Physical contact between mesenchymal stem cells and endothelial precursors induces distinct signatures with relevance to tissue regeneration and engineering

Dissertation zur Erlangung des naturwissenschaftlichen
Doktorgrades der Julius-Maximilians-Universität Würzburg

vorgelegt von
Bettina Hafen

geboren in
Rottweil

Würzburg, 2015

Eingereicht am: 2015-08-11 in Würzburg

Mitglieder der Promotionskommission:

Vorsitzender:	Prof. Dr. Thomas Müller
Gutachter:	Prof. Dr. Norbert Schütze
Gutachter:	Prof. Dr. Georg Krohne

Tag des Promotionskolloquiums: 2015-09-30 in Würzburg

Doktorurkunde ausgehändigt am: _____ in Würzburg

Affidavit

I hereby declare that the present thesis is the result of my own work.
I did not receive any help or support from commercial consultants. All sources and / or materials applied are listed and specified in the thesis.
Furthermore I verify that the thesis has not been submitted as part of another examination process neither in identical nor in similar form.

Eidesstattliche Erklärung

Hiermit erkläre ich an Eides statt, diese Dissertation eigenständig, d. h. insbesondere selbständig und ohne Hilfe eines kommerziellen Promotionsberaters, angefertigt und keine anderen, als die von mir angegebenen Quellen und Hilfsmittel verwendet zu haben.
Ich erkläre außerdem, dass die Dissertation weder in gleicher noch in ähnlicher Form bereits in einem anderen Prüfungsverfahren vorgelegen hat.

Bensheim, 2015-08-08

_____
Bettina Hafen

Table of contents

ACKNOWLEDGEMENT / DANKSAGUNG

Auf meinem Weg hin zu diesem Ziel, haben mich viele Menschen begleitet und unterstützt und ihnen allen gilt zu gleichen Anteilen mein großer Dank. Beginnen möchte ich daher in chronologischer Reihenfolge:

Ein besonderes Dankeschön möchte ich Herrn Dr. Franz Paul Armbruster und der Firma Immundiagnostik AG, Bensheim aussprechen. Lieber Franz Paul, als ich mit dem Wunsch zu promovieren auf Dich zugekommen bin, hast Du nur gelächelt und genickt und mich wieder einmal ziehen lassen – wie zuvor schon nach Australien. Ich danke Dir für die Vermittlung des Kontakts nach Würzburg, die finanzielle Unterstützung und die Bereitstellung des Arbeitsplatzes bei der Firma Immundiagnostik AG.

Ganz herzlich bedanken möchte ich mich in diesem Sinne auch bei Herrn Prof. Norbert Schütze und Herrn Prof. Franz Jakob für die freundliche Aufnahme in ihre Arbeitsgruppe im orthopädischen Centrum für Muskuloskelettale Forschung der Universität Würzburg, die Betreuung dieser Arbeit und die Bereitstellung des Themas. Lieber Norbert, ich danke Dir dafür, dass ich den ersten Teil meiner Doktorarbeit in Deinem Team durchführen durfte. Du ermöglichtest es mir, meine Arbeit auf nationalen und internationalen Kongressen vorzustellen. Ich durfte zwei wundervolle Jahre in Würzburg verbringen und erhielt die Chance, Teil eines EU-Projektes zu sein, bei dem ich viele tolle Wissenschaftler kennengelernt habe, neue Erfahrungen sammeln konnte und sehr viel gelernt habe. Frau PD Dr. Regina Ebert danke ich ganz herzlich für ihren fachlichen Rat. Frau Dr. Katrin Schlegelmilch und Herrn Dr. Alexander Keller danke ich für die Hilfe bei der bioinformatischen Auswertung der Microarrays. Mein ganz besonderer Dank gilt an dieser Stelle auch Frau Susanne Wiesner, sowie dem restlichen Team des wissenschaftlichen Labors und den Mitarbeiter/innen des Osteologie-Zentrums, die mich so nett in ihre Gruppe aufgenommen und immer unterstützt haben. Die Zeit mit euch bleibt unvergesslich!

Ebenfalls bedanken möchte ich mich bei Herrn Prof. Georg Krohne von der Fakultät für Biologie der Universität Würzburg. Vielen Dank, dass Sie sich bereit erklärt haben, diese Arbeit zu betreuen und zu begutachten und mir damit die Promotion an der Fakultät für Biologie der Universität Würzburg ermöglicht haben.

Ganz herzlich bedanken möchte ich mich auch bei den Kollegen und Kolleginnen aus der Firma Immundiagnostik AG, die mich in meinem Wunsch zu promovieren immer bestärkt und unterstützt haben. Insbesondere danke ich den Mitarbeitern aus Labor 6, namentlich Frau Anja Vogt und Herrn Hans Jürgen Grön, die mich nach meiner Rückkehr aus Würzburg so liebevoll in ihren Arbeitskreis aufgenommen haben, sowie Frau Tanja Huhn für ihr Mitwirken am Klotho Projekt. Frau Dr. Susanne Duncker danke ich für ihren fachlichen Rat und ihren unerschöpflichen Rotstift.

Mein abschließender Dank gilt meiner Familie. Euch kann ich nicht genug danken! Ihr wart immer für mich da, egal ob seelischer, moralischer oder finanzieller Beistand gebraucht wurde. Eure Unterstützung und Liebe ist und bleibt für mich mein wertvollstes Gut. DANKE!

This project has received funding from the European Union's Seventh Framework Program for research, technological development and demonstration under grant agreement n°242175

SUMMARY / ZUSAMMENFASSUNG

Zusammenfassung

Das Ziel des durch die europäische Union geförderten Projekts *VascuBone* ist die Entwicklung einer *tool box* zur Knochenregeneration, die einerseits sämtliche Grundanforderungen erfüllt, beispielsweise an die Biokompatibilität, Oberflächenbeschaffenheit und Robustheit der Biomaterialien, und andererseits frei an den Bedarf der individuellen Patientensituation angepasst werden kann. Sie beinhaltet unterschiedlichste biokompatible Materialien und Zelltypen, FDA-zugelassene Wachstumsfaktoren, materialmodifizierende Technologien sowie Simulations- und analytische Werkzeuge, wie die auf molekularer Bildgebung basierende *in-vivo*-Diagnostik (MRI und PET/CT), die für den spezifischen medizinischen Bedarf kombiniert werden können. Die *tool box* wird für die Entwicklung translationaler Ansätze in der regenerativen Medizin für unterschiedliche Arten von Knochendefekten verwendet **(VascuBone 2010)**.

Eingebettet in dieses EU-Projekt sollten in der vorliegenden Arbeit die molekularen Grundlagen und Änderungen der globalen Genexpressionsmuster von endothelialen Vorläuferzellen (EPCs) und mesenchymalen Stammzellen (MSCs) nach direktem Zell-Zell-Kontakt sowie nach Gabe von konditioniertem Medium untersucht werden. EPCs spielen eine wichtige Rolle in der postnatalen Vaskulogenese. Ein intaktes Blutgefäßsystem ist überlebensnotwendig für alle Gewebe, einschließlich Knochen. Neueste Erkenntnisse in der Knochenheilung und -regeneration durch die Nutzung von *Tissue-Engineering*-Konstrukten, die mit MSCs besiedelt wurden, förderten die Idee, MSCs und EPCs zu kombinieren, um die Vaskularisierung – und somit das Überleben – des neu gebildeten Knochengewebes zu begünstigen. Die RNA-Proben aus beiden Versuchsansätzen wurden für die Microarray-Analysen auf Affymetrix GeneChips® HG-U133 Plus 2.0 hybridisiert. Die Array-Daten wurden bioinformatisch ausgewertet und mittels RT-PCR verifiziert.
Die vorliegende Arbeit gibt detailliert Aufschluss darüber, wie MSCs und EPCs miteinander kommunizieren, und erlaubt somit wichtige Einblicke in Signalwege des muskuloskelettalen Systems. Dies wiederum ermöglicht weitere funktionelle Studien auf Proteinebene zum Zwecke der Geweberegeneration. Das bessere Verständnis der Zellkommunikation zwischen MSCs und EPCs und somit die gezielte Adressierung von relevanten Faktoren eröffnet völlig neue Möglichkeiten in der klinischen Anwendung, insbesondere im Bereich *Tissue Engineering*.

Im zweiten Teil dieser Arbeit sollte in Kooperation mit der Firma Immundiagnostik AG, Bensheim, ein ELISA (*enzyme-linked immunosorbent assay*) aufgebaut werden. Ziel war es, für ein geeignetes Protein aus den zu erwartenden Listen regulierter Gene ein *in-vitro*-diagnostisches Nachweisverfahren zu entwickeln, das ggf. später als Qualitätsnachweis für erfolgreich besiedelte *Tissue-Engineering*-Konstrukte herangezogen werden könnte. Als geeigneter Kandidat wurde Klotho ausgewählt. Klotho gilt als *anti-aging*-Protein, da Klotho-*knock-out*-Mäuse alle alterstypischen Erkrankungen wie Osteoporose oder Arteriosklerose zeigen. Als Co-Rezeptor für FGF23 spielt Klotho außerdem eine wichtige Rolle im Knochenstoffwechsel. Diese Studie ist die erste, die zeigt, dass in EPCs nach direktem Zell-Zell-Kontakt mit MSCs Klotho hochreguliert wird. Die Entwicklung eines sensitiven und differenzierten Nachweises von sezerniertem Klotho sowie der von der Membran proteolytisch abgespaltenen Form von Klotho, eröffnet völlig neue Möglichkeiten in der klinischen Diagnostik, insbesondere im Bereich der Knochenstoffwechselerkrankungen.

Summary

The goal of the project VascuBone is to develop a tool box for bone regeneration, which on one hand fulfills basic requirements (e.g. biocompatibility, properties of the surface, strength of the biomaterials) and on the other hand is freely combinable with what is needed in the respective patient's situation. The tool box will include a variation of biocompatible biomaterials and cell types, FDA-approved growth factors, material modification technologies, simulation and analytical tools like molecular imaging-based *in vivo* diagnostics, which can be combined for the specific medical need. This tool box will be used to develop translational approaches for regenerative therapies of different types of bone defects. This project receives funding from the European Union's Seventh Framework Program **(VascuBone 2010)**.

The present study is embedded into this EU project. The intention of this study is to assess the changes of the global gene expression patterns of endothelial progenitor cells (EPCs) and mesenchymal stem cells (MSCs) after direct cell-cell contact as well as the influence of conditioned medium gained from MSCs on EPCs and vice versa. EPCs play an important role in postnatal vasculogenesis. An intact blood vessel system is crucial for all tissues, including bone. Latest findings in the field of bone fracture healing and repair by the use of tissue engineering constructs seeded with MSCs raised the idea of combining MSCs and EPCs to enhance vascularization and therefore support survival of the newly built bone tissue. RNA samples from both experimental set ups were hybridized on Affymetrix GeneChips® HG-U133 Plus 2.0 and analyzed by microarray technology. Bioinformatic analysis was applied to the microarray data and verified by RT-PCR.
This study gives detailed information on how EPCs and MSCs communicate with each other and therefore gives insights into the signaling pathways of the musculoskeletal system. These insights will be the base for further functional studies on protein level for the purpose of tissue regeneration. A better understanding of the cell communication of MSCs and EPCs and subsequently the targeting of relevant factors opens a variety of new opportunities, especially in the field of tissue engineering.

The second part of the present work was to develop an ELISA (*enzyme-linked immunosorbent assay*) for a target protein from the lists of differentially expressed genes revealed by the microarray analysis. This project was in cooperation with Immundiagnostik AG, Bensheim, Germany. The development of the ELISA aimed to have an *in vitro* diagnostic tool to monitor e.g. the quality of cell seeded tissue engineering constructs. The target protein chosen from the lists was klotho. Klotho seemed to be a very promising candidate since it is described in the literature as anti-aging protein. Furthermore, studies with klotho knock-out mice showed that these animals suffered from several age-related diseases e.g. osteoporosis and atherosclerosis. As a co-receptor for FGF23, klotho plays an important role in bone metabolism. The present study will be the first one to show that klotho is up-regulated in EPCs after direct cell-cell contact with MSCs. The development of an assay with a high sensitivity on one hand and the capacity to differentiate between secreted and shedded klotho on the other hand will allow further functional studies of this protein and offers a new opportunity in medical diagnostics especially in the field of metabolic bone disease.

1. INTRODUCTION

The human body utilizes amazing biologic resources and its reparative capability is probably one of the most fascinating and elegant processes in nature. A highly qualified and specialized work force is in charge to control, maintain and repair all systems of our body. Tissue repair requires highly controlled processes such as the proliferation and maturation of specialized cells, the precise coordination of cell signaling and the subsequent homing of cells to specified areas. The orchestrated interaction for example includes a controlled inflammatory cascade at the site of injury or tissue damage to achieve a balanced immune response. This induces the mobilization of tissue-specific host stem or progenitor cells, drives proliferation and differentiation of these recruited cells into the targeted cell types and regenerates functional tissues.
The subsequent chapters will provide some insights into this fascinating world of (bone) tissue regeneration and introduce some of the key players involved in the formation of blood vessels and bone generation, namely the endothelial progenitor cells and the mesenchymal stem cells.

1.1 Blood vessel formation

Blood vessels arose in evolution when organisms outgrew the limits of oxygen diffusion **(Schmidt & Carmeliet 2010).** They are not only important for an adequate supply of oxygen and nutrients, but are also needed for the removal of waste products. The formation of a vascular network is a fundamental process in the growth and maintenance of all tissues. Vascularization – the formation of blood vessels – occurs by three distinct processes: vasculogenesis, angiogenesis and arteriogenesis **(Buschmann & Schaper 1999)**. The processes of vasculogenesis and angiogenesis will be further discussed in this chapter. Arteriogenesis describes the remodeling that occurs to form mature arteries by migration of supporting smooth muscle cells and pericytes from the epicardium during development **(Smart et al. 2009)**.
Understanding how blood vessels form has become a principal, yet challenging, objective of the last decade. Unraveling these mechanisms would offer therapeutic options to ameliorate or perhaps even cure disorders that are now leading causes of mortality **(Carmeliet 2000)**. Vascularization is also a key challenge in tissue engineering. Poor angiogenesis within tissue-engineered grafts has been identified as a main challenge limiting the clinical introduction of bone tissue-engineering approaches for the repair of large bone defects. In several recent review articles, vascularization has been highlighted as a major determinant of the potential size of tissue-engineered scaffolds **(Y. Liu et al. 2012; Novosel et al. 2011; Nguyen et al. 2012)**.

1.1.1 Vasculogenesis

Until recently, it was thought that neovascularization – the process by which new blood vessels form – occurs via angiogenesis in the adult. Angiogenesis is the sprouting of new blood vessels from already established vessels. This is in contrast to vasculogenesis, which refers to the *de novo* formation of blood vessels from endothelial progenitors and was thought to occur only in the embryo **(Patenaude et al. 2010)**. Contrary to the previously held dogma, the process of vasculogenesis is not limited to prenatal development. The differentiation of angioblasts from mesoderm and the formation of primitive blood vessels from angioblasts at or near the site of their origin are the two distinct steps during the onset of vascularization that are defined as vasculogenesis **(Risau & Flamme 1995)**. Vascular endothelial growth factor (VEGF) expression is dramatically up-regulated by hypoxia and results in enhanced neovascularization. Although the role of VEGF in angiogenesis has been well characterized, its role in adult vasculogenesis remains poorly understood **(Li et al. 2006)**. Recently collected data indicate that VEGF is an important factor for the mobilization of endothelial progenitor cells (EPCs) from bone marrow. The similar EPC kinetics

modulation has been observed in response to other hematopoietic stimulators, such as granulocyte colony-stimulating factor (G-CSF), angiopoietin-1, and stroma-derived factor-1 (SDF-1) **(Asahara & Kawamoto 2004)**.

1.1.2 Angiogenesis

Angiogenesis is the generation of new microvessels by endothelial proliferation and migration, either by intussusception, to divide the vessel in two, or by sprouting, to form new branches **(Smart et al. 2009)**. Capillary blood vessels consist of endothelial cells and pericytes. These two cell types carry all of the genetic information to form tubes, branches, and whole capillary networks. Specific angiogenic molecules can initiate this process **(Folkman & Shing 1992)**. When evaluated according to their putative targets, angiogenic molecules appear to fall into two groups: those that act directly on vascular endothelial cells to stimulate locomotion or mitosis, and those that act indirectly by mobilizing host cells (for example, macrophages) to release endothelial growth factors **(Folkman & Klagsbrun 1987)**.
The fibroblast growth factor (FGF) receptor-1 (FGFR1) family of receptor tyrosine kinases is essential for angiogenesis. Unlike classical FGFs, non-classical FGFs (e.g. FGF21) lack affinity for heparin binding and require klotho family member proteins as co-receptors to bind and activate FGFR1 **(Yaqoob et al. 2014)**. Also, the cross-talk among FGFs, vascular endothelial growth factors (VEGFs), and inflammatory cytokines/chemokines may play a role in the modulation of blood vessel growth in different pathological conditions, including cancer **(Presta et al. 2005)**.

1.2 Endothelial progenitor cells (EPCs)

Postnatal neovascularization is thought to result exclusively from the proliferation, migration, and remodeling of fully differentiated endothelial cells (ECs) derived from preexisting blood vessels. This adult paradigm, referred to as angiogenesis, contrasts with vasculogenesis, the term applied to the formation of embryonic blood vessels from EC progenitors, or angioblasts **(Asahara et al. 1997)**.
Since the initial report of EPCs **(Asahara et al. 1997)**, a number of groups have set out to better define this cell population. Because EPCs and hematopoetic stem cells (HSCs) share many surface markers, and because no simple definition of EPCs exists, various methods of EPC isolation have been reported. The term “EPC” may therefore encompass a group of cells existing in a variety of stages ranking from hemangioblasts to fully differentiated ECs (Figure 1). Although the true differentiation lineage of EPCs and their putative precursors remain to be determined, there is overwhelming evidence *in vivo* that a population of EPCs exists in humans **(Asahara & Kawamoto 2004)**.
Growth factors and cytokines released at sites of injury and inflammation play an important role in stimulating EPC migration to these sites and influence favorably EPC angiogenic function. They include SDF-1 (stromal cell-derived factor-1), VEGF (vascular endothelial growth factor), PlGF (placental growth factor), FGF-2 (fibroblast growth factor-2), NGF (nerve growth factor) and IL-1β (interleukin-1 beta). Others, e.g. TNF-α (tumor necrosis factor-alpha), have an unfavorable influence. SDF-1 and VEGF in combination increase chemotactic cell migration and reduce apoptosis caused by serum starvation **(Peplow 2014)**. Beside the endogenous stimulation of the recruitment of EPCs by growth factors, chemokines, cytokines and hormones like VEGF and angiopoietin, SDF-1, GM-CSF (granulocyte-macrophage colony-stimulating factor), erythropoietin and estrogen (e.g. estradiol), respectively, exogenous stimuli like exercise and drugs (e.g. statins) are shown to have a positive effect **(Asahara et al. 1999; Li et al. 2006; Kalka et al. 2000; Hattori et al. 2001; Aicher et al. 2005; Huang & Liu 2011; Takahashi et al. 1999; Heeschen et al. 2003; Bahlmann et al. 2004; Foresta et al. 2007; Strehlow et al. 2003; Iwakura et al. 2003; Li et al. 2013; Wahl et al. 2007; Llevadot et al. 2001; Dimmeler et al. 2001; Vasa et al. 2001; França et al. 2011; Hillen & Griffioen 2007).**
Circulating adult human EPCs were primarily defined as cells positive for CD34/vascular endothelial growth factor receptor-2 (VEGFR-2) or CD133/CD34/VEGFR-2. However, the research on EPC biology is rapidly growing and several recently published data suggested that other populations of bone

marrow-derived, circulating, or tissue resident cells might also possess properties of EPCs. In particular, these sub-populations were characterized by expression of the monocytic marker CD14, together with CD34 or VEGFR-2. Furthermore, "early" isolated EPCs also displayed expression of monocytic marker (CD14, CD11b, CD11c), whereas the "late" endothelial outgrowth were CD14-negative and strongly expressed markers of mature endothelial cells **(Hristov et al. 2007)**.
The originally described EPCs by **Asahara et al. (1997)** were defined as $CD34^+$, $Flk\text{-}1^+$ (also known as CD309), $CD45^+$ and $CD31^+$ cells. Peichev et al. included the hematopoetic surface marker AC133 (also known as CD133) which is not expressed in mature endothelial cells. The authors suggest that circulating $CD34^+$ cells expressing VEGFR-2 (also known as KDR, Flk-1 or CD309) and AC133 constitute a phenotypically and functionally distinct population of circulating endothelial cells **(Peichev et al. 2000)**. Brunt et al. describe EPCs as a heterogeneous group of cells originating from multiple precursors in the bone marrow and present at different stages of differentiation in the circulation (Figure 2) **(Brunt et al. 2007)**.
Adams and colleagues demonstrated in two publications in 2014 that the bone vasculature contains specialized endothelial cells with signaling properties that support bone maturation and regeneration. The authors distinguished two new subpopulations of endothelial cells that they term type H and type L. They found that osteoprogenitor cells, which differentiate into bone-forming osteoblasts, preferentially associate with type H endothelial cells because these cells are a rich source of several growth factors relevant for the survival and proliferation of osteoprogenitors **(Kusumbe et al. 2014; Ramasamy et al. 2014).**
Understanding the nature of the mechanisms linking angiogenesis and bone formation should be of great relevance for improved fracture healing or prevention of bone mass loss.

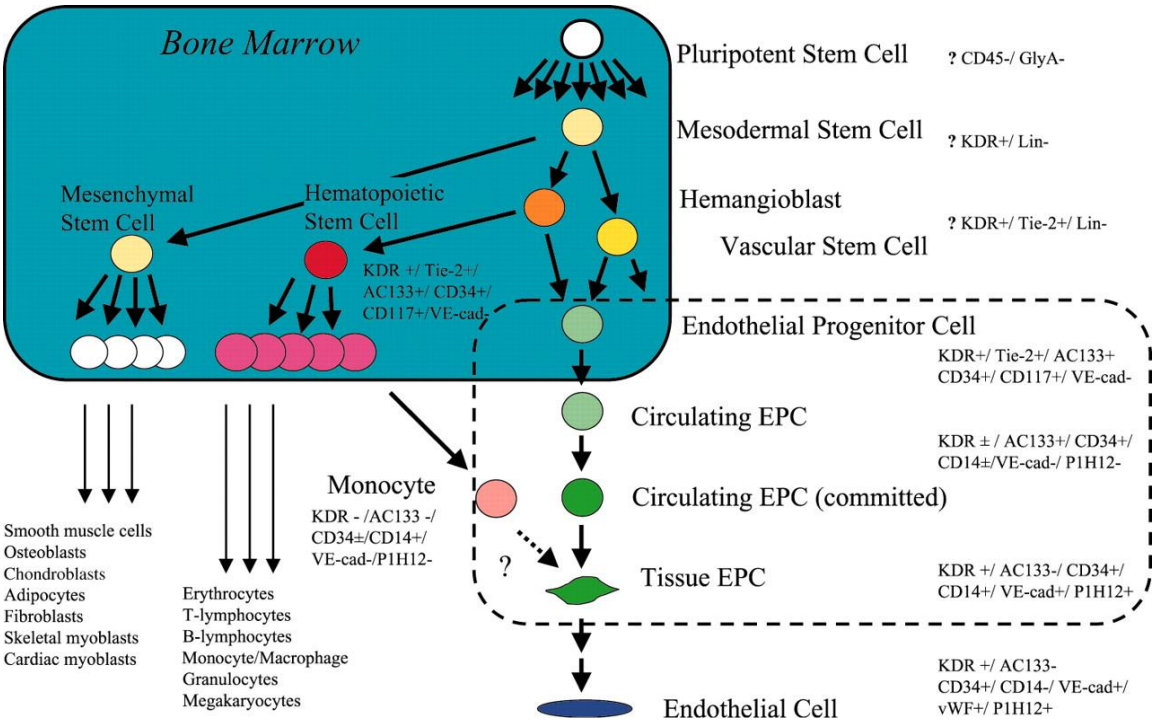

Figure 1: Putative cascade and expressional profiles of human bone marrow-derived endothelial progenitor cell differentiation
EPCs have been isolated along with HSCs in hematopoietic organs. Flk-1 and CD34 antigens were used to detect putative EPCs from the mononuclear cell fraction of peripheral blood. This methodology was supported by former findings that embryonic HSCs and EPCs share certain antigenic determinants, including Flk-1, Tie-2, c-Kit, Sca-1, CD133, and CD34. These progenitor cells have consequently been considered to be derived from a common precursor, putatively termed a hemangioblast. EPC, endothelial progenitor cell; HSC, hemotopoetic stem cell; Flk-1, fetal liver kinase-1; Tie-2, tyrosine kinase, endothelial; c-Kit, tyrosine-protein kinase; Sca-1, spinocerebellar ataxia type 1; KDR = CD309 = VEGFR, vascular-endothelial growth factor receptor; VE-cad, vascular endothelial cadherin (from Asahara & Kawamoto 2004).

Antigen	Alternate name(s)	EC	EPC	MSC	Other
CD10	CALLA, NEP, gp100	-	-	+	T, B, Fibro
CD13	APN, gp150	-	-	+	Mono, Gran
CD14	LPS-R	-	-	-	Mono, Mac, Gran
CD29	Integrin ß1, gp11a	-	-	+	Mono, Gran, Plt, T, B
CD31	PECAM1, Endocam	+	+	-	Mono, Plt, Gran, Lympho, B
CD34	Gp105-120, Mucosialin	+	+	-	HemSC
CD44	H-CAM, Pgp-1, EMCRIII, Ly-24	-	-	+	Leuko
CD45	LCA, T200, B220, Ly-5	-	-	-	T, B, HemP
CD54	ICAM1	+	+/-	†	Mono, Lympho
CD62e	E-Selectin, ELAM1, LECAM2	†	+/-	†	Leuko
CD90	Thy-1	+	+/-	+	Hem
CD105	Endoglin	+	+	+	Mono, Mac
CD106	VCAM1, INCAM	†	†/-	†	HemSC
CD117	c-kit, SCFR	-	+	+	
CD133	AC133[a], Prominin 1[a]	-	+/-	-	HemSC
CD141	Thrombomodulin	+	+/-	-	Mono, Plt, Neutro, SMC
CD144	VE-cadherin, cadherin 5	+	+	+	StemCell
CD146	P1H12, S-endo-1, Muc18	+	-	-	T
CD166	ALCAM	-	-	+	Mono, T, Fib
CD202b	Tie2, Tek, Angiopoietin-R	+	+	+	StemCell
CD309	VEGFR2, Flk1, KDR	+	+	+	StemCell
Sca1		-	+	+	StemCell

Figure 2: Common antigen expression for ECs, EPCs and MSCs
–, antigen negative; +, antigen positive; +/–, subject/age/differentiation dependent; †, antigen activation dependent; B, B cells; EC, endothelial cells; EPC, endothelial progenitor cells; Fib, fibroblast; Gran, granulocyte; Hem, hematopoietic cells; HemP, hematopoeitic progenitors; HemSC, hematopoeitic stem cells; Leuko, leukocytes; Lympho, lymphocytes; Mac, macrophage; MSC, mesenchymal stem cells; Mono, monocyte; Neutro, neutrophil; Plt, platelet; T, T cells; a, murine only (from Brunt et al. 2007).

1.3 Mesenchymal stem cells (MSCs)

Stem cells are undifferentiated cells that can divide asymmetrically to give rise to a copy of the original stem cell as well as to a second daughter programmed to differentiate into a specialized cell. In times of growth or regeneration, stem cells can also divide symmetrically, to produce two identical copies of the original cell. Mesenchymal stem cells (MSCs) are bone marrow populating cells, different from hematopoietic stem cells, which possess an extensive proliferative potential and the ability to differentiate into various cell types, including: osteoblasts, adipocytes, chondrocytes, myocytes, cardiomyocytes and neurons **(Bobis et al. 2006; Bruder et al. 1994)** (Figure 3).
Examples of tissues where MSCs have been characterized include, but are not limited to:
Mesodermal: bone marrow, trabecular bone, synovium, cartilage, fat, muscle, and tonsil; endodermal: thymus; ectodermal: skin, hair follicle, dura mater, and dental pulp (mesoderm and ectoderm-derived); prenatal and perinatal tissues: umbilical cord, umbilical cord blood, and placenta **(Kuhn & Tuan 2010)**.

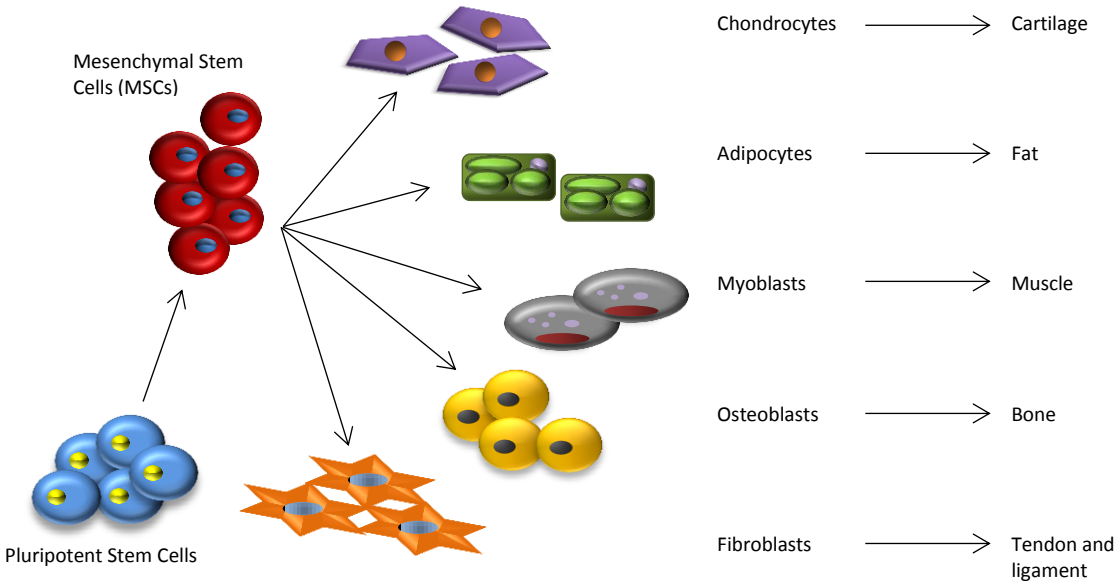

Figure 3: Multilineage potential and differentiation of mesenchymal stem cells
Multipotent MSCs originate from pluripotent stem cells during the embryonic development and persist in the adult organism. MSCs possess an extensive proliferative potential and ability to differentiate into various cell types of various mesenchymal tissues like bone, cartilage, muscle, and adipose tissue.

In addition to regulating normal skeletal homeostasis, MSCs also play an important role in bone formation in the embryo, and during adult fracture repair and remodeling. Bone fracture or injury initiates a series of cellular and molecular pathways that commence with hematoma formation and an inflammatory cascade that regulates MSCs activity leading to fracture healing and the reestablishment of skeletal integrity **(Bielby et al. 2007)**. It has been shown that MSC migrate in response to many chemotactic factors, like platelet-derived growth factor AB (PDGF-AB), insulin-like growth factor 1 (IGF-1), the chemokines RANTES, macrophage-derived chemokine (MDC), and stromal-derived factor 1 (SDF-1). Accordingly, MSC express the tyrosine kinase receptors for PDGF and IGF, as well as the RANTES and MDC receptors CCR2, CCR3, and CCR4, and the SDF-1 receptor CXCR4 **(Eggenhofer et al. 2014)**.
MSCs have generated a great deal of interest because of their potential use in regenerative medicine and tissue engineering and there are some dramatic examples, derived from both pre-clinical and clinical studies, that illustrate their therapeutic value **(Barry & Murphy 2004)**. Some approaches of

the use of MSCs in tissue engineering are summarized in Chapter 1.4. Cell treatment with mesenchymal stem cells (MSCs) has a number of advantages as MSCs: (1) are multipotent cells that can migrate to sites of injury; (2) are capable of suppressing the local immune response; and (3) are available in large quantities from the patients themselves **(Qin et al. 2014)**. MSC-mediated immunosuppression describes the fact that MSC are able to suppress several functions exerted by diverse immunocytes such as T, B, and NK cells **(Hass et al. 2011)**. MSCs have been shown to modulate immunological responses via T cell suppression. As such, they have been investigated as a new therapeutic strategy for T cell-mediated diseases such as graft-versus-host disease (GVHD), Crohn's disease, and the prevention of organ transplantation rejection. MSCs have been reported to express major histocompatibility complex (MHC) molecules, including MHC class II (MHC-II), and the levels of MHC are altered by proinflammatory cytokines **(Yagi et al. 2010)**. A model for the mediation of the immunomodulatory and regenerative effect induced by MSC administration is shown in Figure 4 **(Eggenhofer et al. 2014)**.

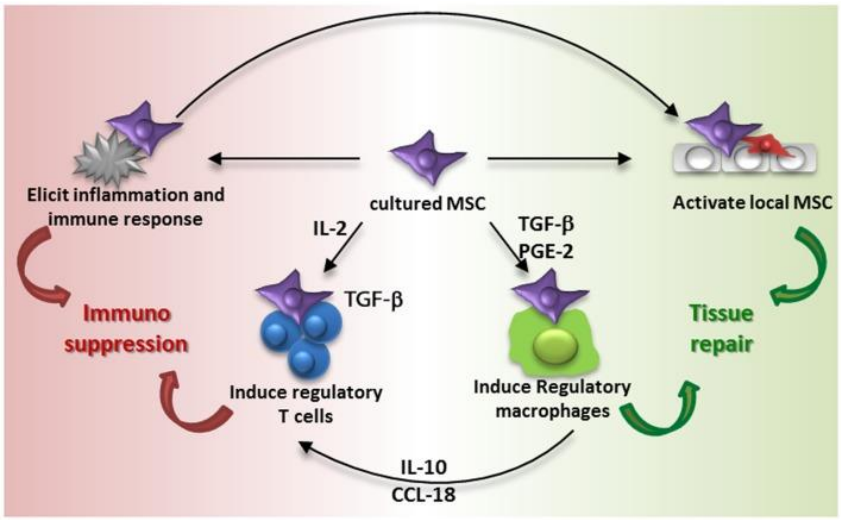

Figure 4: Proposed model of MSC contribution to immune suppression and tissue repair
Intravenous administration of culture-expanded MSCs (violet cells) leads to modulation of the function of endogenous MSCs (red cells) and macrophages via the secretome of the administered cells (e.g., TGF-β, PGE-2, and other factors) and phagocytosis of MSCs by macrophages. The activation of resident MSCs and induction of regulatory macrophages induces tissue regeneration. MSCs furthermore induce regulatory T cells via different mechanisms, including the secretion of TGF-β and an indirect elevation of IL-2. Administration of MSCs also elicits a systemic immune response, which triggers an immunosuppressive response (from Eggenhofer et al. 2014).

1.4 The use of EPCs and MSCs in tissue engineering

Tissue engineering aims to regenerate tissues and organs by using cell and biomaterial-based approaches. One of the current challenges in the field is to promote proper vascularization in the implant to prevent cell death and promote host integration **(Aguirre et al. 2010)**. While reconstruction of small to moderate sized bone defects using engineered bone tissues is technically feasible, the reconstruction of large volume defects remains challenging. Therefore, vascularization concepts gain on interest **(Kneser et al. 2006)**. Endothelial cell-derived tube formation in a scaffold and the dialogue between endothelial cells and mesenchymal stem cells provide promising means of generating vascular bone tissue-engineered constructs **(Grellier et al. 2009)**. An understanding of the cellular and molecular interactions of blood vessels and bone cells will enhance and aid the successful development of future vascularized bone scaffold constructs, enabling survival and integration of bioengineered bone with the host tissue **(Kanczler & Oreffo 2008)**.
Xue et al. showed a significant impact of endothelial cells on MSCs after 5 days and 15 days of co-culture, especially with respect to bidirectional gene regulation of angiogenesis and osteogenesis, through cell signaling, cell adhesion, and cellular matrix **(Xue et al. 2009; Xue et al. 2013)**.
By using a rat calvarial bone defect model, Xing et al. showed *in vivo* that bone regeneration was enhanced by a construct of the polymer scaffold loaded with co-cultured bone marrow stromal cells and endothelial cells **(Xing et al. 2011)**.
Yu et al. established 0.4 cm long segmental femur defects in mice and replaced them with grafts, seeded with osteoblast only or a combination of osteoblasts/endothelial cells. The cell-free scaffolds were denoted as control group. In comparison with the osteoblast group, the osteoblast/endothelial cell group resulted in a widely distributed capillary network, osteoid generated by osteoblasts and absent ischemic necroses. Pre-seeding scaffold with endothelial cells effectively promoted neovascularization in grafts, prevented the ischemic necrosis, and improved osteogenesis **(Yu et al. 2008)**.
Zigdon-Giladi et al. tested vertical bone regeneration in a rat calvarium-guided bone regeneration model. The rats were sacrificed after 4 or 12 weeks. At both time points, new augmented hard tissue filled the space under the dome, and blood vessel density was higher in the EPC/MSC transplanted group vs control. However, bone height and bone area were similar among the groups 4 weeks posttransplantation, but were doubled in the EPC/MSC transplanted group 12 weeks posttransplantation **(Zigdon-Giladi et al. 2013)**.
Although communication between bone marrow stromal cells and endothelial cells is recognized as one of the most important cellular interactions in bone regeneration, the underlying mechanisms of this biological process are not well understood.

1.5 Bone remodeling

Throughout life, bone is constantly being remodeled in a sequence characterized by removal of old bone by osteoclasts and its replacement by osteoblasts (Figure 5). It has been proposed that when osteocytes either sense bone deformation caused by mechanical loading or detect microdamage in old bone, they transmit signals of unknown nature to recruit osteoclast precursors to the specific bone site **(Parfitt 2002)**. Osteoclasts are multinucleated giant cells that differentiate from mononuclear cells of the monocyte/macrophage lineage upon stimulation by two essential factors: the monocyte/macrophage colony-stimulating factor (M-CSF) and the receptor activator of nuclear factor κB (NF-κB) ligand (RANKL) **(Feng & McDonald 2011)**. They have developed an efficient machinery for dissolving crystalline hydroxyapatite and degrading organic bone matrix rich in collagen fibers. When initiating bone resorption, osteoclasts become polarized, and three distinct membrane domains appear: a ruffled border, a sealing zone and a functional secretory domain **(Vaananen et al. 2000)**.

In the reversal phase, osteoblast function (osteoid synthesis) begins to overtake bone resorption as the predominant event **(Feng & McDonald 2011)**. Osteoblasts, the bone-forming cells, are directed to form bone only in the resorption lacunae. Osteoblasts are derived from mesenchymal stem cells (MSCs) through a multistep differentiation pathway, which further differentiate into osteocytes and are embedded in calcified tissues **(Suda et al. 1992)**. Osteocytes remain active in the bone-remodeling process by maintaining connections to the bone surface, to osteoblasts and osteoclasts, and to other osteocytes through an extensive canalicular network **(Rochefort 2014)**. Subsequently, the last phase involves the mineralization of osteoid and concludes the bone-remodeling cycle. The osteoblasts lying on the surface of the newly formed bone packet are quiescent lining cells until activated. It has been suggested that the targeting of pre-osteoclasts for the initiation of remodeling is carried out by lining cells under instruction from osteocytes **(Hill 1998)**.

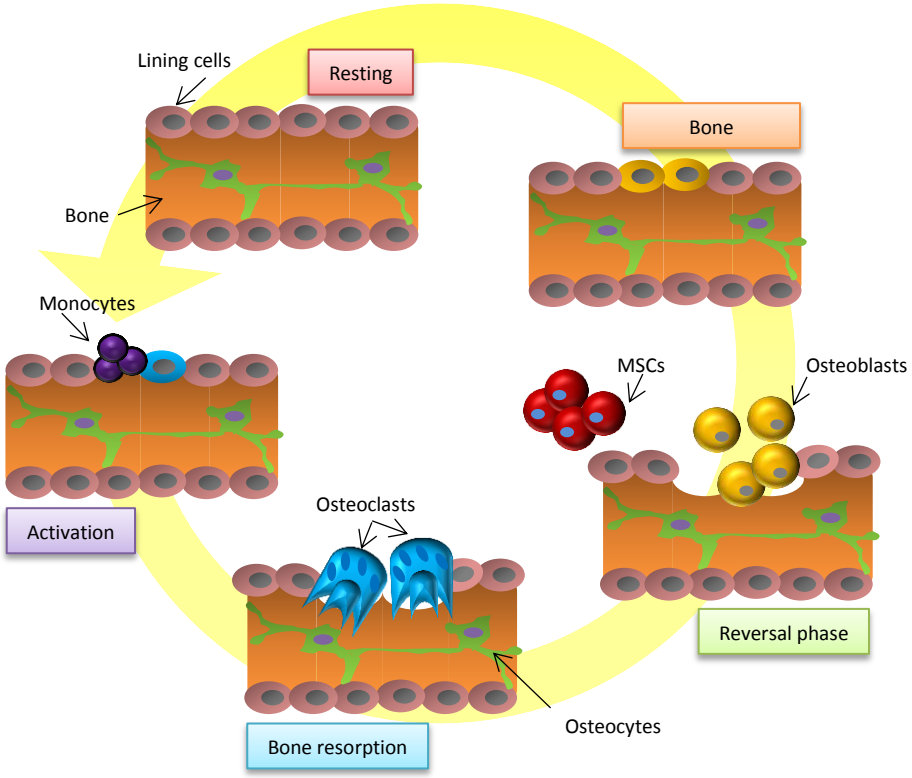

Figure 5: Bone remodeling
Schematic outlines of the bone remodeling cycle of normal bone. In bone tissue, the osteoblasts are involved in new bone formation, while osteoclasts play a major role in bone resorption.

1.6 Calcium and phosphate homeostasis

The skeleton acts as a scaffold by providing support and protection for the soft tissues that make up the rest of the body. The skeletal system also provides attachment points for muscles to allow movements at the joints.

The FGF23-bone-kidney axis is part of newly discovered biological systems linking bone to other organ functions through a complex endocrine network that is integrated with the PTH-vitamin D axis (Figure 6) and which plays an equally important role in health and disease. The discovery that osteoblasts and osteocytes are the principal site for FGF23 production and secretion identified bone not only as the major reservoir for calcium and phosphate, but as an endocrine organ that communicates with other organs involved in mineral homeostasis **(Martin et al. 2012)**. FGF23 is a unique member of the fibroblast growth factor (FGF) family because it acts as a hormone that derives from bone and regulates kidney functions, whereas most other family members are thought to regulate various cell functions at a local level. The renotropic activity of circulating FGF23 indicates the possible presence of an FGF23-specific receptor in the kidney. Urakawa et al. showed in 2006 that a previously undescribed receptor conversion by klotho generates the FGF23 receptor **(Urakawa et al. 2006)**. The recent demonstration that klotho transforms one of the canonical receptors for various FGFs, namely FGFR1(IIIc), into a specific receptor for FGF23, is a major breakthrough. It is still uncertain, however, whether this effect of klotho is strictly limited to this FGFR subtype **(Drüeke & Prié 2007)**.

The traditional model of overall calcium homeostasis has two key components. The first comprises several distinct cell types that sense changes in extracellular Ca^{2+} leading to appropriate changes in the secretion of the calciotropic hormones, parathyroid hormone (PTH), $1,25(OH)_2$ vitamin D and calcitonin. The second key component is the effector systems, specialized calcium-translocating cells of the kidneys, bones and intestine, that respond to the calciotropic hormones **(Lewin & Olgaard 2006)**. Calcium, an essential ion in all organisms, plays a crucial role in processes ranging from formation and maintenance of the skeleton to temporal and spatial regulation of neuronal function. Concentration of blood Ca^{2+} decreases with age in both men and women, and several studies suggest that this is linked to aging-associated disorders. Blood calcium concentration is maintained within a narrow range and the Transient Receptor Potential ion channel TRPV5 has been implicated in this process **(Chang et al. 2005)**. The anti-aging hormone klotho and other glycosidases stimulate TRPV5-dependent Ca^{2+} uptake **(Leunissen et al. 2013)**. For more information about klotho see chapter 1.7.

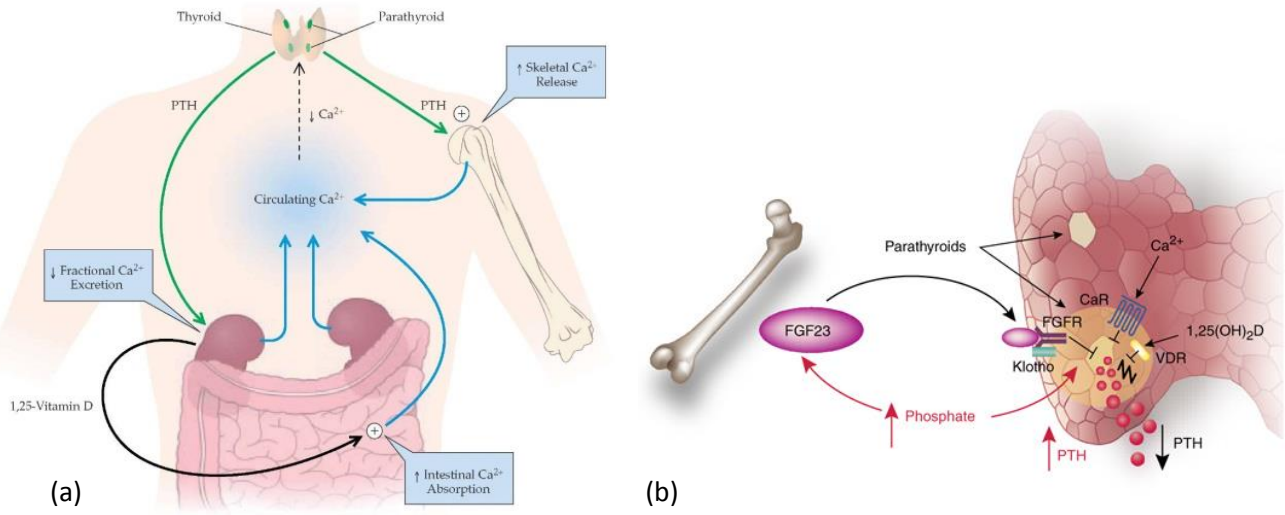

Figure 6: (a) the PTH-vitamin D axis (b) the bone-parathyroid endocrine axis
(a) Circulating concentrations of ionized calcium (Ca^{2+}) are maintained under extremely tight control by the parathyroid hormone (PTH)-vitamin D axis. Absorption of dietary calcium by the gastrointestinal tract, reduction of calcium excretion by the kidneys, and release of stored calcium from bones serve as sources for circulating calcium. Decreases in circulating calcium trigger the release of PTH, which promotes release of calcium into the extracellular space by increasing bone resorption; the release of PTH also causes an increase in calcium reabsorption in the distal nephron, resulting in a decrease in urinary calcium loss. PTH also augments renal production of $1,25(OH)_2$ vitamin D, which secondarily increases calcium absorption in the gut. Source: http://what-when-how.com/acp-medicine/diseases-of-calcium-metabolism-and-metabolic-bone-disease-part-1/; date: 2014-07-24
(b) A high Ca^{2+} or $1,25(OH)_2$ vitamin D level suppresses PTH secretion and stimulates FGF23 secretion. FGF23 is predominantly secreted by osteocytes after the stimulus of a high phosphate (Pi) level. It signals through FGF receptors (FGFRs) bound by the transmembrane protein klotho. As most tissues express FGFRs, the expression of klotho determines FGF23 target organs. In addition to the action of FGF23 on the kidney to cause Pi excretion and decrease the synthesis of $1,25(OH)_2$ vitamin D, it is now shown to act on the parathyroid to decrease PTH synthesis and secretion.
FGF23, fibroblast growth factor 23; FGFR, fibroblast growth factor receptor; CaR, calcium receptor; PTH, parathyroid hormone; VDR, vitamin D receptor. The red arrows indicate stimulatory pathways (Silver & Naveh-Many 2009).

1.7 Klotho

The gene encoding for the klotho protein (KL) is named after Clotho, the youngest of the Three Fates. Clotho was responsible for spinning the thread of human life.
KL has been called an “aging suppressor gene” and has been suggested to delay age-related declines in physiological functioning **(Kuro-o et al. 1997)**. The human klotho gene *(kl)* is composed of 5 exons and ranges over 50 kb on chromosome 13q12. Matsumura et al. identified two transcripts that encode a membrane (1012 amino acids) or secreted (549 amino acids) protein. The sequences are shown in Figure 8. These transcripts arise from a single *kl* gene through alternative RNA splicing. Expression of the putative secreted form (isoform 2) predominates over that of the membrane form (isoform 1) in humans **(Matsumura et al. 1998)**. However, in the mouse, the expression of the transmembrane klotho predominates over the secreted protein in all tissues examined **(Li et al. 2004)**. Compared with the transmembrane form protein, the secreted form does not have the second internal repeat of the extracellular domain (KL2), the transmembrane domain, or the intracellular domain (Figure 7). It only encodes the N-terminal half of klotho with its extracellular domain (KL1), and has a molecular weight of approximately 65–70 kDa **(Wang & Sun 2009)**.

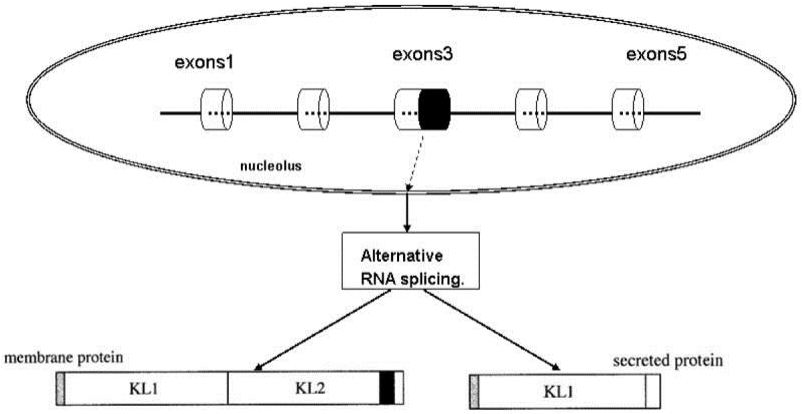

Figure 7: The mouse klotho gene structure and alternative RNA splicing
The mouse klotho gene is composed of 5 exons and 4 introns and resides on chromosome 13. Two transcripts arise from this alternative RNA splicing: a membrane or a secreted form of klotho protein (Wang & Sun 2009).

The single-pass type I membrane protein (Figure 9) can also be cleaved, shed and act as a circulating hormone (soluble KL). KL contains two major cleavage sites: one close to the juxtamembrane region and another between the KL1 and KL2 domains **(C.-D. Chen et al. 2014)**. The extracellular domain of KL protein is released into blood and urine by ectodomain shedding. The two forms of KL protein, membrane klotho and secreted klotho, exert distinct functions. Membrane klotho forms a complex with fibroblast growth factor (FGF) receptors and functions as an obligate co-receptor for FGF23. FGF23 is a bone-derived hormone that regulates phosphate and vitamin D homeostasis **(Kurosu & Kuro-o 2009; Kuro-o 2010)**. Urakawa et al. found that the concerted action of KL and FGFR1(IIIc) reconstitutes the FGF23 receptor **(Urakawa et al. 2006)**. Beside to its important role in phosphate homeostasis via FGF23 signaling, there is also particular focus on its role in the control of calcium homeostasis. Secreted klotho up-regulates the Transient Receptor Potential calcium channel TRPV5 from cell exterior by removing sialic acids from N-glycan of the channel and inhibiting its endocytosis **(Wolf et al. 2014)**.

```
        10         20         30         40         50         60
MPASAPPRRP RPPPPSLSLL LVLLGLGGRR LRAEPGDGAQ TWARFSRPPA PEAAGLFQGT

        70         80         90        100        110        120
FPDGFLWAVG SAAYQTEGGW QQHGKGASIW DTFTHHPLAP PGDSRNASLP LGAPSPLQPA

       130        140        150        160        170        180
TGDVASDSYN NVFRDTEALR ELGVTHYRFS ISWARVLPNG SAGVPNREGL RYYRRLLERL

       190        200        210        220        230        240
RELGVQPVVT LYHWDLPQRL QDAYGGWANR ALADHFRDYA ELCFRHFGGQ VKYWITIDNP

       250        260        270        280        290        300
YVVAWHGYAT GRLAPGIRGS PRLGYLVAHN LLLAHAKVWH LYNTSFRPTQ GGQVSIALSS

       310        320        330        340        350        360
HWINPRRMTD HSIKECQKSL DFVLGWFAKP VFIDGDYPES MKNNLSSILP DFTESEKKFI

       370        380        390        400        410        420
KGTADFFALC FGPTLSFQLL DPHMKFRQLE SPNLRQLLSW IDLEFNHPQI FIVENGWFVS

       430        440        450        460        470        480
GTTKRDDAKY MYYLKKFIME TLKAIKLDGV DVIGYTAWSL MDGFEWHRGY SIRRGLFYVD

       490        500        510        520        530        540
FLSQDKMLLP KSSALFYQKL IEKNGFPPLP ENQPLEGTFP CDFAWGVVDN YIQVDTTLSQ

       550        560        570        580        590        600
FTDLNVYLWD VHHSKRLIKV DGVVTKKRKS YCVDFAAIQP QIALLQEMHV THFRFSLDWA

       610        620        630        640        650        660
LILPLGNQSQ VNHTILQYYR CMASELVRVN ITPVVALWQP MAPNQGLPRL LARQGAWENP

       670        680        690        700        710        720
YTALAFAEYA RLCFQELGHH VKLWITMNEP YTRNMTYSAG HNLLKAHALA WHVYNEKFRH

       730        740        750        760        770        780
AQNGKISIAL QADWIEPACP FSQKDKEVAE RVLEFDIGWL AEPIFGSGDY PWVMRDWLNQ

       790        800        810        820        830        840
RNNFLLPYFT EDEKKLIQGT FDFLALSHYT TILVDSEKED PIKYNDYLEV QEMTDITWLN

       850        860        870        880        890        900
SPSQVAVVPW GLRKVLNWLK FKYGDLPMYI ISNGIDDGLH AEDDQLRVYY MQNYINEALK

       910        920        930        940        950        960
AHILDGINLC GYFAYSFNDR TAPRFGLYRY AADQFEPKAS MKHYRKIIDS NGFPGPETLE

       970        980        990       1000       1010
RFCPEEFTVC TECSFFHTRK SLLAFIAFLF FASIISLSLI FYYSKKGRRS YK
```

Figure 8: Sequence of klotho isoform 1 (membrane-bound)
Sequence length of isoform 1 (membrane-bound): 1012 amino acids. Isoform 1 shedding leads to a soluble peptide. Isoform 2 (secreted) is produced by alternative splicing. The sequence of isoform 2 differs from this sequence as follows:
535-549: DTTLSQFTDLNVYLW → SQLTKPISSLTKPYH
550-1012: missing
Source: http://www.uniprot.org/uniprot/Q9UEF7; 2014-08)

Figure 9: Scheme of the klotho protein structure
Klotho is 1012 amino acids in length and possesses a putative signal sequence at its N-terminus and a transmembrane domain with a short cytoplasmic domain at the C-terminus. The extracellular domain of the klotho protein consists of two internal repeats (KL1 and KL2) that share sequence homology with β-glucosidase (Razzaque 2012).

Secreted klotho functions as a humoral factor that regulates activity of multiple glycoproteins on the cell surface, including ion channels and growth factor receptors such as insulin/insulin-like growth factor-1 receptors **(Kurosu & Kuro-o 2009; Kuro-o 2010)**.
KL is highly expressed in the kidneys, choroid plexus and anterior pituitary **(Shahmoon et al. 2014)**, and is present in lower levels within skeletal muscle and other tissues (Figure 10). KL is a powerful longevity protein that has been linked to the prevention of muscle atrophy, osteopenia, and cardiovascular disease **(Avin et al. 2014)**.

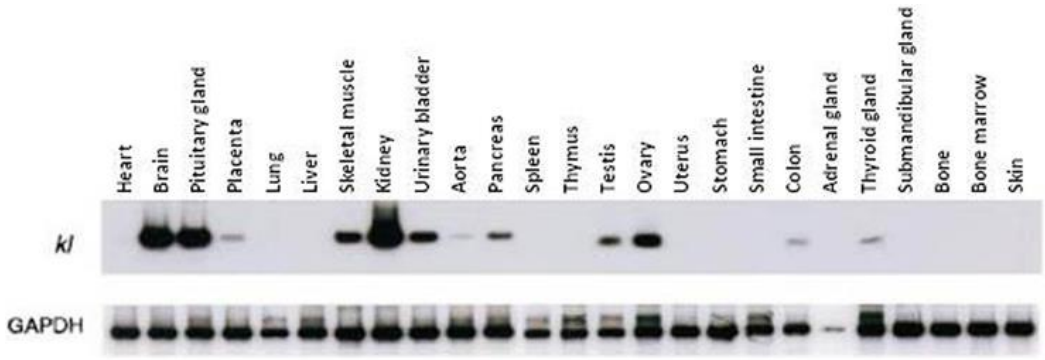

Figure 10: Klotho gene expression in multiple tissues
Kuro-o and colleagues quantified klotho gene expression of multiple tissues using RT–PCR. The kidney, brain and pituitary gland demonstrate the greatest expression, whereas skeletal muscle, ovaries and testes express klotho to a relatively lesser extent (Avin et al. 2014; Kuro-o et al. 1997).

Klotho-hypomorphic mice (*kl/kl* mice) suffer from severe growth deficits, rapid aging, hyperphosphatemia, hyperaldosteronism and extensive vascular and soft tissue calcification **(Voelkl et al. 2013)**. The mechanism by which the number of EPCs is decreased in *kl/kl* mice remains to be determined. A recent study indicated that the klotho protein regulates the bone marrow microenvironment, including macrophages, fibroblasts, endothelial cells and extracellular matrixes, and the 3-dimensional structure composed of these cells is an important environment for hematopoiesis and EPC differentiation **(Shimada et al. 2004; Okada et al. 2000)**.

Chronic kidney disease (CKD) leads as well to increased levels of parathyroid hormone (PTH) and FGF23 as decreased levels of circulating $1,25(OH)_2$ vitamin D. Kitagawa et al. showed that the serum KL level significantly correlated with the $1,25(OH)_2$ vitamin D level and inversely correlated with the PTH level **(Kitagawa et al. 2013)**. Soluble KL may thus represent a new biomarker for the diagnosis of CKD, especially in the early stage **(Shimamura et al. 2012).**

Devaraj et al. reported significant decreases of KL levels with diabetes and increases in CKD. The reference range of 4.7 to 437.6 ng/mL for the klotho assay was derived from samples from 57 healthy control subjects with an age range of 27 to 49 years using the klotho ELISA kit from CUSABIO Biotech, Newark, USA **(Devaraj et al. 2012).**

Immediately after exercise, Avin et al. observed a significant increase in circulating klotho levels in both young and aged mice, although the response was blunted in aged animals when compared to young counterparts **(Avin et al. 2014)**.

Pedersen et al. determined serum KL concentrations in 120 healthy adults aged 19 – 66 years using two different immunoassays (time-resolved fluorescence immunoassay (TRF) compared to the klotho ELISA from IBL). The median serum klotho concentration using TRF was 61 ng/mL (2.5 – 97.5 % reference limits; 11 – 181 ng/mL) for males and 99 ng/mL (2.5 – 97.5 % reference limits; 19 – 316 ng/mL) for females while the ELISA gave a mean value of 472 pg/mL (2.5 – 97.5 % reference limits; 204 – 741 pg/mL) with no difference between genders. No correlation was found between the assays suggesting that the protein exists in human beings in different forms which may function as independent factors and whose role and potential value as biomarkers need to be evaluated separately **(L. Pedersen et al. 2013)**.

Yamazaki et al. developed an ELISA to measure serum KL in healthy volunteers (n = 142, 66 males) of different ages (61.1 ± 18.5 year). Serum levels of KL ranged from 239 to 1266 pg/mL (mean ± SD; 562 ± 146 pg/mL) in normal adults. However, KL levels in normal children (n = 39, 23 males, mean ± SD; 7.1 ± 4.8 years) were significantly higher (mean ± SD; 952 ± 282 pg/mL) than those in adults (mean ± D; 562 ± 146, P<0.001) **(Yamazaki et al. 2010)**.

Heijboer et al. studied within-run variation, between-run variation, matrix effects, linearity, and recovery of added recombinant human KL in the α-klotho assays of IBL (IBL International GmbH, Hamburg, Germany), Cusabio (Cusabio Biotech, Wuhan, China) and USCN (USCN Life Science, Inc., Wuhan, China) using both serum and EDTA plasma. The commercially available methods for the measurement of α-klotho differ in quality. The authors suggested that some of the manufacturers should improve their assays in order to produce accurate results so that reliable conclusions can be drawn from studies in which these assays are used **(Heijboer et al. 2013)**.

The performance characteristics of the assays, as reported by the manufacturers, vary in precision (intraassay CV between 3 % and 10 %), measurement ranges, detection limits, and even sample types (cell culture media, serum, plasma, urine, tissue homogenates, and other biological fluids; Table 1). Importantly, the assays are designed for research use only and do not appear ready for clinical use because they are not harmonized **(Donate-Correa et al. 2014)**.

Table 1: Characteristics of ELISA assays for soluble klotho determinations
BF, biological fluids; CCM, cell culture media; NR, not reported; P, plasma; S, serum; SAL, saliva; TH, tissue homogenates; U, urine. Table modified according to Donate-Correa et al. (2014).

Manufacturer of the ELISA	Units	Sample	Range	Sensitivity	Intraassay CV, %	Interassay CV, %	Interferences
Cusabio	ng/ml	S, P TH	0.156-10	0.39	<8	<10	Hemolysis
IBL International	pg/ml	S, P, U	93.7-6000	6.15	2.7-3.5	2.9-11.4	NR
EIAab	pg/ml	S, P, U, CCM, BF, TH	7.8-500	2.4	NR	NR	NR
My Biosource	ng/ml	S, P, CCM, BF, TH	0.5-10	0.1	<10	<10	Hemolysis, lipemia
My Biosource	ng/ml	S, P, U, TH, SAL	0.05-20	0.01	<10	<12	NR
USCN Life Science	ng/ml	P, S, BF	0.156-10	0.058	<10	<12	Hemolysis

1.8 Aim of the study

Understanding how blood vessels form has become a principal, yet challenging, objective of the last decade. Unraveling these mechanisms would offer therapeutic options to ameliorate or perhaps even cure disorders that are now leading causes of mortality. Vascularization is also a key challenge in tissue engineering. Poor angiogenesis within tissue-engineered grafts has been identified as a main challenge limiting the clinical introduction of bone tissue-engineering approaches for the repair of large bone defects.

The aims of this study are:

- To establish a protocol to isolate endothelial progenitor cells (EPCs) from buffy coat. Unlike peripheral blood, buffy coat is a commercially available source which allows establishing of a standardized method for the isolation of a sufficient number of EPCs needed for the global gene expression studies. Besides the isolation and cultivation, the characterization of these cells is one of the tasks.
- To design an experimental setup to study the changes of the global gene expression pattern of both EPCs and mesenchymal stem cells (MSCs) after direct cell-cell contact as well as after treatment with conditioned medium. Thus, one major goal is to establish necessary molecular and cell biological tools. This included methods to stain the cells, to separate the cells after co-culture as well as to isolate RNA for the microarray analysis.
- To perform microarray analysis to assess the global gene expression pattern of both EPCs and mesenchymal stem cells (MSCs) after direct cell-cell contact as well as after treatment with conditioned medium. Subsequently, this study aimed to analyze the microarray data using bioinformatics and to search the lists of differentially expressed genes for candidates affiliated with angiogenesis and osteogenesis and therefore to achieve a better understanding of the cross-talk of these cells as well as to evaluate the potential benefits of using these cells in tissue engineered constructs.
- To re-evaluate the microarray findings by RT-PCR with selected genes.
- To develop an ELISA for one of the differentially expressed genes. With respect to the experience of Immundiagnostik AG in the development of ELISAs for over 25 years, this study would like to take benefit from an existing cooperation between Immundiagnostik AG and the University of Würzburg to combine basic research and product development. Our study is going to take the outcome of the basic research findings one step further and will develop a new product which will then become a useful tool to the own research group as well as to other researchers. The gene of choice for the development of an ELISA was klotho.

With this thesis, we intend to counter the lack of knowledge about the communication of EPCs and MSCs by a variety of molecular and cell biological methods. The project will thereby contribute to a better understanding of the angiogenic and osteogenic potential of these cells and could provide new options especially in the field of tissue engineering. A better understanding of the cross-talk of EPCs and MSCs might help to overcome the obstacles of large bone defects by actively supporting blood vessel development. The klotho ELISA will be a highly beneficial tool for more detailed basic research studies in the field of bone metabolism and aging.

2 MATERIAL AND METHODS

2.1 Materials

2.1.1 Consumables

Table 2: Consumables

Product	Catalogue number	Purchased from
6-well plates	657160	Greiner
96-well microtiter plates, Lockwell C8 Maxisorp	446469	Thermo Scientific
Cell culture flask, 150 cm² (with filter)	90151	Biochrom
Cell culture flask, 175 cm² (with filter)	660175	Greiner
Cell culture flask, 75 cm² (with filter)	678175	Greiner
Cell culture flask, 75 cm² (with filter)	90076	Biochrom
Cell scratcher	99002	TPP
Cell strainer, sterile, 100µm	ZS10	Hartenstein
Centrifugation tubes, sterile, 15 ml	188271	Greiner
Centrifugation tubes, sterile, 50 ml	227261	Greiner
Disposable cuvettes PS, semi-micro/1.6 ml	KEHM	Hartenstein
Disposable pipettes, sterile, 10 ml	607180	Greiner
Disposable pipettes, sterile, 25 ml	760180	Greiner
Disposable pipettes, sterile, 5 ml	606180	Greiner
Disposable scalpel	5518040	Aesculap (Braun)
Disposable syringe, 10 ml	309110	Becton Dickinson
HiTrap™ Protein G column, 1 ml	17-0404-01	GE-Healthcare
NucleoSEQ® columns	740523.250	Machery & Nagel
PCR reaction tubes with lid	82-1182A	Peqlab
Reaction tubes, 1.5 ml	616201	Greiner
Sterile filter, 0.22 µm	FI02	Hartenstein
Weighing dish	WAE1	Hartenstein

2.1.2 Chemicals

Table 3: Chemicals

Product	Catalogue number	Purchased from
100bp DNA ladder plus	25-2020	Peqlab
2-Mercaptoethanol, 99% p.a.	4227.1	Roth
Accutase	L11-007	PAA
Agarose LE	84004	Biozym
BioScript™ reverse transcriptase	BIO-27036	Bioline
Bradford reagent (Roti®-Quant)	K015.1	Roth
Cell Tracker® Green	PA-3011	Lonza
Cell Tracker® Orange	PA-3012	Lonza
Chloroform, ≥99% p.a.	3313.1	Roth
Dil acetylated low-density lipoprotein (acLDL)	L3484	Invitrogen Molecular Probes
dNTP Set 4x100 µl	BIO-39026	Bioline
Ethanol, 96%, denatured	T171.2	Roth
Ethidium bromide	A1152.0025	Applichem
FBS (fetal bovine serum)	S0115	Biochrom
Ficoll-Paque™ PLUS	17-1440-03	GE-Healthcare
Glycin	CG55	Hartenstein
Isopropanol, p.a.	CP50	Hartenstein
L-Ascorbic acid 2-phosphate sesquimagnesium salt hydrate	A8960	Sigma
MangoTaq™ DNA Polymerase 1000 Units	BIO-21083	Bioline
MangoTaq™ reaction buffer	BIO-21083	Bioline
PBS Dulbecco w/o Ca2+, w/o Mg2+	L182-50	Biochrom
Penicillin / Streptomycin (100x)	P11-010	PAA

Random Hexamer Primers	SO142	Life Technologies GmbH
Sodium acetate	891.1	Roth
Sodium chloride p.a. (NaCl)	A3597	AppliChem
Tris, ultrapure	CT65	Hartenstein
TRIzol® Reagent	15596-018	Invitrogen
Trypanblue solution (0.4%)	T8154	Sigma
Trypsin (10x concentrate)	L11-001	PAA
Trypsin-EDTA (1x)	L11-004	PAA
Ulex Lectin, FITC-conjugate	9006	Sigma Aldrich
VECTASHIELD® Mounting Medium with DAPI	H-1200	Vector Laboratories
Water, HPLC-grade	A511.1	Roth

2.1.3 Kits

Table 4: Kits

Product name	Catalogue number	Purchased from
BigDye® Terminator v3.1 cycle sequencing kit	4337455	Life Technologies GmbH
HisPur™ Cobalt Purification Kit, 3 ml	90092	Thermo Scientific
NucleoSpin® RNA II Kit	740955.250	Macherey-Nagel

2.1.4 Equipment

Table 5: Equipment

Equipment	Catalogue number	Purchased from
Fluorescence filter set no. 09	488009-9901-000	Zeiss
Fluorescence filter set no. 20	488020-9901-000	Zeiss
CO_2 incubator	40042145	Heraeus
ELISA reader, Tecan Spectra Mini AP	F039102	Tecan
Incubator	51015265	Heraeus
Microscope (Axiovert 25)	451210	Zeiss
Peristaltic pump	18-1110-91	GE-Healthcare
Pipettes	P1000, P200, P20	Gilson
Bio Photometer 6131	RS 232 C	Eppendorf
Heater	Type BBA2	Grant Boeckel
Laminar flow hood (HS 15)	51012198	Heraeus
Thermal cycler (peqstar 2x)	95-07002	Peqlab
Water bath	WB 7	Hartenstein
Neubauer cell counting chamber	ZK03	Hartenstein
Centrifuge (Labofuge 400R)	75008162	Heraeus

2.1.5 Antibodies – part I – commercially available

Table 6: Antibodies – part I

Antibody	Catalogue number	Purchased from
goat-anti-klotho (T-19)	SC22218	Santa Cruz
rabbit-anti-klotho (P296)	500-P296	Peprotech
CD34-PE, mouse-IgG	130-081-002	Miltenyi Biotec
CD31-PE (also known as PECAM-1) , mouse-IgG	130-092-653	Miltenyi Biotec
CD45-FITC, mouse-IgG	130-045-801	Miltenyi Biotec
CD133/2-APC, mouse-IgG	130-090-854	Miltenyi Biotec
CD309-PE (also known as VEGFR-2, KDR, flk-1) , mouse-IgG	130-093-598	Miltenyi Biotec
CD144-PE (also known as VE-Cadherin) , mouse-IgG	12-1449-82	eBioscience
mouse IgG1-PE	A07796	Beckman Coulter
mouse IgG2a-FITC	AB81197	Abcam
mouse IgG2b-APC	130-092-217	Miltenyi Biotec

2.1.6 Antibodies – part II – custom made

Table 7: Antibodies – part II

Binder (scFv) / antibody	Antigen	Available at
AF376-D2 scFv	Klotho, recombinant, isoform 2	Immundiagnostik AG, Bensheim, Germany
AF376-D2-rbIgG-Fc	Klotho, recombinant, isoform 2	Immundiagnostik AG, Bensheim, Germany
AF376-E1 scFv	Klotho, recombinant, isoform 2	Immundiagnostik AG, Bensheim, Germany
AF376-E10 scFv	Klotho, recombinant, isoform 2	Immundiagnostik AG, Bensheim, Germany
AF376-E10-rbIgG1-Fc	Klotho, recombinant, isoform 2	Immundiagnostik AG, Bensheim, Germany
AF376-F1 scFv	Klotho, recombinant, isoform 2	Immundiagnostik AG, Bensheim, Germany
AF376-F1-rbIgG1-Fc	Klotho, recombinant, isoform 2	Immundiagnostik AG, Bensheim, Germany
AF376-H9 scFv	Klotho, recombinant, isoform 2	Immundiagnostik AG, Bensheim, Germany

2.1.7 Primer

Table 8: Primer

List of sequences of primers used for reverse transcriptase PCR (RT-PCR) analyses. The table provides information about the primer sequence, annealing temperature (T_A), PCR product size in base pairs (bp) and the sequence ID of the corresponding gene product. Primers were purchased from Eurofins GmbH, Germany.

Gene symbol and name Primer sequences		T_A	Length of PCR product	Sequence ID
EF1-a	**eucaryotic translation elongation factor 1-alpha**			
forward:	5'-CTGTATTGGATTGCCACACG-3'	54 °C	369 bp	NM_001402
reverse:	5'-AGACCGTTCTTCCACCACTG-3'			
IDO1	**indoleamine 2,3-dioxygenase 1**			
forward:	5'- GCGCTGTTGGAAATAGCTTC -3'	55 °C	234 bp	NM_002164.5
reverse:	5'- CAGGACGTCAAAGCACTGAA -3'			
BIRC3	**baculoviral IAP repeat containing 3**			
forward:	5'- GGGAAGAGGAGAGAGAAAGAG -3'	54 °C	243 bp	NM_001165.4
reverse:	5'- CAGTGGCTGCAATATTTCCTT -3'			NM_182962.2
CTGF	**connective tissue growth factor**			
forward:	5'- CCTGGTCCAGACCACAGAGT -3'	54 °C	238 bp	NM_001901.2
reverse:	5'- ATGTCTTCATGCTGGTGCAG -3'			
CXCR4	**chemokine (C-X-C motif) receptor 4**			
forward:	5'- GCACTCACCTCTGTGAGCAG -3'	55 °C	234 bp	NM_001008540.1
reverse:	5'- CAAGACAAAAATCCAACAGC -3'			NM_003467.2
CYR61 ***(CCN1-2)***	**cystein-rich protein 61**			
forward:	5'- CACCCTTCTCCACTTGACC -3'	56 °C	152 bp	NM_001554.4
reverse:	5'- AGTCCTCGTTGAGCTGGCTTG -3'			
CYR61 ***(CCN2-3)***	**cystein-rich protein 61**			
forward:	5'- ACCGCTCTGAAGGGGATCT -3'	56 °C	153 bp	NM_001554.4
reverse:	5'- GGGACACAGAGGAATGCAG -3'			
CYR61 ***(CCN3-4)***	**cystein-rich protein 61**			
forward:	5'- GGTGTGAATATAAACAGACCC -3'	50 °C	481 bp	NM_001554.4
reverse:	5'- CAGGGTTGTCATTGGTAACT -3'			
CYR61 ***(CCN4-5)***	**cystein-rich protein 61**			
forward:	5'- CAACCCTTTACAAGGCCA -3'	54 °C	206 bp	NM_001554.4
reverse:	5'- TGGTCTTGCTGCATTTCTTG -3'			
FST	**follistatin**			
forward:	5'- GTGGGAATGATGGAGTCACC -3'	55 °C	218 bp	NM_006350.3
reverse:	5'- CGACTTACTGTCAGGGCACA -3'			NM_013409.2
FSTL1	**follistatin-like 1**			
forward:	5'- CCATCTTTCAACCCTCCTGA -3'	56 °C	176 bp	NM_007085.4
reverse:	5'- TCCTCCTCTGTCTGGGTCTG -3'			
HLA-DQA1	**major histocompatibility complex, class II, DQ alpha 1**			
forward:	5'- CAGCAAATTTGGAGGTTTTG -3'	59 °C	150 bp	NM_002122.3
reverse:	5'- GTCACGGGAGACTTGGAAAAC -3'			
IL1b	**interleukin 1b**			
forward:	5'- GAAGTACCTGAGCTCGCCATGGAA -3'	54 °C	440 bp	NM_000576.2
reverse:	5'- CGTGCAGTTCAGTGATCGTACAGG -3'			

IL6	**interleukin 6**			
forward:	5'- AAAGCAGCAAAGAAGCACTG -3'	52 °C	194 bp	NM_000600.3
reverse:	5'- GCACAGCTCTGGCTTGTC -3'			
IL8	**interleukin 8**			
forward:	5'- AAGGAAAACTGGGTGCAGAG -3'	52 °C	163 bp	NM_000584.3
reverse:	5'- CCCTACAACAGACCCACACA -3'			
KL (iso1)	**klotho (isoform 1)**			
forward:	5'- CAGCCCCTAGAAGGGACATT -3'	61 °C	301 bp	NM_004795.3
reverse:	5'- GGTTCACCTGGGACTGGTTA -3'			
KL (iso2)	**klotho (isoform 2)**			
forward:	5'- CGAGTGGCACAGAGGTTACA -3'	55 °C	252 bp	NM_004795.3
reverse:	5'- TAGGGCTTGGTGAGACTGCT -3'			
POSTN	**periostin**			
forward:	5'- GAATCATCCATGGGAACCAG -3'	52 °C	177 bp	NM_001135934.1
reverse:	5'- AGTGACCGTCTCTTCCAAGG -3'			
SOCS3	**suppressor of cytokine signaling 3**			
forward:	5'- GCTCCTTTGTGGACTTCACG -3'	52 °C	243 bp	NM_003955.3
reverse:	5'- GGAAACTTGCTGTGGGTGAC -3'			
SOD2	**superoxide dismutase 2**			
forward:	5'- TGCATCTGTTGGTGTCCAAG -3'	55 °C	159 bp	NM_000636.2; NM_001024465.1
reverse:	5'- TAGTAAGCGTGCTCCCACAC -3'			NM_001024466.1
THBS1	**thrombospondin 1**			
forward:	5'- GCAGGACTGTCCAATTGATG -3'	57 °C	167 bp	NM_003246.2
reverse:	5'- AGGCATCAGGCACTTCTTTG -3'			
TNFSF10	**tumor necrosis factor (ligand) superfamily, member 10**			
forward:	5'- TGAGAACCTCTGAGGAAACCA -3'	55 °C	230 bp	NM_001190942.1; NM_003810.3
reverse:	5'- CAAGTGCAAGTTGCTCAGGA -3'			NM_001190943.1
VCAN	**versican**			
forward:	5'- GTTGGGGCAGTCATAGCAAC -3'	55 °C	237 bp	NM_004385.4; NM_001164097.1
reverse:	5'- TGGAACACATCACCATCCAG -3'			NM_001164098.1; NM_001126336.2
VEGFA	**vascular endothelial growth factor A**			
forward:	5'- TCTTCAAGCCATCCTGTGTG -3'	59 °C	164 bp	NM_001025366.2
reverse:	5'- TGTTGTGCTGTAGGAAGCTCA -3'			
Wnt5a	**wingless-type MMTV integration site family, member 5A**			
forward:	5'- GAAGCCAATTCTTGGTGGTC -3'	60 °C	190 bp	NM_001256105.1
reverse:	5'- GGCATTCTTTGATGCCTGTC -3'			NM_003392.4

2.1.8 Buffers and other solutions

- 0.9% NaCl solution
  9 g sodium chloride
  990 ml distilled water
  autoclave
  store at room temperature

- 0.9% NaCl / 1% FBS
  9 g sodium chloride
  990 ml distilled water
  autoclave
  add 10 ml FBS under sterile conditions
  store at 4°C

- Phosphate buffered saline (PBS)
  9.55 g PBS Dulbecco (w/o Ca^{2+}, w/o Mg^{2+})
  ~800 ml distilled water
  adjust pH to 7.4
  ad 1000 ml distilled water and autoclave
  store at room temperature

- 0.1 M Glycine solution, pH 2.2
  3.75 g glycine
  ~450 ml distilled water
  adjust pH to 2.2
  ad 500 ml distilled water
  store at 4°C

- 3 M Tris buffer, pH 8
  18.2 g tris(hydroxymethyl)aminomethane
  25 ml distilled water
  adjust pH to 8
  ad 50 ml distilled water
  store at 4°C

- 50 mg/ml L-Ascorbic acid 2-phosphate solution
  1.25 g L-ascorbic acid 2-phosphate sesquimagnesium salt
  25 ml autoclaved water, HPLC grade
  filter sterile (0.22 µm)
  store in aliquots at -20°C

- CD-buffer for the characterization of EPCs according to the protocol of the manufacturer (Miltenyi Biotec)
  PBS
  0.5 % BSA
  2 mM EDTA
  store at 4°C

- ELISA coating buffer, blocking buffer, antibody dilution buffer, standard dilution buffer, sample dilution buffer and wash buffer
  Buffers made available by Immundiagnostik AG, Bensheim, Germany

2.1.9 Cell culture medium

- Propagation medium for EPCs

500 ml	EBM®-2 medium purchased from Lonza (cat# CC-3156)
25 ml	FBS
5 ml	100x penicillin/streptomycin
0.5 ml	50 mg/ml L-ascorbic acid 2-phosphate solution

- Propagation medium for MSCs

500 ml	DMEM/ Ham's F-12 medium purchased from PAA (cat# E15-813)
50 ml	FBS
5 ml	100x penicillin/streptomycin
0.5 ml	50 mg/ml L-ascorbic acid 2-phosphate solution

- Medium for SF21 cells
  - Culture/propagation medium:
    BacPAK™ Complete medium purchased from Takara Clontech (cat# 631403)
  - Expression medium:
    Insect Express Sf9-S2 medium purchased from PAA (cat# E15-875)

2.2 Methods

2.2.1 Expression and purification of recombinant proteins

2.2.1.1 Expression and purification of recombinant CYR61

The recombinant CYR61 protein was expressed as an IgG-Fc-tagged protein (rCYR61) from baculovirus-infected SF21 insect cells according to **Schütze et al. (2005)**.
The rCYR61 was purified from the cell culture supernatant using a protein G sepharose column (HiTrap™ 1 ml protein G HP column). The column was attached to a peristaltic pump and equilibrated for 15 min with PBS. The flow rate was at 1 ml/min during the whole purification process. All solutions added to the column were sterile filtered to avoid blockage of the column.
Meanwhile, the cell culture supernatant from the SF21 cells was collected and centrifuged at 4000 *g* for 10 min. The supernatant was decanted, sterile filtered and added to the column (Figure 11). To avoid overloading of the column, the maximum volume of supernatant applied was 75 ml. The column was washed with PBS for 15 min before rCYR61 was eluted by adding 5 ml of 0.1 M glycine solution. The eluate was collected as aliquots of 1 ml in 1.5 ml reaction tubes containing 40 µl of 3 M Tris buffer at pH 8. The column was washed with PBS for 15 min. In case of a cell culture supernatant volume greater than 75 ml, the procedure described above was repeated. At the end, the column was washed with 20 % ethanol (= storage buffer) for 10 min. The column was stored at 4 °C. The concentrations of the rCYR61 fractions were determined with a Bradford assay (Chapter 2.2.2). The rCYR61 was either directly used for coating 6-well plates (Chapter 2.2.3) or stored at -20 °C.

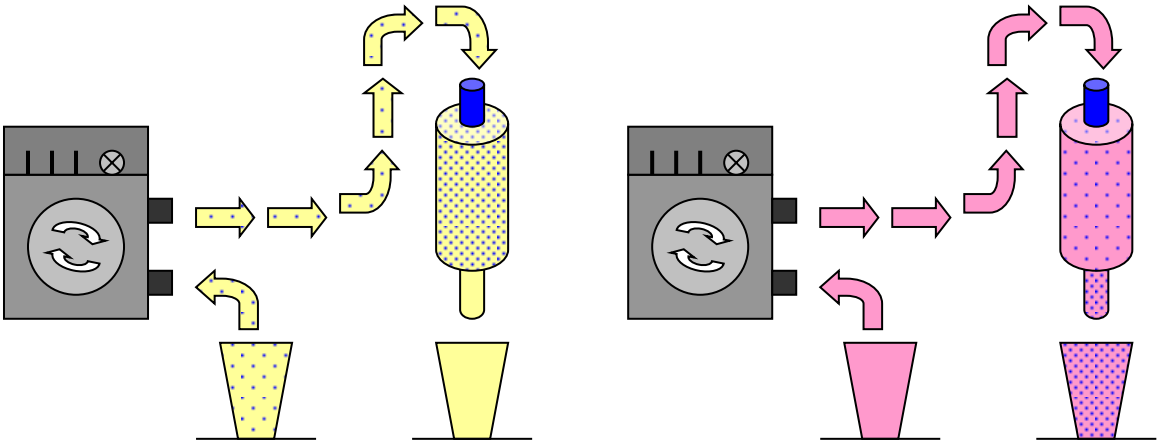

Figure 11: Purification of rCYR61 from cell culture supernatant
(a) Use of a peristaltic pump (gray) to pump cell culture supernatant containing rCYR61 (yellow with blue dots) over a HiTrap™ protein G column. Only the rCYR61 binds to the protein G sepharose of the column. (b) Add elution buffer (pink). Collect rCYR61 (blue dots) in 1.5 ml reaction tubes.

2.2.1.2 Expression and purification of recombinant klotho

The recombinant human klotho protein (isoform 2: secreted) was expressed as a HIS-tagged protein (rKL) from virus-infected HEK293 cells. The HEK cell line (1 vial of HEK pExolN2-klotho: p14) was made available by Dr. Birgit Mentrup of the Orthopedic Centre of Musculoskeletal Research of the University of Würzburg.
The rKL was purified from the cell culture supernatant using the HisPur cobalt purification kit from Thermo Scientific according to the instructions of the manufacturer. Preliminary tests showed that rKL was expressed, but at low levels. The production of the protein using this method was very time consuming, expensive and not suitable to produce the amounts of protein needed for the generation of antibodies and the development of an ELISA. Therefore, the expression and purification of the rKL was outsourced to InVivo BioTech Services GmbH. InVivo is a leading contract manufacturing organization (CMO) dedicated to the development and production of monoclonal antibodies and expression of recombinant proteins. Based in Hennigsdorf, Germany, just outside Berlin, InVivo is an DIN ISO 9001 certified company with over ten years of experience in mammalian cell culture and protein production. As a trusted provider of cost-effective outsourcing solutions and as a long-standing business partner of Immundiagnostik AG, InVivo was chosen for the up-scaled production (10 L bioreactor) of the rKL.

2.2.2 Determination of protein concentration

Concentrations of the rCYR61 fractions were determined after each purification and prior to each application by the Micro-Bradford method by using the Roti®-Quant assay. This assay relies on binding of the dye Coomassie Brilliant Blue G250 to proteins, based on the method originally described by **Bradford (1976)**. The binding of the dye to protein causes a shift in the absorption maximum of the dye from 465 to 595 nm, and it is the increase in absorption at 595 nm which is monitored (Figure 12). Therefore, 10 µl of sample, standard (25-250 µg/ml BSA in Tris/Glycin buffer) or buffer (blank), respectively, were added to disposable semi-micro cuvettes and mixed with 500 µl diluted Roti®-Quant solution. Absorption was determined using an Eppendorf biophotometer which calculates absolute protein concentrations according to the obtained calibration curve.

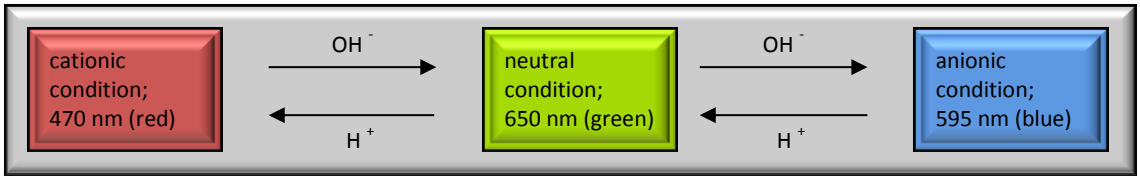

Figure 12: The three absorbing conditions of the dye Coomassie Blue G250
The shift of the dye from its cationic condition to its anionic condition when binding to proteins and therefore the shift of its absorption maximum from 470 to 595 nm allows a quantitative measurement of the protein concentration.

2.2.3 Coating 6-well plates with rCYR61

Recombinant CYR61-coated 6-well plates were used to seed buffy coat-derived endothelial progenitor cells (EPCs). The positive effect of rCYR61-coated plates for the *ex vivo* expansion of EPCs and the optimal coating concentration were shown by Rita Schenk in her PhD thesis **(Schenk 2007)**.
The 6-well plates were coated with 5 µg/1.5 ml PBS/well for 3 h at room temperature. The coating solution was aspirated and the cells were seeded directly into the plates (Chapter 2.2.5.1). Excess plates were stored at -20 °C for up to 2 months without a loss of quality.

2.2.4 Cell counting

A counting chamber, also known as hemocytometer, is a microscope slide that is especially designed to enable cell counting (Figure 13). The cell suspension was diluted with an equal volume of a 0.4 % trypan blue solution (dilution factor A = 2). Trypan blue is a vital stain used to selectively color dead cells. Cell suspensions with a high cell number were diluted with medium prior to dilution with trypan blue (e.g. 10 µl of cell suspension + 450 µl of medium; dilution factor B = 50). A cover slip was placed on the counting chamber and 10 µl of diluted and colored cell suspension was applied to the chamber. The cell number was determined under the microscope by counting the cells in each of the four large corner squares of the gridded area (mean value = MV).

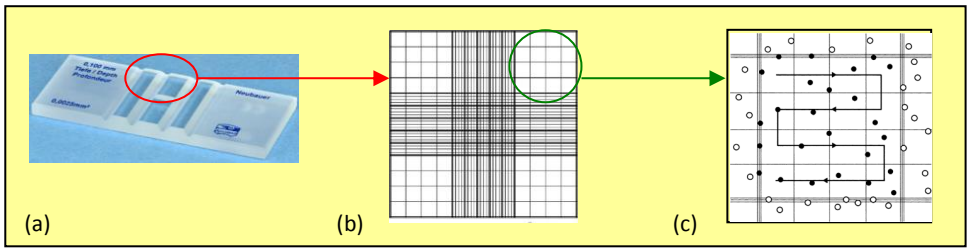

Figure 13: Counting cells with a Neubauer counting chamber
(a) Neubauer counting chamber with 2 counting chambers. (b) Gridded area of the chamber with the four large corner squares. (c) Large corner square. Counting the cells in each of the 16 small squares by starting in the upper right corner. (sources: (a) www.neolab.de; (b) www.praxisdienst-vet.de; (c) Schmitz 2011; date: 2014-06-28)

The cell number per milliliter was calculated as followed:

$$\textit{Cell number/ml} = \textit{MV} \times \textit{f} \times \textit{A} \times \textit{B}$$

(MV = mean value; A = dilution factor A; B = dilution factor B; f = chamber factor [= 10^4])

2.2.5 Isolation of cells

2.2.5.1 Isolation of buffy coat-derived EPCs

A protocol for the isolation and cultivation of human endothelial progenitor cells (EPCs) from fresh peripheral blood was already established in the lab **(Hofmann 2010)**. However, fresh peripheral blood is a limited source as well as limited in its volume. Therefore, part of this work was to adapt the existing protocol to buffy coat and to establish a standardized method to isolate EPCs from a commercially available source.
The buffy coat is the fraction of an anticoagulated blood sample that contains most of the white blood cells and platelets following density gradient centrifugation of the blood (about 1 % of the total blood volume). The buffy coat was produced by and purchased from the Blood Donation Service of the Bavarian Red Cross (Blutspendedienst des bayerischen Roten Kreuzes). They gain the buffy coat from a blood sample by filtration and centrifugation in a sterile multi-chamber bag system. One bag contains 30 ml ± 5 ml of buffy coat. The buffy coat was transferred to the lab and used for the isolation of EPCs within 18 – 24 h after donation. For the reason of privacy, only the age and the gender of the donors were known. The use of the buffy coat was approved by the Local Ethics Committee of the University of Würzburg.
The content of one bag of buffy coat was decanted into a sterile 175 cm² cell culture flask and diluted 1:4 with 0.9 % NaCl/1 % FBS solution. 15 ml of Ficoll-Paque™ density gradient solution were placed at the bottom of four 50 ml centrifugation tubes each. Then 30 ml of diluted buffy coat were slowly layered above the Ficoll solution of each tube. The tubes were centrifuged at 1000 *g* for 25 min without using the brake (Figure 14). The mono-nuclear cell layer was carefully pipetted into a fresh 50 ml tube including some of the plasma and some of the Ficoll solution but strictly without any of the erythrocytes/granulocytes.

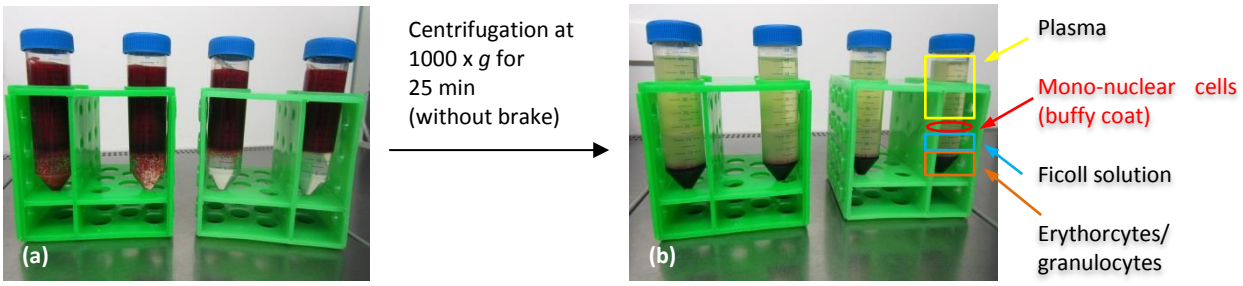

Figure 14: Ficoll-Paque density gradient centrifugation
(a) Ficoll solution overlaid with diluted buffy coat. (b) After being centrifuged, the following layers were visible in the tube, from top to bottom: plasma and other constituents, a layer of mono-nuclear cells called buffy coat, Ficoll solution, and erythrocytes & granulocytes.

The mono-nuclear cells were centrifuged at 300 *g* for 10 min. The supernatant was discarded and the cell pellet was washed with 30 ml of 0.9 % NaCl/1 % FBS solution. The cell suspension again was centrifuged and the washing procedure was repeated once. The cell pellet was resuspended in 30 ml of EPC medium and filtered through a 100 µm cell strainer. Cell number and vitality were determined by diluting the cell suspension 1:50 with medium and mixing the diluted cell suspension 1:2 with trypan blue and counting in a Neubauer counting chamber (Chapter 2.2.4).
The cells were seeded at a density of 2×10^7 cells/well into rCYR61 coated 6-well plates in a total volume of 5 ml EPC medium and incubated at 37 °C in a humidified atmosphere with 5 % CO_2.

2.2.5.2 Isolation of bone marrow-derived MSCs

Isolation of human mesenchymal stem cells (MSCs) was performed under the approval of the Local Ethics Committee of the University of Würzburg as well as with the informed consent of each patient. The MSCs were isolated by staff members of the group of Prof. Jakob/Prof. Schütze at the Orthopedic Centre of Musculoskeletal Research of the University of Würzburg according to a standardized protocol **(Nöth et al. 2002; Schütze et al. 2005).** In brief, the femoral heads of patients were removed during total hip joint replacement surgery. The cancellous bone was collected and washed once with MSC medium (propagation medium) by centrifugation at 1200 *g* for 5 min. Any fatty components were removed by discarding the supernatant. Subsequent washing of the remaining pellet released the stromal cells. After each vortexing step, the propagation medium enriched with stromal cells was filtered through a cell strainer to hold back bone fragments and collected in a fresh tube. After final centrifugation at 1200 *g* for 5 min, the cell pellet was resuspended in a known volume of propagation medium. Cell number and vitality were determined by mixing 50 µl cell suspension with 50 µl trypan blue and counting in a Neubauer counting chamber (Chapter 2.2.4). The stromal cells were seeded at a density of more than 10^6 cells/cm² into 175 cm² cell culture flasks and incubated at 37 °C in a humidified atmosphere with 5 % CO_2. About 3 days after isolation, the supernatant containing non-adherent blood cells was removed, the MSCs selected by plastic adherence were washed with PBS and further incubated in fresh propagation medium. The MSCs were provided in 175 cm² cell culture flask at 60 – 80 % confluence.

2.2.6 Culture and propagation of primary cells and cell lines

2.2.6.1 Culture of EPCs

Propagation medium was replaced on day 2 and day 6 after isolation. Prior to the change of medium, the cells were washed 2x or 1x with 0.9 % NaCl/1 % FBS at day 2 or day 6, respectively. Subsequently, EPCs of passage 0 were detached earliest on day 7 and latest on day 9 by exposure to 1 ml/well accutase and further incubation for 30 min at 37 °C and the use of a cell scratcher. The cells were pelleted by centrifugation (1200 *g* for 5 min), resuspended in fresh propagation medium, and the cell number was assessed. The cells were seed at a density of 1x 10^6/well into none-coated 6-well plates in a total volume of 5 ml of medium and incubated at 37 °C in a humidified atmosphere with 5 % CO_2. Propagation medium was replaced every 3 – 4 days.
Experiments were performed with EPCs of passage 1.

2.2.6.2 Culture of MSCs

The MSCs were provided in fresh propagation medium at 60 – 80 % confluence and passaged within 3 days without any further change of medium. Cells were detached by exposure to 1x Trypsin-EDTA and further incubation for 5 min at 37 °C. Addition of propagation medium inactivated the trypsin. The cells were pelleted by centrifugation (1200 *g* for 5 min), resuspended in fresh propagation medium, and the cell number was assessed. Cells were seeded at a density of 2x 10^5 – 1.2x 10^6 cells/75 cm² into cell culture flasks at a total volume of 15 ml of medium and incubated at 37 °C in a humidified atmosphere with 5 % CO_2. Propagation medium was replaced every 3 – 4 days.
Experiments were performed with MSCs of passage 1.

2.2.6.3 Culture of SF21 cells

For propagation, cells were split every 7 days at a ratio of 1:10 into new 75 cm² cell culture flasks at a total volume of 16 ml culture medium and incubated at 27 °C. Cells were detached by using a cell scratcher.
For infection with baculovirus (chapter 2.2.1), cells were split 1:2. Subsequently, cells were detached by using a cell scratcher. The cells were pelleted by centrifugation (1200 *g* for 5 min), resuspended in expression medium and transferred into a 150 cm² cell culture flask. The cells were incubated in a total volume of 25 ml at 27 °C and infected with baculovirus 20 – 24 h later. The cell culture supernatant containing the rCYR61 was harvested after 1 week.

2.2.7 Characterization of EPCs

2.2.7.1 By flow cytometry

The characterization of the buffy coat-derived primary EPCs was performed using monoclonal mouse antibodies against the surface markers CD34, CD31 (also known as PECAM-1), CD45, CD133, CD144 (also known as VE-Cadherin) and CD309 (also known as VEGFR-2, KDR, flk-1). The antibodies were conjugated to the dyes PE, FITC or APC. The immunofluorescent staining of the cells was performed according to the instructions of the manufacturer Miltenyi Biotec.
The cells were stained at two different time points of *in vitro* cultivation: day 7, passage 0 and day 14, passage 1 (n = 3). The following isotype controls were used as controls: mouse IgG1-PE, mouse IgG2a-FITC, mouse IgG2b-APC.
In brief, 1x 10^5 cells were resuspended in 100 µl of CD-buffer in centrifugation tubes for each staining. 5 µl of respective antibody or isotype control antibody was added to the tubes, mixed well and incubated for 15 min in the dark on ice. Subsequently, the cells were centrifuged at 300 *g* for 10 min, the supernatant aspirated and the pellets resuspended in 100 µl of CD-buffer. The stained EPCs were analyzed by flow cytometry at the Institute for Virology and Immunology of the University of Würzburg in cooperation with Christian Linden using established protocols.

2.2.7.2 By fluorescence microscopy

Several markers for endothelial cells are routinely used for confirmation that established cell lines are of endothelial origin including the uptake of DiI acetylated low-density lipoprotein (DiI acLDL).
Voyta et al. demonstrated that labeling endothelial cells with DiI acLDL is an improved method for specifically visualizing endothelial cells **(Voyta et al. 1984)**. Some cells, including EPCs, utilize a specific metabolic pathway, the low-density lipoprotein (LDL) pathway, to supply themselves with cholesterol. Acetylated-low density lipoprotein (acLDL) is taken up by macrophages and endothelial cells via the "scavenger cell pathway" of LDL metabolism.
A second specific marker commonly used for the identification of endothelial cells is ulex europaeus I agglutinin (ulex lectin), a lectin specific for some alpha-L-fucose-containing glycocompounds **(Holthöfer et al. 1982)**. Lectins are carbohydrate-binding proteins, macromolecules that are highly specific for sugar moieties.
The EPCs were cultivated in a 12-well plate and stained on day 14 (passage 1) of the *in vitro* cultivation (n = 3). The cells were washed 3x with PBS. Before adding 0.5 ml/well of the DiI acLDL, the solution was diluted with propagation medium to a final concentration of 5 µg/ml. The EPCs were incubated for 1 h at 37 °C in a humidified atmosphere with 5 % CO_2. The cells were washed 3x with PBS and subsequently fixed with 4 % PFA (paraformaldehyde) for 15 min at room temperature. The cells were washed 3x with 0.9 % NaCl solution. Before adding 0.5 ml/well of the Ulex Lectin, the solution was diluted with 0.9 % NaCl solution to a final concentration of 50 µg/ml. The EPCs were incubated for 1 h at room temperature in the dark. The cells were washed 3x with 0.9 % NaCl solution and 1x with distilled water. To mount the cells, VECTASHIELD® Mounting Medium with DAPI was dispensed onto the fixed cells and cover slipped. The fluorescence staining was made visible using a fluorescence microscope (red = acLDL uptake; green = ulex lectin; blue = DAPI).

2.2.8 Experiments with conditioned medium

This experimental setting was designed to assess the influence of conditioned medium gained from MSCs on EPCs and vice versa (Figure 15). For each experiment (n = 4), two 75 cm² flasks with MSCs and two 6-well plates with EPCs were employed. Donors of the EPCs were male and aged 35 – 60 years, in average 49 ± 9 years (mean ± standard deviation). Donors of the MSCs were of both genders and aged 56 – 72 years, in average 67 ± 6 years (mean ± standard deviation).
Both types of cells were at passage 1 and 90 % confluence. The experiment started with a change of medium at day 0: 3 ml/10 cm² of EPC propagation medium or MSC propagation medium were applied to the EPCs or MSCs, respectively. After 24 h incubation at 37 °C in a humidified atmosphere with 5 % CO_2, the conditioned medium was collected and centrifuged at 4000 *g* for 5 min. Meanwhile, the cells were washed with 1x with PBS. The distribution of the conditioned medium is shown in Table 9. The conditioned medium was mixed with 50 % fresh medium. Both types of cells received equal amounts of medium (3 ml/10 cm²). The controls received fresh medium instead of conditioned medium.

Table 9: Distribution of conditioned and fresh medium
EPCs were in 6-well plates at 90 % confluence and passage 1.
MSCs were in 75 cm² cell culture flasks at 90 % confluence and passage 1.

Experimental set up	Conditioned medium gained from EPCs	Fresh EPC medium	Conditioned medium gained from MSCs	Fresh MSC medium
EPCs + conditioned medium	-	1.5 ml/well	1.5 ml/well	-
EPC control group	-	1.5 ml/well	-	1.5 ml/well
MSCs + conditioned medium	11.2 ml/flask	-	-	11.2 ml/flask
MSC control group	-	11.2 ml/flask	-	11.2 ml/flask

The optimal ratio of 50 % conditioned medium and 50 % fresh medium was shown by Gerhard Martin in his medical doctoral thesis (own working group; data not published). He showed that MSC medium in this equation has neither pure nor mixed an effect on the gene expression pattern of EPCs and vice versa.
The cells were incubated for 24 h at 37 °C in a humidified atmosphere with 5 % CO_2. Subsequently, the medium was aspirated, the cells were washed 1x with PBS and lysed with 1 ml/10 cm² TRIzol® for 5 min at room temperature. The lysed monolayers were detached using a cell scratcher, transferred into 15 ml tubes and stored at -80 °C until further use. For the RNA isolation, the lysed cell suspension was thawed on ice and allowed to stand for further 5 min at room temperature. For each ml of TRIzol®, 0.2 ml chloroform were added to each tube and shaked vigorously for 15 s. The mixture was incubated for 2 min at room temperature before the two phases were separated by centrifugation at 4500 *g* for 15 min at 4 °C. The upper aqueous phase was transferred into a fresh 15 ml tube and mixed with 2.5 ml 2-propanol (isopropyl alcohol). The mixture was incubated for 10 min at room temperature before the two phases were separated by centrifugation at 4500 *g* for 10 min at 4 °C. The supernatant was discarded and the cell pellet resuspended in a mixture of 350 µl RA1 buffer from the NucleoSpin® RNA Kit from Macherey-Nagel + 3.5 µl 2-mercaptoethanol. The further RNA isolation was performed according to the protocol of the manufacturer (Chapter 2.2.12).

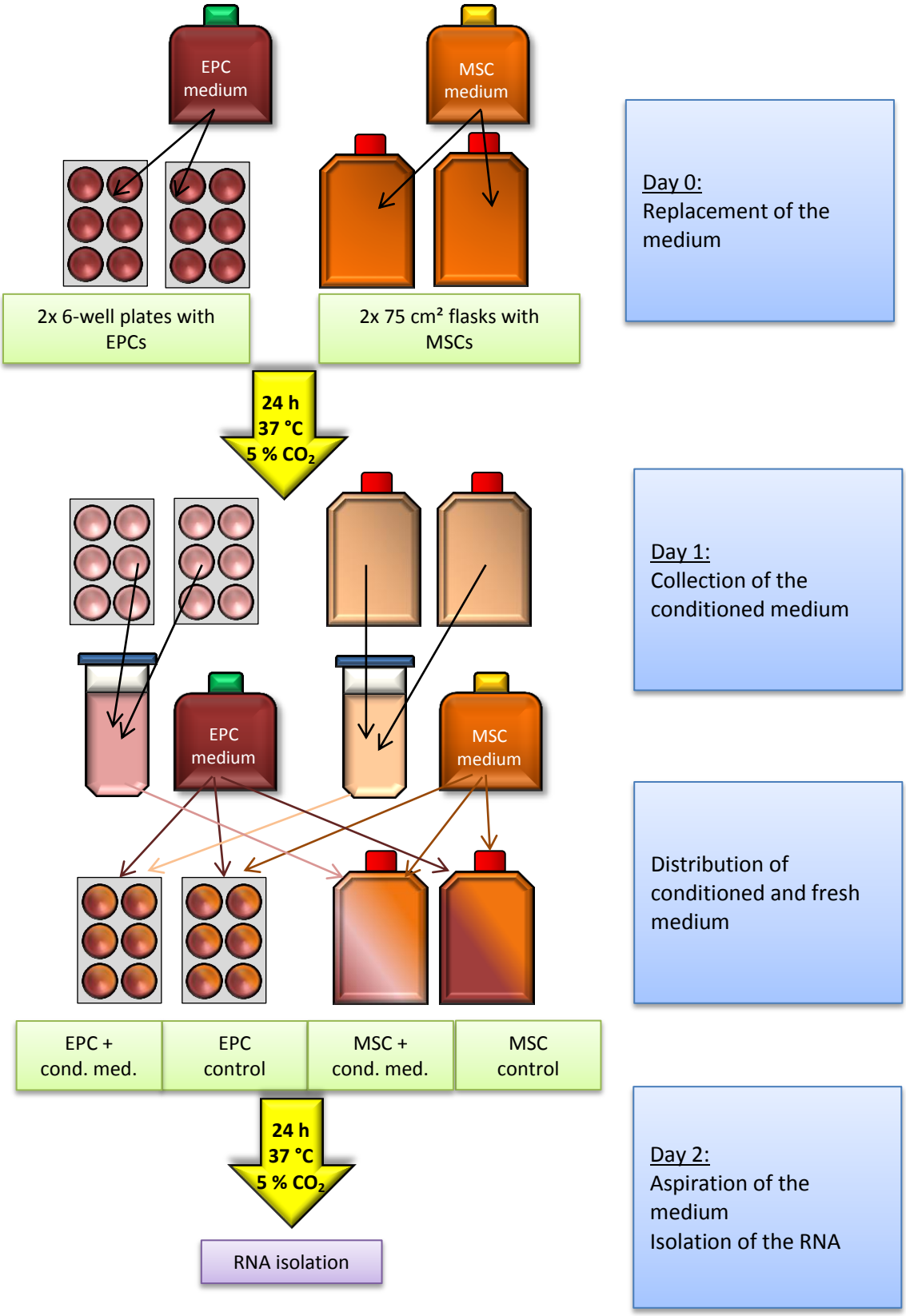

Figure 15: Experimental setting for the experiments with conditioned medium
The conditioned medium was collected 24 h after the medium had been replaced. The conditioned medium was mixed with 50 % fresh medium and distributed to the cells as shown. The control cells received 50 % fresh medium of the respective other cell type instead of conditioned medium. cond. med. = conditioned medium

2.2.9 Staining of cells with Cell Tracker®

Cell Tracker® Green CMFDA (5-chloromethylfluorescein diacetate) and Cell Tracker® Orange CMTMR (5-(and-6)-(((4-chloromethyl)benzoyl)amino)tetramethylrhodamine) are thiol-reactive fluorescent probes suitable for long-term cell-labeling. These dyes have been designed to freely pass through cell membranes into cells, where the dye is transformed into cell membrane-impermeant reaction products. Cell Tracker® Green is colorless and nonfluorescent until the acetate groups are cleaved by intracellular esterases. Cell Tracker® Orange does not require enzymatic cleavage to activate its fluorescence. Cell Tracker dyes are retained in living cells. According to the manufacturer (Lonza), cells labeled with Cell Tracker dye are brightly fluorescent for at least 72 h after incubation in fresh medium at 37 °C and through at least four cell divisions.
The Cell Tracker dyes were used according to the protocol of the manufacturer. Shortly, the dye was loaded into the cells simply by adding 10 ml of 2 µM reagent solution in serum free medium to a 150 cm² cell culture flask containing MSCs or EPCs at 80 – 90 % confluence. The cells were incubated for 45 min at 37 °C in a humidified atmosphere with 5 % CO_2 and then briefly washed with fresh medium. Subsequently, the stained cells were further incubated in propagation medium.
Absorption (abs) and fluorescence emission (em) maxima of Cell Tracker® Green or Cell Tracker® Orange are at abs/em (nm): 492/517 or abs/em (nm): 541/565, respectively. The stained cells were detected with a fluorescence microscope using the Zeiss filter sets no. 09 and 20 (Figure 16).

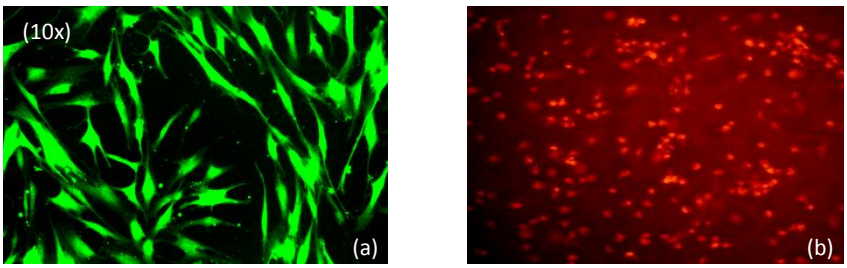

Figure 16: Staining cells with Cell Tracker® dye
(a) MSCs stained with Cell Tracker® Green. (b) EPCs stained with Cell Tracker® Orange

2.2.10 Co-cultivation of EPCs and MSCs

To assess the changes of the global gene expression patterns after direct cell-cell contact, MSCs and EPCs were co-cultured for 24 h (n = 4). Donors of the EPCs were male and aged 26 – 59 years, in average 46 ± 11 years (mean ± standard deviation). Donors of the MSCs were of both genders and aged 49 – 77 years, in average 64 ± 10 years (mean ± standard deviation).
Preliminary tests showed that EPCs adhere comparatively poor. Therefore EPCs were seeded 24 h prior to the addition of MSCs as well as at a higher cell density. The experiment started when EPCs and MSCs of passage 0 reached 80 – 90 % confluence. On day 0 of the experiment, EPCs were seeded into two 150 cm² cell culture flasks at a density of $2x\ 10^7$ cells in a total volume of 24 ml EPC propagation medium. One flask served for the co-culture experiment, the other flask for the EPC control group. The cells were incubated for 24 h at 37 °C in a humidified atmosphere with 5 % CO_2.
On day 1 of the experiment, the prepared EPCs were stained with Cell Tracker® Orange. In parallel, MSCs at passage 0 were stained with Cell Tracker® Green (Chapter 2.2.9.). Subsequently, the MSCs were added to one flask of EPCs as well as into an empty flask (MSC control group) at a density of $2x\ 10^6$ cells. The co-culture as well as the single control cultures contained a total volume of 24 ml medium of which 50 % consisted of EPC propagation medium and 50 % of MSCs propagation medium. The cell density and medium distribution is summarized in Table 10.
The co-culture as well as the control groups were incubated for 24 h at 37 °C in a humidified atmosphere with 5 % CO_2. Subsequently, the cells of the co-culture were separated using fluorescence-activated cell sorting (FACS; Chapter 2.2.11). Although the controls were single cell cultures, the same procedure was applied to avoid differences caused by mechanical stress (Figure 17). The sorted cells were centrifuged at 4500 *g* for 10 min at 4 °C. The supernatant was discarded and the cell pellet of each tube was resuspended in a mixture of 350 µl RA1 buffer from the NucleoSpin® RNA Kit from Macherey-Nagel + 3.5 µl 2-mercaptoethanol. The further RNA isolation was performed according to the protocol of the manufacturer (Chapter 2.2.12).

Table 10: Cell density and medium composition of the co-culture and the control groups
EPCs were seeded 24 h prior to the addition of MSCs. EPCs and MSCs were stained with Cell Tracker® Orange and Green, respectively. The cells were seeded into 150 cm² cell culture flasks in a mixture of 50 % EPC medium and 50 % MSC medium.

Experimental set up	Cell density of EPCs	Volume of EPC medium	Cell density of MSCs	Volume of MSC medium
Co-culture of EPCs + MSCs	$2x\ 10^7$ cells	12 ml	$2x\ 10^6$ cells	12 ml
EPC control group	$2x\ 10^7$ cells	12 ml	-	12 ml
MSC control group	-	12 ml	$2x\ 10^6$ cells	12 ml

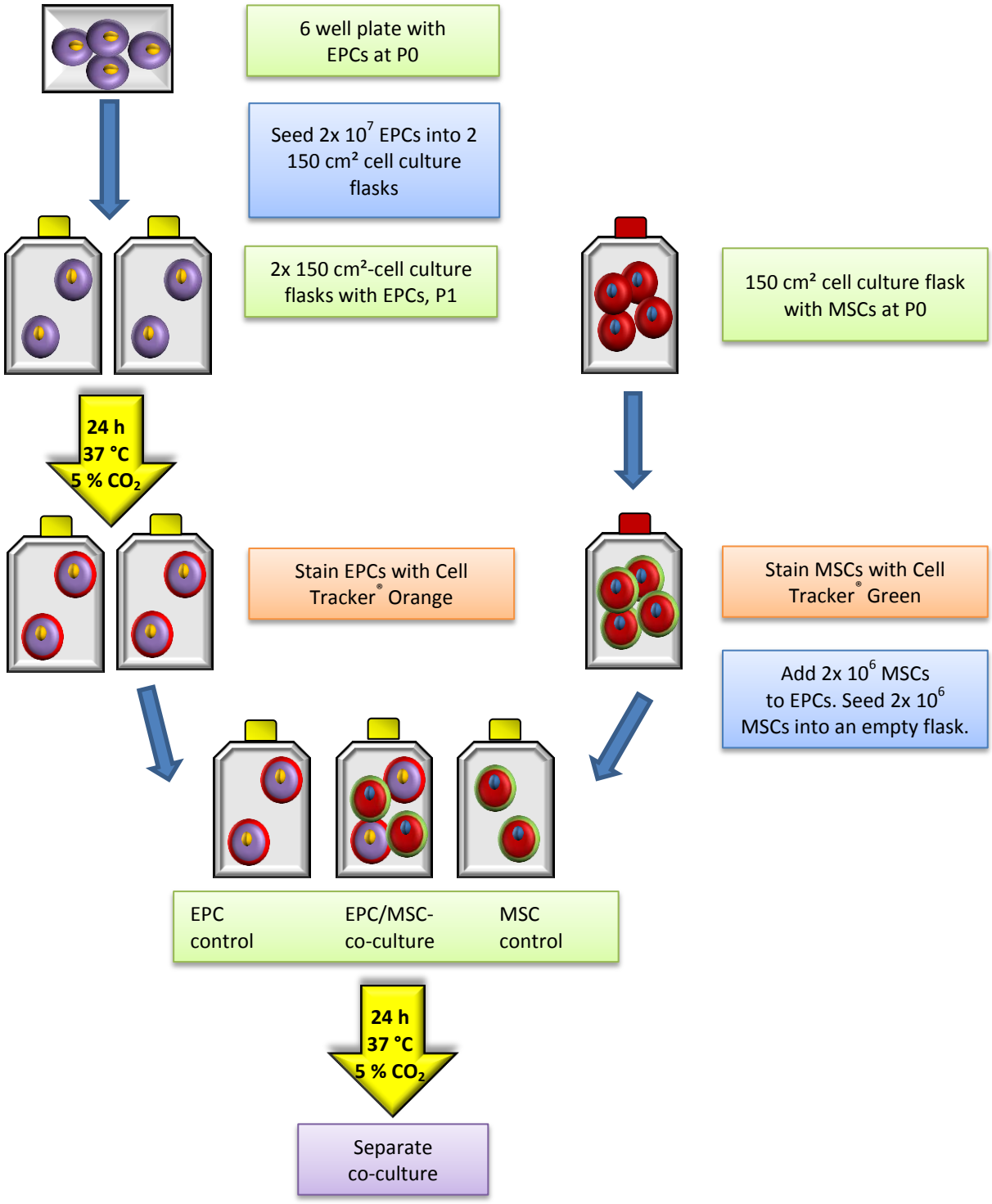

Figure 17: Experimental setting for the assessment of direct cell-cell contact
EPCs and MSCs were stained with Cell Tracker® Orange and Green, respectively. Cells were co-cultured for 24 h in a mixture of 50 % EPC propagation medium and 50 % MSC propagation medium. Single cultures of EPCs and MSCs served as control groups. Subsequently the cells were separated by fluorescence-activated cell sorting (FACS). P0 = passage 0; P1 = passage 1

2.2.11 Fluorescence-activated cell sorting (FACS)

Fluorescence-activated cell sorting (FACS) is a special type of flow cytometry. It provides a method for sorting a heterogeneous mixture of cells into two or more containers, one cell at a time, based upon the specific light scattering and fluorescent characteristics of each cell (Figure 18).
Light scattering occurs when a particle deflects incident laser light. Forward-scattered light (FSC) is proportional to cell-surface area or size. Side-scattered light (SSC) is proportional to cell granularity or internal complexity. In a mixed population of cells, different fluorochromes (e.g. Cell Trackers®) can be used to distinguish separate subpopulations. The staining pattern of each subpopulation, combined with FSC and SSC data, can be used to identify which cells are present in a sample and to count their relative percentages. The cells can also be sorted if desired.
To sort particles or cells, the cytometer first needs to identify the cells of interest, then separate out the individual cells. Once the population of interest has been identified on a data acquisition plot, a region is drawn around that population. A logical gate is created from the regions. This gate is then loaded into the cytometer's software as the sort gate. The sort gate identifies cells of interest to be sorted out of the stream. A stream-in-air flow cytometer isolates a cell of interest by vibrating the entire stream. The sample stream vibrates along its axis and breaks up into drops. The distance between drops is fixed. When the sheath velocity and the vibration speed of the nozzle tip are constant, the pattern of drop formation is fixed. With the fixed drop formation, the FACS is able to calculate the distance between the drops precisely, which allows for the isolation of individual cells. The FACS applies a voltage charge to drops containing a cell that meets the predefined sorting criteria. Positively and negatively charged plates are present on either side of the vibrating stream. As the charged drops pass by the charged plates, the droplets are deflected to the collection tubes, depending on the droplet's charge polarity. Once collected, the cells can be analyzed microscopically, biochemically, or functionally **(BD Biosciences, pt.11–11032–01)**.
The separation of the co-culture of the Cell Tracker® Orange and Green stained EPCs and MSCs, respectively, was performed at the Institute for Virology and Immunology of the University of Würzburg in cooperation with Christian Linden using established protocols.

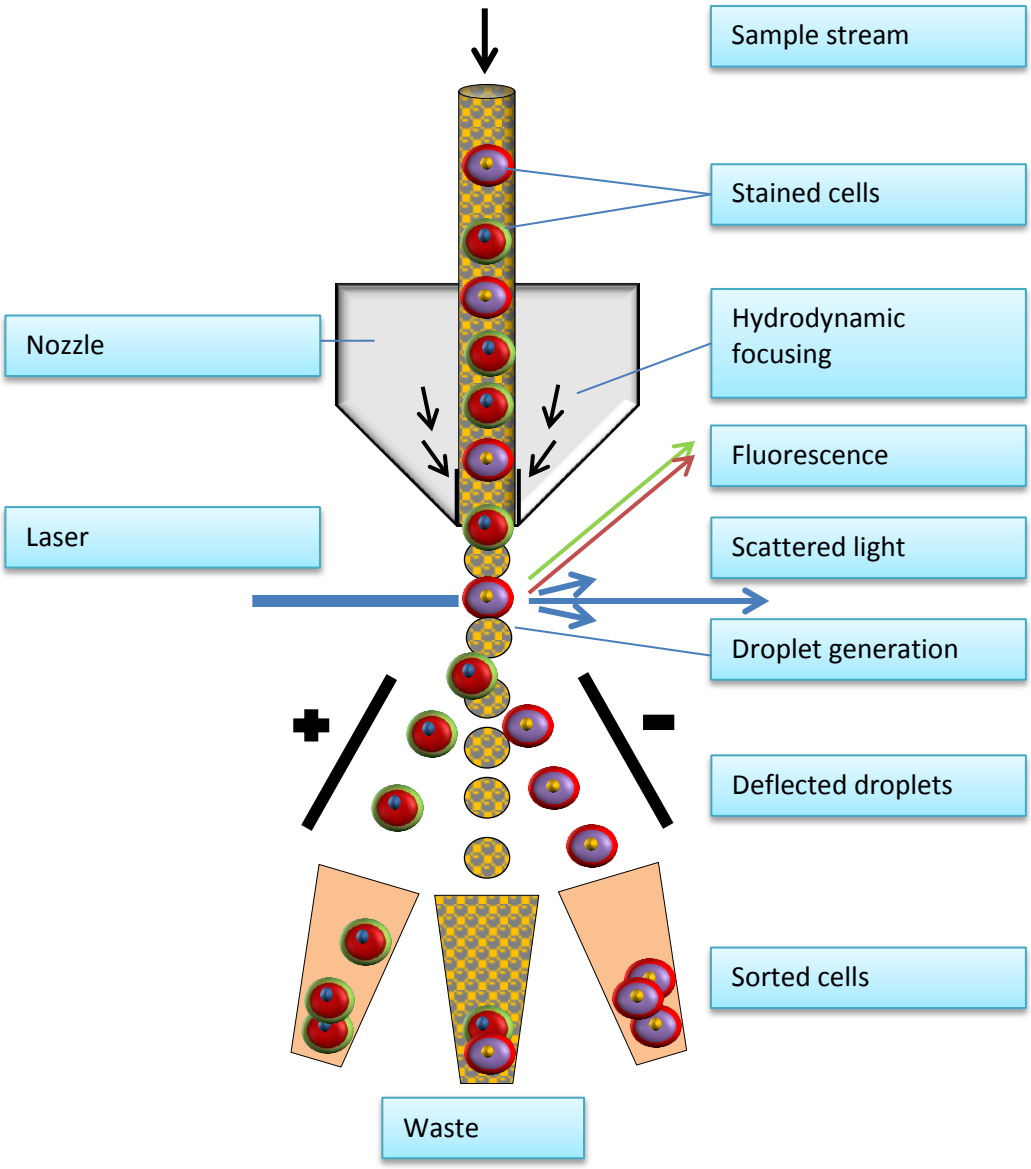

Figure 18: Principle of the flow cytometric cell sorting (FACS)
Fluorescence-activated cell sorting (FACS) is a specialized type of flow cytometry. It provides a method for sorting a heterogeneous mixture of cells into two or more containers, one cell at a time, based upon the specific light scattering and fluorescent characteristics of each cell.

2.2.12 Isolation of cellular RNA

The RNA was isolated using the NucleoSpin® RNA Kit from Macherey-Nagel according to the protocol of the manufacturer.
In brief, the cell pellet was lysed in 350 µl of RA1 buffer containing 3.5 µl 2-mercaptoethanol (Chapter 2.2.8 and 2.2.10). After lysis, homogenization and reduction of viscosity was achieved by filtration with NucleoSpin® filter units provided with the kit. The flow through was mixed with 350 µl 70 % ethanol and loaded onto a second column to bind nucleic acids. The column was centrifuged at 11500 *g* for 1 min and washed with 350 µl of a specific desalting buffer (MDB buffer). Contaminating DNA bound to the silica membrane was removed by adding 95 µl of rDNase solution which was directly applied onto each column and incubated for 15 min at room temperature. The DNase was inactivated by adding 200 µl of RA2 buffer. The column was washed with 600 µl RA3 buffer, followed by a second washing step with 250 µl RA3 buffer. To dry the column, it was centrifuged at 11500 *g* for 3 min. Subsequently, the RNA was eluted in 30 – 50 µl of nuclease-free water and either used immediately or stored at -80 °C. Concentration of total RNA was measured at $OD_{260/280}$ and accepted if the ratio was in-between 1.8 – 2.0.

2.2.13 Synthesis of cDNA

The cDNA was synthesized from the RNA templates via reverse transcription. Therefore, 1 µg of RNA was reverse transcribed using the BioScript™ reverse transcriptase from Bioline, which is a Moloney Murine Leukemia Virus (MMLV) reverse transcriptase. The necessary volume of RNA was mixed with 1 µl random hexamer primer (1 µg/µl) and added up to a total volume of 14.75 µl with water (HPLC grade). The mixture was incubated at 70 °C for 5 min, followed by a further incubation of 5 min on ice. 5.25 µl cDNA master mix (Table 11) were added and incubated for 10 min at room temperature, followed by a further incubation for 60 min at 42 °C. Subsequently the reverse transcriptase was heat inactivated for 10 min at 70 °C and 30 µl of nuclease-free water were added (total volume of 50 µl). The resulting cDNA was used immediately or stored at -20 °C.

Table 11: cDNA master mix for 1 sample

Volume	Component
4 µl	Reaction buffer
1 µl	10 mM dNTPs
0.25 µl	200 U/µl BioScript™ reverse transcriptase

2.2.14 Reverse transcriptase polymerase chain reaction (RT-PCR)

The technique of RT-PCR is commonly used in molecular biology to detect RNA expression. In the first step a RNA template is reverse transcribed into cDNA (Chapter 2.2.13). In the second step, the polymerase chain reaction is performed using the cDNA specimen and gene specific primers. The pipetting scheme for the RT-PCR mix and the protocol to run the RT-PCR are shown in Table 12. In brief, gene specific primers anneal on different strands in the DNA sequence of the gene of interest. *Taq* DNA polymerase elongates the annealed primers yielding double stranded PCR products specific for this gene. The used primers are listed in Table 8. Several of the PCR primers used were already established in the laboratory, others were designed using the free online software Primer3Plus (www.primer3plus.com). If possible, primers were chosen spanning the intron-exon junction to exclude contamination with genomic material. The annealing temperature was identified by a temperature gradient. Specificity of the primer was assured by sequencing the PCR product.
RT-PCR products and molecular weight marker were loaded onto a 1.5 % agarose gel containing 5 % ethidium bromide. Ethidium bromide intercalates into double-stranded DNA or RNA and fluoresces when exposed to UV light. The gel was run at 145 V for approximately 1 h. Bands in the gel were visualized by UV-light and recorded by a snapshot. Densitometric evaluation of transcript amounts was performed using the open source software GelAnalyzer2010A (www.gelanalyzer.com), whereas band intensities of different specimens were normalized onto those of EF1α serving as housekeeping gene.

Table 12: RT-PCR pipetting scheme for 1 sample and run protocol

Volume	Component
18.7 µl	Water, HPLC grade
6 µl	MangoTaq reaction buffer
1 µl	50 mM $MgCl_2$
1 µl	10 mM dNTPs
1 µl	5 pmol/µl forward primer
1 µl	5 pmol/µl reverse primer
0.3 µl	5000 U/ml MangoTaq polymerase
1 µl	cDNA-template or water, HPLC grade
30 µl	**Total volume**

Step	Temperature	Time
1	94 °C	5 min
2	95 °C	30 sec
3	Anneal.-temp.	30 sec
4	72 °C	30 sec
5	Go to step 2, repeat for x cycles	
6	72 °C	5 min
7	12 °C	Store forever

2.2.15 Sequencing

DNA sequencing allows for identification of the nucleotide order of a given DNA fragment. The method applied was the Sanger sequence method using the BigDye® Terminator v3.1 cycle sequencing kit. This chain termination method uses normal deoxynucleosidetriphosphates (dNTPs) (unlabelled) as well as modified di-deoxynucleosidetriphosphates (ddNTPs) (labelled) for the PCR. In the mix of the labelled ddNTPs, each of the di-deoxynucleotide chain-terminators is labelled with a separate fluorescent dye, which fluoresces at a different wavelength. These chain-terminating nucleotides lack a 3'-OH group required for the formation of a phosphodiester bond between two nucleotides, causing DNA polymerase to cease extension of DNA when a modified ddNTP is incorporated. Subsequently, differently sized DNA fragments, each with a fluorescent dye at its end, are separated by electrophoresis. The analysis results in an electropherogram, displaying the determined nucleic base sequence.
In order to sequence a PCR product, the agarose gel electrophoresis of the product must result in a single band. The pipetting scheme and the protocol to run the sequencing PCR are shown in Table 13. Free labelled ddNTPs can disturb the read out. Therefore, for the fast and effective clean-up of these nucleic acids, NucleoSEQ® columns were used. The column was centrifuged at 1133 *g* for 30 sec, equilibrated with 600 µl water (HPLC grade) for 30 min and loaded with 20 µl of the sequence PCR product. The column was centrifuged again at 1133 *g* for 5 min. For the precipitation of the DNA, the flow through was mixed with 3 µl 3 M sodium acetate (pH 4.3) and 80 % ethanol and incubated for 15 min at room temperature before the solution was centrifuged at 16090 *g* for 20 min. The supernatant was discarded, whereas 250 µl 70 % ethanol were added to the pellet, thoroughly mixed and centrifuged at 16090 x *g* for 10 min. The supernatant was discarded and the pellet air dried before resuspended in 30 µl Hi-Di™ formamide. The solution was transferred into a 96-well plate and further processed at the Institute of Human Genetics of the University of Würzburg by Prof. Feichtinger.

Table 13: Sequencing PCR pipetting scheme for 1 sample and run protocol

Volume	Component
4 µl	BigDye® Terminator v3.1 Ready Reaction Mix (2.5x)
2 µl	BigDye® Sequencing v3.1 Buffer (5x)
1 µl	5 pmol/µl primer (forward or reverse)
1-2 µl	PCR product
ad 20µl	Water, HPLC grade

Step	Temperature	Time
1	94 °C	4 min
2	94 °C	30 sec
3	50 °C	1 min
4	60 °C	1 min
5	Go to step 2, repeat for 24 cycles	
6	72 °C	5 min
7	12 °C	Store forever

2.2.16 Affymetrix GeneChip® Human Genome U133 Plus 2.0 Array

A DNA microarray is a collection of microscopic DNA spots attached to a solid surface (GeneChip). Each DNA spot contains picomoles of a specific DNA sequence, known as probes. Given mRNA molecules are able to bind specifically to the DNA template from which they originated. Comparison of separate chips probed with RNA specimens obtained from differently treated cells enables estimation of gene expression differences of the distinct conditions. Microarrays were performed using the Affymetrix GeneChip® Human Genome U133 Plus 2.0 Array. The Affymetrix GeneChip® covers the complete human genome U133 set plus 6500 additional genes for analysis of over 47000 transcripts.
Affymetrix GeneChip® hybridization, staining, and scanning of the chips were performed by PD Dr. L. Klein-Hitpass at the Institute of Cell Biology, University of Duisburg-Essen, Germany. Computation and pairwise comparison of the obtained signals were performed by Dr. Katrin Schlegelmilch, Orthopedic Centre of Musculoskeletal Research, University of Würzburg, Germany and Dr. Alexander Keller, DNA-Analytics, Biocentre, University of Würzburg, Germany.

For the assessment of the changes of the global gene expression patterns of human primary EPCs after having been subjected to conditioned medium of human primary MSCs or after direct cell-cell contact and verse vica, mRNA specimens were collected and analyzed using Affymetrix GeneChip® technology. RNA specimens (n = 4 each) of treated samples were compared to untreated controls, whereas sample and control specimens were taken under same conditions and at the same time point, 24 h after the experiment (Chapter 2.2.8, 2.2.10 and 2.2.12). In total, n = 16 Affymetrix GeneChip® arrays were performed (Table 14).

Table 14: List of Affymetrix GeneChip® analyses
Group A and B: experiments with conditioned medium (n = 4); Donors of the EPCs were male and aged 35-60 years, in average 49 ± 9 years (mean ± standard deviation). Donors of the MSCs were of both genders and aged 56-72 years, in average 67 ± 6 years (mean ± standard deviation)
Group C and D: co-culture experiments (n = 4); Donors of the EPCs were male and aged 26-59 years, in average 46 ± 11 years (mean ± standard deviation). Donors of the MSCs were of both genders and aged 49-77 years, in average 64 ± 10 years (mean ± standard deviation).

Group	Microarray no.	Assessed cells	Treatment
A	1	EPCs	Conditioned medium
	2	EPCs	Conditioned medium
	3	EPCs	Conditioned medium
	4	EPCs	Conditioned medium
B	5	MSCs	Conditioned medium
	6	MSCs	Conditioned medium
	7	MSCs	Conditioned medium
	8	MSCs	Conditioned medium
C	9	EPCs	Co-culture
	10	EPCs	Co-culture
	11	EPCs	Co-culture
	12	EPCs	Co-culture
D	13	MSCs	Co-culture
	14	MSCs	Co-culture
	15	MSCs	Co-culture
	16	MSCs	Co-culture

The comparison of the expression profiles of treated cells to those of the control group allowed for detection of differentially expressed probe sets. Statistical analyses of the regulated probe sets were performed with the statistics software R and its additional component for microarray analyses, Bioconductor. To analyze the Affymetrix GeneChip®, the analysis add-on package Affy was used. Raw data were visually quality controlled by looking for defective or inadequately spotted regions of the chip itself. Further, RNA degradation plots were used to determine the quality of all samples. All samples passed these controls and were used for further analyses. The raw data were normalized using quantiles (Q) without background correction and the robust multi-array average expression measure (RMA) with background correction. However, only the method that yielded the best normalization was used in the following analytical steps, which was determined by comparison of density plots. The AFFX cut-off filter was used to reduce the data to the most significantly differentially expressed probe sets. Gene ontology (GO) analyses regarding differentially regulated genes were performed using GOstats and KEGG. GO enrichment for cellular compounds (CC), molecular function (MF) and biological processes (BP) as well as KEGG enrichment analyses were performed to detect over- and under-represented GO and KEGG terms. Color-coded heat maps that include significant probe sets of interesting pathways or functional groups of genes were plotted using the package gplots **(Schlegelmilch 2012; Schlegelmilch et al. 2014)**.

2.2.17 Production of highly specific anti-hKL antibodies

For the development of an a-hKL sandwich ELISA, two highly specific antibodies are needed. Commercially available a-hKL antibodies are hardly available, very expensive and quite often not suitable for ELISA applications. Therefore, Immundiagnostik AG decided to generate own antibodies. The antibody production was outsourced to YUMAB GmbH, a business partner of Immundiagnostik AG. YUMAB is a privately-held German biotechnology company in Braunschweig, Germany, that provides tailored solutions for human antibody development and antibody engineering problems.
The main feature of recombinant antibodies is the availability of their gene sequences, which are directly obtained during an *in vitro* selection process. These antibody gene sequences allow immediate access to further genetic engineering and to different expression systems.
The principle of antibody phage display is based on large libraries of bacteriophage particles, each carrying the genetic information and the unique phenotypic binding function of one antibody clones. *In vitro* selection is performed by the molecular interaction of target (rKL) and antibody phage. Several selection rounds result in the enrichment of antigen-specific antibody phage. Monoclonal antibodies are finally identified by soluble expression and screening using different types of immunoassays. The standard recombinant antibody format for rapid and large-scale custom antibody generation is “yumab” (scFv-Fc), which has IgG equivalent properties like bivalency and Fc mediated functions (Figure 19). Yumabs are produced in mammalian cells under serum-free conditions and are delivered as purified proteins. According to the manufacturer, yumabs have been shown to successfully replace IgGs in all tested applications. Yumabs are fully compatible with standard Fc-specific secondary antibody conjugates used for detection as well as protein A based purification.
For the generation of klotho specific antibodies by panning the proprietary universal naive human antibody gene libraries (HAL), 100 µg rKL from InVivo (Chapter 2.2.1.2) were made available to YUMAB. Antibodies were generated and delivered as scFv and rabbit-Fc-scFv.

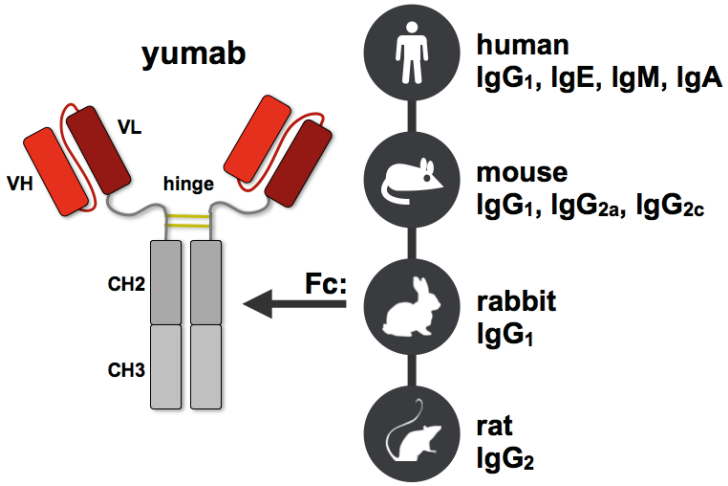

Figure 19: Yumab antibody generation by YUMAB
Yumabs are bivalent scFv-Fc antibodies that are functionally equivalent to IgG in almost all assays. The Fc origin can be chosen from different species (human, mouse, rabbit, rat) and isotypes (see selection in the picture) by the customer. Yumabs are produced in mammalian cells under serum-free conditions and are delivered as purified proteins (source: http://yumab.com/antibody-generation/; date: 2014-06-29).
scFv = single-chain variable fragment; Fc = fragment crystallizable region; VH or VL = heavy or light chain of an immunoglobulin, respectively; Ig = immunoglobulin;

2.2.18 Enzyme-linked immunosorbent assay (ELISA)

The enzyme-linked immunosorbent assay (ELISA) is a popular format of "wet-lab" type analytic biochemistry assay and widely recognized and accepted as a user-friendly tool in diagnostic procedures as well as for research studies. For the development of an ELISA, highly specific antibodies are needed (ideally two different antibodies). For the present study, the target protein was klotho (KL). Therefore, in the first step, recombinant KL was produced (Chapter 2.2.1.2). Due to a lack of commercially available high quality antibodies for the ELISA development, specific anti-KL antibodies were generated (Chapter 2.2.17). For the assay design, the classical (indirect) sandwich ELISA format was chosen (Figure 20), so called after the layers of a sandwich.
First of all, the optimal combination of capture antibody and detection antibody needs to be assessed. Secondly, each of these reactants requires a special buffer (coating buffer, blocking buffer, sample dilution buffer etc.) and the ideal concentration as well as incubation time needs to be optimized. Subsequently, in quantitative ELISA, the optical density (OD) of the sample is compared to a standard curve, which is typically a serial dilution of a known-concentration solution of the target molecule.
Table 15 shows a pipetting scheme describing the volumes of each reactant added to one well of a 96-well microtiter plate as well as the incubation time, temperature, condition and the following washing steps. Each experiment required variations in one or more of these factors/parameters. Therefore each result will list such a table to describe the specific conditions under which the result was obtained.

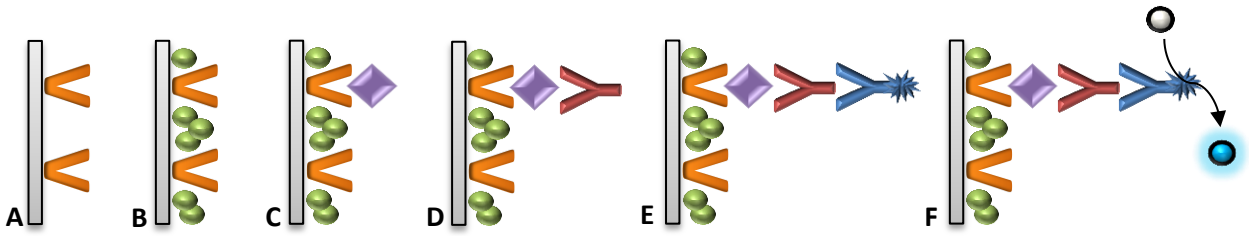

Figure 20: Principle of the sandwich ELISA
Each step requires an incubation time to allow the reactant to bind to its reaction partner. Excess solution is discarded, followed by a washing step.
A: Coating of a 96-well plate with target specific scFv (single-chain variable fragment) which is the capture antibody. B: Adding a blocking solution. Blocking of any non-specific binding sites on the surface C: Adding the sample. Binding of the target to the scFv fragments. D: Adding a target specific bivalent scFv-Fc antibody. Binding of the antibody to the target. E: Adding a species-specific, peroxidase-conjugated antibody (conjugate). Binding of the conjugate to the Fc-part of the target specific antibody. F: Adding the substrate. Enzymatic reaction and color change. Not shown in the figure: Stopping of the enzymatic reaction by adding stop solution and detection of the optical density of the solution using an ELISA reader.

Table 15: Pipetting scheme for the klotho ELISA
ON = over night incubation; RT = room temperature; shake = shake microtiter plate on a horizontal shaker.

Volume per well	Reactant	Time / Temperature	Condition	Washing steps
100 µl	Capture antibody	ON / 4 °C	-	-
200 µl	Blocking buffer	1 h / RT	shake	5x
100 µl	Standard curve / sample	1 h / RT	shake	5x
100 µl	Detection antibody	1 h / RT	shake	5x
100 µl	Conjugate	1 h / RT	shake	5x
100 µl	Substrate	15 – 20 min / RT	-	-
50 µl	Stop solution	Read plate at 450 nm (reference filter: 620 nm)		

3 RESULTS – PART I

3.1 Expression and purification of recombinant CYR61

The recombinant CYR61 protein was expressed as an IgG-Fc-tagged protein (rCYR61) from baculovirus-infected SF21 insect cells according to **Schütze et al. 2005**. The rCYR61 was purified from the cell culture supernatant (75 ml/run) using a protein G sepharose column (Chapter 2.2.1.1). 5 eluates were collected from each run and the protein concentration of each eluate was determined using the Micro-Bradford method (Chapter 2.2.2).
The highest concentration of rCYR61 was always found in eluate number 2 (277 µg/ml ± 101 µg/ml; mean ± standard deviation), independent of the passage of the SF21 cells or the age of the column (n = 34; Figure 21). Hence, eluate 2 was preferably used to coat the 6-well plates for the cultivation of the buffy coat-derived EPCs.
Excess rCYR61 was stored at -20 °C. Prior to its use, the protein concentration was assessed again. The comparison of the rCYR61 concentration determined before and after the freeze-thawing showed a decrease of the protein concentration of up to 59 % (n = 14; Figure 22).

The average yield of rCYR61 from 75 ml cell culture supernatant in eluate 2 of each purification run was 277 µg/ml ± 101 µg/ml (mean ± standard deviation) (n = 34). Excess rCYR61 can be stored at -20 °C with a loss of protein of up to 59 % (n = 14).

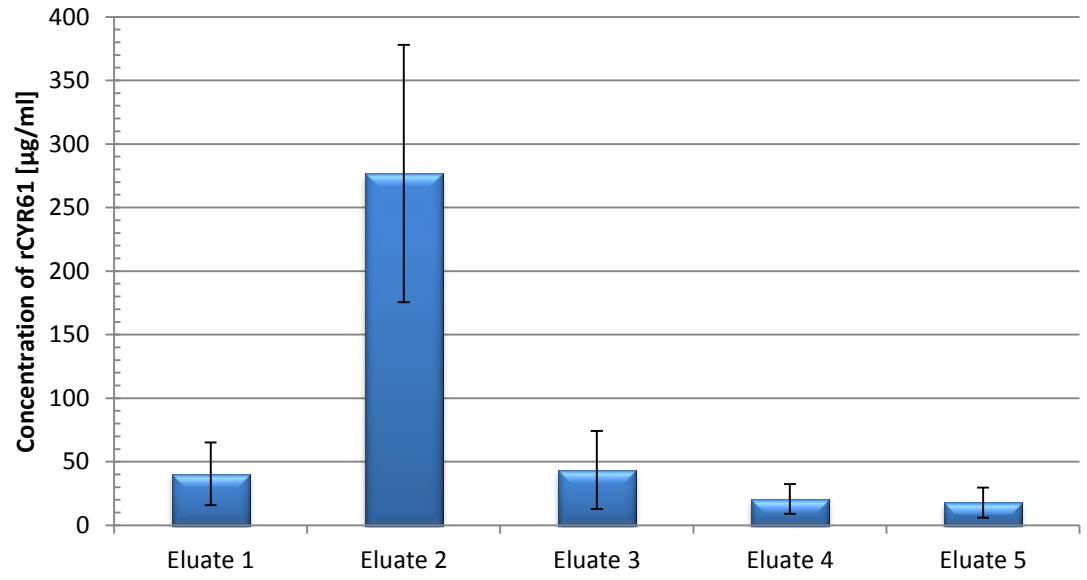

Figure 21: Yield of rCYR61 in different eluates after chromatographic purification
The rCYR61 was purified from 75 ml cell culture supernatant using a protein G sepharose column (n = 34). The concentration of protein in the 5 individual eluates of each run was determined using the Micro-Bradford method. The graph shows the rCYR61 concentrations as mean values ± standard deviation of 34 independent experiments.
Eluate 1: 41 µg/ml ± 25 µg/ml; Eluate 2: 277 µg/ml ± 101 µg/ml; Eluate 3: 44 µg/ml ± 31 µg/ml; Eluate 4: 21 µg/ml ± 12 µg/ml; Eluate 5: 18 µg/ml ± 12 µg/ml.

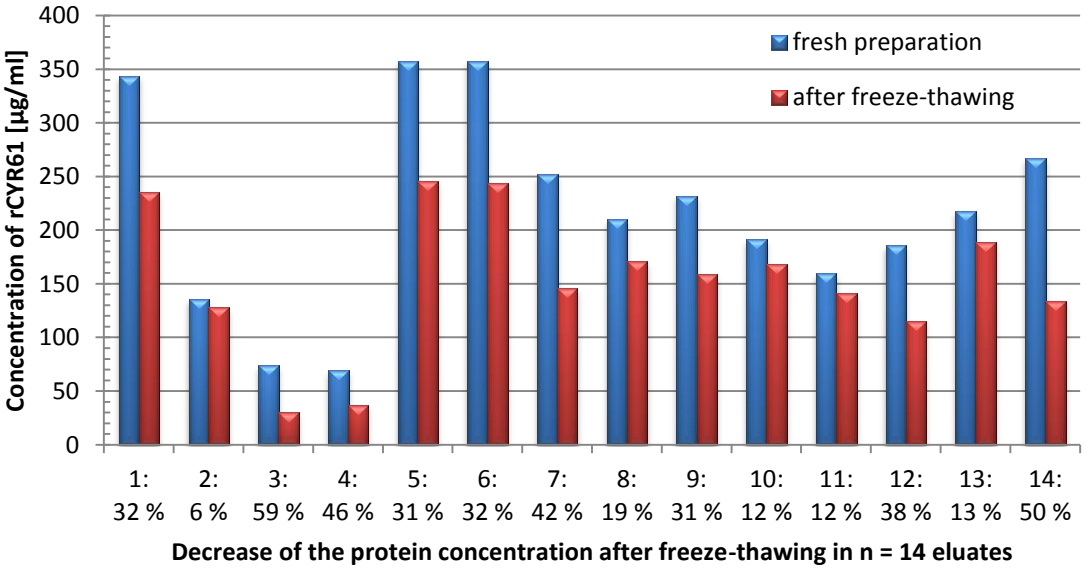

Figure 22: Concentration of rCYR61 in eluate 2 before and after freeze-thawing
Excess rCYR61 was stored at -20 °C. Before coating 6-well plates, the protein concentration was determined again (n = 14). After freeze-thawing the eluate 2, the rCYR61 concentration was decreased up to 59 %.

3.2 Morphological observations of buffy coat-derived EPCs

Buffy coat-derived EPCs adhere as small, round-shaped cells. From day 2 onwards, cells start to become spindle-shaped. Eventually the cells form a cobblestone monolayer in average at day 12.
Figure 23 shows a representative example of the morphological changes of *in vitro* cultured buffy coat-derived EPCs over a time period of 3 weeks.
The EPCs were isolated from buffy coat as described in Chapter 2.2.5.1 latest 24 h after blood sample donation. The buffy coat was purchased from the Blood Donation Service of the Bavarian Red Cross (Blutspendedienst des bayerischen Roten Kreuzes). Each bag contained 30 ml ± 5 ml buffy coat which was gained from 500 ml ± 50 ml blood from 1 donor.
The mono-nuclear cells were isolated from the buffy coat by Ficoll-Paque™ density gradient centrifugation and seeded onto CYR61-coated 6-well plates (= day 0). In average, $1.9 \times 10^6 \pm 0.4 \times 10^6$ mono-nuclear cells/ml blood were isolated from 1 bag of buffy coat (n = 29).
After the first change of medium on day 2, the cell culture showed adherent, small round-shaped cells, which were evenly spread over the bottom of the 6-well plate (Figure 23 A). For the experiments, only cell cultures that showed continuous proliferation over the following 7 days were chosen by meaning only cells that reached 80 – 90 % confluence and showed as well predominantly spindle-shaped cells by that time as a high vitality were chosen for further experiments. 75 % of the cell preparations fulfilled these criteria.
If these criteria were fulfilled, the cells were passaged earliest at day 7 and latest at day 9 (EPCs on day 7 prior to the passaging are shown in Figure 23 B). To observe the morphological changes and to compare cells from passage 0 with cells from passage 1, some of the cells of the current trial were post-confluent cultured in passage 0 in parallel to passaged cells (Figure 23 C-K versus L-N).
The passaged cells showed in the first a small, round-shaped morphology similar to their original shape. Within 24 h, the cells sprout spindle-shaped, and latest after 48 h the morphology of the cells was comparable to the morphology of non-passaged cells of the same age (Figure 23 E and M, passage 0 and 1, respectively, day 10; Figure 23 F and N, passage 0 and 1, respectively, day 12).
The post-confluent cultured cells showed in addition to the slim spindle-shaped cells thickened oblong-shaped cells from day 8 – 9 onwards. From day 11 – 12 onwards, the culture showed predominantly cobblestoned cells (Figure 23 G and H, day 13 and 14, respectively). The cells were still proliferating.
From day 17 onwards the morphology became more and more inhomogeneous showing a higher number of enlarged granular cells (Figure 23 I). After a further 6 days, the culture showed cell aggregates and the cell layer was fragmentary.

In conclusion, the buffy coat-derived EPCs went through 3 different morphological stages during the propagation culture: stage 1: small, round-shaped cells, stage 2: slim, spindle-shaped cells after 1 week of *in vitro* cultivation, stage 3: cobblestone morphology from day 12 onwards. These morphological changes were observed in all experimental settings.

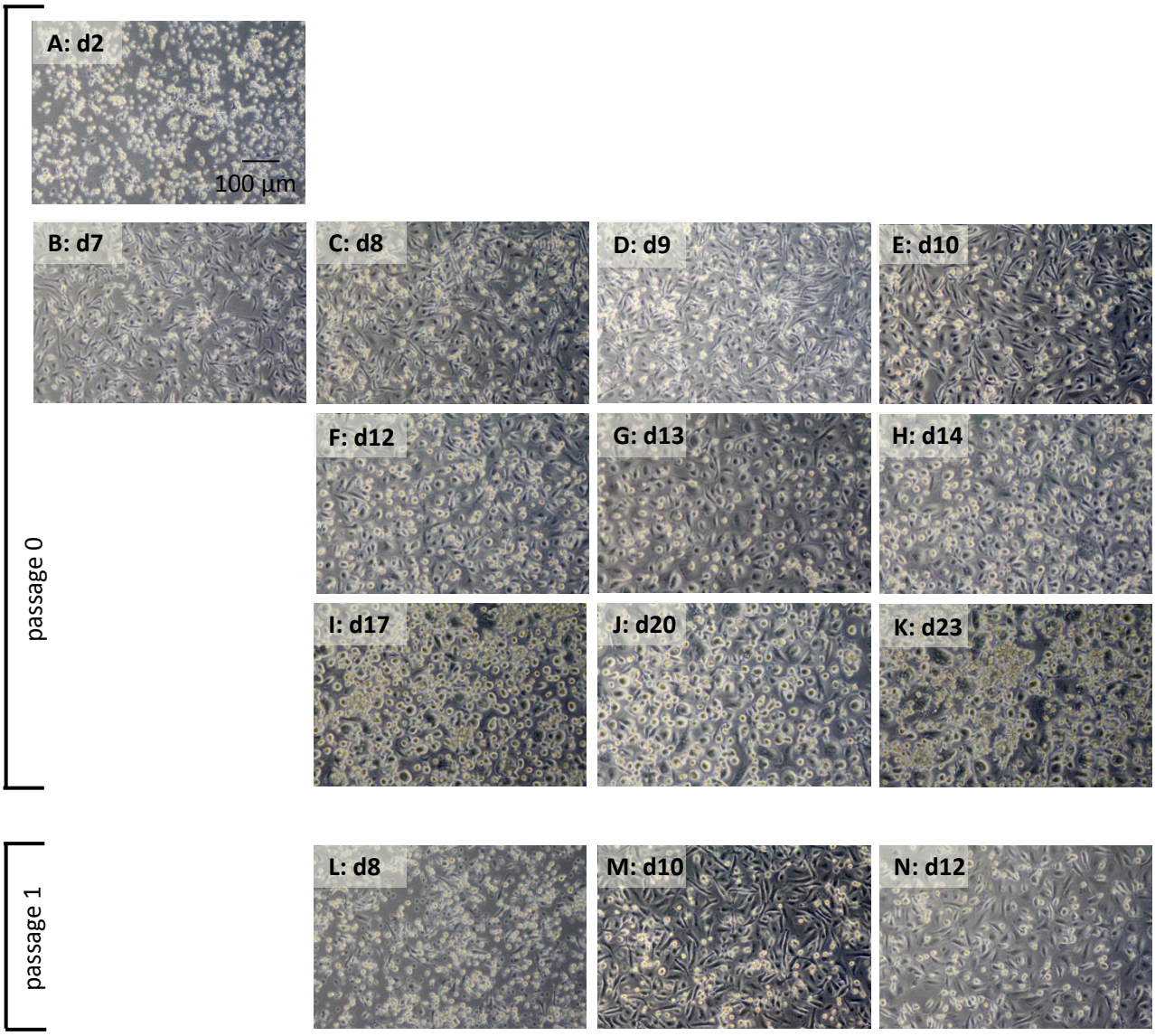

Figure 23: Representative example of the morphological changes of buffy coat-derived EPCs
The figure shows the morphology of buffy coat-derived EPCs over a time of 23 days in passage 0 and in addition cells in passage 1 over a time of 5 days that had been passaged at day 7.
A-K: EPCs (passage 0) at day (d) 2, 7, 8, 9, 10, 12, 13, 14, 17, 20 and 23, respectively of the *in vitro* cultivation in EPC propagation medium. L-N: EPCs (passage 1) at day (d) 8, 10 and 12, respectively of the *in vitro* cultivation in EPC propagation medium.

3.3 Characterization of buffy coat-derived EPCs

Mono-nuclear cells from buffy coat were seeded on CYR61-coated plates. The CYR61 protein, also known as CCN1, is known as an angiogenic inducer. The positive effect of rCYR61-coated plates for the *ex vivo* expansion of EPCs as well as the characterization of EPCs derived from fresh peripheral blood were shown by Rita Schenk in her PhD thesis **(Schenk 2007)**. To assess the expression of surface markers of buffy coat-derived EPCs, the cells were stained with monoclonal mouse antibodies for CD31, CD34, CD45, CD133, CD309 and CD144 at day 7 (passage 0) and day 14 (passage 1) of *in vitro* cultivation. Control cells were stained with mouse IgG1-PE, mouse IgG2a-FITC and mouse IgG2b-APC (isotype control). The stained cells were analyzed using flow cytometry.
Figure 24 A shows a representative image out of 3 independent experiments. The cells are positive for the endothelial cell marker CD31 (also known as PECAM-1), the hematopoietic cell marker CD45, and the endothelial cell marker CD144 (also known as VE-cadherin) with a fraction additionally positive for CD34 at both time points. The cells are in addition positive for the hematopoietic stem cell marker CD34 at day 14. The cells are negative for CD133, a marker found on multipotent progenitor cells, including immature hematopoietic stem and progenitor cells at both time points. The cells are also negative for the endothelial progenitor, endothelial and hematopoietic cell marker CD309 (also known as VEGFR-2/KDR) at both time points.
In addition, the buffy coat-derived EPCs were analyzed for the uptake of acetylated low-density lipoprotein (acLDL) and the binding of Ulex Lectin (UEA) at day 14. The result shown in Figure 24 B is representative for 3 independent experiments. Fluorescence microscopy shows that adherent cells are positive for the uptake of acLDL (red) and the binding of Ulex Lectin (green). DAPI staining shows nuclei (blue).

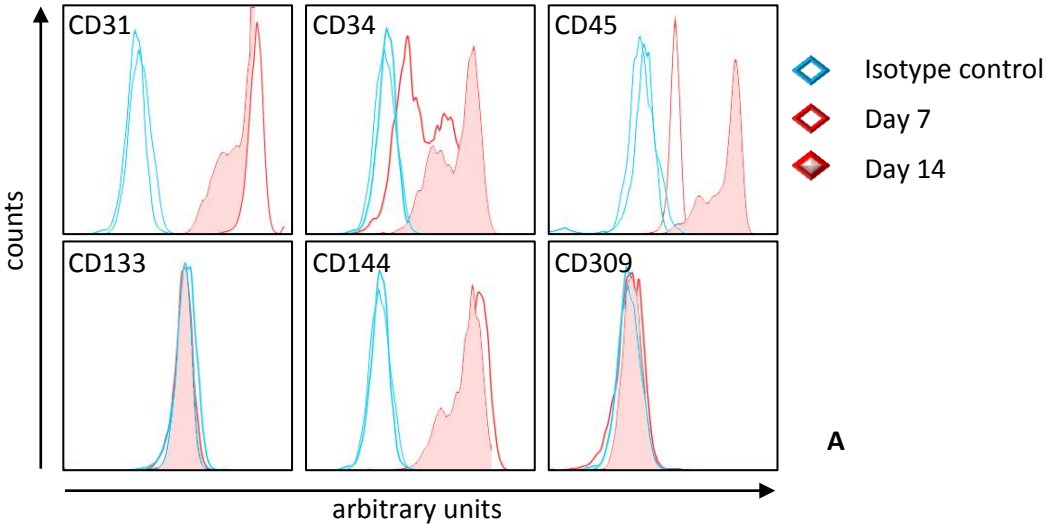

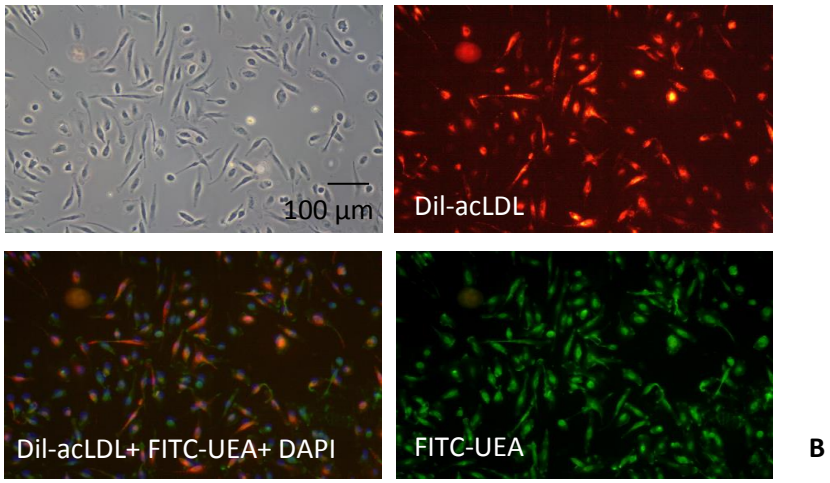

Figure 24: Representative images of the characterization of primary buffy coat-derived EPCs by fluorescence microscopy
A: *In vitro* cultured EPCs are positive for the cell surface markers CD31 (also known as PECAM-1), CD45 and CD144 (also known as VE-Cadherin) on day 7 and in addition positive for CD34 on day 14. The cells are negative for the markers CD133 and CD309 (also known as VEGFR-2/KDR) at both time points.
B: The fluorescence microscopy shows positive results for the staining with Ulex Lectin (FITC-UEA) and the uptake of acetylated low density lipoprotein (Dil-acLDL) on day 14.

3.4 Experimental setup for the analysis of the cross-talk of EPCs and MSCs

A better understanding of the interactions of cells used in the field of bone tissue regeneration on tissue engineered constructs will help to improve this technology. A better knowledge of the molecular functions, the regulatory mechanisms and the factors involved in e.g. angiogenic and osteogenic processes could help to support or positively influence cell survival, proliferation and function. Therefore, a model to assess the communication of these cells was needed.
This study aimed to investigate the cross-talk of EPCs and MSCs within the first 24 h of contact. To assess the response of the cells after humoral contact, experiments with conditioned medium were performed (see Chapter 2.2.8. for details on the experimental setup and Chapter 3.4.1 for the results). To assess the changes of the global gene expression patterns after direct cell-cell contact, co-culture experiments were performed (see Chapter 2.2.10. for details on the experimental setup and Chapter 3.4.2 for the results).

3.4.1 Experiments with conditioned medium

The experimental setting was designed to assess the influence of conditioned medium gained from MSCs on EPCs and *vice versa* and subsequently to assess the changes of the global gene expression patterns of both cell types (n = 4). Donors of the EPCs were male and aged 35 – 60 years, in average 49 ± 9 years (mean ± standard deviation). Donors of the MSCs were of both genders and aged 56 – 72 years, in average 67 ± 6 years (mean ± standard deviation).
Figure 25 shows a representative example of an *in vitro* culture of EPCs and MSCs at the time the conditioned medium was collected and distributed in combination with fresh medium to the respective other cell type. Control cells received a composition of fresh EPC/MSC medium. Subsequently, RNA was isolated 24 h later. The amount of RNA isolated from the cell fractions was 3.8 – 76.5 µg. This amount of RNA was sufficient to be used for the microarray analyses. The results of the microarray analyses are shown in Chapter 3.5.

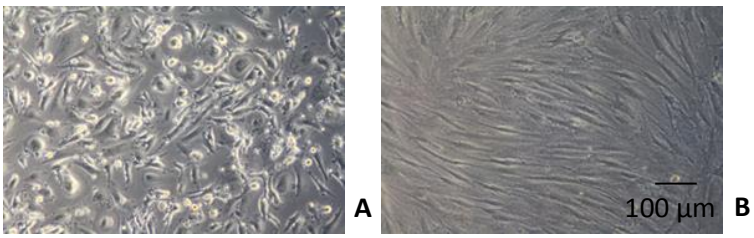

Figure 25: Representative example of EPCs and MSCs used for the experiments with conditioned medium
Example of an *in vitro* culture of EPCs (A) and MSCs (B) at the time point of the collection of the conditioned medium and distribution to the respective other cell type (n = 4).

3.4.2 Co-cultivation of EPCs and MSCs

To assess the changes of the global gene expression patterns after direct cell-cell contact, MSCs and EPCs were co-cultured for 24 h (n = 4). Donors of the EPCs were male and aged 26 – 59 years, in average 46 ± 11 years (mean ± standard deviation). Donors of the MSCs were of both genders and aged 49 – 77 years, in average 64 ± 10 years (mean ± standard deviation).
To separate the MSCs and EPCs after the co-culture experiment, the cells were stained with Cell Tracker® Green and Orange, respectively, prior to the experiment (Figure 26). Subsequently, the cells were sorted by flow cytometry (fluorescence-activated cell sorting, FACS). Control cells were stained and sorted as well to apply the same procedure.
An aliquot of the sorted cells from each co-culture experiment was re-sorted (post-analyzed) to determine the purity of separated cell fractions. The post-analysis showed in average a purity of 99.1 % ± 0.3 % (mean ± standard deviation). The amount of RNA isolated from these cell fractions was 1.4 – 20.0 µg. This amount of RNA was sufficient to be used for the microarray analyses. The results of the microarray analyses are shown in Chapter 3.5.

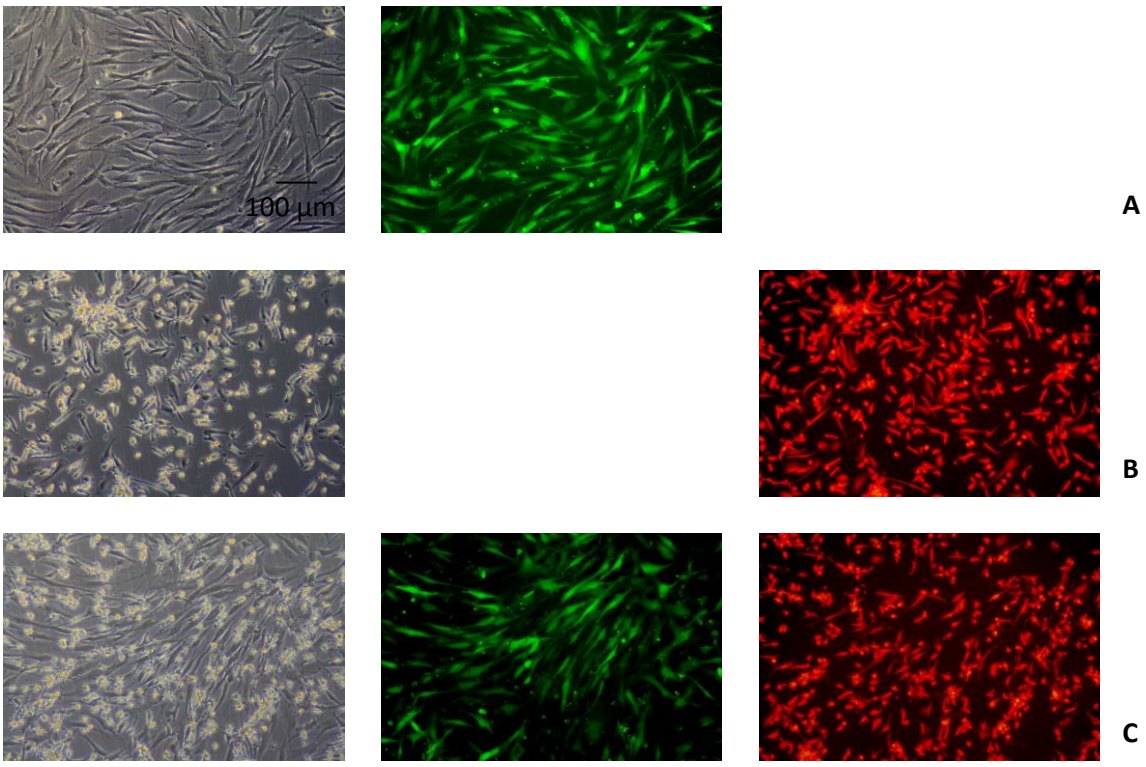

Figure 26: Representative example of EPCs and MSCs stained with Cell Tracker® Orange and Green, respectively
Cells were stained with Cell Trackers prior to the co-culture experiment (n = 4). A: MSC control cells stained with Cell Tracker® Green. B: EPC control cells stained with Cell Tracker® Orange. C: Co-culture of MSCs and EPCs stained with Cell Tracker® Green and Orange, respectively.

3.5 Microarray analyses

Assays with the co-cultured EPCs and MSCs and the corresponding controls were performed (n = 4). In addition, assays with EPCs and MSCs treated with conditioned medium and the corresponding controls were performed (n = 4; Chapter 2.2.16, Table 14). Total RNA was isolated 24 h after the experiment to detect gene regulations in an early stage of cell communication. Microarrays were performed using the Affymetrix GeneChip® Human Genome U133 Plus 2.0 Array and by comparing treated and control cells (Figure 27).

The data of the microarrays was analyzed using the statistical software R and its additional component for microarray analyses, namely Bioconductor. Raw data was visually quality controlled and the RNA degradation plot (Chapter 3.5.1) was used to determine the quality of all samples. Subsequently, a normalization step was applied for each sample using the robust multi-array average expression measure (RMA) with background correction (Chapter 3.5.2). The AFFX cut-off (maximum differentially expressed AFFX labelled probe set as threshold) was used to reduce the data to the most significant probe sets.

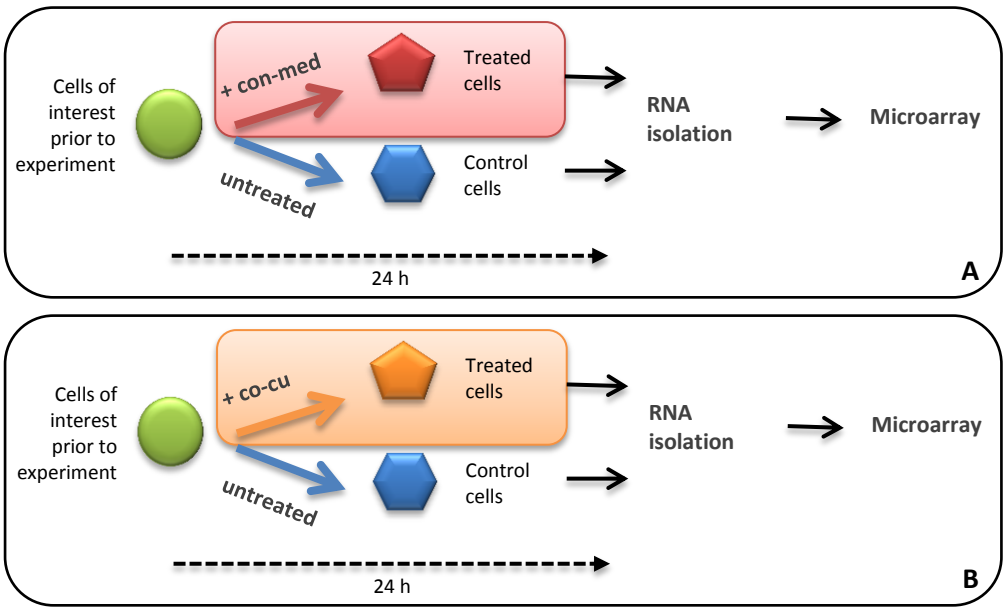

Figure 27: Chart of the experimental setting applied to the cells of interest
Cells of interest were both EPCs and MSCs. Untreated cells were used as controls. RNA specimens isolated 24 h after the treatment were applied for the microarray analyses. A: Cells were treated with conditioned medium (con-med) of the respective other cell type. B: Cells were co-cultured (co-cu) with the respective other cell type.

3.5.1 RNA degradation plot

The RNA degradation plot serves as a quality control of the used RNA. RNA is degraded from the 5' end of a sequence, therefore intensities of probes at the 3' end of a probe set are higher than those at the 5' end. High slopes indicate degradation. More important than the slope is the agreement between arrays. Mean intensities of all RNA specimens were lower in RNA parts of the 5’ region compared to mean intensities of parts within the 3’ region. However, all RNA samples reflect the same expected intensity gradients and were used for further analyses (Figure 28).

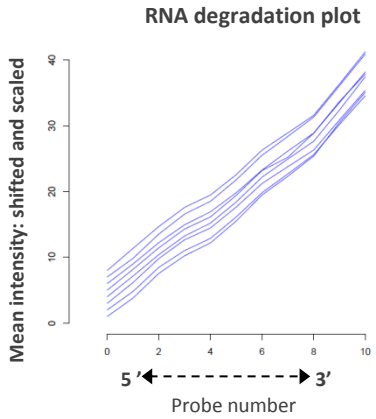

Figure 28: Representative example of a diagnostic plot of microarray raw data prior to normalization
RNA degradation from 5’ to 3’ end of the probe sets. Displayed are mean intensity values for the 4 individual experiments/arrays of EPCs co-cultured with MSCs and the respective controls. All samples were comparable according to their ascendant slope and parallelity.

3.5.2 Normalization

Normalization is needed to ensure that differences in intensities are indeed due to differential expression, and not some printing, hybridization, or scanning artifact. Normalization is necessary before any analysis which involves within or between slides comparisons of intensities. The normalization method applied to all microarray data was RMA (Figure 29).

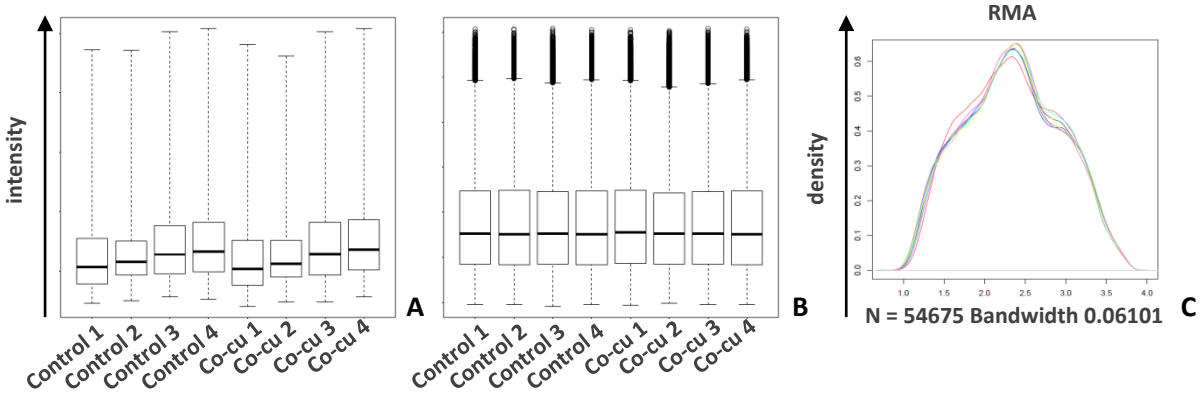

Figure 29: Representative result of a normalization of the microarray data using RMA
A+B: Boxplots before (A) and after (B) normalization with RMA of the EPCs co-cultured with MSCs (co-cu) and the respective control EPCs (control) of 4 independent experiments. Each box shows the distribution of expression values of one array. C: Densities of normalized expression intensities.

3.5.3 Microarray results

Microarrays were performed using RNA specimens of co-cultured EPCs and MSCs and the corresponding controls (n = 4). In addition, assays with EPCs and MSCs treated with condition medium and the corresponding controls were performed (n = 4). Thus, data sets were generated by comparing treated and non-treated cells for both EPCs and MSCs each consisting of 4 individual experiments (array group A – D). The bioinformatic analysis of the microarray data revealed a number of differentially expressed probe sets. The results are displayed in subsequent chapters and summarized in Figure 30. Detailed lists showing the differentially expressed probe sets of each experiment are listed according to their descending statistical score (logFc) from highest up-regulation to highest down-regulation in appendix A – D.

3.5.3.1 Array group A: EPCs treated with conditioned medium ($EPCs^{con\text{-}med}$)

The comparison between EPCs treated with conditioned medium ($EPCs^{con\text{-}med}$) and the respective control cells revealed 769 differentially expressed probe sets corresponding to 514 genes of which 343 genes were significantly up-regulated and 171 significantly down-regulated.

3.5.3.2 Array group B: MSCs treated with conditioned medium ($MSCs^{con\text{-}med}$)

The comparison between MSCs treated with conditioned medium ($MSCs^{con\text{-}med}$) and the respective control cells revealed 180 differentially expressed probe sets corresponding to 119 genes of which 97 genes were significantly up-regulated 22 significantly down-regulated.

3.5.3.3 Array group C: EPCs co-cultured with MSCs ($EPCs^{co\text{-}cu}$)

The comparison between co-cultured EPCs ($EPCs^{co\text{-}cu}$) and the respective control cells revealed 923 differentially expressed probe sets corresponding to 613 genes of which 501 genes were significantly up-regulated 112 significantly down-regulated.

3.5.3.4 Array group D: MSCs co-cultured with EPCs ($MSCs^{co\text{-}cu}$)

The comparison between co-cultured MSCs ($MSCs^{co\text{-}cu}$) and the respective control cells revealed 458 differentially expressed probe sets corresponding to 319 genes of which 207 genes were significantly up-regulated 112 significantly down-regulated.

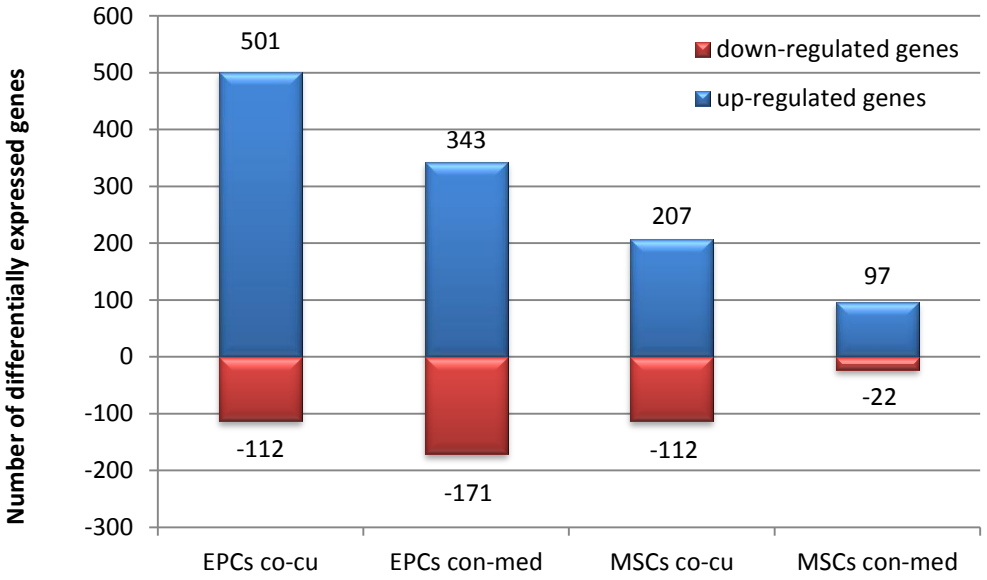

Figure 30: Number of significantly up- or down-regulated genes
The bioinformatics evaluation of the microarray data revealed a certain number of differentially expressed genes comparing treated with untreated cells. Co-cu = co-culture experiments; con-med = conditioned medium experiments.

3.6 Gene ontology analysis

Each of the 4 microarray groups consist of 4 individual experiments (Chapter 2.2.16, Table 14, Page 40). Each experiment consists of treated cells and control cells that, compared to each other, resulted in 1 microarray result. For the bioinformatical analysis, the microarray results of the 4 individual experiments have been grouped and compared to each other (array group). Significantly regulated genes of the array data of each group were analyzed for their affiliation regarding the main Gene Ontology (GO) categories biological process, cellular component and molecular function as well as for Kyoto Encyclopedia of Genes and Genomes (KEGG) pathway over-representation. The results are shown group-wise in the subsequent chapters.
Within one chapter/group, the differentially expressed genes are displayed in tables according to their affiliation to a certain pathway or biological process, e.g. angiogenesis or osteogenesis. In addition, the differentially regulated genes are arranged in alphabetical order to disburden the search for certain gene names. To search for differentially expressed genes sorted by their degree of regulations (logarithmic fold change), please view the tables in appendix A – D. The tables also provide information about the probe set ID, their corresponding gene symbol and name as well as the adjusted (corrected for multiple comparisons) p-value.

3.6.1 EPCs treated with conditioned medium (array group A)

To assess the changes of the global gene expression patterns of EPCs after incubation with conditioned medium, the medium of *in vitro* cultured MSCs was collected and distributed to cultured EPCs. After 24 h, RNA was isolated and used for microarray analyses (n = 4). The comparison between EPCs$^{con\text{-}med}$ and the respective control cells revealed 769 differentially expressed probe sets corresponding to 514 genes of which 343 genes were significantly up-regulated and 171 significantly down-regulated. These significantly regulated genes were analyzed for their affiliation regarding the GO database and KEGG pathway over-representation (Figure 33). The analysis revealed several important cellular processes affiliated with cytokine-cytokine receptor interaction and chemokine signaling. In the GO class of biological processes, clusters of differentially expressed genes belonging to different subclasses of inflammation (e.g. inflammatory response, immune response and response to wounding) were discovered. Similarly, proteins associated with e.g. cell adhesion, proliferation, migration and angiogenesis such as vascular endothelial growth factor (VEGFA), versican (VCAN) and interleukin 8 (IL8) could be assigned along the main GO-categories (Table 16).

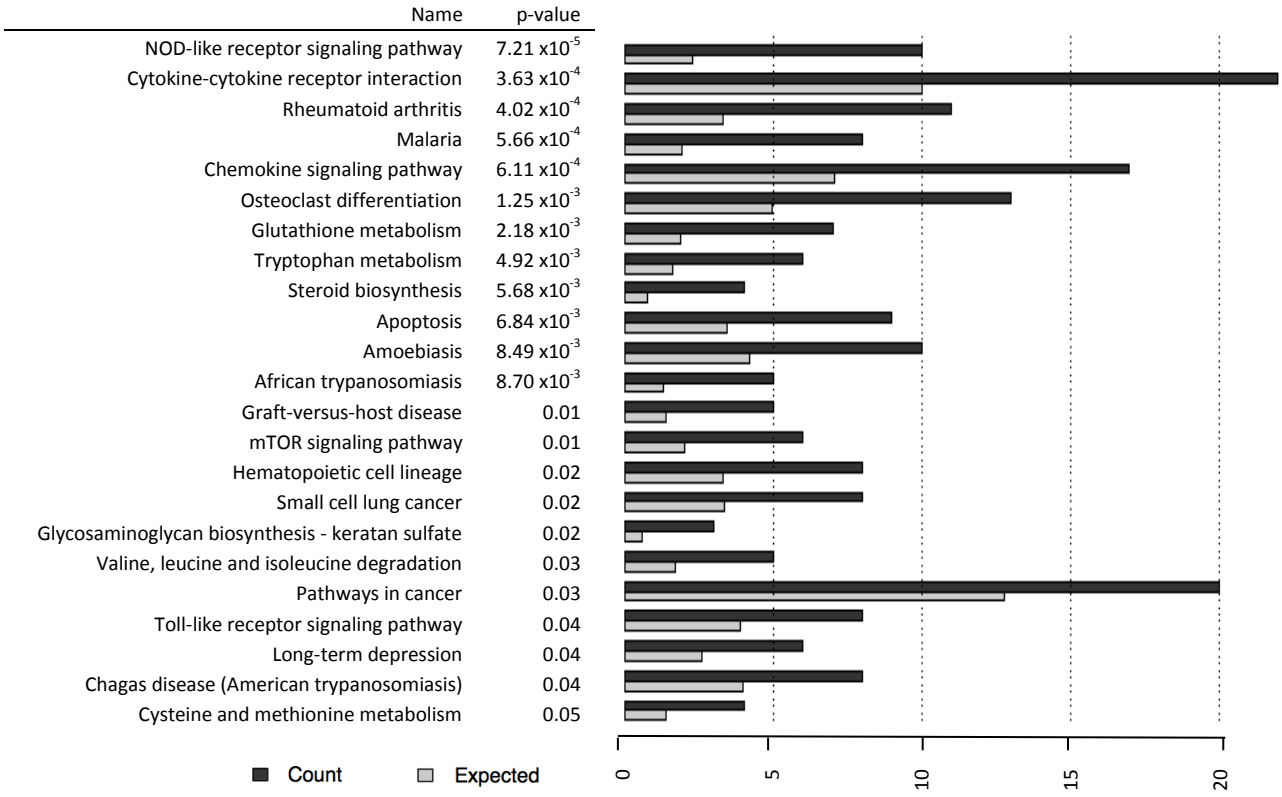

Figure 31: KEGG pathway over-representation of EPCs$^{con\text{-}med}$ (array group A)
All 514 significantly regulated genes were assigned to KEGG signaling pathways. Illustrated are all pathways which were over-represented according to their corresponding p-values. Grey bars indicate the expected count of gene regulations for each pathway, whereas black bars demonstrate the actual count. Corresponding p-values are results of the hyper-geometric tests.

Table 16: Selection of genes differentially expressed in EPCs$^{con\text{-}med}$ (array group A)
Shown is a selection of differentially expressed genes revealed by the microarray analysis of EPCs after treatment with conditioned MSC medium. The table provides information about the degree of regulation (logFC) and the corresponding p-value. Positiv logFCs indicate up-regulation of the corresponding gene compared to the control cells. GeneCards Summary provides information about the function of the protein (source: www.genecards.org; November 2014).
logFC = logarithmic fold change; adj.P.Val = adjusted p-value

Symbol	GeneName	logFC	adj.P.Val	Function (GeneCards Summary)
CD86	CD86 molecule	1.01	6.60×10^{-4}	This gene encodes a type I membrane protein that is a member of the immunoglobulin superfamily. This protein is expressed by antigen-presenting cells, and it is the ligand for two proteins at the cell surface of T cells.
CXCL1	Chemokine (C-X-C Motif) Ligand 1	4.54	9.60×10^{-4}	The encoded protein is a secreted growth factor that signals through the G-protein coupled receptor, CXC receptor 2. This protein plays a role in inflammation and as a chemoattractant for neutrophils. May play a role in inflammation and exerts its effects on endothelial cells in an autocrine fashion.
CXCL2	Chemokine (C-X-C Motif) Ligand 2	3.57	8.95×10^{-4}	Produced by activated monocytes and neutrophils and expressed at sites of inflammation. Hematoregulatory chemokine, which, in vitro, suppresses hematopoietic progenitor cell proliferation.
CXCL3	Chemokine (C-X-C Motif) Ligand 3	4.22	1.19×10^{-3}	Ligand for CXCR2 (By similarity). Has chemotactic activity for neutrophils. May play a role in inflammation and exert its effects on endothelial cells in an autocrine fashion.
EREG	Epiregulin	4.51	2.35×10^{-5}	Epiregulin is a member of the epidermal growth factor family. It can function as a ligand of EGFR (epidermal growth factor receptor). May be a mediator of localized cell proliferation. As a mitogen it may stimulate cell proliferation and/or angiogenesis.
IL1A	Interleukin 1, alpha	5.03	1.80×10^{-4}	This cytokine is a pleiotropic cytokine involved in various immune responses, inflammatory processes, and hematopoiesis. This cytokine is produced by monocytes and macrophages as a proprotein, which is proteolytically processed and released in response to cell injury, and thus induces apoptosis.
IL6	Interleukin 6	3.99	7.24×10^{-4}	The protein is primarily produced at sites of acute and chronic inflammation, where it is secreted into the serum and induces a transcriptional inflammatory response through interleukin 6 receptor, alpha.
IL8	Interleukin 8	4.18	6.89×10^{-4}	The protein encoded by this gene is a member of the CXC chemokine family. This chemokine is one of the major mediators of the inflammatory response. This chemokine is secreted by several cell types. It functions as a chemoattractant, and is also a potent angiogenic factor.
ITGB8	Integrin, beta 8	3.97	4.86×10^{-5}	This gene is a member of the integrin beta chain family and encodes a single-pass type I membrane protein which noncovalently binds to an alpha subunit to form a heterodimeric integrin complex. Integrin alpha-V/beta-8 is a receptor for fibronectin.
LAMB1	Laminin, beta 1	2.54	6.32×10^{-4}	Laminins, a family of extracellular matrix glycoproteins, are the major noncollagenous constituent of basement membranes. Binding to cells via a high affinity receptor, laminin is thought to mediate the attachment, migration and organization of cells into tissues.
OSM	Oncostatin M	3.02	6.44×10^{-4}	It regulates cytokine production, including IL-6, G-CSF and GM-CSF from endothelial cells. It also regulates osteoblast to osteocyte transition.
PECAM1	Platelet/endothelial cell adhesion molecule 1	1.39	4.81×10^{-4}	The protein encoded by this gene is found on the surface of platelets, monocytes, neutrophils, and some types of T-cells, and makes up a large portion of endothelial cell intercellular junctions. The encoded protein is a member of the immunoglobulin superfamily and is likely involved in leukocyte migration, angiogenesis, and integrin activation.
THBS1	Thrombospondin	6.15	4.94×10^{-4}	This protein is an adhesive glycoprotein that mediates cell-to-cell and cell-to-matrix interactions. This protein can bind to fibrinogen, fibronectin, laminin, type V collagen and integrins alpha-V/beta-1. This protein has been shown to play roles in platelet aggregation, angiogenesis, and tumorigenesis.
TNFAIP6	Tumor Necrosis Factor, Alpha-Induced Protein 6	4.34	3.60×10^{-4}	The protein encoded by this gene is a secretory protein. The hyaluronan-binding domain is known to be involved in extracellular matrix stability and cell migration. This gene can be induced by proinflammatory cytokines such as tumor necrosis factor alpha and interleukin-1.
VCAN	Versican	5.06	3.18×10^{-4}	This protein is a major component of the extracellular matrix. It is involved in cell adhesion, proliferation, migration and angiogenesis and plays a central role in tissue morphogenesis and maintenance.
VEGFA	Vascular endothelial growth factor A	3.47	3.20×10^{-4}	This protein is a glycosylated mitogen that specifically acts on endothelial cells and has various effects, including mediating increased vascular permeability, inducing angiogenesis, vasculogenesis and endothelial cell growth, promoting cell migration, and inhibiting apoptosis.

3.6.2 MSCs treated with conditioned medium (array group B)

To assess the changes of the global gene expression patterns of MSCs after incubation with conditioned medium, the medium of *in vitro* cultured EPCs was collected and distributed to cultured MSCs. After 24 h, RNA was isolated and used for microarray analyses (n = 4). The comparison between MSCs$^{con\text{-}med}$ and the respective control cells revealed 180 differentially expressed probe sets corresponding to 119 genes of which 97 genes were significantly up-regulated and 22 significantly down-regulated. These significantly regulated genes were analyzed for their affiliation regarding the GO database and KEGG pathway over-representation (Figure 32). The analysis revealed several genes affiliated with inflammatory processes, e.g. BIRC3, PTGS2 and IL6 (Table 17).

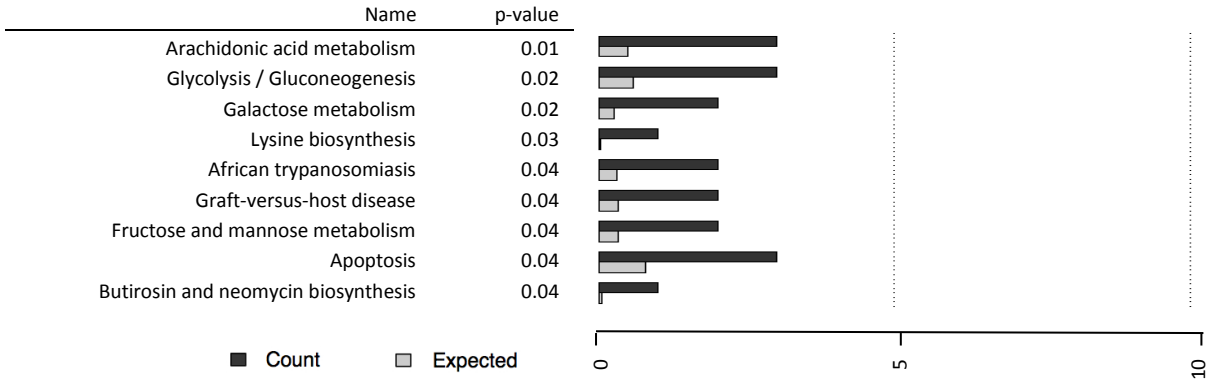

Figure 32: KEGG pathway over-representation of MSCs$^{con\text{-}med}$ (array group B)
All 119 significantly regulated genes were assigned to KEGG signaling pathways. Illustrated are all pathways, which were over-represented according to their corresponding p-values. Gray bars indicate the expected count of gene regulations for each pathway, whereas black bars demonstrate the actual count. Corresponding p-values are results of the hyper-geometric tests.

Table 17: Selection of genes differentially expressed in MSCs$^{con\text{-}med}$ (array group B)
Shown are differentially expressed genes with logFc >1. Results were revealed by the microarray analysis of MSCs after treatment with conditioned EPC medium. The table provides information about the degree of regulation (logFC) and the corresponding p-value. Positiv logFCs indicate up-regulation of the corresponding gene compared to the control cells. GeneCards Summary provides information about the function of the protein (source: www.genecards.org; 2014-11). logFC = logarithmic fold change; adj.P.Val = adjusted p-value

Symbol	GeneName	logFC	adj.P.Val	Function (GeneCards Summary)
BIRC3	baculoviral IAP repeat containing 3	1.85	4.39 x10^{-3}	Multi-functional protein which regulates not only caspases and apoptosis, but also modulates inflammatory signaling and immunity, mitogenic kinase signaling and cell proliferation, as well as cell invasion and metastasis. Member of the IAP family of proteins that inhibit apoptosis by binding to tumor necrosis factor receptor-associated factors TRAF1 and TRAF2.
PTGS2	prostaglandin-endoperoxide synthase 2 (prostaglandin G/H synthase and cyclooxygenase)	1.48	7.02 x10^{-3}	This gene encodes the inducible isozyme. It is regulated by specific stimulatory events, suggesting that it is responsible for the prostanoid biosynthesis involved in inflammation and mitogenesis. Critical component of colonic mucosal wound repair. Mediates the formation of prostaglandins from arachidonate.
CPM	carboxypeptidase M	1.34	0.01	Specifically removes C-terminal basic residues (Arg or Lys) from peptides and proteins. It is believed to play important roles in the control of peptide hormone and growth factor activity at the cell surface, and in the membrane-localized degradation of extracellular proteins.
STC1	stanniocalcin 1	1.32	4.64 x10^{-3}	This gene encodes a secreted, homodimeric glycoprotein that is expressed in a wide variety of tissues and may have autocrine or paracrine functions. The protein may play a role in the regulation of renal and intestinal calcium and phosphate transport, cell metabolism, or cellular calcium/phosphate homeostasis.
SOD2	superoxide dismutase 2, mitochondrial	1.25	7.02 x10^{-3}	Mitochondrial protein that forms a homotetramer and binds one manganese ion per subunit. This protein binds to the superoxide byproducts of oxidative phosphorylation and converts them to hydrogen peroxide and diatomic oxygen. Mutations in this gene have been associated with idiopathic cardiomyopathy (IDC), premature aging, sporadic motor neuron disease, and cancer.
IL6	interleukin 6 (interferon, beta 2)	1.21	0.01	This gene encodes a cytokine that functions in inflammation and the maturation of B cells. The protein is primarily produced at sites of acute and chronic inflammation, where it is secreted into the serum and induces a transcriptional inflammatory response through interleukin 6 receptor, alpha.
GCH1	GTP cyclohydrolase 1	1.20	6.51 x10^{-3}	The encoded protein is the first and rate-limiting enzyme in tetrahydrobiopterin (BH4) biosynthesis, catalyzing the conversion of GTP into 7,8-dihydroneopterin triphosphate. BH4 is an essential cofactor required by aromatic amino acid hydroxylases as well as nitric oxide synthases.
SPAG4	sperm associated antigen 4	1.13	6.51 x10^{-3}	May assist the organization and assembly of outer dense fibers, a specific structure of the sperm tail.
PION (GSAP)	pigeon homolog (Drosophila); (Gamma-Secretase Activating Protein)	1.09	7.02 x10^{-3}	Regulator of gamma-secretase activity, which specifically activates the production of beta-amyloid protein (beta-amyloid protein 40 and beta-amyloid protein 42), without affecting the cleavage of other gamma-secretase targets such has Notch.
C7orf63	chromosome 7 open reading frame 63	1.07	8.97 x10^{-3}	-
CD200	CD200 molecule	1.05	7.02 x10^{-3}	The protein encoded by this gene is a type-1 membrane glycoprotein, which contains two immunoglobulin domains, and thus belongs to the immunoglobulin superfamily. Studies of the related genes in mouse and rat suggest that this gene may regulate myeloid cell activity and delivers an inhibitory signal for the macrophage lineage in diverse tissues.

3.6.3 EPCs co-cultured with MSCs (array group C)

To assess the changes of the global gene expression patterns of EPCs after direct cell-cell contact with MSCs, both types of cells were co-cultured for 24 h before being separated by FACS. RNA was isolated and used for microarray analyses (n = 4). The comparison between EPCs$^{co\text{-}cu}$ and the respective control cells revealed 923 differentially expressed probe sets corresponding to 613 genes of which 501 genes were significantly up-regulated and 112 significantly down-regulated. These significantly regulated genes were analyzed for their affiliation regarding the GO database and KEGG pathway over-representation (Figure 33). An overview of selected results is provided in Table 18. The analysis revealed several important cellular processes affiliated with extracellular matrix (ECM) interactions, focal adhesion, osteoclast differentiation and TGF-beta signaling. In the GO class of biological processes, clusters of differentially expressed genes belonging to different subclasses of vasculature development (e.g. angiogenesis, blood vessel development and response to wounding) were discovered. Similarly, regulations associated with e.g. growth factor binding, cytokine and chemokine activities could be assigned along the main GO categories. Gene regulation in subclasses of higher interest is shown in detail in subsequent sections.

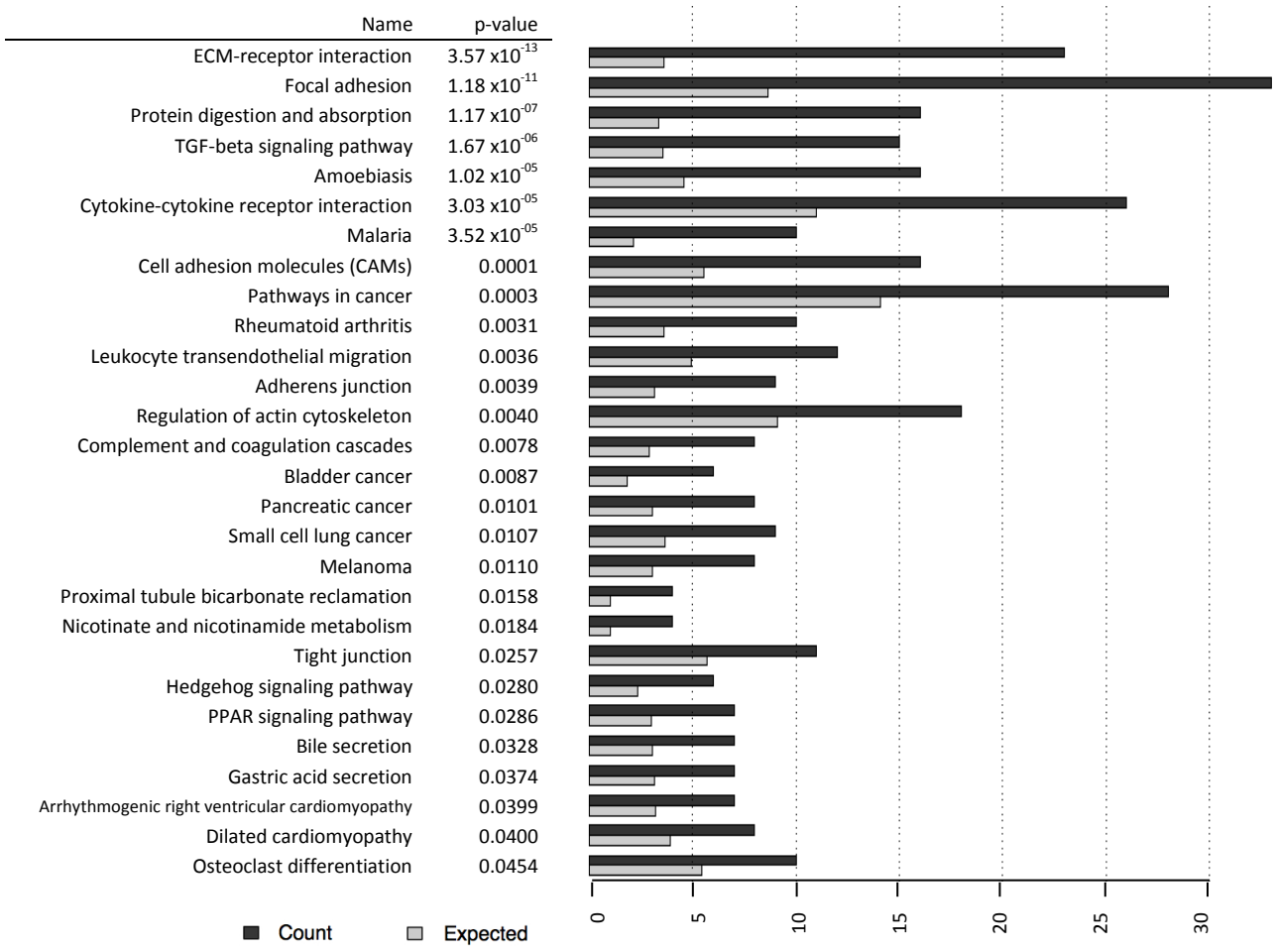

Figure 33: KEGG pathway over-representation of EPCs$^{co\text{-}cu}$ (array group C)
All 613 significantly regulated genes were assigned to KEGG signaling pathways. Illustrated are all pathways, which were over-represented according to their corresponding p-values. Grey bars indicate the expected count of gene regulations for each pathway, whereas black bars demonstrate the actual count. Corresponding p-values are results of the hyper-geometric tests.

Table 18: Gene Ontology (GO) analysis and KEGG pathway over-representation for EPCs$^{co\text{-}cu}$ (array group C)
All 613 significantly regulated genes were continuatively assigned to GO terms and KEGG signaling pathways. Illustrated are, in addition to the corresponding subclass name, the expected count, actual count and overall number of genes (N) associated to the GO/KEGG term. These values were related to and corrected by the total number of all and differentially expressed corresponding genes present on the chip. Odds ratio of corrected values is provided by the fraction (N/actual count). Corresponding p-values are results of the hyper-geometric tests.

GO/KEGG term	p-value	Odds ratio	Expected count	Actual count	N
KEGG pathways					
ECM-receptor interaction	3.57×10^{-13}	9.13	3.63	23	84
Focal adhesion	1.18×10^{-11}	4.92	8.65	33	200
TGF-beta signaling pathway	1.67×10^{-06}	5.22	3.54	15	82
Cytokine-cytokine receptor interaction	3.03×10^{-05}	2.71	10.99	26	254
Cell adhesion molecules (CAMs)	1.10×10^{-4}	3.31	5.53	16	128
PPAR signaling pathway	0.028	2.54	2.98	7	69
Osteoclast differentiation	0.045	1.94	5.45	10	126
Molecular functions (MF)					
Growth factor binding	3.94×10^{-17}	10.19	3.80	28	104
Polysaccharide binding	9.58×10^{-14}	5.95	6.62	32	181
Glycosaminoglycan binding	1.37×10^{-13}	6.33	5.89	30	161
Extracellular matrix structural constituent	4.73×10^{-13}	9.88	2.89	21	79
Insulin-like growth factor binding	3.99×10^{-10}	21.10	0.91	11	25
Platelet-derived growth factor binding	4.58×10^{-10}	71.26	0.40	8	11
Vascular endothelial growth factor receptor binding	8.98×10^{-4}	26.46	0.21	3	6
Platelet-derived growth factor receptor binding	9.75×10^{-4}	11.77	0.47	4	13
Low-density lipoprotein particle binding	9.75×10^{-4}	11.77	0.47	4	13
Cytokine receptor binding	1.04×10^{-3}	2.50	7.28	17	199
Biological processes (BP)					
Cardiovascular system development	1.35×10^{-25}	4.40	25.81	89	681
Vasculature development	3.66×10^{-25}	5.23	17.63	72	465
Cell migration	1.31×10^{-24}	4.19	27.18	90	717
Blood vessel development	2.44×10^{-24}	5.26	16.75	69	442
Cell adhesion	5.92×10^{-23}	3.70	33.25	98	877
Response to wounding	1.40×10^{-19}	3.20	38.86	101	1025
Blood vessel morphogenesis	8.24×10^{-19}	4.75	14.78	57	390
Cell differentiation	9.37×10^{-18}	2.40	88.07	166	2323
Chemotaxis	3.30×10^{-17}	3.84	20.73	66	547
Angiogenesis	2.20×10^{-15}	4.58	12.39	47	327
Cell communication	4.82×10^{-15}	2.03	163.60	247	4315
Regulation of endothelial cell proliferation	3.37×10^{-8}	7.22	2.61	15	69
Endothelial cell proliferation	2.68×10^{-7}	6.00	3.03	15	80
Endothelial cell migration	2.72×10^{-7}	5.55	3.45	16	91
Sprouting angiogenesis	7.78×10^{-7}	9.56	1.40	10	37
Regulation of angiogenesis	1.10×10^{-6}	4.16	5.23	19	138
Blood vessel endothelial cell migration	2.04×10^{-6}	7.29	1.89	11	50
Cellular components (CC)					
Extracellular region part	5.29×10^{-35}	4.44	37.66	126	1026
Extracellular matrix	1.48×10^{-32}	6.82	14.68	75	400
Extracellular region	2.83×10^{-26}	3.02	69.85	162	1903
Collagen	7.35×10^{-10}	7.59	3.01	18	82

3.6.3.1 Selection of genes involved in ECM-receptor interaction

The bioinformatical investigation of the data set identified a cluster of differentially expressed genes associated with extracellular matrix (ECM) interactions and focal adhesion such as cell adhesion molecules (CAMs, e.g. VCAN, VCAM1, PECAM1), collagens (type I, II, IV, V, and VI) and proteoglycans (lumican, versican, decorin). All 49 regulated genes affiliated to these pathways are listed in alphabetical order in Table 19 with their gene name and symbol. In addition, the logarithmic fold change (logFC) shows the degree of regulation (positive logFC = up-regulation; negative logFC = down-regulation). Genes with regulations of more than one probe set were reduced to the probe set with the highest logFC. 6 genes were found to be down-regulated.

To compare the degree of regulation of the individual experiments within an array group, heat maps were generated for all over-represented pathways. Heat maps are color-coded tables that show the levels of gene expression by color subclass-coding, i.e. heat-colors with white representing high expression, over yellow and orange as medium expression and red representing low expression of the corresponding probe set. Table 20 shows the top 5 differentially regulated genes affiliated with ECM interactions and focal adhesion with their corresponding heat map. The first 4 columns of the heat map reflect regulations in the control EPCs and the following 4 columns the corresponding gene regulation after co-culturing EPCs with MSCs. The heat map illustrates that regulations occurred uniformly in all 4 individual experiments.

3.6.3.2 Selection of genes affiliated to angiogenesis

In addition to the bioinformatic analysis of the microarray data, a google search using the search criteria “genes involved in angiogenesis” (2014-11) as well as a search on NCBI PubMed (2014-11) were used to identify genes affiliated to angiogenesis. The findings included growth factors and their receptors, chemokines and cytokines, matrix and adhesion molecules, proteases and their inhibitors, as well as transcription factors. This list was compared to the list of significantly regulated genes. The analysis revealed 28 differentially expressed genes, all involved in the development of new blood vessels, of which 1 gene was down-regulated. The results are shown in alphabetical order with additional information about the degree of the regulation indicated by the logarithmic fold change (logFC) as well as information from the literature about the function (Table 21).

3.6.3.3 Selection of genes affiliated to osteogenesis

The analysis of the microarray data revealed a cluster of significantly regulated genes belonging to the KEGG pathway osteoclast differentiation (KEGG ID: 04380). In addition to the bioinformatical analysis, the lists of significantly regulated genes were searched for genes known to be affiliated with bone metabolism and remodeling. The analysis revealed 18 differentially expressed genes e.g. klotho, TNFRSF11b (OPG), BMP2 and FGF2 of which 2 genes were down-regulated (CSF-1 and MITF) (Table 22). The corresponding heat map shows gene regulations within the osteoclast differentiation pathway. Levels of gene expression are visualized by color-coding with white representing high expression, over yellow and orange as medium expression and red representing low expression of the corresponding probe set. The first 4 columns of the heat map reflect regulations in the control EPCs and the following 4 columns the corresponding gene regulation after co-culturing EPCs with MSCs. The heat map illustrates that regulations occurred uniform in all 4 individual experiments.

3.6.3.4 Selection of genes affiliated with the Wnt signaling pathway

The bioinformatical analysis of the data set identified 15 differentially expressed genes associated with the wingless (Wnt) signaling pathway, e.g. klotho (KL), dickkopf Wnt signaling pathway inhibitor 1 (DKK1), insulin-like growth factor binding protein 4 (IGFBP4), wingless-type MMTV integration site family, member 5A (Wnt5A) and Wnt5B. In addition to the bioinformatic analyses of the microarray data, a search on NCBI PubMed (2015-02) and the Wnt homepage (http://web.stanford.edu/group/nusselab/cgi-bin/wnt/; 2015-02) were used to identify genes affiliated to the Wnt signaling pathway. The results are shown in alphabetical order with additional information about the degree of the regulation indicated by the logarithmic fold change (logFC) as well as information from the literature about the function (Table 23).

Table 19: Differentially regulated genes in EPCs$^{co\text{-}cu}$ affiliated with the KEGG pathways ECM-receptor interaction, focal adhesion and cell adhesion molecules (CAMs) (array group C)

Differentially regulated genes are shown in alphabetical order next to the degree of regulation (logFC) and the corresponding p-value. Positiv logFCs indicate up-regulation, negativ logFCs indicate down-regulation of the corresponding gene compared to the control cells. Affiliations to a specific pathway are indicated as follows: [a] = KEGG ID 04510 – focal adhesion, [b] = KEGG ID 04512 – ECM-receptor interaction, [c] = KEGG ID 04514 – cell adhesion molecules (CAMs); logFC = logarithmic fold change; adj.P.Val = adjusted p-value

Symbol	GeneName	logFC	adj.P.Val
ALCAM[c]	activated leukocyte cell adhesion molecule	-1.16	0.03
BIRC3[a]	baculoviral IAP repeat containing 3	-1.78	0.01
CADM1[c]	cell adhesion molecule 1	1.47	0.03
CAV1[a]	caveolin 1, caveolae protein, 22kDa	5.59	2.71×10^{-6}
CAV2[a]	caveolin 2	3.07	1.07×10^{-4}
CD226[c]	CD226 molecule	1.04	0.04
CD36[b]	CD36 molecule (thrombospondin receptor)	-1.57	0.03
CD40[c]	CD40 molecule, TNF receptor superfamily member 5	-1.04	0.04
CDH2[c]	cadherin 2, type 1, N-cadherin (neuronal)	2.50	8.40×10^{-4}
CLDN11[c]	claudin 11	1.24	0.02
CLDN23[c]	claudin 23	1.19	0.02
COL11A1[a b]	collagen, type XI, alpha 1	2.08	2.46×10^{-3}
COL1A1[a b]	collagen, type I, alpha 1	8.32	8.17×10^{-8}
COL1A2[a b]	collagen, type I, alpha 2	7.84	8.09×10^{-8}
COL3A1[a b]	collagen, type III, alpha 1	7.14	9.21×10^{-8}
COL4A1[a b]	collagen, type IV, alpha 1	3.09	2.82×10^{-5}
COL4A2[a b]	collagen, type IV, alpha 2	2.58	6.68×10^{-4}
COL5A1[a b]	collagen, type V, alpha 1	2.91	2.37×10^{-4}
COL5A2[a b]	collagen, type V, alpha 2	5.10	1.09×10^{-6}
COL6A1[a b]	collagen, type VI, alpha 1	1.95	0.01
COL6A2[a b]	collagen, type VI, alpha 2	1.04	0.05
COL6A3[a b]	collagen, type VI, alpha 3	5.32	1.32×10^{-5}
EGFR[a]	epidermal growth factor receptor	1.17	0.02
F11R[c]	F11 receptor	1.22	0.02
FLT1[a]	fms-related tyrosine kinase 1 (vascular endothelial growth factor/vascular permeability factor receptor)	-1.00	0.08
FN1[a b]	fibronectin 1	2.29	0.03
IBSP[a b]	integrin-binding sialoprotein	2.04	0.02
ITGAL[c]	integrin, alpha L (antigen CD11A (p180), lymphocyte function-associated antigen 1; alpha polypeptide)	-1.32	0.02
ITGB3[a b]	integrin, beta 3 (platelet glycoprotein IIIa, antigen CD61)	1.30	0.02
ITGB8[a bc]	integrin, beta 8	2.98	0.01
JAM3[c]	junctional adhesion molecule 3	1.00	0.03
LAMA4[a b]	laminin, alpha 4	2.77	9.86×10^{-4}
LAMB1[a b]	laminin, beta 1	3.53	3.78×10^{-5}
LAMC1[a b]	laminin, gamma 1 (formerly LAMB2)	1.95	4.29×10^{-3}
MET[a]	met proto-oncogene (hepatocyte growth factor receptor)	3.43	5.99×10^{-4}
MYLK[a]	myosin light chain kinase	2.75	8.70×10^{-4}
NEGR1[c]	neuronal growth regulator 1	1.14	0.05
PARVA[a]	parvin, alpha	2.37	6.32×10^{-4}
PDGFRA[a]	platelet-derived growth factor receptor, alpha polypeptide	3.61	1.11×10^{-4}
PDGFRB[a]	platelet-derived growth factor receptor, beta polypeptide	1.20	0.02
PECAM1[c]	platelet/endothelial cell adhesion molecule 1	1.42	0.02
SDC2[bc]	syndecan 2	1.72	8.87×10^{-3}
THBS1[a b]	thrombospondin 1	4.80	2.49×10^{-3}
THBS2[a b]	thrombospondin 2	3.84	9.52×10^{-5}
TNC[a b]	tenascin C	3.50	7.05×10^{-4}
VCAM1[c]	vascular cell adhesion molecule 1	2.34	0.01
VCAN[c]	versican	4.31	6.93×10^{-5}
VEGFA[a]	vascular endothelial growth factor A	1.74	0.01
VEGFC[a]	vascular endothelial growth factor C	3.48	1.46×10^{-5}

Table 20: Representative example of a heat map for the top 5 differentially regulated genes in EPCs$^{co\text{-}cu}$ from Table 19 (array group C)

Levels of gene expression are visualized by colorsubclass-coding, i.e. heat-colors with white representing high expression, over yellow and orange as medium expression and red representing low expression of the corresponding probe set. logFC = logarithmic fold change; adj.P.Val = adjusted p-value; control = control EPCs; CoCu = co-cultured EPCs; C9-C12 = array identification number (array group C, array no. 9-12)

Symbol	GeneName	logFC	adj.P.Val
COL1A1	collagen, type I, alpha 1	8.32	8.17 x10^{-8}
COL1A2	collagen, type I, alpha 2	7.84	8.09 x10^{-8}
COL3A1	collagen, type III, alpha 1	7.14	9.21 x10^{-8}
CAV1	caveolin 1, caveolae protein, 22kDa	5.59	2.71 x10^{-6}
COL6A3	collagen, type VI, alpha 3	5.32	1.32 x10^{-5}
CD40	CD40 molecule, TNF receptor superfamily member 5	-1.04	0.04
ALCAM	activated leukocyte cell adhesion molecule	-1.16	0.03
ITGAL	integrin, alpha L (antigen CD11A (p180), lymphocyte function-associated antigen 1; alpha polypeptide)	-1.32	0.02
CD36	CD36 molecule (thrombospondin receptor)	-1.57	0.03
BIRC3	baculoviral IAP repeat containing 3	-1.78	0.01

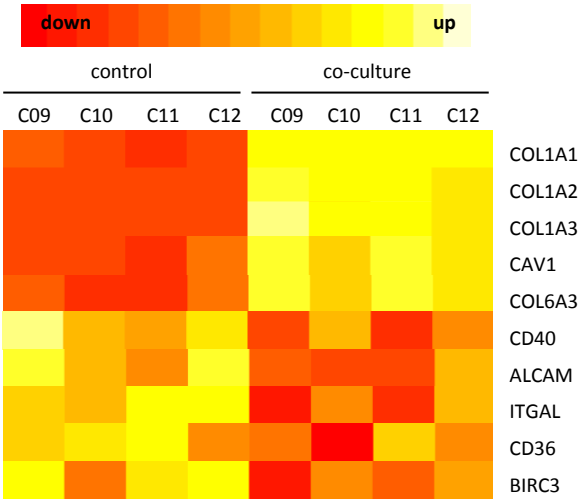

Table 21: Differentially regulated genes in EPCs$^{co\text{-}cu}$ affiliated with angiogenesis and blood vessel development (array group C)

Differentially regulated genes are shown in alphabetical order next to the degree of regulation (logFC) and the corresponding p-value. Positive logFCs indicate up-regulation, negative logFCs indicate down-regulation of the corresponding gene compared to the control cells. logFC = logarithmic fold change; adj.P.Val = adjusted p-value; [1] = source: www.genecards.org (2014-11)

Symbol	GeneName	logFC	adj.P.Val	Function related to angiogenesis
ANPEP (CD13)	alanyl (membrane) aminopeptidase	1.39	0.03	CD13 is a large cell surface peptidase expressed on the monocytes and activated endothelial cells that is important for homing to and resolving the damaged tissue at sites of injury (Subramani et al. 2013).
CTGF (CCN2)	connective tissue growth factor	6.29	8.23×10^{-8}	CTGF can be produced by and act on many cell types, including fibroblasts, smooth muscle, endothelial, neural, and cancer cells. It can influence several functions of endothelial cells, including in vitro proliferation and tube formation, cell adhesion and migration, and induction of angiogenesis in vivo (Chang et al. 2006).
CXCL5	chemokine (C-X-C motif) ligand 5	3.70	4.29×10^{-3}	This protein is proposed to bind the G-protein coupled receptor chemokine (C-X-C motif) receptor 2 to recruit neutrophils, to promote angiogenesis and to remodel connective tissues.[1]
CXCL6	chemokine (C-X-C motif) ligand 6 (granulocyte chemotactic protein 2)	3.22	0.01	HIF-1α is upregulated in hepatocellular carcinoma cell lines and tissues and its effect on promoting invasion and metastasis is mediated by its direct interaction with the pro-angiogenic chemokine CXCL6 (Tian et al. 2014). Sun et al. developed a microcarrier-based *in vitro* angiogenesis system and showed CXCL6 to be differentially regulated during endothelial capillary morphogenesis (Sun et al. 2005)
CYR61 (CCN1)	cysteine-rich, angiogenic inducer, 61	4.78	1.77×10^{-6}	Both CTGF and CYR61 can promote endothelial cell growth, migration, adhesion and survival in vitro. Both members of the CCN family participate in a variety of direct and indirect mechanisms by which angiogenesis is regulated through their autocrine action as products of endothelial cells as well as in paracrine action (Brigstock 2002).
EREG	epiregulin	3.16	3.86×10^{-3}	Epiregulin is involved in certain physiological processes such as maintenance or development of normal cell growth, and the progression of carcinomas (Toyoda et al. 1997). As a mitogen it may stimulate cell proliferation and/or angiogenesis.[1]
FGF2	fibroblast growth factor 2 (basic)	2.66	2.98×10^{-4}	Treatment of surgical periodontal defect in early diabetic rats with the single application of FGF-2 provided beneficial effects on new bone formation via increasing cell proliferation and regulating angiogenesis (Bizenjima et al. 2014).
FLT1	fms-related tyrosine kinase 1 (vascular endothelial growth factor/vascular permeability factor receptor)	-1.00	0.08	Placental growth factor (PlGF) is a proangiogenic factor sharing high homology with vascular endothelial growth factor, whereas soluble FMS-like tyrosine kinase-1 (sFlt1) is a potent antagonist of vascular endothelial growth factor (VEGF) and PlGF signaling (Korevaar et al. 2014). Flt1, a naturally occurring inhibitor of VEGF suppresses angiogenesis (Ambati et al. 2006).
HEY1	hairy/enhancer-of-split related with YRPW motif 1	1.08	0.05	This gene encodes a nuclear protein belonging to the hairy and enhancer of split-related (HESR) family of basic helix-loop-helix (bHLH)-type transcriptional repressors. Downstream effector of Notch signaling which may be required for cardiovascular development.[1]
HPSE	heparanase	1.86	0.02	Facilitates cell migration associated with metastasis, wound healing and inflammation. Enhances shedding of syndecans, and increases endothelial invasion and angiogenesis in myelomas. Enhances angiogenesis through up-regulation of SRC-mediated activation of VEGF. [1] HPSE participates in angiogenesis and bone formation. It is involved in the osteogenic differentiation of rat MSCs (Han et al. 2013).
ID1	inhibitor of DNA binding 1, dominant negative helix-loop-helix protein	2.19	5.34×10^{-3}	Increased expression of Id1 and Id3 promotes tumorigenicity by enhancing angiogenesis and suppressing apoptosis in small cell lung cancer (D. Chen et al. 2014). The Id1-Id3 double knockout mice display vascular malformations in the forebrain and an absence of branching and sprouting of blood vessels into the neuroectoderm (Lyden et al. 1999). The Id1 and 3 proteins have a critical role in promoting angiogenesis during development, tumor growth and wound repair (Lee et al. 2014).
ID3	inhibitor of DNA binding 3, dominant negative helix-loop-helix protein	2.07	0.01	
ITGB3	integrin, beta 3 (platelet glycoprotein IIIa, antigen CD61)	1.30	0.02	The ITGB3 protein product is the integrin beta chain beta 3. Integrins are integral cell-surface proteins composed of an alpha chain and a beta chain.[1] Integrins such as αvβ3 play a key role in angiogenesis regulation, invasion and metastasis, inflammation, wound healing (Bi & Yi 2014). Sumimoto et al. found that vascular endothelial cells promote neurite elongation in an integrin β3-dependent manner. Vascular endothelial cells may therefore play a role in the development and repair of neural networks in the central nervous system (Sumimoto et al. 2014).

MMP2	matrix metallopeptidase 2 (gelatinase A, 72kDa gelatinase, 72kDa type IV collagenase)	1.51	0.03	This gene encodes an enzyme which degrades type IV collagen, the major structural component of basement membranes. The enzyme plays a role in endometrial menstrual breakdown, regulation of vascularization and the inflammatory response.[1] Rivilis et al. observed that MMP-2 regulation occurs independent of VEGF signaling. Their data suggest that the involvement of MMPs in capillary growth is dependent on the nature of the angiogenic stimulus (Rivilis et al. 2002).
PECAM-1	platelet/endothelial cell adhesion molecule 1	1.42	0.02	Endothelial cells plated in the presence of anti-PECAM-1 antibodies adhered normally to the culture plate but failed to establish tight cell-cell contacts and the normal cobblestone appearance. These findings provide evidence that PECAM-1 is involved in angiogenesis (DeLisser et al. 1997).
PROK2	prokineticin 2	1.40	0.04	Both PROK1 and PROK2 have been found to regulate a dazzling array of biological functions throughout the body. During development, *PROK2* appears to act as a chemoattractant factor (Balasubramanian et al. 2011).
SEMA3C	sema domain, immunoglobulin domain (Ig), short basic domain, secreted, (semaphorin) 3C	1.40	0.01	In vitro, Sema3C treatment preserved alveolar epithelial cell viability in hyperoxia and accelerated alveolar epithelial cell wound healing. Sema3C preserved lung microvascular endothelial cell vascular network formation in vitro under hyperoxic conditions. In vivo, Sema3C treatment of hyperoxic rats decreased lung neutrophil influx and preserved alveolar and lung vascular growth (Vadivel et al. 2013).
SERPINE 1 (PAI-1)	serpin peptidase inhibitor, clade E (nexin, plasminogen activator inhibitor type 1), member 1	2.35	5.02×10^{-3}	Plasminogen activator inhibitor-1 (PAI-1) regulates angiogenesis via effects on extracellular matrix proteolysis and cell adhesion (Wu et al. 2014).
TGF-α	transforming growth factor, alpha	1.31	0.02	This gene encodes a growth factor that is a ligand for the epidermal growth factor receptor, which activates a signaling pathway for cell proliferation, differentiation and development.[1] Prolyl hydroxylase-4 overexpression in tumor cells stimulated the expression of TGF-α, which was necessary and sufficient to promote angiogenic sprouting of endothelial cells (Klotzsche-von Ameln et al. 2013).
TGF-β2	transforming growth factor, beta 2	1.63	0.01	TGF-β2 may mediate repair after injury and promote wound healing by inducing morphological changes and regulating synthesis and secretion of ECM. TGF-β2 has alterative effect on the morphology of human corneal endothelial cells from polygonal phenotype to enlarged spindle-shaped phenotype, in dose and time-dependence manner by inducing more, elongation and alignment of F-actin, rearrangement of microtubule and larger spread area of collagen type IV (Wang et al. 2014).
THBS1	thrombospondin 1	1.11	0.05	Implication of THBS1 in inhibiting angiogenesis is by direct mechanism through interaction with specific receptors and indirect by influencing the activity of other mediators of angiogenesis (Surlin et al. 2014). The exact role of THBS1 in angiogenesis has been controversial: both stimulatory and inhibitory effects of THBS1 have been reported. Qian et al found that THBS1 is a multifunctional modulator of angiogenesis and are consistent with the dynamic presence of THBS1 in remodeling tissues in which matrix degradation is required (Qian et al. 1997).
THBS2	thrombospondin 2	3.84	9.52×10^{-5}	Vascular remodeling is essential for tissue repair and is regulated by multiple factors THBS2 and hypoxia/VEGF-induced activation of Akt (Bancroft et al. 2014). THBS2 is an inhibitor of angiogenesis with pro-apoptotic and anti-proliferative effects on endothelial cells. A lack of THBS2 leads to aberrant extracellular matrix remodeling providing evidence for a newly proposed function of TSP2 as a modulator of extracellular matrix remodeling (Maclauchlan et al. 2009).
TIMP1	TIMP metallopeptidase inhibitor 1	1.51	7.72×10^{-3}	The proteins encoded by this gene family are natural inhibitors of the matrix metalloproteinases (MMPs), a group of peptidases involved in degradation of the extracellular matrix.[1] Inhibition of TIMP1 increased angiogenesis into a PVA sponge in vivo and enhanced the migration of dermal human microvascular endothelial cells and fibroblasts on collagen I in vitro (Reed et al. 2003).
VCAM1	vascular cell adhesion molecule 1	2.34	0.01	Cell adhesion molecules (CAMs), such as VCAM1, modulate EC-leukocyte interactions (Rafat et al. 2012). This gene is a member of the Ig superfamily and encodes a cell surface sialoglycoprotein expressed by cytokine-activated endothelium. This type I membrane protein mediates leukocyte-endothelial cell adhesion and signal transduction.[1]
VCAN	versican	3.90	6.61×10^{-5}	This gene is a member of the aggrecan/versican proteoglycan family. The protein encoded is a large chondroitin sulfate proteoglycan and is a major component of the extracellular matrix. This protein is involved in cell adhesion, proliferation, proliferation, migration and angiogenesis and plays a central role in tissue morphogenesis and maintenance.[1]
VEGFA	vascular endothelial growth factor A	1.74	0.01	VEGFA regulates most of the endothelial response, such as the proliferation and migration of endothelial cells, vascular permeability and the selection of tip and stalk cells (Matsumoto & Ema 2014).

VEGFC	vascular endothelial growth factor C	3.48	1.46×10^{-5}	Growth factor active in angiogenesis, and endothelial cell growth, stimulating their proliferation and migration and also has effects on the permeability of blood vessels.[1] To form the coronary vasculature VEGFC is required, revealing its role as a tissue-specific mediator of blood endothelial development (H. I. Chen et al. 2014).
WNT5A	wingless-type MMTV integration site family, member 5A	3.87	4.97×10^{-4}	Overexpression of Wnt5a promotes angiogenesis in non-small-cell lung cancer (Yao et al. 2014).

Table 22: Significantly regulated genes in EPCs$^{co\text{-}cu}$ associated with osteoclast differentiation and osteogenesis (array group C)

Differentially regulated genes are shown in alphabetical order next to the degree of regulation (logFC) and the corresponding p-value. In additon, levels of gene expression by the KEGG over-representation osteoclast differentiation (ID 04380) are visualized by colorsubclass-coding, i.e. heat-colors with white representing high expression, over yellow and orange as medium expression and red representing low expression of the corresponding probe set. logFC = logarithmic fold change; adj.P.Val = adjusted p-value; control = control EPCs; CoCu = co-cultured EPCs; C9-C12 = array identification number (array group C, array no. 9-12)

Symbol	GeneName	logFC	adj.P.Val
BMP2	bone morphogenetic protein 2	1.80	0.01
CDH11	cadherin 11, type 2, OB-cadherin (osteoblast)	1.64	5.78 x10^{-3}
CSF1	colony stimulating factor 1 (macrophage)	-1.67	0.01
CTGF	connective tissue growth factor	6.29	8.23 x10^{-8}
FCGR2A	Fc fragment of IgG, low affinity IIa, receptor (CD32)	1.26	0.01
FCGR2C	Fc fragment of IgG, low affinity IIc, receptor for (CD32) (gene/pseudogene)	1.01	0.03
FGF2	fibroblast growth factor 2 (basic)	2.66	2.98 x10^{-4}
FHL2	four and a half LIM domains 2	3.97	5.15 x10^{-5}
FOSL2	FOS-like antigen 2	1.62	8.52 x10^{-3}
IBSP	integrin-binding sialoprotein	2.04	0.02
ITGB3	integrin, beta 3 (platelet glycoprotein IIIa, antigen CD61)	1.30	0.02
KL	klotho	2.94	6.42 x10^{-3}
MITF	microphthalmia-associated transcription factor	-1.11	0.02
NID2	nidogen 2 (osteonidogen)	2.22	3.01 x10^{-3}
SOCS3	suppressor of cytokine signaling 3	1.21	2.96 x10^{-2}
TGF-ß2	transforming growth factor, beta 2	1.63	1.81 x10^{-2}
TNFRSF 11B (OPG)	tumor necrosis factor receptor superfamily, member 11b	2.27	7.18 x10^{-4}
VEGFA	vascular endothelial growth factor A	1.74	0.01

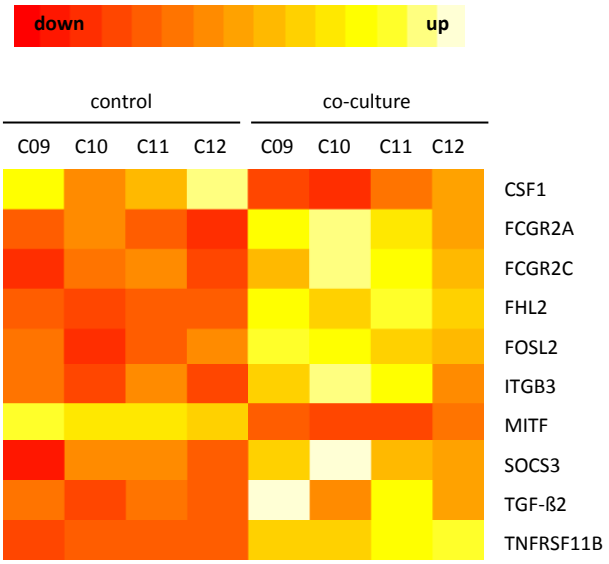

Table 23: Differentially regulated genes in EPCs$^{co\text{-}cu}$ affiliated to the Wnt signaling pathway (array group C)
Differentially regulated genes are shown in alphabetical order next to the degree of regulation (logFC) and the corresponding p-value. Positive logFCs indicate up-regulation, negative logFCs indicate down-regulation of the corresponding gene compared to the control cells. logFC = logarithmic fold change; adj.P.Val = adjusted p-value; [1] = www.genecards.org (2015-02); [2] = www.ncbi.nlm.nih.gov (2015-02)

Symbol	GeneName	logFC	adj.P.Val	Function
APCDD1L	adenomatosis polyposis coli down-regulated 1-like	1.21	0.02	May function as a Wnt inhibitor. Soluble APCDD1 binds to Wnt3a and to the extracellular domain of LRP5 in vitro, and it inhibits Wnt/β-catenin signaling in cultured cells, possibly by preventing Fz from binding to Wnt (Cruciat & Niehrs 2013).
DKK1	dickkopf 1 homolog (Xenopus laevis); Dickkopf WNT Signaling Pathway Inhibitor 1	1.54	6.30×10^{-3}	Antagonizes canonical Wnt signaling by inhibiting low density lipoprotein receptor-related protein (LRP) 5/6 interaction with Wnt and by forming a ternary complex with the transmembrane protein KREMEN that promotes internalization of LRP5/6. In the adult, DKKs are implicated in bone formation and bone disease, cancer and Alzheimer disease.[1] DKK1 antagonizes Wnt–LRP5 signaling to regulate physiological levels of bone mass (Cruciat & Niehrs 2013).
DKK3	dickkopf 3 homolog (Xenopus laevis); Dickkopf WNT Signaling Pathway Inhibitor 3	2.53	1.97×10^{-3}	In contrast to other DKK family members, DKK3 does not bind LRP6 and does not affect Wnt signaling, but rather regulates transforming growth factor-β (TGF-β) signaling (Cruciat & Niehrs 2013).
IGFBP3	insulin-like growth factor binding protein 3	6.14	4.39×10^{-7}	Wnt stimulation exerted its antiproliferative effects through a previously unappreciated activation of IGFBP3, which requires intact IGF binding site for its action (Oikonomopoulos et al. 2011).
IGFBP4	insulin-like growth factor binding protein 4	1.47	0.01	Antagonizes Wnt/β-catenin signaling. It binds directly to LRP6 and Fz8 via the carboxy-terminal thyroglobulin domain and blocks binding of Wnt3a to the receptors (Cruciat & Niehrs 2013) .
IGFBP5	insulin-like growth factor binding protein 5	1.08	0.02	IGFBP5 regulation is mediated by the β-catenin-dependent Wnt pathway (B. Y. Liu et al. 2012).
IGFBP6	insulin-like growth factor binding protein 6	1.71	4.17×10^{-3}	IGFBP1, 2, and 6, but not IGFBP3 and 5, are also able to bind directly to LRP6 and Fz8 and to inhibit Wnt/β-catenin signaling, albeit with a lower efficiency compared with IGFBP4 (Cruciat & Niehrs 2013).
KL	Klotho	2.93	6.42×10^{-3}	α-klotho regulates WNT signaling. It binds to different types of Wnt ligands to suppress the downstream signaling transduction. Recombinant α-klotho protein has been shown to inhibit Wnt5A internalization and signaling in cells that overexpress Wnt5A. Klotho may therefore suppress Wnt signaling (Xu & Sun 2015).
KREMEN1	kringle containing transmembrane protein 1	1.22	0.02	This gene encodes a high-affinity dickkopf homolog 1 (DKK1) transmembrane receptor that functionally cooperates with DKK1 to block wingless (Wnt)/beta-catenin signaling.[1] Kremens bind both DKK1 and DKK2 but not DKK3 (Cruciat & Niehrs 2013).
PRKACB	protein kinase, cAMP-dependent, catalytic, beta	-1.40	0.04	The protein encoded by this gene is a member of the Ser/Thr protein kinase family and is a catalytic subunit of cAMP-dependent protein kinase. cAMP is a signaling molecule important for a variety of cellular functions. cAMP exerts its effects by activating the cAMP-dependent protein kinase, which transduces the signal through phosphorylation of different target proteins.[2]
RHOH	ras homolog family member H	1.15	0.05	The Rho family of small guanine nucleotide binding proteins belongs to one of the branches of the Ras superfamily. Whereas Rac and CDC42 have been shown to activate the c-Jun N-terminal kinase (JNK) and p38 MAP kinase pathway and mediate nuclear signaling via NFkB, RhoB and RhoH inhibit these signaling pathways in various cell systems (Troeger & Williams 2013).
SMAD3	SMAD family member 3	1.01	0.03	SMAD proteins are signal transducers and transcriptional modulators that mediate multiple signaling pathways. Regulator of chondrogenesis and osteogenesis and inhibits early healing of bone fractures.[1]
WISP1	WNT1 inducible signaling pathway protein 1	1.57	0.02	Member of the family of CCN proteins (also known as CCN4). Downstream regulator in the Wnt/Frizzled-signaling pathway. Associated with cell survival.[1]
WNT5A	wingless-type MMTV integration site family, member 5A	3.29	3.23×10^{-4}	Ligand for members of the frizzled family of seven transmembrane receptors. Can activate or inhibit canonical Wnt signaling, depending on receptor context. In the presence of ROR2, inhibits the canonical Wnt pathway by promoting beta-catenin degradation through a GSK3-independent pathway.[1] Camilli et al. suggest that Wnt5A antagonizes the expression of klotho (Camilli et al. 2011).
WNT5B	wingless-type MMTV integration site family, member 5B	1.29	0.02	Ligand for members of the frizzled family of seven transmembrane receptors.[1]

3.6.4 MSCs co-cultured with EPCs (array group D)

To assess the changes of the global gene expression patterns of MSCs after direct cell-cell contact with EPCs, both types of cells were co-cultured for 24 h before being separated by FACS. RNA was isolated and used for microarray analyses (n = 4). The comparison between $MSCs^{co\text{-}cu}$ and the respective control cells revealed 458 differentially expressed probe sets corresponding to 319 genes of which 207 genes were significantly up-regulated and 112 significantly down-regulated. These significantly regulated genes were analyzed for their affiliation regarding the GO database and KEGG pathway over-representation (Figure 34). An overview of selected results is provided in Table 24. The analysis revealed several important cellular processes affiliated with immunomodulation, cytokine and chemokine activity and osteoclast differentiation. In the GO class of biological processes, clusters of differentially expressed genes belonging to different subclasses of immune response (e.g. immune system process, regulation of immune response, antigen processing and presentation, T cell activation) were discovered. Similarly, regulations associated with e.g. cytokine-cytokine receptor interaction, chemokine signaling pathway and cell adhesion molecules (CAMs) could be assigned along the main GO categories. Gene regulation in subclasses of higher interest will be discussed in detail in subsequent sections.

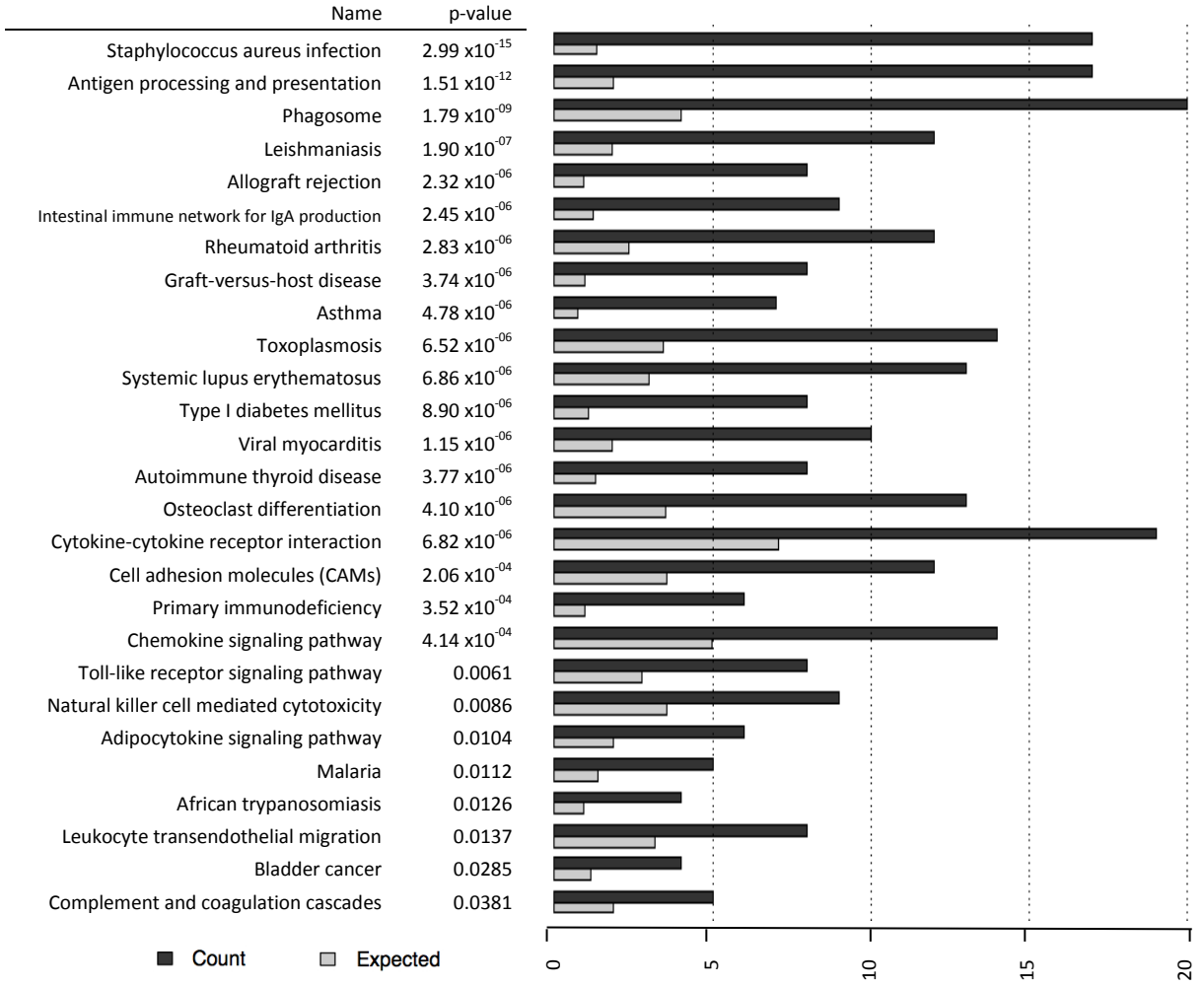

Figure 34: KEGG pathway over-representation in $MSCs^{co\text{-}cu}$ (array group D)
All 319 significantly regulated genes were assigned to KEGG signaling pathways. Illustrated are all pathways which were over-represented according to their corresponding p-values. Gray bars indicate the expected count of gene regulations for each pathway, whereas black bars demonstrate the actual count. Corresponding p-values are results of the hyper-geometric tests.

Table 24: Gene Ontology (GO) analysis and KEGG pathway over-representation for MSCs$^{co\text{-}cu}$ (array group D)
All 319 significantly regulated genes were continuatively assigned to GO terms and KEGG signalling pathways. Illustrated are, in addition to the corresponding subclass name, the expected count, actual count and overall number of genes (N) associated to the GO/KEGG term. These values were related to and corrected by the total number of all and differentially expressed corresponding genes present on the chip. Odds ratio of corrected values is provided by the fraction (N/actual count). Corresponding p-values are results of the hyper-geometric tests.

GO/KEGG term	p-value	Odds ratio	Expected count	Actual count	N
KEGG pathways					
Antigen processing and presentation	1.15×10^{-12}	13.25	1.86	17	67
Graft-versus-host disease	3.76×10^{-06}	10.86	0.97	8	35
Osteoclast differentiation	4.10×10^{-05}	4.30	3.51	13	126
Cytokine-cytokine receptor interaction	6.82×10^{-05}	3.08	7.07	19	254
Cell adhesion molecules (CAMs)	2.06×10^{-04}	3.83	3.56	12	128
Chemokine signaling pathway	3.52×10^{-04}	3.16	4.98	14	179
Molecular functions (MF)					
MHC protein binding	5.92×10^{-08}	27.95	0.38	7	20
Chemokine receptor binding	3.51×10^{-07}	11.74	0.94	9	49
Chemokine activity	9.81×10^{-07}	12.61	0.79	8	41
Cytokine activity	6.03×10^{-06}	4.06	3.77	15	195
Cytokine receptor binding	7.72×10^{-06}	4.09	3.85	15	199
MHC class II receptor activity	9.07×10^{-06}	51.36	0.15	4	8
MHC class I protein binding	8.58×10^{-05}	22.82	0.25	4	13
Biological processes (BP)					
Immune response	8.96×10^{-48}	8.77	18.65	100	949
Immune system process	3.34×10^{-45}	6.84	30.97	122	1576
Defense response	1.07×10^{-34}	6.70	18.98	86	966
Cellular response to cytokine stimulus	2.88×10^{-18}	6.85	7.13	39	363
Antigen processing and presentation	2.81×10^{-17}	11.85	2.75	25	140
Response to cytokine stimulus	6.10×10^{-17}	5.72	9.08	42	462
T cell activation	7.01×10^{-16}	6.89	5.89	33	300
Inflammatory response	2.96×10^{-15}	5.58	8.29	38	422
Cellular components (CC)					
MHC class II protein complex	5.87×10^{-10}	74.41	0.22	7	12
Cell surface	4.97×10^{-08}	3.73	8.12	27	430
Extracellular space	7.46×10^{-08}	2.91	14.70	38	778
Extracellular region part	9.91×10^{-08}	2.63	19.39	45	1026

3.6.4.1 Selection of genes involved in immunomodulation

The analysis of the microarray data revealed a cluster of significantly regulated genes belonging to the KEGG pathway graft-versus-host disease (KEGG ID: 05332). In addition to the analysis of KEGG over-representation, the lists of significantly regulated genes were searched for genes known to be affiliated with immune-regulatory processes. The analysis revealed several differentially expressed genes, e.g. IDO1, BIRC3 and a set of cell surface molecules belonging to the major histocompatibility complex (MHC). A selection of 24 genes is shown in Table 25. All of these significantly expressed genes were found to be up-regulated.

3.6.4.2 Selection of genes affiliated to osteogenesis

The analysis of the microarray data revealed a cluster of significantly regulated genes belonging to the KEGG pathway osteoclast differentiation (KEGG ID: 04380). In addition to the bioinformatical analysis, the lists of significantly regulated genes were searched for genes known to be affiliated with bone metabolism and remodeling. The analysis revealed 14 differentially expressed genes e.g. SOCS3 (Table 26). The heat map shows gene regulations within the osteoclast differentiation pathway.

Table 25: Significantly regulated genes in MSCs$^{co\text{-}cu}$ associated with immune-regulatory processes (array group D)
Differentially regulated genes are shown in alphabetical order next to the degree of regulation (logFC) and the corresponding p-value. The table also provides information about the function.
In additon, levels of gene expression of the KEGG over-representation graft-versus-host disease are visualized in a heat map, i.e. heat-colors with white representing high expression, over yellow and orange as medium expression and red representing low expression of the corresponding probe set.
logFC = logarithmic fold change; adj.P.Val = adjusted p-value; control = control MSCs; CoCu = co-cultured MSCs; D13-D16 = array identification number (array group D, array no. 13-16); MHC = major histocompatibility complex; [1] = source: www.genecards.org (2014-12)

Symbol	GeneName	logFC	adj.P.Val	Function
ALOX5	arachidonate 5-lipoxygenase	2.31	4.04 x10^{-3}	This gene encodes a member of the lipoxygenase gene family and plays a dual role in the synthesis of leukotrienes from arachidonic acid. The encoded protein is expressed specifically in bone marrow-derived cells. Leukotrienes are important mediators of a number of inflammatory and allergic conditions.[1]
B2M	Beta-2-microglobulin	1.37	3.57 x10^{-3}	Component of the class I MHC. Involved in the presentation of peptide antigens to the immune system.[1]
BIRC3	baculoviral IAP repeat containing 3	3.32	2.97 x10^{-3}	Also known as c-IAP2 (cellular inhibitor of apoptosis 2). IAP proteins are key regulators of the signaling pathways that activate NF-kB transcription factors and expression of genes controlling innate and adaptive immunity, inflammation, and cell survival and migration (Damgaard & Gyrd-Hansen 2011).
CD86	CD86 molecule	2.47	2.78 x10^{-3}	This gene encodes a type I membrane protein that is a member of the immunoglobulin superfamily. It is expressed by antigen-presenting cells.[1]
CTSH	Cathepsin H	1.30	3.57 x10^{-3}	Important for the overall degradation of proteins in lysosomes.[1]
CTSS	Cathepsin S	3.84	5.19 x10^{-4}	Cathepsin S is responsible for the generation of the MHC class I epitope (MHC class I cross-presentation pathway) (Hari et al. 2014). Key protease responsible for the removal of the invariant chain from MHC class II molecules.[1]
CXCL9	chemokine (C-X-C motif) ligand 9	4.93	3.17 x10^{-3}	Cytokine that affects the growth, movement, or activation state of cells that participate in immune and inflammatory response. Chemotactic for activated T-cells.[1]
CXCL11	chemokine (C-X-C motif) ligand 11	5.48	3.57 x10^{-3}	CXCL9 and CXCL11 bind to the CXCR3 receptor and are associated with a variety of human diseases including chronic inflammation, immune dysfunction, cancer and metastasis (Billottet et al. 2013). CXCR3 signaling pathway may serve as a coordinator of wound remodeling (Huen & Wells 2012).
CXCL16	chemokine (C-X-C motif) ligand 16	1.19	1.34 x10^{-3}	CXCL16 is a recently discovered chemokine produced by several inflammatory cells and representing an important pathogenic mediator in the development of progressive heart failure (Borst et al. 2014, p.16).
HLA-DMB	major histocompatibility complex, class II, DM beta	2.10	1.12 x10^{-3}	The MHC is a set of cell surface molecules encoded by a large gene family which controls a major part of the immune system in all vertebrates. In humans, the MHC is also called the human leukocyte antigen (HLA). MHC class II (MHC II) determinants present antigens to $CD4^+$ T cells, which are the main regulators of the immune response (Drozina et al. 2005). Peptides presented by MHC class II molecules are predominantly from materials acquired by endocytosis (external antigens) (Hari et al. 2014). Recent studies involving MSCs demonstrated that interferon (IFN)–γ stimulation induces MHC class II–mediated antigen presentation in MSCs both in vitro and in vivo (François et al. 2009). MSCs function as immune suppressors, express MHC-II, are phagocytic, and support T-cell cytotoxicity. Chan et al. showed that these contradictory properties of MSCs are important for BM homeostasis and occur partly through antigen presentation within a narrow window (Chan et al. 2006).
HLA-DPA1	major histocompatibility complex, class II, DP alpha 1	2.14	3.26 x10^{-3}	
HLA-DPB1	major histocompatibility complex, class II, DP beta 1	1.25	3.44 x10^{-3}	
HLA-DQA1	major histocompatibility complex, class II, DQ alpha 1	4.29	1.11 x10^{-4}	
HLA-DQB1	major histocompatibility complex, class II, DQ beta 1	3.04	1.83 x10^{-3}	
HLA-DRA	major histocompatibility complex, class II, DR alpha	3.63	1.86 x10^{-3}	
HLA-E	major histocompatibility complex, class I, E	1.20	3.57 x10^{-3}	The majority of nucleated cells present endogenous antigenic peptides on major histocompatibility complex (MHC) class I molecules to $CD8^+$ T cells (François et al. 2009).
IDO1	indoleamine 2,3-dioxygenase 1	3.68	3.63 x10^{-3}	Recent data has shown a role for IDO in human MSC mediated immune suppression. IDO is involved in the inhibition of T cell proliferation by dendritic cells. MSC do not constitutively express IDO, however when stimulated with IFNγ, but not TNF-α, MSCs can be induced to express IDO (Yagi et al. 2010). As IDO-mediated T-cell inhibition depends on MSC activation, modulation of IDO activity

				might alter the immunosuppressive properties of MSCs in different therapeutic applications (Meisel et al. 2004).
IFI30	interferon, gamma-inducible protein 30	1.65	1.35 x10^{-3}	The protein encoded by this gene is a lysosomal thiol reductase. The enzyme is expressed constitutively in antigen-presenting cells and induced by gamma-interferon in other cell types. This enzyme has an important role in MHC class I and II-restricted antigen processing.[1]
IRF8	interferon regulatory factor 8	0.85	3.23 x10^{-3}	IRF8 is a transcription factor of the interferon (IFN) regulatory factor (IRF) family. It specifically binds to the upstream regulatory region of type I IFN and IFN-inducible MHC class I genes.[1]
LYZ	lysozyme	4.99	1.34 x10^{-3}	Lysozymes have primarily a bacteriolytic function; those in tissues and body fluids are associated with the monocyte-macrophage system and enhance the activity of immunoagents.[1]
S100A8	S100 calcium binding protein A8	4.48	1.27 x10^{-4}	S100A8 is a calcium- and zinc-binding protein which plays a prominent role in the regulation of inflammatory processes and immune response.[1] It has been shown to be associated with osteoblast differentiation (Zreiqat et al. 2007, p.8). Grevers et al. demonstrated that the alarmin S100A8 stimulates both osteoclast formation and osteoclast function (Grevers et al. 2011, p.8).
SOCS3	suppressor of cytokine signaling 3	2.12	8.54 x10^{-4}	Studies in different mouse models have proven the critical importance of SOCS3 in restraining inflammation and allowing optimal levels of protective immune responses against infections (Carow & Rottenberg 2014).
SOD2	superoxide dismutase 2, mitochondrial	2.82	1.34 x10^{-3}	Downregulation of SOD2 contributes to the establishment of chronic oxidative stress in aged vessels. This is accompanied by a chronic low-grade inflammatory phenotype that participates in defective endothelial vasodilation (Assar et al. 2013).
TNFSF13B (BAFF)	tumor necrosis factor (ligand) superfamily, member 13b	2.73	1.36 x10^{-3}	This cytokine is involved in the stimulation of B- and T-cell function and the regulation of humoral immunity.[1]

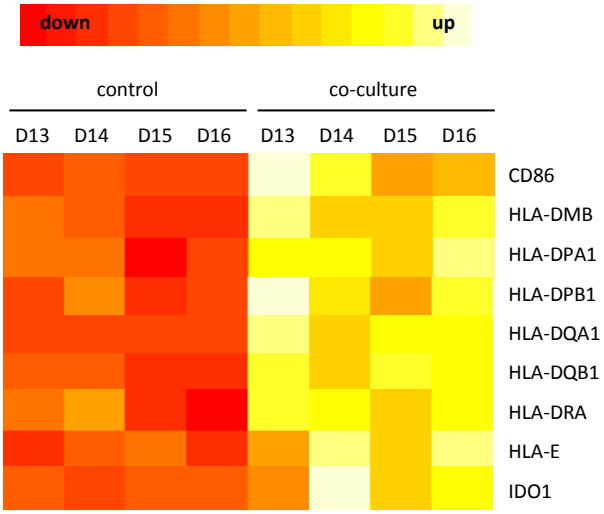

Table 26: Significantly regulated genes in MSCs$^{co\text{-}cu}$ associated with osteoclast differentiation (array group D)
Differentially regulated genes are shown in alphabetical order next to the degree of regulation (logFC) and the corresponding p-value. In additon, levels of gene expression of the KEGG pathway over-representation osteoclast differentiation are visualized by colorsubclass-coding, i.e. heat-colors with white representing high expression, over yellow and orange as medium expression and red representing low expression of the corresponding probe set. logFC = logarithmic fold change; adj.P.Val = adjusted p-value; D13-D16 = array identification number (array group D, array no. 13-16)

Symbol	GeneName	logFC	adj.P.Val
CYBB	cytochrome b-245, beta polypeptide	3.85	2.85 x10^{-4}
FCGR2A	Fc fragment of IgG, low affinity IIa, receptor (CD32)	1.84	2.72 x10^{-3}
FCGR2B	Fc fragment of IgG, low affinity IIb, receptor (CD32)	1.03	4.93 x10^{-3}
FCGR2C	Fc fragment of IgG, low affinity IIc, receptor for (CD32) (gene/pseudogene)	0.65	6.56 x10^{-3}
IFNAR2	interferon (alpha, beta and omega) receptor 2	0.61	3.82 x10^{-3}
JUNB	jun B proto-oncogene	0.93	2.78 x10^{-3}
LCP2	lymphocyte cytosolic protein 2 (SH2 domain containing leukocyte protein of 76kDa)	2.30	5.19 x10^{-4}
LILRB1	leukocyte immunoglobulin-like receptor, subfamily B (with TM and ITIM domains), member 1	1.82	3.65 x10^{-3}
NCF2	neutrophil cytosolic factor 2	1.69	3.67 x10^{-3}
NCF4	neutrophil cytosolic factor 4, 40kDa	1.02	3.86 x10^{-3}
RELB	v-rel reticuloendotheliosis viral oncogene homolog B	0.91	4.48 x10^{-3}
S100A8	S100 calcium binding protein A8	4.48	1.27 x10^{-4}
SOCS3	suppressor of cytokine signaling 3	2.12	8.54 x10^{-4}
TYROBP	TYRO protein tyrosine kinase binding protein	3.19	1.15 x10^{-3}

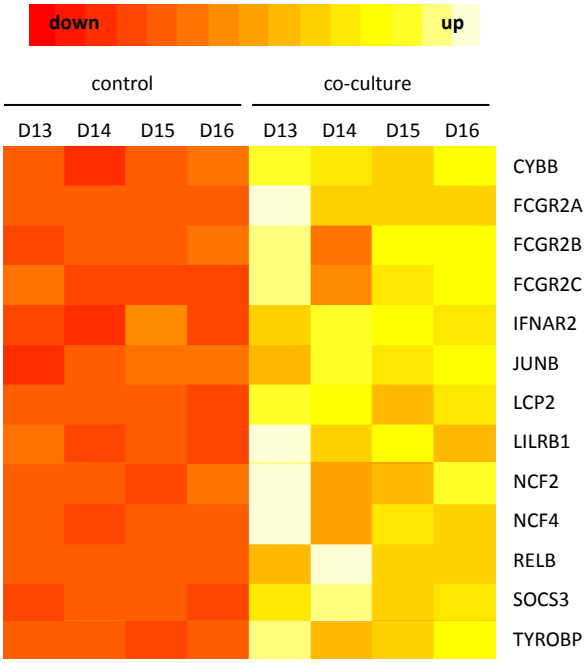

3.7 Re-evaluation of microarray data by semi-quantitative RT-PCR

The results of differential gene regulation obtained by Affymetrix array analyses employing the GeneChip® Human Genome U133 Plus 2.0 were re-evaluated by semi-quantitative RT-PCR after establishment of the respective PCR reactions and densitometric evaluation of RT-PCR bands on agarose gels. Amongst regulated genes, a selection of genes was chosen for the re-evaluation of each array group. These genes were selected due to their high fold change obtained by microarray analysis and under consideration of their functional properties. The results are shown group-wise in the subsequent chapters.
Re-evaluation by RT-PCR was accomplished with the same RNA samples, previously used for the microarray analysis (n = 4) as well as, if available, from additional experiments (indicated with AE).

3.7.1 EPCs treated with conditioned medium (array group A)

To assess the changes of the global gene expression patterns of EPCs due to humoral mediated effects by MSCs, the EPCs were incubated with conditioned medium for 24 h. Subsequently, RNA was isolated and used for microarray analyses. The comparison between $EPCs^{con\text{-}med}$ and the respective control cells revealed 514 differentially expressed genes. The results were re-evaluated by semi-quantitative RT-PCR and confirmed with densitometric analysis of the corresponding gel bands.
For this purpose, a selection of 9 regulated genes was used for the re-evaluation of the array data. The RT-PCR was performed with the same RNA probes previously used for the microarray analysis. In addition, 1 RNA sample from an additional experiment was used for the re-evaluation (Figure 37).
The densitometric analysis of the corresponding gel bands confirmed the RT-PCR findings. Accordance between microarray analysis and RT-PCR analysis was assessed under the following criteria (Table 29): same algebraic sign and a logarithmic fold change (logFC) of at least ≥ 0.5 or ≤ -0.5, respectively. Regulations with -0.5 > logFC < 0.5 were considered to be not significant in accordance with the filter used for the bioinformatical analysis of the microarray data.

8 of the 9 regulated genes showed accordance with the microarray data for all assessed samples, including the additional RNA specimen. For vascular endothelial growth factor A (VEGFA) the RT-PCR revealed no significant regulation for 1 out of the 4 RNA samples previously used for the microarray analysis. A comparison of the result with the heat map showed a similar result for the corresponding probe set.

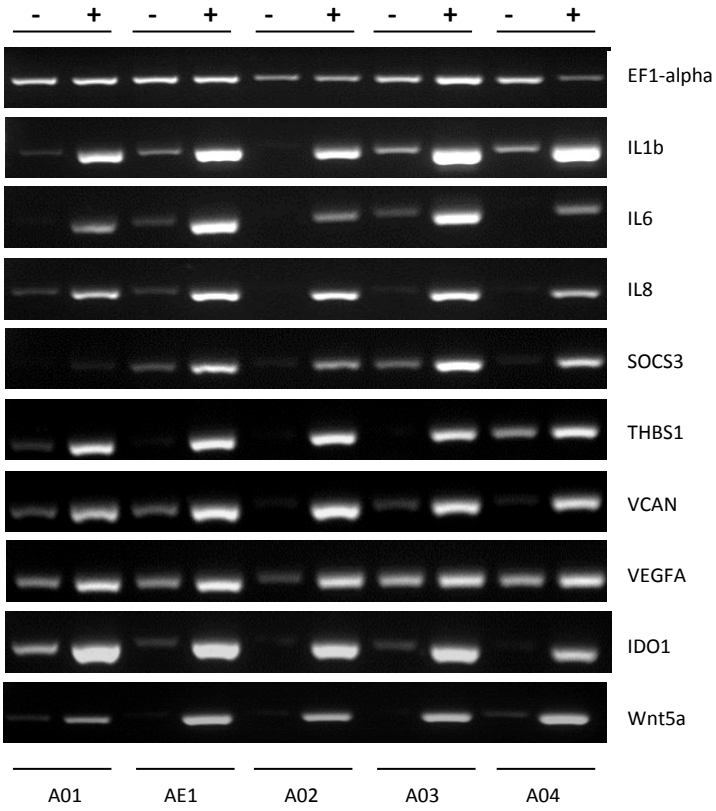

Figure 35: RT-PCR of gene regulations of EPCs$^{con\text{-}med}$ (array group A)
The EPCs treated with conditioned medium (+) were compared with non-treated (control) EPCs (-). The mRNA levels of the housekeeping gene EF1-alpha were used as internal controls. The re-evaluation of the microarray was performed with the same RNA samples used for the microarray analysis (indicated with A01 – A04) as well as with RNA from an additional experiment (indicated with AE1).
+ = EPCs$^{con\text{-}med}$; - = control EPCs; A01 – A04 = array identification number (array group A, array no. 1 - 4); AE = additional experiment; IDO1 = indoleamine 2,3-dioxygenase 1; IL1b = interleukin 1b; IL6 = interleukin 6; IL8 = interleukin 8; SOCS3 = suppressor of cytokine signaling 3; THBS1 = Thrombospondin 1; Wnt5a = wingless-type MMTV integration site family, member 5A ; VCAN = versican; VEGFA = vascular endothelial growth factor A.

Table 27: Accordance of microarray data and RT-PCR analyses of EPCs$^{con\text{-}med}$ (array group A)
Microarray data and densitometric evaluation of logarithmic fold changes (logFC) of gene regulation in EPCs$^{con\text{-}med}$. The RNA used for the RT-PCR was the same as previously used for the microarrays (A01 – A04) as well as RNA from an additional experiment (AE1). Genes with regulations of more than one probe set within the microarray data set were reduced to the probe set with the highest logFC. Levels of gene expression are also visualized by colorsubclass-coding (heat map), i.e. heat-colors with white representing high expression, over yellow and orange as medium expression and red representing low expression of the corresponding probe set.
A01 – A04 = array identification number (array group A, array no. 1 - 4); AE = additional experiment; IDO1 = indoleamine 2,3-dioxygenase 1; IL1b = interleukin 1b; IL6 = interleukin 6; IL8 = interleukin 8; SOCS3 = suppressor of cytokine signaling 3; THBS1 = thrombospondin 1; Wnt5a = wingless-type MMTV integration site family, member 5A ; VCAN = versican; VEGFA = vascular endothelial growth factor A; *italic* = no significant regulation.

Gene symbol	Identical RNA probes					Additional RNA probes	Number of accordance with microarray data
	LogFC					LogFC	
	Micro-array analysis	RT-PCR				RT-PCR	
		A01	A02	A03	A04	AE1	
IDO1	4.41	1.19	2.49	1.55	3.22	2.09	5
IL1b	3.59	2.35	2.54	1.11	2.56	1.77	5
IL6	4.00	1.61	1.47	0.92	2.71	1.67	5
IL8	4.18	1.22	1.87	1.53	2.40	1.74	5
SOCS3	2.76	0.68	0.83	0.66	2.64	1.12	5
THBS1	6.16	1.33	1.30	1.43	1.47	1.96	5
Wnt5a	3.94	1.18	2.36	2.83	3.32	2.88	5
VCAN	5.06	0.97	1.64	0.82	2.56	0.98	5
VEGFA	3.47	0.67	0.67	*0.08*	1.42	0.55	4

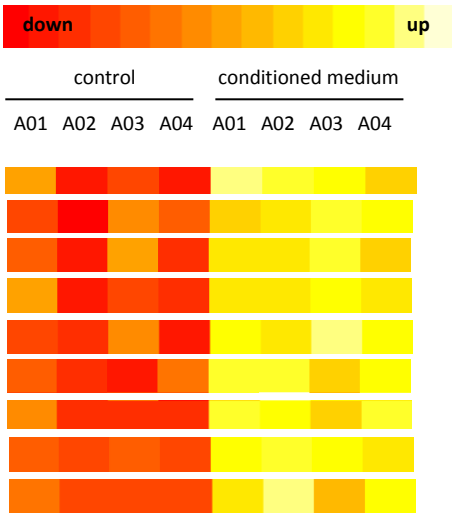

3.7.2 MSCs treated with conditioned medium (array group B)

To assess the changes of the global gene expression patterns of MSCs due to humoral mediated effects by EPCs, the MSCs were incubated with conditioned medium for 24 h. Subsequently, RNA was isolated and used for microarray analyses. The comparison between $MSCs^{con\text{-}med}$ and the respective control cells revealed 119 differentially expressed genes. The results were re-evaluated by semi-quantitative RT-PCR and confirmed with densitometric analysis of the corresponding gel bands.
For this purpose, a selection of 5 regulated genes was used for the re-evaluation of the array data. The RT-PCR was performed with the same RNA probes previously used for the microarray analysis (Figure 36). The densitometric analysis of the corresponding gel bands confirmed the RT-PCR findings. Accordance between microarray analysis and RT-PCR analysis was assessed under the following criteria (Table 28): same algebraic sign and a logarithmic fold change (logFC) of at least ≥ 0.5 or ≤ -0.5, respectively. Regulations with -0.5 > logFC < 0.5 were considered to be not significant in accordance with the filter used for the bioinformatical analysis of the microarray data.

3 of 5 evaluated genes showed accordance with 3 of 4 specimens previously used for the microarray performance. 2 of 5 evaluated genes showed accordance with 1 or 0 of 4 specimens previously used for the microarray analysis, respectively. However, the RT-PCR results reflect the very low signals/regulations obtained for $MSCs^{con\text{-}med}$ by microarray analysis (highest logFC for $MSCs^{con\text{-}med}$ = 1.85). A comparison of the corresponding heat maps confirmed the RT-PCR findings.

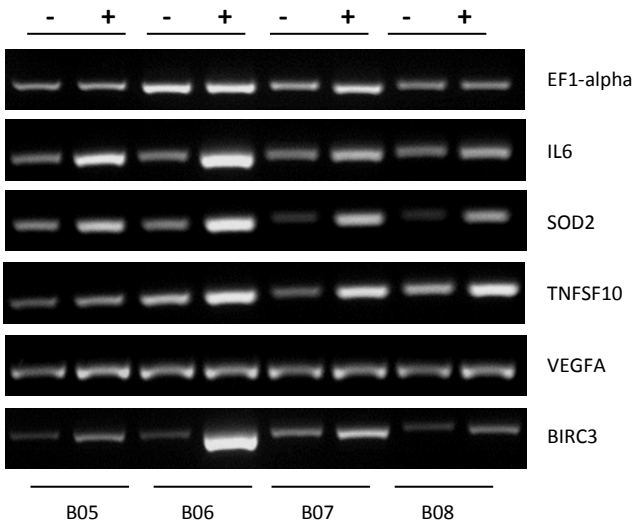

Figure 36: RT-PCR of gene regulations of MSCs$^{con\text{-}med}$ (array group B)
The MSCs treated with conditioned medium (+) were compared with non-treated (control) MSCs (-). The mRNA levels of the housekeeping gene EF1-alpha were used as internal controls. The re-evaluation of the microarray was performed with the same RNA samples used for the microarray analysis (indicated with B05 – B08).
+ = MSCs$^{con\text{-}med}$; - = control MSCs; B05 – B08 = array identification number (array group B, array no. 5 - 8); BIRC3 = baculoviral IAP repeat containing 3; IL6 = interleukin 6; SOD2 = superoxide dismutase 2; TNFSF10 = tumor necrosis factor (ligand) superfamily, member 10; VEGFA = vascular endothelial growth factor A.

Table 28: Accordance of microarray data and RT-PCR analyses of MSCs$^{con\text{-}med}$ (array group B)
Microarray data and densitometric evaluation of logarithmic fold changes (logFC) of gene regulation in MSCs$^{con\text{-}med}$. The RNA used for the RT-PCR was the same as previously used for the microarrays (B05 – B08). Genes with regulations of more than one probe set within the microarray data set were reduced to the probe set with the highest logFC. Levels of gene expression are also visualized by colorsubclass-coding (heat map), i.e. heat-colors with white representing high expression, over yellow and orange as medium expression and red representing low expression of the corresponding probe set.
B05 – B08 = array identification number (array group B, array no. 5 - 8); BIRC3 = baculoviral IAP repeat containing 3; IL6 = interleukin 6; SOD2 = superoxide dismutase 2; TNFSF10 = tumor necrosis factor (ligand) superfamily, member 10; VEGFA = vascular endothelial growth factor A; *italic* = no significant regulation.

Gene symbol	Identical RNA probes					Number of accordance with microarray data
	LogFC					
	Micro-array analysis	RT-PCR				
		B05	B06	B07	B08	
BIRC3	1.85	0.69	1.99	*0.24*	0.58	3
IL6	1.21	0.73	1.02	*0.12*	0.50	3
SOD2	1.25	*0.26*	0.89	0.89	1.15	3
TNFSF10	0.86	*0.16*	*0.46*	0.66	0.50	2
VEGFA	0.72	*0.15*	*-0.09*	*-0.15*	*0.41*	0

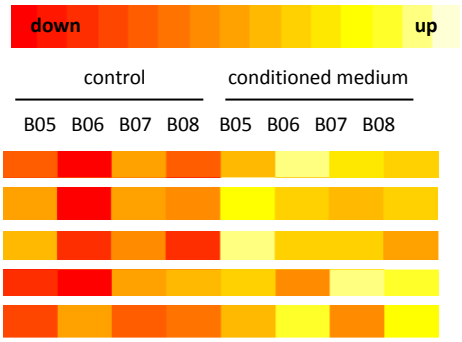

3.7.3 EPCs co-cultured with MSCs (array group C)

To assess the changes of the global gene expression patterns of EPCs after direct cell-cell contact with MSCs, both types of cells were co-cultured for 24 h before separated by FACS. RNA was isolated and used for microarray analyses. The comparison between $EPCs^{co\text{-}cu}$ and the respective control cells revealed 613 differentially expressed genes. The results were re-evaluated by semi-quantitative RT-PCR and confirmed with densitometric analysis of the corresponding gel bands. For this purpose, a selection of 7 regulated genes was used for the re-evaluation of the array data. In addition, 2 genes were included that showed no differential expression according to the microarray analysis (control). The RT-PCR was performed with the same RNA probes previously used for the microarray analysis. In addition, up to 4 RNA samples from additional experiments were used for the re-evaluation (Figure 37). Densitometric analysis of the corresponding gel bands confirmed the RT-PCR findings. Accordance between microarray analysis and RT-PCR analysis was assessed under the following criteria (Table 29): same algebraic sign and a logarithmic fold change (logFC) of at least ≥ 1 or ≤ -1, respectively. Regulations with $-1 > logFC < 1$ were considered to be not significant in accordance with the filter used for the bioinformatical analysis of the microarray data.

4 of the 7 regulated genes showed accordance with the microarray data for all assessed samples, including the additional RNA specimens. For follistatin (FST) the RT-PCR revealed no significant regulation for 1 of the RNA samples used for the microarray analysis. A comparison of the result with the heat map showed a similar result for the corresponding probe set. 1 of the 2 genes which showed no differential regulation in the microarray (control) showed no significant regulation in the RT-PCR, except for 1 RNA specimen. The other gene showed very diffuse results by meaning the results ranged from up-regulated over no significant regulation to down-regulated.
The RT-PCR for klotho showed a double-band for klotho isoform 1. The sequence analyses revealed that the lower band (300 bp) represents full-length klotho (isoform 1) while the higher band includes 50 bp of the intron sequence that is located between exon 3 and 4.

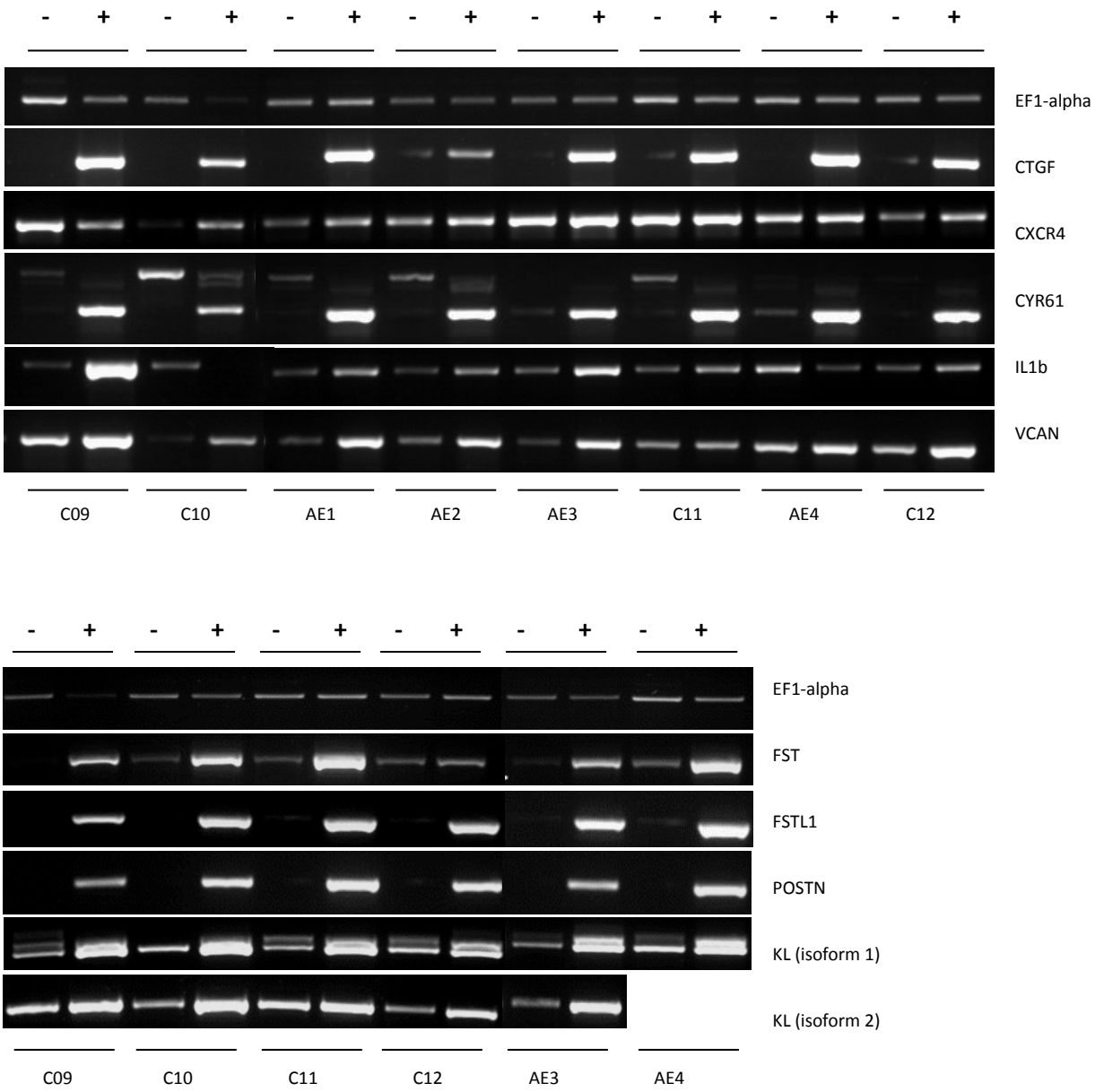

Figure 37: RT-PCR of gene regulations of EPCs$^{co\text{-}cu}$ (array group C)
The co-cultered EPCs (+) were compared with non-treated (control) EPCs (-). The mRNA levels of the housekeeping gene EF1-alpha were used as internal controls. The re-evaluation of the microarray was performed with the same RNA samples used for the microarray analysis (indicated with C09 - C12) as well as with RNA from additional experiments (indicated with AE1 - AE4).
+ = EPCs$^{co\text{-}cu}$; - = control EPCs; C09 - C12 = array identification number (array group C, array no. 9 - 12); AE = additional experiments; CTGF = connective tissue growth factor; CXCR4 = chemokine (C-X-C motif) receptor 4; CYR61 = cystein-rich protein 61; IL1b = interleukin 1b; VCAN = versican; FST = follistatin; FSTL1 = follistatin-like 1; POSTN = periostin; KL = klotho.

Table 29: Accordance of microarray data and RT-PCR analyses of EPCs$^{co\text{-}cu}$ (array group C)
Microarray data and densitometric evaluation of logarithmic fold changes (logFC) of gene regulation after co-culture of EPCs with MSCs. The RNA used for the RT-PCR was the same as previously used for the microarrays (C09-12) as well as RNA from additional experiments (AE1-4). Genes with regulations of more than one probe set within the microarray data set were reduced to the probe set with the highest logFC. Levels of gene expression are also visualized by colorsubclass-coding (heat map), i.e. heat-colors with white representing high expression, over yellow and orange as medium expression and red representing low expression of the corresponding probe set.
C09-C12 = array identification number (array group C, array no. 09-12); AE = additional experiments; CTGF = connective tissue growth factor; CXCR4 = chemokine (C-X-C motif) receptor 4; CYR61 = cystein-rich protein 61; IL1b = interleukin 1b; VCAN = versican; FST = follistatin; FSTL1 = follistatin-like 1; POSTN = periostin; KL = klotho; n.a = no regulation in microarray; n.r = not re-evaluated; *italic* = no significant regulation.

Gene symbol	Identical RNA probes					Additional RNA probes				Number of accordance with microarray data
	LogFC					LogFC				
	Micro-array analysis	RT-PCR				RT-PCR				
		C09	C10	C11	C12	AE1	AE2	AE3	AE4	
CTGF	6.29	5.31	4.82	3.68	3.40	3.94	1.89	3.62	4.64	8
CXCR4	n.a	*0.05*	4.23	*0.46*	*0.97*	*0.76*	*0.62*	*0.01*	*0.26*	-
CYR61	4.78	3.91	1.56	2.35	3.69	2.13	2.02	2.66	2.78	8
IL1b	n.a	3.97	*-0.82*	1.27	1.06	*0.84*	1.21	1.09	-1.18	-
VCAN	4.30	1.75	3.60	*0.74*	1.20	1.83	1.52	1.89	*0.61*	6
FST	3.47	2.79	2.14	2.06	*0.09*	n.r	n.r	2.28	2.21	5
FSTL1	5.39	3.66	3.95	3.21	2.84	n.r	n.r	3.38	3.44	6
POSTN	6.87	3.21	3.05	2.64	2.07	n.r	n.r	3.27	2.72	6
KL (iso1)	2.93	2.46	1.80	1.65	*0.47*	n.r	n.r	1.55	*0.82*	4
KL (iso2)		*0.99*	1.45	*0.39*	*0.84*	n.r	n.r	1.48	n.r	2

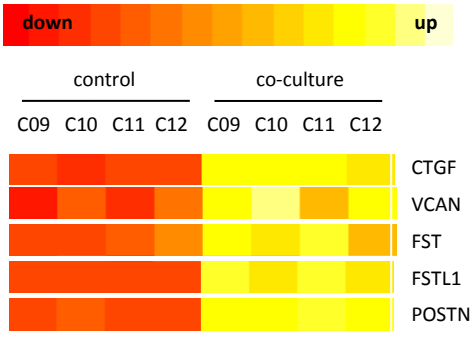

3.7.3.1 Alternative splicing of CYR61 mRNA

The RT-PCR of EPCs$^{co\text{-}cu}$ using intron 4 spanning primers for CYR61 (*CCN1 4-5*) showed 2 bands of different sizes for the treated cells in comparison to the control cells suggesting the expression of two alternate mRNA forms. CYR61 is a member of the CCN protein family (also known as CCN1). The production of CCN truncated proteins have been reported in the case of CCN2 (CTGF), CCN3 (NOV), CCN4 (WISP-1) and CCN6 (WISP-3) **(Perbal 2009)**. Julia Dotterweich from our group recently demonstrated that the interleukin-6 (IL-6)-dependent myeloma cell line INA-6 displays increased transcription and induction of splicing of intron-retaining *CCN1* pre-mRNA when cultured in contact with MSC **(Dotterweich et al. 2014)**.

To evaluate if this effect seen in INA-6 cells also affects EPCs and to assess if splicing is restricted to intron 4, additional primer pairs were used to span the remaining three exon-intron transitions (*CCN1 1-2, CCN1 2-3, CCN1 3-4*). The RT-PCR was performed using RNA specimens of 6 individual co-culture experiments.

The results show a single band for the EPCs$^{co\text{-}cu}$ representing the intron-free isoform when RT-PCR was performed using the intron 1 or intron 2 spanning primers. The respective control cells show no band. The RT-PCR of *CCN1 3-4* or *CCN1 4-5* shows two bands of different sizes representing intron-retained and intron-free *CCN1* mRNA. However, intron-free mRNA is expressed to a greater extend in the treated cells.

The results indicate that intron 3 and intron 4 of *CCN1* are affected by splicing upon contact with MSCs (Figure 38).

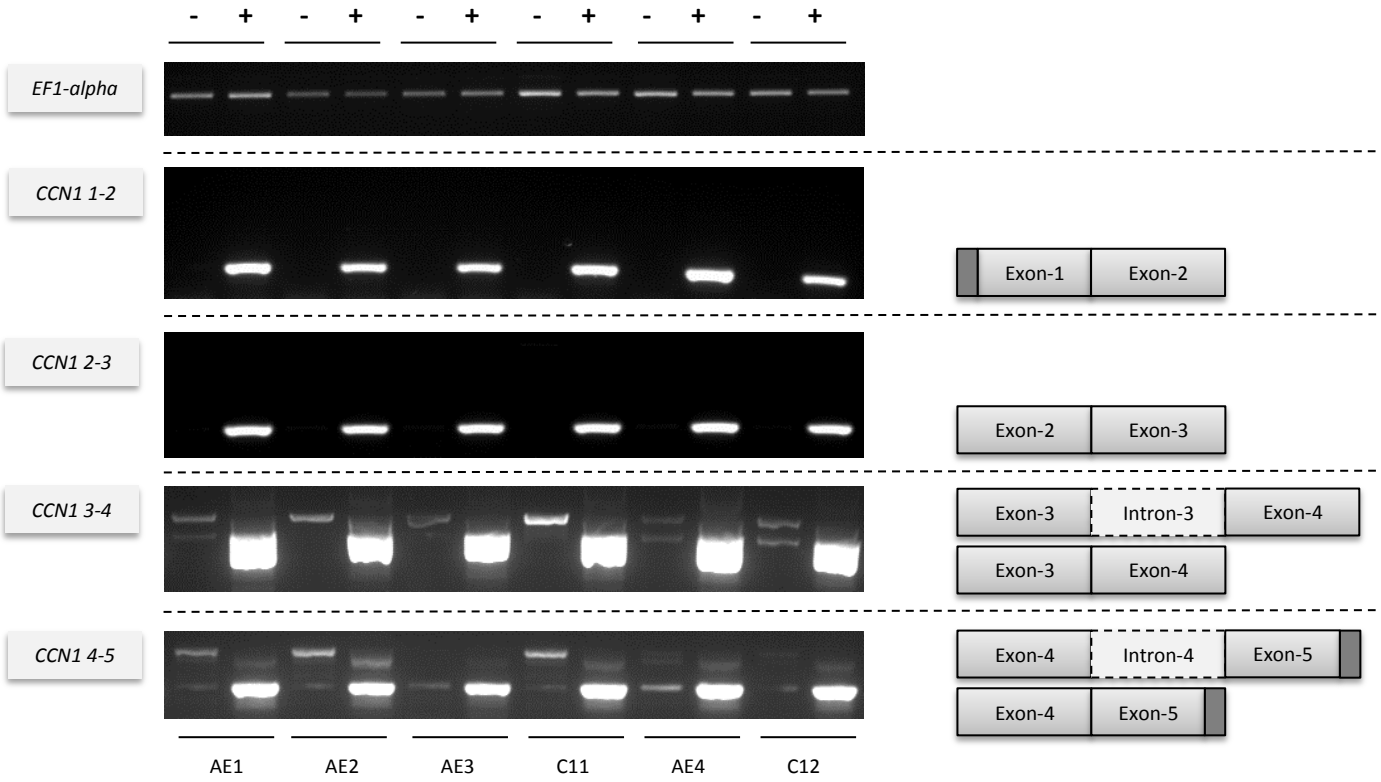

Figure 38: Splicing of *CCN1* pre-mRNA in EPCs upon contact with MSCs
The RT-PCR was performed using RNA specimens of 6 individual experiments (AE1-4, C11-C12). Co-cultured cells (+) were compared to control cells (-) using 4 different primer pairs, each spanning one of the 4 exon-intron transitions (*CCN1 1-2, CCN1 2-3, CCN1 3-4, CCN1 4-5*).

3.7.4 MSCs co-cultured with EPCs (array group D)

To assess the changes of the global gene expression patterns of MSCs after direct cell-cell contact with EPCs, both types of cells were co-cultured for 24 h before being separated by FACS. RNA was isolated and used for microarray analyses. The comparison between $MSCs^{co\text{-}cu}$ and the respective control cells revealed 319 differentially expressed genes. The results were re-evaluated by semi-quantitative RT-PCR and confirmed with densitometric analysis of the corresponding gel bands. For this purpose, a selection of 6 regulated genes was used for the re-evaluation of the array data. The RT-PCR was performed with the same RNA probes previously used for the microarray analysis. In addition, 2 RNA samples from additional experiments (AE) were used for the re-evaluation (Figure 39). Densitometric analysis of the corresponding gel bands confirmed the RT-PCR findings. Accordance between microarray analysis and RT-PCR analysis was assessed under the following criteria (Table 30): same algebraic sign and a logarithmic fold change (logFC) of at least ≥ 0.5 or ≤ -0.5, respectively. Regulations with -0.5 > logFC < 0.5 were considered to be not significant in accordance with the filter used for the bioinformatic analysis of the microarray data.
4 of the 6 regulated genes used for the re-evaluation showed accordance with the microarray data for all assessed samples, including the additional RNA specimens. The RT-PCR of superoxide dismutase 2 (SOD2) showed no significant regulation for 1 RNA specimen previously used for the microarray analysis and 1 additional RNA specimen (logFC = 0.41 or 0.47, respectively). The RT-PCR of thrombospondin 1 (THBS1), which was found to be down-regulated in microarray analysis, showed no significant regulation for 4 of the 6 assessed RNA specimens. Of the remaining two RNA specimens, 1 sample was found to be up-regulated and the other sample was found to be down-regulated.

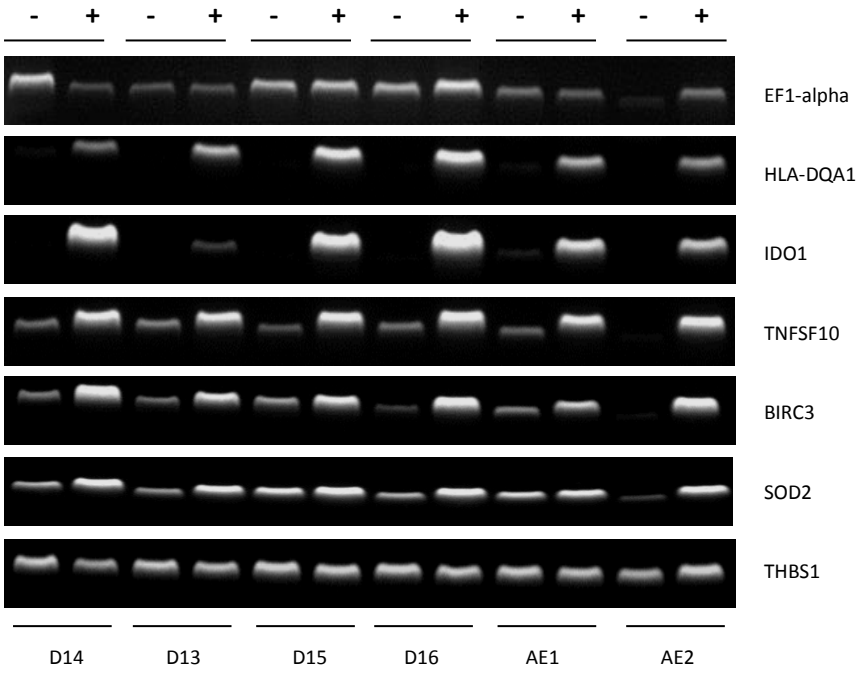

Figure 39: RT-PCR of gene regulations of MSCs^{co-cu} (array group D)
The co-cultered MSCs (+) were compared with non-treated (control) MSCs (-). The mRNA levels of the housekeeping gene EF1-alpha were used as internal controls. The re-evaluation of the microarray was performed with the same RNA samples used for the microarray analysis (indicated with D13 – D16) as well as with RNA from additional experiments (indicated with AE1 – AE2).
+ = MSCs^{co-cu}; - = control MSCs; D13 – D16 = array identification number (array group D, array no. 13 – 16); AE = additional experiments; BIRC3 = baculoviral IAP repeat containing 3; HLA-DQA1 = major histocompatibility complex, class II, DQ alpha 1; IDO1 = indoleamine 2,3-dioxygenase 1; SOD2 = superoxide dismutase 2; THBS1 = thrombospondin 1; TNFSF10 = tumor necrosis factor (ligand) superfamily, member 10.

Table 30: Accordance of microarray data and RT-PCR analyses of MSCs$^{co\text{-}cu}$ (array group D)
Microarray data and densitometric evaluation of logarithmic fold changes (logFC) of gene regulation after co-culture of MSCs with EPCs. The RNA used for the RT-PCR was the same as previously used for the microarrays (D13 – D16) as well as RNA from additional experiments (AE1 – AE2). Genes with regulations of more than one probe set within the microarray data set were reduced to the probe set with the highest logFC. Levels of gene expression are also visualized by colorsubclass-coding (heat map), i.e. heat-colors with white representing high expression, over yellow and orange as medium expression and red representing low expression of the corresponding probe set.
D13 – D16 = array identification number (array group D, array no. 13 – 16); AE = additional experiments; BIRC3 = baculoviral IAP repeat containing 3; HLA-DQA1 = major histocompatibility complex, class II, DQ alpha 1; IDO1 = indoleamine 2,3-dioxygenase 1; SOD2 = superoxide dismutase 2; THBS1 = thrombospondin 1; TNFSF10 = tumor necrosis factor (ligand) superfamily, member 10; *italic* = no significant regulation.

Gene symbol	Identical RNA probes					Additional RNA probes		Number of accordance with microarray data
	LogFC					LogFC		
	Micro-array analysis	RT-PCR				RT-PCR		
		D13	D14	D15	D16	AE1	AE2	
BIRC3	3.32	1.21	2.66	0.64	1.77	0.87	2.16	6
HLA-DQA1	4.29	2.51	2.71	2.57	2.43	2.01	1.36	6
IDO1	3.68	1.43	4.73	3.06	3.02	2.40	2.10	6
SOD2	2.82	1.13	2.11	*0.41*	0.54	*0.47*	1.21	4
THBS1	-1.79	*-0.06*	0.90	*-0.08*	*-0.44*	*0.12*	-0.50	1
TNFSF10	4.28	1.23	2.36	1.39	0.95	1.31	2.09	6

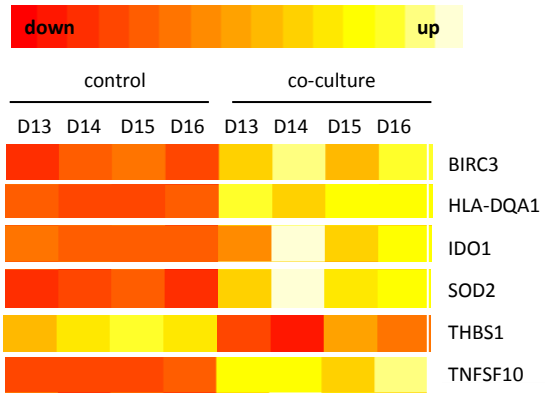

4 Results – Part II

The first part of this thesis was cell-based research at the University of Würzburg, Germany. This part was embedded in the EU project VascuBone and aimed to assess the changes of the global gene expression patterns of endothelial progenitor cells (EPCs) and mesenchymal stem cells (MSCs) after humoral contact as well as direct cell-cell contact. Therefore microarray analyses have been performed. As a result, lists with differentially regulated genes were generated.
The second part of the present study was to choose one promising candidate from these lists and to develop an ELISA (enzyme-linked immune sorbent assay) in cooperation with Immundiagnostik AG, Bensheim, Germany. The candidate of choice was klotho, a very promising and yet not well understood protein involved in important processes affiliated with bone metabolism and aging.

4.1 Klotho: Production of recombinant protein

For the development of an ELISA as well as for the generation of highly specific antibodies, target protein is needed. The recombinant human klotho protein (isoform 2: secreted) was expressed as a HIS-tagged protein (rKL) from virus-infected HEK293 cells. The HEK cell line (1 vial of HEK pExolN2-klotho: p14) was made available by Dr. Birgit Mentrup of the Orthopedic Centre of Musculoskeletal Research of the University of Würzburg. The up-scaled production (10 L bioreactor) of the rKL using the cell line was outsourced to InVivo BioTech Services GmbH in Hennigsdorf, Germany. The outcome was 1.37 mg rKL. The material was purified, sterile filtered and provided at a protein concentration of 0.28 mg/ml in PBS, pH 7.4 (batch number: RP_SZ_293/02). The certificate of analysis showed that the material had passed the quality control (Figure 40). The molecular weight of the product was stated with 60,676 Da.

Certificate of Analysis

Electrophoresis:
ID #3396
Sample identification:

1. hKlotho RP_SZ_293/02, 20µl
2. hKlotho RP_SZ_293/02, 10µl
L Prestained Protein Marker Thermo Fisher

SDS-PAGE (4-20%Tris/HEPES gele, reduced, Coomassie Blue stain)

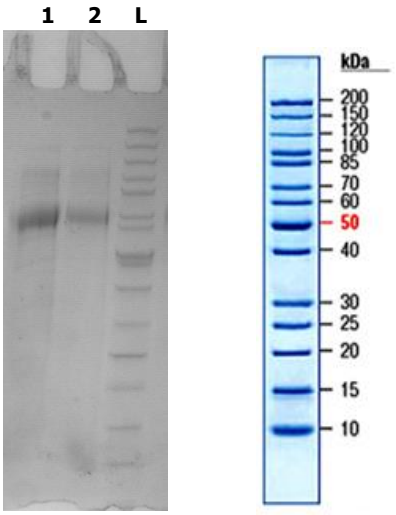

Figure 40: Quality control (certificate of analysis) of the recombinant human klotho protein
The recombinant klotho protein was produced in a 10 L bioreactor by InVivo BioTech Services GmbH. It was expressed as a HIS-tagged protein (rKL), purified, sterile filtered and provided at a concentration of 0.28 mg/ml in PBS. The purity of the rKL was determined using gel electrophoresis. The gel shows a single band at 60 kDa.

4.2 Klotho: Generation of specific antibodies

The recombinant klotho protein (Chapter 4.1) was used to generate specific antibodies. The generation and production of the antibodies was outsourced to YUMAB GmbH, Braunschweig, Germany.

4.2.1 Screening

Within the selection process to identify suitable scFv (single chain variable fragment) from the YUMAB library, 3 panning rounds have been applied. Subsequently, 92 antibody clones were screened for their binding capacity to the target antigen (klotho) and the negative control (bovine serum albumin, BSA). In brief, 100 ng of klotho and BSA, respectively, were immobilized on a microtiter plate. Supernatant of 92 antibody clones from panning round number 3 were added and detected by adding an anti-c-myc antibody followed by a goat-anti-mouse-Gc-HRP antibody. Subsequently, the substrate (TMB) was added and incubated for 30 min before the color reaction was stopped by adding 1 N sulfuric acid. The optical density was determined at 450 nm using an ELISA reader. An anti-lysozyme antibody served as positive control. 5 of the 92 clones have been identified to be positive for klotho: AF376-D2, E1, E10, F1 and H9 (Figure 41).

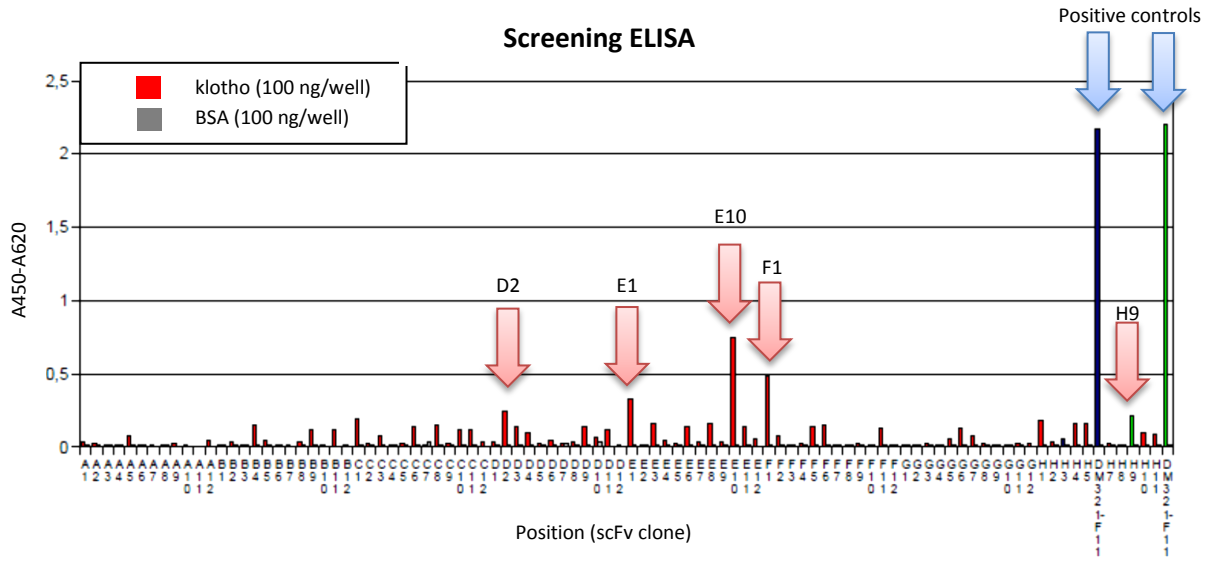

Figure 41: Screening of 92 antibody clones from panning round number 3
100 ng of klotho and BSA, respectively, have been immobilized on a microtiter plate. Supernatant of 92 different antibody clones of panning round number 3 were added and detected with an anti-c-myc antibody followed by a goat-anti-mouse-Gc-HRP antibody. The results were obtained using an ELISA reader. An anti-lysozyme antibody served as positive control. 5 clones were found to be positive to klotho: AF376-D2, E1, E10, F1 and H9.

4.2.2 Validation

In the next step, the selected antibodies from the initial screening were validated. Therefore the positive antibodies from the first screening have been re-produced and tested for their binding capacity to the target protein using a titration ELISA. Thus, the supernatant of an independent expression was applied in different dilutions to a microtiter plate coated with klotho and BSA, respectively. The detection was performed as described before for the screening ELISA.
The titration ELISA verified the results of the screening ELISA. All clones showed, in comparison to the control antigen (BSA), an elevated specific signal (Figure 42). The binding capacity seems to be lower with higher concentrations. The antibody AF376-D2 shows a very low signal.

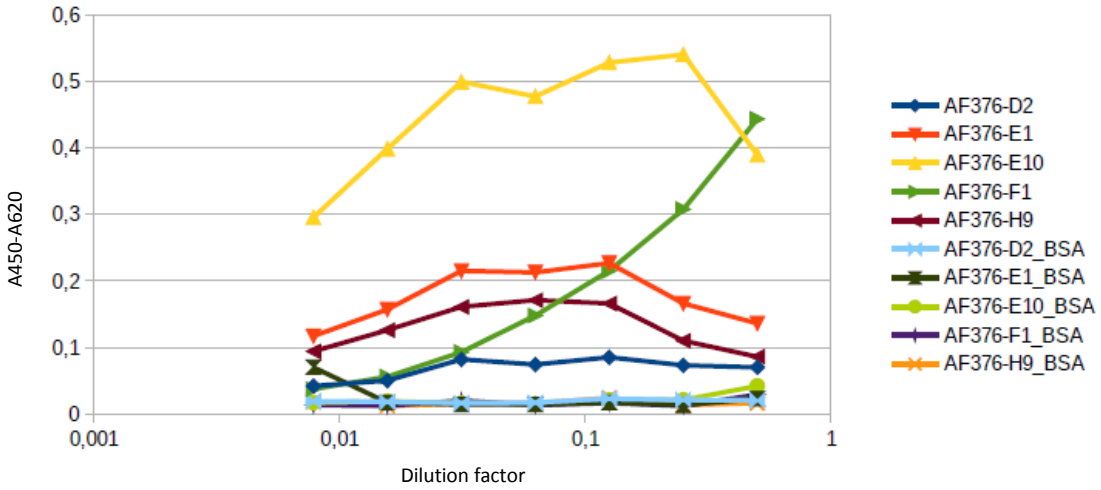

Figure 42: Titration ELISA for the positive antibody clones
To verify the results of the screening ELISA, supernatants of all positive antibody clones were re-produced (independent expression) and added in different dilutions to a microtiter plate coated with klotho and BSA, respectively. Subsequently, the same detection protocol/procedure as used for the screening ELISA was applied.

4.2.3 Sequence analysis

All positive antibody clones have been sequenced and bioinformatically analyzed by the manufacturer. All clones have been identified as being different in their sequence and therefore specific to different epitopes of the klotho protein, except for the clones D2 and H9 which have been identified to be sequence-identical.

4.2.4 Testing the antibodies for the klotho isoform 2 specific amino acid sequence

Matsumura et al. identified two transcripts that encode a membrane (1012 amino acids, isoform 1) or secreted (549 amino acids, isoform 2) klotho protein **(Matsumura et al. 1998)**. Compared with the transmembrane form protein, the secreted form does not have the second internal repeat of the extracellular domain (KL2), the transmembrane domain, or the intracellular domain (Figure 7, page 11). The KL1 subunit of the transmembrane form differs only in the 15 most C-terminal amino acid residues (Figure 8, page 12) from the KL1 domain of isoform 2.
The antibodies were generated using recombinant klotho isoform 2 protein (rKL). The following experiment aimed to test whether the antibodies are able to differentiate between isoform 1 and isoform 2 by recognizing the isoform 2 specific amino acid sequence. Therefore, the klotho isoform 2 specific amino acid sequence was synthesized. The manufacturing process was outsourced to JPT Peptide Technologies GmbH, Berlin, Germany. The outcome was 1.2 mg klotho peptide, with the

sequence H-SQLTKPISSLTKPYH-OH, a molecular weight of 1699.97 g/mol and a purity of > 95 % (confirmed by HPLC). 100 ng of the klotho peptide were made available to the manufacturer of the antibodies to test the antibody clones for their ability to bind this specific sequence. The manufacturer used the same experimental setup (direct sandwich ELISA technique) as used for the testing of the antibodies against the target protein (rKL). The test showed that the antibodies do not bind to the specific sequence H-SQLTKPISSLTKPYH-OH which differs in the KL1 domain of the secreted klotho form (isoform 2) and the soluble klotho form that is a cleaved product of the full-length transmembrane form (isoform 1). To confirm the results, the antibodies were tested in parallel at Immundiagnostik using a competitive ELISA. Therefore, a 96-well microtiterplate was coated with 1 µg/ml rKL. Uncoated wells served as negative controls. The detailed pipetting scheme is displayed in Table 32. In brief, after incubation over night at 4 °C, blocking and washing of the plate, a mixture of 0.1 µg/ml klotho specific antibodies and 40 µg/ml klotho peptide was added to respective wells. During the following incubation time, the antibody had the choice of either binding to the immobilized rKL on the plate or to a putative binding site on the klotho peptide (competition; Figure 43). Control solutions containing only klotho peptide or only klotho antibody were pipetted to respective wells. The plate was incubated for 1 h at room temperature on a horizontal shaker, before the anti-rabbit-HRP conjugate was added. After incubation for 1 h at room temperature on a horizontal shaker, the substrate (TMB) was added. The color reaction was stopped by adding stop solution and the plate was read at 450 nm. All values were determined in duplicates.

Table 31: Pipetting scheme for experiment 4.2.4
ON = over night incubation; RT = room temperature; shake = shake microtiter plate on a horizontal shaker.

Volume per well	Reactant	Time / Temperature	Condition	Washing steps
100 µl	rKL, 1 µg/ml in coating buffer or PBS 2 % BSA	ON / 4 °C	-	-
200 µl	Blocking buffer	1 h / RT	shake	5x
100 µl	0.1 µg/ml klotho antibody only or with 40 µg/ml klotho peptide or peptide only, in wash buffer	1 h / RT	shake	5x
100 µl	Conjugate: a-rabbit-HRP antibody, 1:10000 in wash buffer	1 h / RT	shake	5x
100 µl	Substrate: TMB	3 min / RT	-	-
50 µl	Stop solution	Read plate at 450 nm (reference filter: 620 nm)		

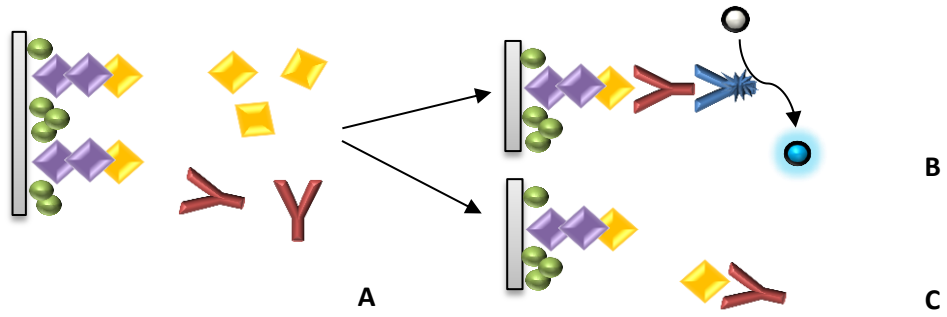

Figure 43: Principle of the competitive ELISA
A: 96-well plate coated with rKL (purple/yellow). Klotho-specific antibody (red) and klotho peptide (yellow; the 15 most C-terminal amino acids of klotho subunit KL1) were added. The klotho peptide and the rKL compete now for the binding sites of the antibody. B: The antibody binds to rKL and gets immobilized on the plate. The conjugate (blue) binds to the antibody and by adding a substrate a color reaction is visible. C: In a balanced reaction some of the antibody binds to the klotho peptide. This antibody is no longer available for the conjugate and therefore does not participate in the color reaction. Subsequently, the signal is expected to be lower than in case B.

The competition reaction showed that all 3 tested antibodies bound only to the rKL (Figure 44).
If the antibodies would recognize the 15 most C-terminal amino acids of the KL1 subunit (klotho peptide), the OD was expected to be significantly lower than for the version without klotho peptide where all antibody was free to bind to the immobilized protein. All controls were negative, indicating that no unspecific bindings took place. The result shows that the generated klotho specific antibodies recognize all klotho isoforms containing the subunit KL1, independent of the 15 amino acids that differ in the two isoforms. The test also confirmed the findings of the manufacturer of the antibodies.

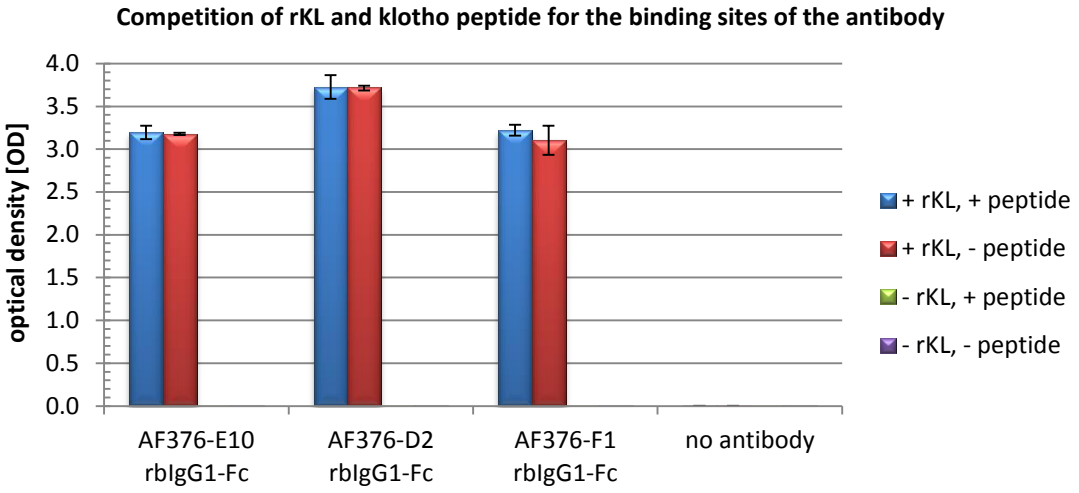

Figure 44: Competitive ELISA to determine the specificity of the antibodies for klotho isoform 2
Recombinant klotho protein (isoform 2, rKL) was immobilized on a 96-well microtiter plate (+ rKL). Control wells were uncoated (- rKL). Klotho peptide (isoform 2 specific amino acid sequence) and klotho-specific antibodies were added. Controls were with either no peptide or no antibody.
The figure shows that the signal (OD) for rKL is only the same as for the version containing klotho peptide with all 3 antibodies, indicating that no competition reaction took place. The results show that none of the antibodies recognizes the klotho isoform 2-specific amino acid sequence and therefore are specific to all klotho isoforms containing the KL1 subunit. All controls were negative showing that no unspecific bindings occurred.

4.2.5 Summary

- In total, 4 klotho specific scFv antibody clones were identified during the screening procedure.
- These clones were found to be different in their sequence in subsequent analysis.
- The antibodies bind specific to klotho and not the negative antigen (BSA).
- The antibodies recognize all klotho isoforms containing the KL1 subunit, independent of the amino acid sequence of the 15 most C-terminal amino acid residues.
- Selected antibodies were produced as scFv antibodies as well as rabbit-Fc-scFv antibodies (both provided in PBS) and delivered to Immundiagnostik AG as followed:

Name	Concentration	Lot	Amount
AF376-D2 rbIgG1-Fc	0.2 mg/ml	AF396.8	3 x 1 ml
AF376-F1 rbIgG1-Fc	0.48 mg/ml	AF396.9	1 x 1 ml
AF376-E10 rbIgG1-Fc	0.19 mg/ml	AF396.6	3 x 1 ml
AF376-D2 scFv	0.1 mg/ml	AF398.2	3 x 1 ml
AF376-F1 scFv	0.56 mg/ml	AF398.3	1 x 1 ml
AF376-E1 scFv	0.1 mg/ml	AF396.5	3 x 1 ml
AF376-E10 scFv	0.4 mg/ml	AF396.1	1 x 1 ml
AF376-H9 scFv	0.28 mg/ml	AF396.2	2 x 1 ml

4.3 Klotho: Development of an ELISA

4.3.1 Identification of suitable antibody pairs

The first step in the development of an ELISA is to test the antibodies. For the classical sandwich ELISA, two antibodies are needed: the capture antibody and the detection antibody. Usually these two antibodies are different from each other, unless the target protein possesses two identical epitopes in favorable steric configuration. A good match of antibodies should show a high signal for the target protein and a signal as low as possible for the blank. The difference between standard signal and the blank should be at least 1x OD (optical density).
The klotho specific antibody production at YUMAB GmbH resulted in 4 different antibody clones. The antibodies were made available to Immundiagnostik AG as scFv (single chain fragment variable) as well as in the format rb-IgG1-Fc (equivalent to the classical IgG antibody with rabbit (rb)-Fc fragment). To identify suitable antibody combinations, 16 wells of a 96-well plate were coated with 3 µg/ml of each of the scFv antibodies. In addition, a commercially available rabbit-anti-klotho antibody (P296 from PeproTech) was used to compare the custom-made antibodies with commercial antibodies. The pipetting scheme for this experiment is displayed in Table 32. After blocking and washing the microtiter plate, 0.5 µg/ml klotho were added to the respective wells (in duplicates). PBS was used as a negative control (blank). The plate was incubated on a horizontal shaker for 1 h at room temperature before the detection antibodies were added. Therefore 0.5 µg/ml of 3 different rb-IgG1-Fc antibodies were added to the respective wells. In addition, a commercially available goat-anti-klotho antibody was used (T-19 from Santa Cruz). The plate was incubated on a horizontal shaker for 1 h at room temperature before the conjugate (anti-rabbit-HRP and anti-goat-HRP, respectively) was added. Subsequently the substrate (TMB) was added, the color reaction was stopped by adding stop solution and the plate was read at 450 nm using an ELISA reader. The results are shown in Figure 45.

Table 32: Pipetting scheme for experiment 4.3.1
ON = over night incubation; RT = room temperature; shake = shake microtiterplate on a horizontal shaker.

Volume per well	Reactant	Time / Temperature	Condition	Washing steps
100 µl	Capture antibody: 3 µg/ml scFv antibody or P296, 1:5000 in coating buffer	ON / 4 °C	-	-
200 µl	Blocking buffer	1 h / RT	shake	5x
100 µl	0.5 µg/ml or 0 µg/ml klotho in PBS	1 h / RT	shake	5x
100 µl	Detection antibody: 0.5 µg/ml rb-IgG1-Fc antibody or T-19, 1:200 in wash buffer	1 h / RT	shake	5x
100 µl	Conjugate: a-rabbit- or a-goat-HRP antibody, 1:10000 in wash buffer	1 h / RT	shake	5x
100 µl	Substrate: TMB	7 min / RT	-	-
50 µl	Stop solution	Read plate at 450 nm (reference filter: 620 nm)		

The evaluation of the ELISA read out revealed which antibody combinations were suitable for further analysis and which combinations were unfavorable. All values were determined in duplicates. The average standard deviation of the duplicates was on the plate coated with AF376-D2 scFv mean OD ± 0.038, on AF376-F1 scFv mean OD ± 0.016, on AF376-E1 scFv mean OD ± 0.022, on AF376-E10 scFv mean OD ± 0.046, on AF376-H9 scFv mean OD ± 0.042.
Using AF376-D2 rb-IgG1-Fc as detection antibody resulted in high signals for the standard (OD > 3.5) but also very high blanks, independent of the coating antibody used (OD > 0.5 when used with AF376-F1 scFv, OD > 1.0 when used with AF376-E10 scFv and AF376-H9 scFv, OD > 3.0 when used with AF376-D2 scFv and AF376-E1 scFv).
AF376-F1-rb-IgG1-Fc showed a signal > 3.0 for the standard in all cases. Using this detection antibody, the blank was found to be < 0.05 when the plate was coated with AF376-D2 scFv, AF376-F1 scFv and AF376-H9 scFv, while the blank was slightly higher (OD = 0.102) with AF376-E1 scFv and significantly higher (OD = 0.610) with AF376-E10 scFv.
Similar results were obtained using AF376-E10 rb-IgG1-Fc as detection antibody. This antibody showed an OD > 3.0 for the standard, except for the combination with AF376-E10 scFv (OD = 1.206). The blank wasat an OD < 0.08, except for the combination with AF376-E1 (OD = 0.117).
The commercially available detection antibody T-19 showed in average a signal 7 times lower than the custom-made antibodies. The blank was in in all cases at ab OD < 0.06. The combination of the two commercial antibodies (P296 as coating antibody and T-19 as detection antibody) resulted in significantly lower results (OD = 0.259 for the standard, OD = 0.047 for the blank) than with the custom-made antibodies.

In summary, following combinations met the requirements for the development of an ELISA which are a high signal for the standard and a low signal for the blank, and are therefore favorable for further analysis (coating / detection antibody):

- AF376-**D2** scFv / AF376-**F1** rb-IgG1-FC in short: D2/F1
- AF376-**F1** scFv / AF376-**F1** rb-IgG1-FC in short: F1/F1
- AF376-**H9** scFv / AF376-**F1** rb-IgG1-FC in short: H9/F1
- AF376-**D2** scFv / AF376-**E10** rb-IgG1-FC in short: D2/E10
- AF376-**F1** scFv / AF376- **E10** rb-IgG1-FC in short: F1/E10
- AF376-**H9** scFv / AF376-**E10** rb-IgG1-FC in short: H9/E10

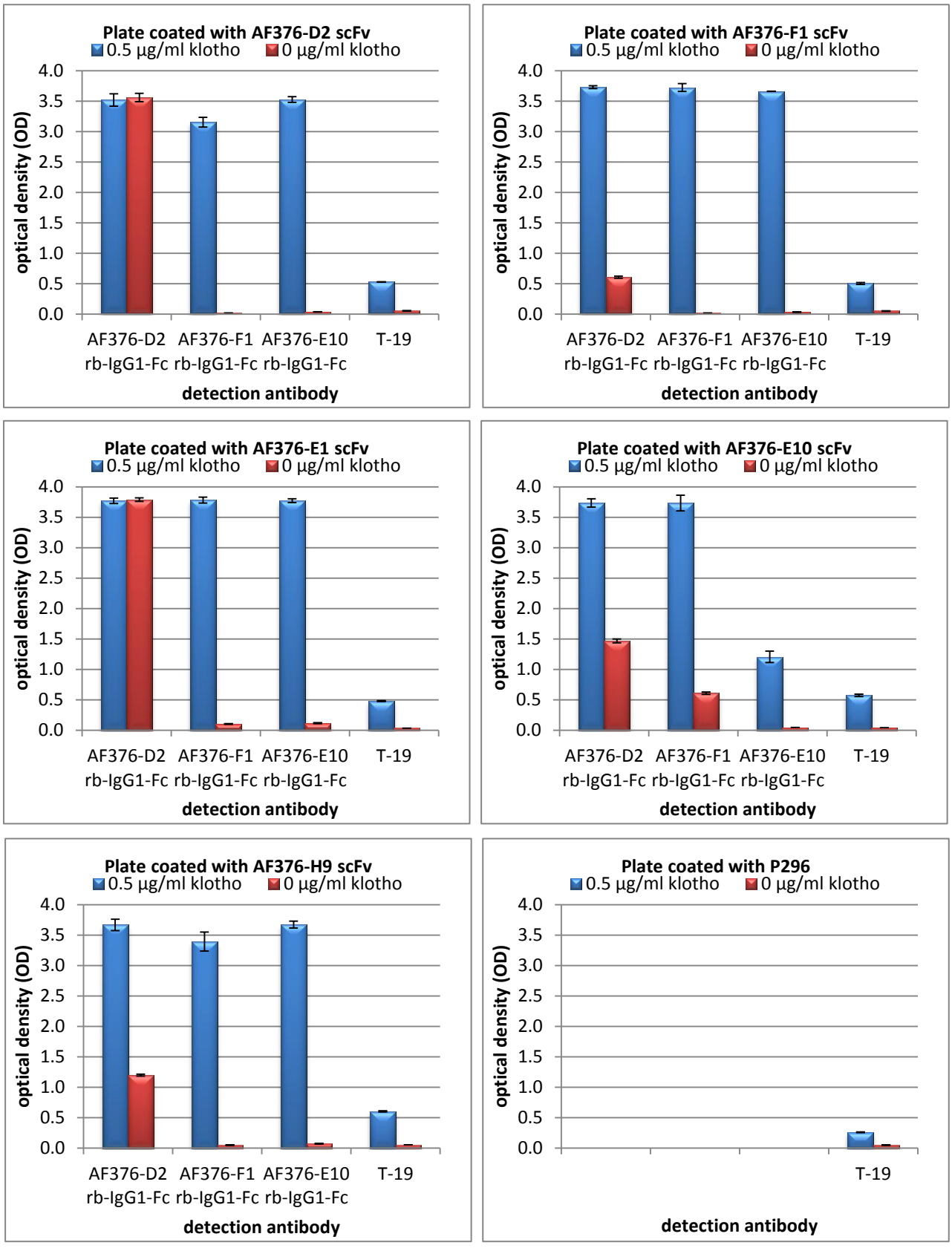

Figure 45: Identification of suitable antibody combinations

A 96-well microtiter plate was coated with different custom-made antibodies (format: scFv) and 1 commercially available antibody (P296, rabbit-a-klotho IgG from Pepro Tech). 3 different custom-made antibodies (format: rb-IgG1-Fc) and 1 commercial antibody (T-19, goat-anti-klotho IgG from Santa Cruz) were used as detection antibodies. All combinations were tested using 0.5 µg/ml klotho in PBS as a positive standard and PBS (0 µg/ml klotho) as negative standard/blank.

4.3.2 Standard curve and optimization of standard dilution buffer

To determine the concentration of a sample, each ELISA needs a standard curve (calibration curve) with known concentrations of the target protein. The standard curve is usually diluted in standard dilution buffer, which possesses similar characteristics as the sample. Therefore buffers containing protein, e.g. BSA, are very common as standard dilution buffer.
In the previous experiment, suitable pairs of antibodies have been defined. The calibrators used were 0.5 µg/ml and 0 µg/ml klotho in PBS. In the next step, a small standard curve (0, 0.125, 0.25, 0.5 µg/ml klotho) was generated to test if the standard material is dilutable. In addition, 2 different dilution buffers were compared: PBS and PBS 2 % BSA. Both versions were tested in duplicates using different antibody combinations (coating / detection antibody):

- AF376-**D2** scFv / AF376-**F1** rb-IgG1-FC in short: D2/F1
- AF376-**F1** scFv / AF376-**F1** rb-IgG1-FC in short: F1/F1
- AF376-**D2** scFv / AF376-**E10** rb-IgG1-FC in short: D2/E10
- AF376-**F1** scFv / AF376- **E10** rb-IgG1-FC in short: F1/E10

The pipetting scheme for this experiment is displayed in Table 33.

Table 33: Pipetting scheme for experiment 4.3.2
ON = over night incubation; RT = room temperature; shake = shake microtiterplate on a horizontal shaker.

Volume per well	Reactant	Time / Temperature	Condition	Washing steps
100 µl	Capture antibody: 1 µg/ml scFv antibody in coating buffer	ON / 4 °C	-	-
200 µl	Blocking buffer	1 h / RT	shake	5x
100 µl	Klotho standard curve in PBS or PBS 2 % BSA	1 h / RT	shake	5x
100 µl	Detection antibody: 0.1 µg/ml rb-IgG1-Fc antibody in wash buffer	1 h / RT	shake	5x
100 µl	Conjugate: a-rabbit-HRP antibody, 1:10000 in wash buffer	1 h / RT	shake	5x
100 µl	Substrate: TMB	10 min / RT	-	-
50 µl	Stop solution	Read plate at 450 nm (reference filter: 620 nm)		

The results are shown in Figure 46. All values were determined in duplicates. The standard deviation of the duplicates was in average mean OD ± 0.030.
The standard material was dilutable in both buffers. However, the standard curves in PBS 2 % BSA were significant lower than the standard curves in PBS for all antibody combinations, e.g. the highest calibrator in PBS was at OD = 3.757 ± 0.072 (average of all 4 different antibody combinations ± standard deviation). Setting this OD to 100 %, the highest standard in PBS 2 % BSA was 71.7 %, 37.8 %, 52.2 %, and 68.2 % lower in version D2/F1, D2/E10, F1/F1 and F1/E10, respectively. The blank was < 0.03 OD for both buffers and with all antibody combinations.
The standard curves in PBS flattened at the top end of the standard curve (formation of a plateau). The standard curves in PBS 2 % BSA showed a linear shape.

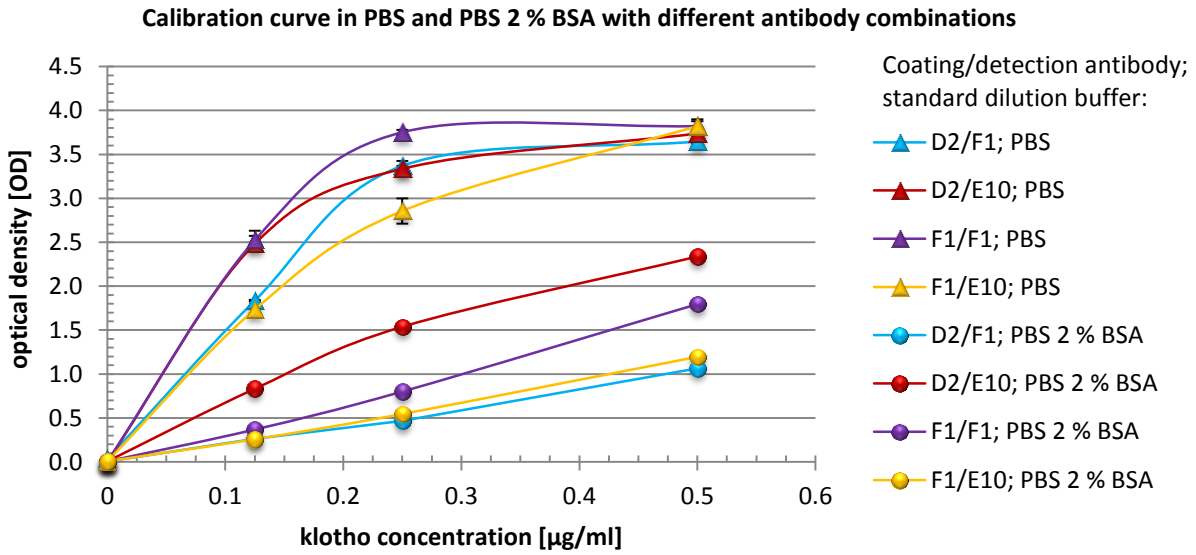

Figure 46: Standard curve in different dilution buffers with different antibody combinations
The standard curves in PBS are significantly higher than the curves in PBS 2 % BSA. The curves in PBS flatten at the top end, while the curves in PBS 2 % BSA show a linear shape.

4.3.3 Optimization of the antibody concentrations

The previous experiment showed that PBS 2 % BSA is suitable as standard dilution buffer. The standard curve was linear in the range of 0 – 0.5 µg/ml klotho with all 4 tested antibody combinations. In the next step, 4 serum samples and 4 corresponding EDTA-plasma samples were measured using the same experimental setting as described in Table 33 with the antibody combination D2/E10. The samples were from healthy donors, 2x male, 2x female, age 38 ± 5 years (mean ± standard deviation) from the blood donation service of the University of Mainz. The klotho concentration of all samples was found to be < 0.1 µg/ml. This preliminary test showed that samples from healthy donors range between the blank and the lowest standard. As shown in Figure 47, the OD of the standard with the concentration 0.125 µl/ml klotho was for all 4 antibody combinations < 1. Thus, diluting the standard material further would not result in a suitable standard curve for the determination of samples from healthy donors. Therefore the next step aimed to optimize the concentration of the capture antibody as well as the detection antibody to obtain higher ODs at lower klotho concentrations. The pipetting scheme for this experiment is shown in Table 34. The test was performed with the antibody combination D2/E10 (coating/detection antibody) using 1 µg/ml and 3 µg/ml AF376-D2 scFv in combination with 0.1 µg/ml and 1 µg/ml AF376-E10 rb-IgG1-Fc. The klotho standard curve ranged from 0 – 100 ng/ml in PBS 2 % BSA. All values were measured in duplicates.

Table 34: Pipetting scheme for experiment 4.3.3
ON = over night incubation; RT = room temperature; shake = shake microtiterplate on a horizontal shaker.

Volume per well	Reactant	Time / Temperature	Condition	Washing steps
100 µl	Capture antibody: 1 or 3 µg/ml scFv antibody in coating buffer	ON / 4 °C	-	-
200 µl	Blocking buffer	1 h / RT	shake	5x
100 µl	Klotho standard curve in PBS 2 % BSA	1 h / RT	shake	5x
100 µl	Detection antibody: 0.1 or 1 µg/ml rb-IgG1-Fc antibody in wash buffer	1 h / RT	shake	5x
100 µl	Conjugate: a-rabbit-HRP antibody, 1:10000 in wash buffer	1 h / RT	shake	5x
100 µl	Substrate: TMB	20 min / RT	-	-
50 µl	Stop solution	Read plate at 450 nm (reference filter: 620 nm)		

Using higher concentrations of the antibodies improved the ODs of the standard curve (Figure 47), therefore allowing to detect klotho concentrations in the range of 1.5 – 100 ng/ml. The best results were obtained using 3 µg/ml AF376-D2 scFv as coating antibody in combination with 1 µg/ml E10 rb-IgG1-Fc as detection antibody. These concentrations led to a 14 times higher OD for the highest standard compared to the originally used concentrations of 1 µg/ml coating antibody and 0.1 µg/ml detection antibody. Using higher concentrations of either the coating antibody or the detection antibody led to a 4 times or 3 times higher OD for the highest standard, respectively.

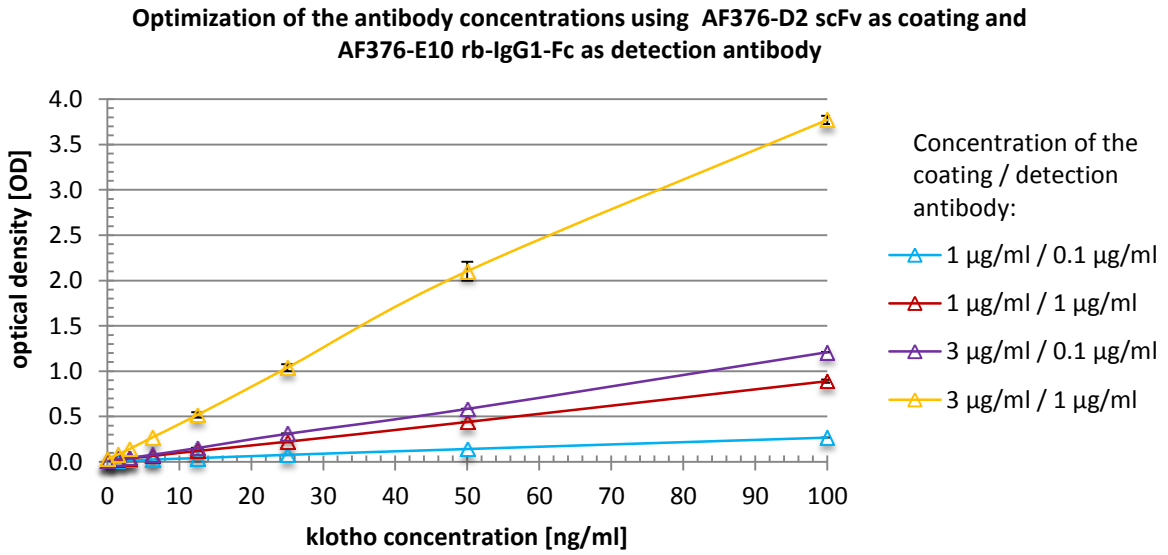

Figure 47: Optimization of the concentration of the coating and the detection antibody
The standard curve in PBS 2 % BSA ranges between 0 – 100 ng/ml. Independent of the antibody concentration, all curves are linear. Using 3 times or 10 times higher concentrations of the coating antibody or the detection antibody leads to a 4 times or 3 times higher OD for the highest standard, respectively. Using 3 times and 10 times higher concentrations of the coating antibody and the detection antibody, respectively, leads to a 14 times higher OD for the highest standard in comparison to the originally used concentration.

4.3.4 Testing the optimized ELISA version with samples of normal subjects

The optimized ELISA (standard curve in PBS 2 % BSA, coating antibody: 3 µg/ml AF376-D2 scFv, detection antibody: 1 µg/ml E10 rb-IgG1-Fc) was used to measure samples of healthy donors to determine whether this version was suitable to detect klotho in normal serum samples. At the same time, this experiment aimed to test if normal serum samples were dilutable. The linearity of a sample dilution row gives information about the specificity of the antigen-antibody binding. The samples were from healthy donors, 1x male, 5x females, and age 38 ± 5 years (mean ± standard deviation) from the blood donation service of the University of Mainz. The pipetting scheme for this experiment is shown in Table 35. All values were determined in duplicates.

Table 35: Pipetting scheme for experiment 4.3.4
ON = over night incubation; RT = room temperature; shake = shake microtiterplate on a horizontal shaker.

Volume per well	Reactant	Time / Temperature	Condition	Washing steps
100 µl	Capture antibody: 3 µg/ml scFv antibody in coating buffer	ON / 4 °C	-	-
200 µl	Blocking buffer	1 h / RT	shake	5x
100 µl	Klotho standard curve in PBS 2 % BSA, sample in PBS	1 h / RT	shake	5x
100 µl	Detection antibody: 1 µg/ml rb-IgG1-Fc antibody in wash buffer	1 h / RT	shake	5x
100 µl	Conjugate: a-rabbit-HRP antibody, 1:10000 in wash buffer	1 h / RT	shake	5x
100 µl	Substrate: TMB	25 min / RT	-	-
50 µl	Stop solution	Read plate at 450 nm (reference filter: 620 nm)		

To determine the linearity of the samples, all samples were diluted 1:2, 1:4 and 1:8 in PBS. The klotho concentrations were determined using the optimized ELISA. All samples were found within the range of the standard curve. However, all samples were located within the lower half of the curve.
Figure 48 shows the mean values of the 3 different dilutions for each sample. The error bars indicate the standard deviations. Following klotho concentrations were measured: sample 1: 29.27 ng/ml ± 2.45 ng/ml, sample 2: 21.67 ng/ml ± 1.96 ng/ml, sample 3: 41.70 ng/ml ± 6.60 ng/ml, sample 4: 35.77 ng/ml ± 7.80 ng/ml, sample 5: 7.73 ng/ml ± 1.10 ng/ml, sample 6: 50.87 ng/ml ± 0.97 ng/ml (mean ± standard deviation).

The experiment showed that the current version of the ELISA is suitable to determine samples of normal subjects. All samples were dilutable, indicating that there are no unspecific bindings, and were within the range of the standard curve. The klotho concentration ranged between 7.73 ng/ml and 50.87 ng/ml. The deviation calculated from 3 different dilutions was minimum ± 1.9 % and maximum ± 21.8 %.

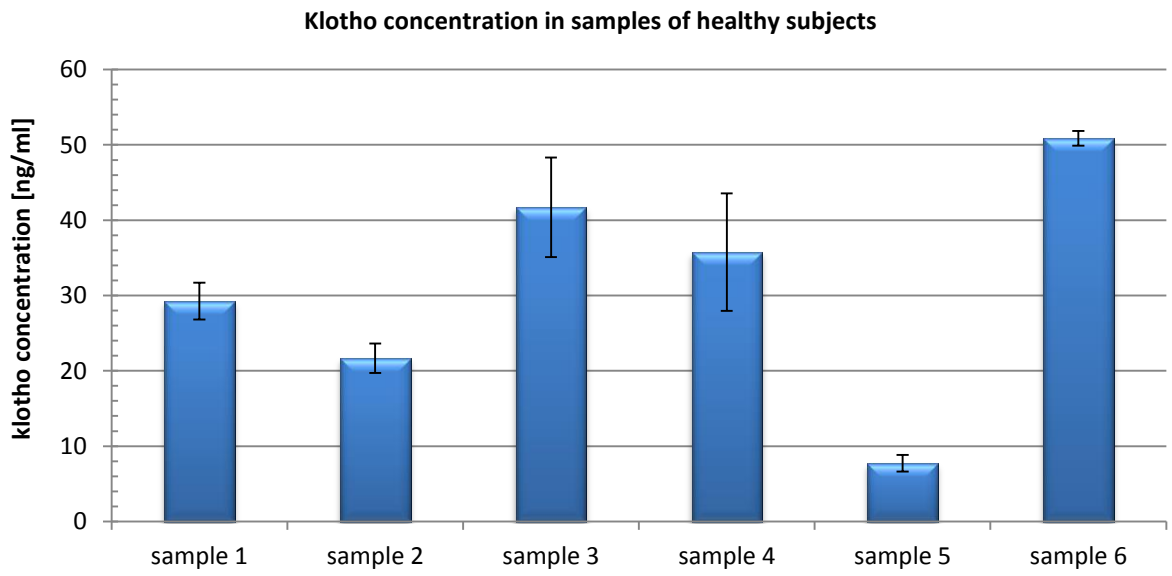

Figure 48: Klotho concentration in samples of healthy subjects
Serum samples of normal donors were diluted 1:2, 1:4 and 1:8 in PBS. The klotho concentration was determined using the optimized ELISA version. The figure shows the mean values of the klotho concentration from three different dilutions for each sample. The error bars indicate the standard deviation. Sample 1: 29.27 ng/ml ± 2.45 ng/ml, sample 2: 21.67 ng/ml ± 1.96 ng/ml, sample 3: 41.70 ng/ml ± 6.60 ng/ml, sample 4: 35.77 ng/ml ± 7.80 ng/ml, sample 5: 7.73 ng/ml ± 1.10 ng/ml, sample 6: 50.87 ng/ml ± 0.97 ng/ml (mean ± standard deviation).

5 DISCUSSION

The survival of all tissues, including bone, depends on an adequate blood supply. This very simple sounding fact of life yet remains a quite challenging task, especially in the field of tissue engineering. Rapid establishment of functional blood vessels is a prerequisite for successful tissue engineering and a limiting factor for the reconstruction of larger defects **(Pedersen et al. 2014)**.

Mesenchymal stem cells (MSCs) are investigated primarily as progenitor cells capable of regenerating bone, cartilage and adipose tissue, thus being an attractive cell source for tissue engineering. Vascularization, the formation of blood vessels is a fundamental process in tissue regeneration, maintained by endothelial progenitor cells (EPCs). The idea of VascuBone, a project funded by the European Union, was to comprise MSCs and EPCs on novel tissue engineered constructs to generate pre-vascularized bone implants **(VascuBone 2010)**.

The present study focused on the crosstalk of these 2 types of important progenitor cells by establishing 2 cell culture models to assess the changes of the global gene expression patterns after direct cell-cell contact (co-culture) as well as humoral-mediated gene regulations (conditioned medium).

The MSCs were isolated according to a standardized protocol **(Nöth et al. 2002; Schütze et al. 2005)** from femoral heads. A protocol for the isolation and cultivation of EPCs using buffy coat and rCYR61-coated plates was optimized in the present study, including the characterization of the progenitor cells. The results are discussed in subsequent chapters.

Subsequently, microarray analyses have been performed. The bioinformatical analysis revealed lists of differentially expressed genes and the gene ontology (GO) analysis unraveled KEGG pathway overrepresentations as well as cluster of differentially regulated gene affiliated with certain pathways. The findings are discussed in detail in the following chapters.

5.1 Cultivation and expansion of buffy coat-derived EPCs

Part of the present study was to establish a method for the *ex vivo* cultivation and expansion of EPCs from buffy coat for the study of the crosstalk of EPCs with MSCs in 2 *in vitro* cell culture models to better understand the underlying mechanisms of this cell communication.

When looking for a reliable, cost-efficient and sufficient source of primary human EPCs, the decision fell on buffy coat. Buffy coat is a commercially available product, produced and tested according to defined protocols, which is the main advantage compared to peripheral blood. In addition, buffy coat is a concentrate (30 ml) from a total volume of 500 ml blood. This is an approximately 5 times greater volume than usually received from a peripheral blood donation. At the same time, the use of a concentrate reduced the amount of reagents needed to isolate the mononuclear cell fraction and speeded up the isolation process.

Preliminary tests showed that the mono-nuclear cell fraction isolated by Ficoll-Paque™ density gradient centrifugation did not adhere on uncoated plates. Therefore, rCYR61-coated plates were used to allow the EPCs to attach to the plate. The positive effect of CYR61 on the proliferation and differentiation of EPCs is known from the literature **(Yu et al. 2010; Brigstock 2002; Maity et al. 2014; Lienau et al. 2006; Grote et al. 2007; Schenk 2007)** and was also described by Anke Hofmann for the isolation of EPCs from peripheral blood. With her protocol, she isolated in average 1.44 x 10^6 ± 0.59 x 10^6 mono-nuclear cells/ml blood (n = 32; mean ± standard deviation) **(Hofmann 2010)**. Using this existing protocol and adapting it for the use of buffy coat resulted in 1.9 x 10^6 ± 0.4 x 10^6 mono-nuclear cells/ml blood (n = 29; mean ± standard deviation).

In summary, these results show that EPCs have been successfully isolated from buffy coat using rCYR61-coated plates. The number of cells was sufficient to establish protocols for the 2 *in vitro* cell culture models (conditioned medium and co-culture experiments).

However, the number of cells was not sufficient to supply partners of the VascuBone consortium with cells for the seeding of scaffolds and therefore to perform subsequent experiments (*in vitro* in bioreactors and *in vivo* in animal models). With the procedure applied, no expansion of the cell culture was possible. The limiting factor was the ability to passage the cells more than 2 times.

Presumably, the reason for this was the medium used. The medium did not contain supplements. The medium composition was chosen from the point of view for the above mentioned experiments to study the crosstalk of the 2 cell types. Therefore, a different composition may be needed for the *ex vivo* expansion. Within the VascuBone consortium, the task of establishing an expansion protocol for EPCs was shared with another partner (Medicyte GmbH, Heidelberg, Germany). Medicyte was responsible for the development of a medium for the cultivation and expansion of EPCs for the up-scaled experiments. In addition, Medicyte was working on an increased expansion by upcyte® and vericyte® technology. Taking together the efforts of both working groups, the task of the isolation, cultivation and expansion of EPCs was successfully solved (data not published. Results were presented during the bi-annual meeting of the VascuBone consortium in 2014).

5.2 Characterization of buffy coat-derived EPCs

The vasculature contributes to many different physiological and pathological conditions. Therefore, it is no surprise that EPCs gain growing interest in many scientific fields, e.g. in tissue regeneration **(T. O. Pedersen et al. 2013; Xue et al. 2013; Pedersen et al. 2014; Bartaula-Brevik et al. 2014)**, cancer **(Hillen & Griffioen 2007; Ahn et al. 2010; Patenaude et al. 2010)**, coronary artery disease **(Vasa et al. 2001; França et al. 2011)** or diabetes **(Fadini et al. 2006; Georgescu et al. 2011; António et al. 2010)**. Nevertheless, no simple definition of EPCs exists and various methods of EPC isolation have been reported. Since the initial report of EPCs **(Asahara et al. 1997)**, a number of groups have set out to better define this cell population. The term "EPC" may therefore encompass a group of cells existing in a variety of stages ranking from hemangioblasts to fully differentiated ECs.

The characterization of the EPCs used in the present study resulted in the following profile: The buffy coat-derived EPCs incorporated acLDL and bound to Ulex Lectin. The results also showed that the cells expressed the surface markers CD31 (also known as PECAM-1), CD45 and CD144 (also known as VE-Cadherin) and in addition age-dependent CD34, and were negative for the surface markers CD133 and CD309 (also known as VEGFR-2, KDR, flk-1). The characterization was performed on day 7 and day 14 of the *in vitro* cultivation.

In most studies addressing the identity of EPCs, the surface marker CD34 was included **(Hillen & Griffioen 2007; França et al. 2011; Estes et al. n.d.; Schmidt-Lucke et al. 2010; Yin et al. 1997; Yang et al. 2011; Giannotti et al. 2010; Fadini et al. 2006; Murohara et al. 2000)**. Many investigators have identified or designated putative (circulating) EPCs with flow cytometry using a single surface marker such as CD34 or CD133 in humans, or various combinations of surface markers were used, which has actually resulted in a complicated list of putative EPC immunophenotypes in men and mice. Timmermans et al. summarized in their review in 2009 some of the conflicting results that have been reported in the field **(Timmermans et al. 2009**). However, the topic still is a subject of much discussion. For example, Sato et al. used a mouse transplantation model to address the recent controversy about CD34 expression by hematopoietic stem cells. Interestingly, the authors observed that CD34 expression reflects the activation state of hematopoietic stem cells and that this is reversible **(Sato et al. 1999)**. Subsequently, this gives rise to the question: $CD34^+$ or $CD34^-$, does it really matter? Goodell et al. addressed this question and concluded from recent findings that in normal murine bone marrow, the long-term repopulating activity was found entirely in the $CD34^{-/low}$ compartment. During culture, the $CD34^-$ stem cells expanded and acquired CD34, and the $CD34^+$ cells contained all detectable hematopoietic repopulating activity **(Goodell 1999)**. In addition, strong evidence demonstrates that CD34 is expressed not only by EPCs, but by a multitude of other nonhematopoietic cell types including muscle satellite cells, corneal keratinocytes, interstitial cells, epithelial progenitors, and MSCs. In many cases, the $CD34^+$ cells only represent a small proportion of the total cell population **(Sidney et al. 2014)**. In the present study, the EPCs were not selected by flow cytometry using a single surface marker and therefore excluding certain cell populations, but were seeded on rCYR61-coated plates. The results showed that the cells on day 7 were $CD34^-$, while they were found to be $CD34^+$ on day 14, supporting the theories of Sato and Goodell.

One of the issues in the discussion is also the functional overlap between EPCs, haematopoietic cells (HCs) and mature endothelial cells (ECs). In addition, the surface expression profile changes during maturation. For example, Sugimoto et al. defined EPCs as $CD34^+/CD133^+$ cells and circulating ECs as $CD34^+/CD144^+$ cells **(Sugimoto et al. 2014)**. Taking this definition and applying it to the findings of the present study would place the $CD34^+/CD144^+/CD133^-$ cells at the more mature end of a scale, ranking from primitive progenitors to fully mature cells. Controversy, Case et al. found in 2007 that $CD34^+/CD133^+/VEGFR\text{-}2^+$ cells were HPCs (hematopoietic progenitor cells) that do not yield EC progeny. The authors described that these cells did not form EPCs and were devoid of vessel forming activity and expressed the hematopoietic lineage-specific antigen, CD45 **(Case et al. 2007)**. Untergasser et al. reported in 2006 the isolation of a homogeneous population of CEP (circulating endothelial precursor cells) from $CD34^+/CD133^-$ cells of peripheral blood that could be expanded

easily on collagen type I-coated plastic. CEP displayed a phenotype of mature endothelial cells (vWF, CD31, CD34, VEGFR-2, CD105, CD146) similar to that of cord-blood CEP and umbilical vein endothelial cells. The cells bound Ulex Lectin and incorporated acLDL **(Untergasser et al. 2006)**.

In conclusion, currently, there is no uniform definition of an EPCs. It is known that ECs are highly heterogeneous and acquire specialized functional properties in local microenvironments **(Ribatti et al. 2002; Garlanda & Dejana 1997)**. There is growing evidence for the existence of many subpopulations of EPCs, too. Recent findings support this theory of highly specialized endothelial cells. In two papers in this issue, Adams and colleagues demonstrated that the bone vasculature contains specialized endothelial cells with signaling properties that support bone maturation and regeneration **(Kusumbe et al. 2014; Ramasamy et al. 2014)**. The authors distinguished two new subpopulations of ECs that they term type H and type L ECs.

While significant progress has been made in our understanding that neovasculogenesis is a multicellular event and is unlikely to occur from a single recruited progenitor cell type, further progress will require the development of novel assays and conscientious read-out criteria that specifically identify the functional ability of putative EPCs to directly participate in postnatal vasculogenesis **(Timmermans et al. 2009)**.

Supported by the use of state-of-the-art information, we conclude that as well the morphological observations (spindle-shape and cobblestone morphology) as the expression of endothelial and stem cell specific surface markers ($CD34^+/CD31^+/CD45^+/CD144^+$) show that the cells used for the present study are a subpopulation of EPCs. The EPCs described in the present study were in addition $acLDL^+/Ulec\ Lectin^+/CD133^-/CD309^-$ at the time of use.

5.3 Experimental design

5.3.1 Experiments with conditioned medium

The experimental setting was designed to assess the influence of conditioned medium gained from human primary MSCs on human primary EPCs and *vice versa* and subsequently to assess the changes of the global gene expression patterns of both cell types. The experiment aimed to analyze the early humoral mediated effects. Therefore the cells were treated with conditioned medium for 24 h before the RNA was collected. 4 individual experiments were performed.
The conditioned medium itself was collected from the respective other cell type 24 h after the medium had been changed and applied to the cells as a composition of 50 % conditioned medium and 50 % fresh medium. Since the propagation medium of EPCs and MSCs differs in its composition, the control cells received a mixture of 50 % fresh EPC medium and 50 % fresh MSC medium to treat the control cells equally. The experimental design was suitable to analyze the changes of the global gene expression patterns of both cell types. The amount of RNA collected from each experiment was suitable to perform microarray analyses as well as to re-evaluate the results by RT-PCR.

5.3.2 Co-cultivation of EPCs and MSCs

To assess the early changes of the global gene expression patterns after direct cell-cell contact, human primary MSCs and human primary EPCs were co-cultured for 24 h.
4 individual experiments were performed.
To separate the MSCs and EPCs after the co-culture experiment, the cells were stained with Cell Tracker® Green and Orange, respectively, prior to the experiment. Subsequently, the cells were separated by flow cytometry (fluorescence-activated cell sorting, FACS). Control cells were stained and sorted as well to apply the same procedure.
An aliquot of the sorted cells from each co-culture experiment was re-sorted (post-analyzed) to determine the purity of the separated cell fractions. The post-analysis showed in average a purity of 99.1 % ± 0.3 % (mean ± standard deviation). This result shows that the cross-contamination was < 1 %. The separation method applied allowed to observe the changes of the global gene expression patterns for each cell type individually. The minimal cross-contamination of the cell fractions used for the microarray analyses allowed to show gene regulations caused in one type of cells compared to non-treated cells after direct cell-cell contact with the other type of cells. In conclusion, the experimental design including the cell staining and the cell sorting was suitable to analyze the changes of the global gene expression patterns of both cell types. The amount of RNA collected from each experiment was suitable to perform microarray analyses as well as to re-evaluate the results by RT-PCR.

5.4 Re-evaluation of the microarray data

The re-evaluation of the microarray results was performed using RNA specimens that had previously been used for the microarray analyses as well as with RNA specimens of additional experiments (if available). The RT-PCRs were performed with a selection of genes found to be differentially regulated in the respective microarray. The densitometric analysis of the corresponding gel bands confirmed the RT-PCR findings. The acceptance criteria were chosen according to the filters used for the microarray analyses to determine the significance of the observed regulations as well as under consideration of the same algebraic sign.

5.4.1 EPCs treated with conditioned medium (array group A)

For the re-evaluation of the microarray data of the $EPCs^{con\text{-}med}$, a selection of 9 differentially regulated genes was used for the RT-PCR which was performed with RNA specimens of 5 individual experiments. For 8 of the 9 assessed genes the RT-PCR showed accordance for all analyzed samples. For 1 gene, the RT-PCR revealed no significant regulation for 1 RNA sample previously used for the microarray analyses. A comparison with the corresponding heat map showed that the regulation of this sample was indeed lower than for the other 3 RNA specimens. Since the quality of all RNA samples used for the microarray analyses was controlled by RNA degradation plots and the sample showed good results for all other assessed genes, the re-evaluation of the microarray data for $EPCs^{con\text{-}med}$ was considered as being successful.

5.4.2 MSCs treated with conditioned medium (array group B)

The microarray analysis of the $MSCs^{con\text{-}med}$ showed the lowest number of differentially regulated genes ($EPCs^{con\text{-}med}$, $MSCs^{con\text{-}med}$, $EPCs^{co\text{-}cu}$, and $MSCs^{co\text{-}cu}$ = 514, 119, 613, and 319 differentially expressed genes, respectively) as well as the lowest degrees of regulation (highest logFC in $EPCs^{con\text{-}med}$, $MSCs^{con\text{-}med}$, $EPCs^{co\text{-}cu}$, and $MSCs^{co\text{-}cu}$ = 6.27, 1.85, 8.32, and 5.48, respectively). For the re-evaluation of the microarray findings, 4 RNA specimens of individual experiments were used and analyzed for 5 selected genes. 3 genes showed accordance with the microarray results in 3 of 4 samples, 1 gene was confirmed in only 1 sample and 1 gene did not match the microarray findings for all assessed RNA specimens. A comparison of the results with the corresponding heat map showed that the regulations for the $MSCs^{con\text{-}med}$ are not as evenly distributed as for the other microarrays. This result correlates with the in total low number of differentially regulated genes as well as with the comparatively low degree of regulation (logFC). The results of the re-evaluation also show that the lower the logFC of the assessed gene the worse the accordance with the microarray results.
Thus, although the RT-PCR confirmed the microarray results of the $MSCs^{con\text{-}med}$, the reliability of results with a logFC < 1 were accepted under reserve for subsequent analyses and conclusions.

5.4.3 EPCs co-cultured with MSCs (array group C)

The RT-PCR of the assessed RNA specimens confirmed the microarray findings. The re-evaluation was performed with a selection of 9 genes of which 2 genes were not represented in the lists of the differentially expressed genes. These genes were included as controls. As expected, the RT-PCR showed very diffuse results for these 2 genes demonstrating that the bioinformatic analysis of the microarray data did not accept or include non-regulated genes. Out of the 7 regulated genes, 4 specimens showed accordance with the microarray data for all assessed samples, including the additional RNA specimens. 2 of the differentially regulated genes showed the same algebraic sign for the desitometric analyses of the RT-PCR bands but did not match the acceptance criteria for the logFC value. The acceptance criteria were chosen very stringently and in accordance with the filter used for the microarray analysis. A comparison of the RT-PCR results with the respective heat map that allows a more detailed view on the performance of individual specimens showed a similar result for the corresponding probe set. Therefore, the re-evaluation of these 2 genes has also been considered to be successful and reliable.
The RT-PCR for KL (klotho) showed a double-band for KL isoform 1. The sequence analyses revealed and confirmed that the lower band (300 bp) represents full-length KL (isoform 1) while the higher band includes 50 bp of the intron sequence that is located between exon 3 and 4 which codes for the C-terminus of KL isoform 2 and therefore leads to an alternative spicing variant. 4 out of 6 assessed RNA specimens using a primer pair for KL isoform 1 and 2 out of 5 samples using a primer pair detecting KL isoform 2 showed accordance with the microarray results. The remaining RNA specimens showed an up-regulation, too, but did not match the very stringent acceptance criteria for the logFC value. In conclusion, the re-evaluation of the microarray analyses was successful and confirmed the reliability of the results.
In addition, the RT-PCR for CYR61 revealed an alternative splicing variant which will be discussed more detailed in Chapter 5.5.2.2.

5.4.4 MSCs co-cultured with EPCs (array group D)

4 of the 6 regulated genes used for the re-evaluation of the $MSCs^{co\text{-}cu}$ showed accordance with the microarray data for all assessed samples, including the additional RNA specimens. The RT-PCR of 1 gene showed no significant regulation for 1 RNA specimen previously used for the microarray analysis and 1 additional RNA specimen (logFC = 0.41 or 0.47, respectively; cut off = 0.5). Although two RNA specimens did not match the acceptance criteria for 1 gene, the obtained logFC values show a correlation with the array data. The acceptance criteria were chosen very stringently and in accordance with the filter used for the microarray analysis. Thus, the re-evaluation of these 5 up-regulated genes was regarded to be successful.
The RT-PCR of 1 down-regulated gene showed no significant regulation for 4 of the 6 assessed RNA specimens. Of the remaining two RNA specimens, 1 sample was found to be up-regulated and the other sample was found to be down-regulated for this gene. These results indicate that the re-evaluation of down-regulated genes is less precise than the RT-PCR of up-regulated genes most likely caused by a limited sensitivity of the method. 5 of the 6 assessed RNA specimens for this gene showed a down-regulation (indicated by the negative algebraic sign), but only 1 sample was considered to be significantly regulated in accordance to the very stringent acceptance criteria.
In conclusion, the summary of the results showed that the microarray has been successfully validated with biological replicates through RT-PCR, thus confirming the reliability of the microarray results.

5.5 Microarray analysis

Although communication between MSCs and EPCs is recognized as one of the most important cellular interactions in bone regeneration, the underlying mechanism of this biological process is not well understood. Understanding the nature of the mechanism linking angiogenesis and bone formation should be of great relevance for the improved fracture healing or prevention of bone mass loss **(Ramasamy et al. 2014)**.
The present study aimed to unravel some of these mechanisms by giving detailed information about the changes of the global gene expression patterns of EPCs and MSCs after treatment with conditioned medium (EPCs$^{con\text{-}med}$ or MSCs$^{con\text{-}med}$) as well as after direct cell-cell contact (EPCs$^{co\text{-}cu}$ or MSCs$^{co\text{-}cu}$).

The findings of the microarray and gene ontology analysis will be discussed in subsequent chapters, with special focus on bone regeneration and angiogenesis. The first chapter will reflect on the results of MSCs after treatment with conditioned medium of EPCs as well as after direct cell-cell contact with EPCs. It will provide information about selected genes affiliated with inflammation, immunomodulation and osteogenesis and link the findings of the present study to current state-of-the-art knowledge in this field. The next chapter will focus on the changes of the global gene expression patterns of EPCs mediated either in a humoral manner by conditioned medium of MSCs or direct cell-cell contact with MSCs. Selected genes found to be differentially regulated will be pointed out and their role in angiogenesis and osteogenesis will be discussed. Finally, a summary will focus on the combined findings and shed light on the interactions of the crosstalk of MSCs and EPCs.

5.5.1 The impact of EPCs on MSCs

The impact of human primary EPCs on the global gene expression patterns of human primary MSCs was studied in two different cell culture models:

- after having been subjected to conditioned medium of EPCs (MSCs$^{con\text{-}med}$, array group B)
- after direct cell-cell contact with EPCs (MSCs$^{co\text{-}cu}$, array group D)

To assess the changes of the global gene expression patterns, microarrays were performed using the Affymetrix GeneChip® Human Genome U133 Plus 2.0 Array and by comparing treated and control cells for both experimental settings. The Affymetrix GeneChip® covers the human genome U133 set plus 6500 additional genes allowing the analysis of over 47000 transcripts.
The treatment with conditioned medium resulted in 180 differentially expressed probe sets corresponding to 119 genes of which 97 genes were significantly up-regulated and 22 significantly down-regulated. The comparison between co-cultured MSCs and the respective control cells revealed 458 differentially expressed probe sets corresponding to 319 genes of which 207 genes were significantly up-regulated and 112 significantly down-regulated.
The results show clearly that there are more genes differentially regulated after direct cell-cell contact than by humoral mediated effects. There is also significant difference in the degree of regulation, shown by the logFC value (logarithmic fold change). While the highest up-regulated gene in array group B (MSCs$^{con\text{-}med}$) showed a logFC of 1.85, the highest up-regulated gene in array group D (MSCs$^{co\text{-}cu}$) showed a logFC of 5.48. Both results are expected findings since humoral mediated effects are in general weaker than effects observed by direct cell-cell interactions.
In both experimental setups, genes affiliated with inflammatory processes were found to be differentially expressed, e.g. BIRC3 (baculoviral IAP repeat containing 3) with a logFC of 1.85 or 3.31, CTSS (cathepsin S) with a logFC of 0.97 or 3.84, SOD2 (superoxide dismutase 2, mitochondrial) with a logFC of 1.24 or 2.82 in MSCs$^{con\text{-}med}$ or MSCs$^{co\text{-}cu}$, respectively. The gene ontology analysis revealed several KEGG pathway overrepresentations, e.g. graft-versus-host disease. The findings have been grouped and analyzed for their affiliation to certain biological processes, e.g. immunomodulation or osteogenesis. The results will be discussed in subsequent chapters.

5.5.1.1 MSCs: Reflection on results affiliated to inflammation and immunomodulation

The humoral mediated effects are significantly lower than the effects seen by direct cell-cell contact. Nevertheless, amongst the top 10 differentially regulated genes in $MSC^{con\text{-}med}$, the up-regulation of BIRC3, PTGS2 (prostaglandin-endoperoxide synthase 2) and IL6 shows an increase of inflammation factors. For example, BIRC3 provides a feed-forward loop, which, with BIRC2, is required to moderate the normal speed of nuclear factor kappa-B (NF-κB) activation. Thus BIRC3 is involved in the fine-tuning of NF-κB and c-Jun N-terminal kinase (JNK) signaling to ensure transcriptional responses are appropriately matched to extracellular inputs. NF-κB signaling appears downstream of the TNF signaling cascades that converge on pathways important for cell survival and inflammation **(Tan et al. 2013)**. Activated NF-κB increases the transcription of genes encoding chemokines (e.g. IL8), cytokines (e.g. tumor necrosis factor alpha (TNF-α), IL1, IL6, and granulocyte-macrophage colony-stimulating factor (GM-CSF)), adhesion molecules (e.g. intercellular adhesion molecule 1 (ICAM-1), vascular cell adhesion molecule 1 (VCAM-1)), acute phase proteins and enzymes (e.g. COX-2) **(Damgaard & Gyrd-Hansen 2011)**. Cyclooxygenase (COX) is the key enzyme required for the conversion of arachidonic acid to prostaglandins. In humans, prostaglandins are involved in diverse functions, including bone metabolism, wound healing, blood vessel tone, and immune responses **(Dubois et al. 1998)**. PTGS2 (also known as COX-2) is an immediate-early response gene normally absent from most cells but is mainly induced at sites of inflammation in response to inflammatory stimuli including pro-inflammatory cytokines **(Wang et al. 2011)**. Another important key player involved in inflammation and infection responses but also in the regulation of metabolic, regenerative, and neural processes is the cytokine IL6 **(Scheller et al. 2011)**.

Inflammation is basically a protective response that ensures the removal of injurious agents and healing of damaged tissue. Healing occurs in three distinct but overlapping stages: 1) the early inflammatory stage; 2) the repair stage; and 3) the late remodeling stage **(Kalfas 2001)**.

Although the regulations of differentially expressed genes in $MSCs^{con\text{-}med}$ were at low levels, the data show that EPCs release signal molecules that affect MSCs in a humoral manner and lead to an up-regulation of some key players in inflammatory processes subsequently initiating phase 1 of the tissue regeneration process. In accordance with these findings, MSCs co-cultured with EPCs ($MSCs^{co\text{-}cu}$) show a significantly higher number of differentially regulated genes involved in inflammation and immunomodulation, e.g. BIRC3, CTSS, chemokine (C-X-C motif) ligands (CXCL9, CXCL11), human leukocyte antigens (HLA-DQA1, HLA-DQB1, HLA-DRA), indoleamine 2,3-dioxygenase 1 (IDO1), lysozyme (LYZ) and S100 calcium binding protein A8 (S100A8) ($logFC > 3$; for detailed information see Chapter 3.6.4.1, Table 25, Page 76). For example, as chemokine (C-X-C motif) receptor 3 (CXCR3) activating chemokines, CXCL9 and CXCL11 specifically attract activated T cells. These chemokines are strongly induced by cytokines, particularly interferon γ (IFN-γ), during infection, injury or immunoinflammatory responses. Consequently, their major function is to selectively recruit immune cells at inflammation sites, but they also play a role in angiogenesis mechanisms **(Müller et al. 2010; Lacotte et al. 2009)**. CTSS is a lysosomal cysteine protease of antigen-presenting cells (APCs) that is secreted during inflammation **(Zhao et al. 2014)**. It is known that MSCs possess antigen-presenting properties. Chan et al. verified in 2006 APC functions of MSCs to recall antigens. MSCs also express MHC class II antigens **(Chan et al. 2006; Chan et al. 2004)**. The MHC is a set of cell surface molecules encoded by a large gene family which controls a major part of the immune system in all vertebrates. In humans, the MHC is also called the human leukocyte antigen (HLA). The microarray analysis of $MSCs^{co\text{-}cu}$ revealed an up-regulation of 6 genes belonging to the MHC class II family and 1 gene belonging to the MHC class I family. Unlike professional APCs, non-professional APCs do not constitutively express the MHC class II proteins required for interaction with naive T cells. These are expressed only upon stimulation, e.g. by IFN-γ **(Nickoloff & Turka 1994)**.

Beside these reports showing the immunostimulatory properties of MSCs, various studies have demonstrated that MSCs are strongly immunosuppressive in vitro and in vivo. Indeed, there is evidence to support the duality in MSC immune status **(Shi et al. 2010; Yagi et al. 2010)**. It is thought

that MSCs need to be activated to exert their immunomodulation skills. There is great controversy concerning the mechanisms and molecules involved in the immunosuppressive effect of MSCs. Prostaglandin E2, transforming growth factor beta (TGF-β), IL6 and interleukin 10 (IL10), human leukocyte antigen G5, matrix metalloproteinases, IDO and nitric oxide (NO) are all candidates under investigation **(De Miguel et al. 2012)**. Chan et al. showed that the antigen-presenting property of MSCs occurs during a narrow window at low levels of IFN-γ. This could explain the roles of MSCs as both APCs and as immune suppressor cells as a function of IFN-γ levels balancing the immune stimulatory and inhibitory properties of MSCs **(Chan et al. 2006)**. Shi et al. showed in their study that there is a species variation in the mechanisms of MSC-mediated immunosuppression: immunosuppression by cytokine-primed mouse MSCs is mediated by NO, whereas immunosuppression by cytokine-primed human MSCs is executed through IDO. Therefore, the authors suggest that immunosuppression by inflammatory cytokine-stimulated MSCs occurs via the concerted action of chemokines and immune-inhibitory NO or IDO produced by MSCs **(Shi et al. 2010)**. IDO, one of the genes up-regulated in $MSCs^{co\text{-}cu}$, is a cytosolic monomeric hemoprotein enzyme that catalyzes tryptophan to kynurenine. It appears that some of the biological effects of IDO can be mediated via local depletion of tryptophan, whereas others are mediated via immunomodulatory tryptophan metabolites, subsequently suppressing T cell responses. IDO seems to be a counter-regulatory mechanism to suppress excessive immune activation. Such counter regulatory pathways are important in the immune system because uncontrolled immune responses can cause unacceptable damage to the host **(Jalili et al. 2007)**.

In conclusion, these results show that MSCs up-regulate a cluster of important key players in inflammation and immunomodulation within 24 h after contact with EPCs, suggesting the initiation of phase 1 of the tissue regeneration process. Inflammatory conditions induce the release of a variety of chemokines and cytokines, are chemo-attractive for other cells and pave the way for the repair of the surrounding tissue. For the survival of the host, inflammation is a necessary and beneficial process that needs to be tightly regulated. Our study demonstrates that amongst the differentially regulated genes are also genes affiliated with immunomodulatory effects. These findings shed light on the mechanisms involved in early tissue repair, especially in the orchestrated function of MSCs as both APCs and immune suppressor cells and provide a platform for further studies.

5.5.1.2 MSCs: Reflection on results affiliated to osteogenesis

Osteogenesis is an important part of the bone remodeling process, referring to the formation of bone tissue. It is the most commonly occurring process in fracture healing. The complex array of interdependent biological events that occur during fracture repair are represented by inflammation, signaling, gene expression, cellular proliferation and differentiation, osteogenesis, chondrogenesis, angiogenesis, and remodeling.

In bone regeneration and remodeling processes, MSCs have a crucial role, and their differentiation during these processes is regulated by specific signaling molecules (growth factors/cytokines and hormones) and their activated intracellular networks. Especially the utilization of the molecular machinery seems crucial to consider prior to developing bone implants, bone-substitute materials, and cell-based constructs for bone regeneration **(Hayrapetyan et al. 2014)**.

To gain knowledge of these complex mechanisms, the main protagonists in angiogenesis and osteogenesis, namely EPCs and MSCs, were co-cultured for 24 h before the cells were separated, RNA collected and microarray analysis performed. The gene ontology analysis of the microarray data of $MSCs^{co\text{-}cu}$ shows a KEGG overrepresentation for the osteoclast differentiation pathway. The differentially expressed genes related to this pathway are displayed in Chapter 3.6.3.3, Table 26 on Page 78 with additional genes identified from the literature to be involved in osteogenesis, e.g. suppressor of cytokine signaling 3 (SOCS3), jun B proto-oncogene (JUNB) and S100A8. However, common bone marker genes like alkaline phosphatase (ALP) or runt-related transcription factor-2 (RUNX2) were not found to be regulated. The time point and culture system chosen likely caused this result, as we have found that several important regulators of inflammation and immunomodulation were differentially regulated indicating that phase 1 of the repair process was activated. Kon et al. analyzed the expression of a number of cytokines and receptors that are of functional importance to bone remodeling (osteoprotegerin (OPG), colony-stimulating factor 1 (M-CSF) and OPG ligand (RANKL)), as well as inflammation (TNF-α and its receptors and IL1-alpha and -beta and their receptors) over a 28-day period after the generation of simple transverse fractures in mouse tibias. The authors found distinct expression profiles that occurred at certain time points, e.g. within the first 24 h after fracture, during the initial period of inflammation on day 1 and day 3 postfracture, during the period of cartilage formation on day 7, or on day 21 and day 28 when bone remodeling was initiated **(Kon et al. 2001)**. However, the upregulation of wingless-type MMTV integration site family, member 5A (Wnt5A) by the $EPCs^{co\text{-}cu}$ in combination with proinflammatory cytokines such as IL6 and IL8 may initiate frizzled-receptor-mediated osteogenic signaling in a self-sustaining loop of inflammation induced wnt/ROR2 signaling as we and others were recently able to describe in the early phase of osteogenic differentiation **(Ebert et al. 2015; Rauner et al. 2012; Ferreira et al. 2013)**.

The appearance of SOCS3 in $MSC^{co\text{-}cu}$, which is a significant player in bone-associated inflammatory responses, is another candidate to show the orchestrated regulatory mechanisms of bone tissue regeneration mediated by the contact with EPCs. Studies in different mouse models have proven the critical importance of SOCS3 in restraining inflammation and allowing optimal levels of protective immune responses against infections. A main role of SOCS3 results from its binding to both the JAK kinase and the cytokine receptor, which results in the inhibition of signal transducer and activator of transcription 3 (STAT3) activation **(Carow & Rottenberg 2014)**. However, the underlying mechanisms and signaling pathways regulating SOCS3 expression in osteoblasts, osteoclasts, and other types of bone cells are still not well understood. Although there are discrepancies in the reports of the function of SOCS3, it has been clearly established that SOCS3 plays a key role in regulation of both inflammation and bone **(Gao & Van Dyke 2014)**.

5.5.2 The impact of MSCs on EPCs

The impact of human primary MSCs on the global gene expression patterns of human primary EPCs was studied in two different cell culture models:

- after having been subjected to conditioned medium of MSCs ($EPCs^{con\text{-}med}$, array group A)
- after direct cell-cell contact with MSCs ($EPCs^{co\text{-}cu}$, array group C)

To assess the changes of the global gene expression patterns, microarrays were performed using the Affymetrix GeneChip® Human Genome U133 Plus 2.0 Array and by comparing treated and control cells for both experimental settings. The Affymetrix GeneChip® covers the human genome U133 set plus 6500 additional genes allowing the analysis of over 47000 transcripts.

The treatment with conditioned medium resulted in 769 differentially expressed probe sets corresponding to 514 genes of which 343 genes were significantly up-regulated and 171 significantly down-regulated. The comparison between co-cultured EPCs and the respective control cells revealed 923 differentially expressed probe sets corresponding to 613 genes of which 501 genes were significantly up-regulated 112 significantly down-regulated.
Compared by the number of regulated genes, the direct cell-cell contact unraveled more differentially expressed genes than produced by humoral effects. This is an expected result, since the direct cell-cell contact allows a more intense crosstalk. Comparing the two different experimental settings, there is also difference in the degree of the regulation shown by the logFC value (logarithmic fold change). The highest up-regulated gene in array group A ($EPCs^{con\text{-}med}$) showed a logFC of 6.27, the highest up-regulated gene in array group C ($EPCs^{co\text{-}cu}$) showed a logFC of 8.32.
Both the number of regulated genes as well as the very high logFC values indicate that MSCs exert a very strong impact on EPCs in both cell culture models. The gene ontology analysis threw light on some of these effects by unraveling several KEGG pathway overrepresentations all belonging to cytokine, chemokine and cell adhesion molecule activities, ECM-receptor interactions, focal adhesion and remodeling processes. In addition, gene regulations affiliated with angiogenesis and osteogenesis were unraveled. The subsequent chapters will discuss these findings in detail.

5.5.2.1 EPCs: Reflection on results affiliated to ECM-receptor interaction

The extracellular matrix (ECM) consists of a complex mixture of structural and functional macromolecules such as collagens, laminins, fibrilins, elastins, fibronectins and several proteoglycans and serves an important role in tissue and organ morphogenesis and in the maintenance of cell and tissue structure and function (Figure 49). Cells interact with the ECM through ECM receptors, including the syndecans, a four member group of transmembrane cell surface proteoglycans, dystroglycan, a heterodimer component of muscle dystrophin-glycoprotein complex, discoidin domain receptors, a two member family of tyrosine kinase receptors activated by native collagen, and heterodimeric integrins, which constitute the major class of ECM receptors **(Barber et al. 2014)**.

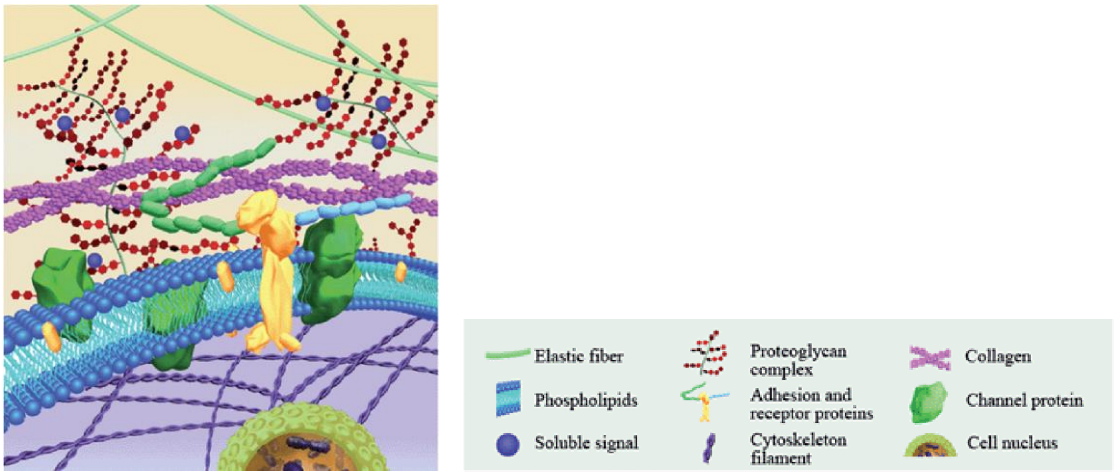

Figure 49: Schematic illustration of the composition of the extracellular matrix (ECM)
The ECM regulates cellular tension and polarity, differentiation, migration, proliferation, and survival. The ECM consists of collagen, elastin, multidomain glycoproteins (e.g. fibronectin), and proteoglycans and glycosaminoglycans; the exact composition of the ECM varies by tissue and by the state of the tissue, e.g. intact adult tissue, healing wound, cancer, etc. (He et al. 2014; Schultz et al. 2011).

Remodeling of the ECM is an essential component of the complex vascular biology that drives each step within the angiogenic cascade. A balance between pro- and anti-angiogenic proteins, known as the "angiogenic switch", is crucial for the control of angiogenesis. In healthy adults, the switch is typically maintained in the "off" position, unless a pathological state which requires the formation of new vasculature occurs, such as cancer, wound healing, or ischemic disease **(Grainger & Putnam 2013)**. Angiogenesis, in response to tissue injury, is a dynamic process that is highly regulated by signals from both serum and the surrounding ECM environment. Migration of endothelial cells and development of new capillary vessels during wound repair is dependent on not only the cells and cytokines present but also the production and organization of ECM components both in granulation tissue and in endothelial basement membrane. In addition, inflammatory cells require the interaction with and transmigration through the endothelial basement membrane to enter the site of injury **(Li et al. 2003)**.

The microarray analysis of EPCs$^{con\text{-}med}$ revealed an up-regulation of several genes affiliated with ECM interactions, such as thrombospondin (THBS), laminin beta 1 (LAMB1), integrin beta 8 (ITGB8) and versican (VCAN). In addition to these genes, EPCs$^{co\text{-}cu}$ expressed clusters of genes affiliated with ECM-receptor interactions, focal adhesion and cell adhesion, such as collagens of different subtypes (type I, III, IV, V, VI, XI), fibronectin 1 (FN1), syndecan 2 (SDC2), tenascin C (TNC), parvin alpha (PARVA), and integrin-binding sialoprotein (IBSP). These results show that the production and organization of ECM components is stimulated by EPCs through humoral mediated signals from MSCs but even more by

direct cell-cell contact with MSCs. The results lead to the conclusion that the platelet-derived growth factor (PDGF) signaling pathway gets dominant which subsequently stimulates the remodeling process. For example, platelet-derived growth factor receptor alpha and beta (PDGFRA and PDGFRB) – both genes were found to be differentially expressed in EPCs$^{co\text{-}cu}$ – play a crucial role in wound healing. The two PDGF receptors are structurally similar and consist of extracellular domains with 5 immunoglobulin (Ig)-like domains and intracellular parts with kinase domains. Ligand binding occurs preferentially to domains 2 and 3, and domain 4 stabilizes the dimer by a direct receptor-receptor interaction. Ligand-induced dimerization induces autophosphorylation of the receptors, which activates their kinases and creates docking sites for SH2 domain-containing signaling molecules. Activation of these signaling pathways promotes cell growth, survival, migration and actin reorganization **(Heldin 2013)**.

Collagens play an important role in determining cell attachment and spreading. The types 1, 2, and 3 are the most abundant collagens of the human body that form fibrils responsible for the tensile strength of the tissue **(Rosso et al. 2004)**. Other proteins, such as fibronectin and laminin, also participate in building the matrix network as connectors or linking proteins **(Daley et al. 2008)**. Both, the up-regulation of genes encoding ECM proteins as well as their receptors (integrins), were observed in EPCs$^{co\text{-}cu}$. Integrins are heterodimeric transmembrane receptors that link the ECM to the internal cytoskeleton by binding directly to ECM proteins, such as fibronectin and laminins, and indirectly to actin via cytoplasmic binding proteins **(Daley et al. 2008)**. As endothelial cells migrate into the wound, integrin expression is spatiotemporally controlled, with ECM adhesions being assembled and disassembled at various times and places **(Schultz et al. 2011)**.

Temporal and spatial regulation of extracellular matrix remodeling events allow for local changes in net matrix deposition or degradation, which in turn contributes to control of cell growth, migration, and differentiation during different stages of angiogenesis. Extracellular matrix molecules, such as thrombospondin-1 and -2 (THBS1 and THBS2) can exert anti-angiogenic effects by inhibiting endothelial cell proliferation, migration and tube formation **(Sottile 2004)**. The most significant enzymes in ECM remodeling are metalloproteinases. Two main families of metalloproteinases, including matrix metalloproteinase (MMP) and a disintegrin and metalloproteinase with thrombospondin motifs (ADAMTS) families, are specialized in degrading the ECM **(Lu et al. 2011)**.

The microarray analysis of EPCs$^{co\text{-}cu}$ unraveled an up-regulation of the genes encoding for ADAM8, ADAM12, ADAMTS1, ADAMTS2, ADAMTS5 and ADAMTS6 as well as MMP1, MMP2 and MMP3.

MMP3, for instance, targets proteoglycans, fibronectin, and laminin, whereas MMP1 prefers collagen type III. ADAMTSs can degrade aggrecan, versican, brevican, and other proteoglycans. While ADAMTSs are mainly responsible for the degradation of ECM components, a related family of proteins, a disintegrin and metalloproteinase (ADAM) family members are often involved with cytokine processing and growth factor receptor shedding **(Lu et al. 2011)**. These findings seem to be controversial to the above mentioned results. However, it is known from the literature that in humans, capillary sprouts begin to migrate into the wound by day 4 post injury. This process depends on the degradation of existing basement membrane by MMPs and other enzymes **(Schultz et al. 2011)**. ECM remodeling is important in wound repair and in developmental processes. Like the 2 sides of a coin, the remodeling process is defined by 2 events: degradation and reconstruction. Fragments of ECM molecules with biological functions distinct from those of the parental protein are called matrikines and were identified about two decades ago. Due to their activity, matrikines may play a significant role in physiological or pathological processes such as wound healing or tumor invasion. They are also under investigation in the context of inflammation-induced angiogenesis **(Arroyo & Iruela-Arispe 2010)**.

The findings of the present study show that the contact of EPCs with MSCs is highly beneficial for the process of wound healing by enhancing the degradation of damaged tissue on one hand and on the other hand by promoting synthesis of ECM components, e.g. collagens, subsequently supporting angiogenesis and tissue repair. The results demonstrate that the process of ECM remodeling is a highly balanced process. The present study unravels some key players in the orchestrated process of ECM-cell interactions and provides insights into the underlying mechanisms how cells interact with and remodel the ECM.

5.5.2.2 EPCs: Reflection on results affiliated to angiogenesis

The microarray analysis of both, $EPCs^{con\text{-}med}$ and $EPCs^{co\text{-}cu}$, revealed several differentially expressed genes directly involved in angiogenesis, e.g. vascular endothelial growth factor A (VEGFA). However, significantly more differentially expressed genes affiliated with angiogenesis are observed in $EPCs^{co\text{-}cu}$, e.g. cysteine-rich angiogenic inducer 61 (CYR61) and connective tissue growth factor (CTGF), both members of the CCN protein family as well as fibroblast growth factor 2 (FGF2) and transforming growth factor alpha and beta (TGF-α and TGF-β).

FGF2, a key player in the regulation of angiogenesis, is an example of a growth factor that must be bound to the ECM to exert its effects. FGF2 is made by multiple types of cells (e.g. macrophages during the inflammatory phase and fibroblasts and endothelial cells during the proliferative phase) during wound healing **(Schultz et al. 2011)**. Endothelial cell-derived FGF2 may mediate angiogenesis with an autocrine mode of action. In vivo, FGF2 has been detected in the basal lamina of blood capillaries, primarily at sites of vessel branching, and in the endothelium of the capillaries of some tumors. Seghezzi et al. showed in an *in vivo* angiogenesis experiment with the mouse cornea that (endogenous or exogenous) FGF2 modulates endothelial cell expression of VEGF *in vivo*, and that endothelial cell VEGF is an important autocrine effector of FGF2–induced angiogenesis. FGF2 and VEGF have synergistic effects on angiogenesis **(Seghezzi et al. 1998)**. They are released into the wound bed during hemostasis and promote the formation of new blood vessels **(Przybylski 2009)**.

More than a decade of research on VEGF and angiogenesis has provided evidence that VEGF has multiple roles in endothelial cells, controlling both physiological and pathological angiogenesis **(Gerhardt 2008)**. Among the different VEGF ligands, the role of VEGFA signaling in vascular endothelial cells is understood best. VEGFA interacts with fetal liver kinase 1 (Flk1, also known as VEGFR2) and Fms-like tyrosine kinase 1 (Flt1, also known as VEGFR1). Flt1 is alternatively spliced to produce both a membrane-localized form (mFlt1) and a soluble form (sFlt1) that is secreted from endothelial cells. Soluble Flt1 is capable of binding VEGFA, which inhibits the pro-angiogenic functions of the ligand **(Matsumoto & Ema 2014)**. While the gene encoding VEGFA was found to be up-regulated in $EPCs^{co\text{-}cu}$, the gene encoding Flt1 was down-regulated. Thus, these results show a preferable pro-angiogenic fate of EPCs after direct cell-cell contact with MSCs.

These findings are supported by the appearance of two more differentially expressed genes affiliated with angiogenesis. Through their paracrine action as products of cells such as fibroblasts or smooth muscle cells or through their autocrine action as products of endothelial cells, the two members of the CCN family, CYR61 (CCN1) and CTGF (CCN2), can promote endothelial cell growth, migration, adhesion and survival *in vitro*. Both proteins are transcriptionally activated in endothelial cells in response to FGF2 or VEGF. The expression pattern of CTGF and CYR61 in endothelial cells of vessels *in situ* supports a role for these molecules in normal endothelial homeostasis, as well as participating in the angiogenic process during embryonic development, placentation, tumor formation, fibrosis, and wound healing **(Brigstock 2002)**.

CCN proteins share a modular structure, with an N-terminal secretory peptide followed by four conserved domains with sequence homologies to insulin-like growth factor-binding protein (IGFBP), von Willebrand factor type C repeat (vWC), thrombospondin type I repeat (TSR), and a carboxyl-terminal (CT) domain that contains a cysteine knot motif (Figure 50). Each conserved structural domain is encoded by a separate exon, suggesting that CCN genes arose through exon shuffling **(Lau 2011)**.

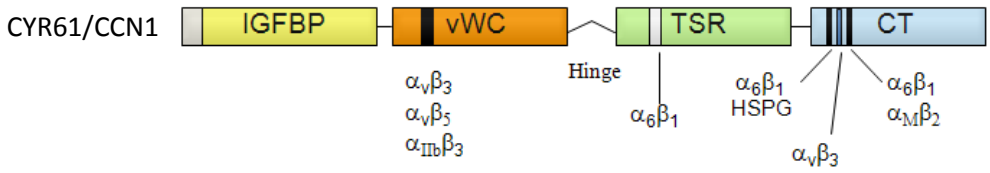

Figure 50: Schematic diagram of CYR61/CCN1 and its receptor binding sites
Each domain is depicted as a box with a unique color, with the domain name shown in the box. The grey box represents the secretory signal peptide. Integrin/HSPGs binding sites are marked as stripes. IGFBP, insulin-like growth factor-binding protein; vWC, von Willebrand factor type C repeat; TSR, thrombospondin type I repeat; CT, carboxyl-terminal domain; HSPG, heparan sulfate proteoglycans (www.atlasgeneticsoncology.org, 2015-02).

CYR61 is an immediate-early gene expressed at a very low level in quiescent cells, but is transcriptionally activated within minutes of stimulation by e.g. FGF2, TGF-ß1, IL1, TNF-α and prostaglandin E2 **(Lau 2011)**.
CYR61 was amongst the top 50 up-regulated genes in EPCs$^{co\text{-}cu}$ (logFC = 4.78). The re-evaluation of the microarray data by RT-PCR showed bands at different sizes for the treated cells and the respective control cells when used an intron 4-spanning primer pair (*CCN1 4-5*). These findings indicated the existence of intron-retaining *CCN1* mRNA in control EPCs and an enhanced transcription and production of intron-free *CCN1* mRNA in EPCs upon contact with MSCs. To evaluate if splicing is restricted to intron 4, additional primer pairs were used to span the remaining three exon-intron transitions (*CCN1 1-2, CCN1 2-3, CCN1 3-4*). The RT-PCR was performed using RNA specimens of 6 individual co-culture experiments.
The preliminary tests show *CCN1* intron splicing in EPCs for at least two introns (intron 3 and 4) of the *CCN1* mRNA and enhanced transcription of *CCN1* after co-culture with MSC. A similar effect was recently reported for the interleukin-6 (IL-6)-dependent myeloma cell line INA-6 after contact with MSCs by Julia Dotterweich from our group **(Dotterweich et al. 2014)**. She showed that INA-6 cells display an increased transcription and induction of splicing of intron-retaining *CCN1* pre-mRNA when cultured in contact with MSC. INA-6 control cells express the intron-retaining pre-mRNA, whereas INA-6 cells in contact with MSC express both the intron-retaining pre-mRNA and, to a greater extent, the intron-free isoform. The results were confirmed on protein level by western blot using the polyclonal antibody CYR61 H-78, raised against amino acids located in the hinge region. In addition, she showed that exogenous stimulation by recombinant CYR61-Fc protein induces *CCN1* pre-mRNA splicing and transcription in INA-6 cells in a concentration-dependent manner.
The production of truncated CCN proteins as well as variants of CCN proteins via alternative splicing have been reported by several groups **(Perbal 2009; Hirschfeld et al. 2009; Leng et al. 2002; Dotterweich et al. 2014)**. There is growing evidence that the production of CCN variants deprived of one or more elementary modules has profound biological effects. However, up to this date, there is little known about the variants and their biological function in physiological and pathological conditions. Their potential regulatory functions have only recently begun to be widely accepted **(Perbal 2009)**. The contact with MSCs seems to be a switch from intron retention to intron skipping, but further functional studies are required to determine the role of alternative splicing of *CCN1* mRNA in EPCs. Experiments to verify the results obtained in the present study are currently in progress. Since CYR61 is also a key player in tumor angiogenesis, a better knowledge of specific inducers of alternative *CCN1* splicing toward the intron skipping mRNA isoform and the underlying mechanisms in physiological conditions would be highly beneficial for a better understanding of the potential biological consequences in tumor cells.
Thrombospondin 1 and 2 (THBS1 and THBS2) – two other genes found to be up-regulated in EPCs$^{co\text{-}cu}$ – were among the first protein inhibitors of angiogenesis to be identified. A major pathway by which THBS1 or THBS2 inhibits angiogenesis involves an interaction with CD36 on endothelial cells, which

leads to apoptosis of both the liganded and adjacent cells **(Bornstein 2009)**. Interestingly, the microarray analysis of EPCs$^{co\text{-}cu}$ showed an up-regulation for the genes encoding for THBS1 and THBS2, and a down-regulation for CD36. Silverstein et al. identified in 2007 a circulating protein, histidine-rich glycoprotein (HRGP), that contains a CD36 homology domain and that acts as a soluble decoy to block the anti-angiogenic activities of THBSs, thereby promoting angiogenesis **(Silverstein & Febbraio 2007)**. The context dependent role of the THBS-CD36-HRGP axis in (tumor) angiogenesis is subject to current studies **(Hale et al. 2012; Chu et al. 2013)**. The review by Bornstein et al. on THBSs as regulators of angiogenesis included the initial work by Armstrong et al. (2002) that indicates that both THBS1 and THBS2 can inhibit the proliferation of human microvascular endothelial cells in the absence of cell death, and that the mechanisms responsible for inhibition of cell cycle progression differs from those leading to apoptosis. Both suggested pathways – the apoptotic and homeostatic – are shown in Figure 51. The authors take into consideration that in the event of trauma, it would seem preferable for endothelial cells in the periphery of a wound to become quiescent rather than to undergo apoptosis in response to THBS1, because the exposure of additional sub-endothelial matrix could lead to more extensive and undesirable thrombosis. As shown in Figure 51, the coordinated interaction of THBS1 or THBS2 bound to the very low density lipoprotein receptor (VLDLR), and VEGF bound to the VEGF receptor (VEGFR) leads to an inhibition of the PI3K and MAPK pathways, and consequently to the inhibition of cell cycle progression in endothelial cells **(Bornstein 2009)**.
In conclusion, the findings of the present study show that upon contact with MSCs, EPCs up-regulate several important key players in angiogenesis. Although some of the differentially expressed genes are known to exert anti-angiogenic effects, the sum of all these different molecules reflects the tight regulations and orchestrated mechanisms needed to support and to maintain an appropriate response to situations where angiogenesis is required.

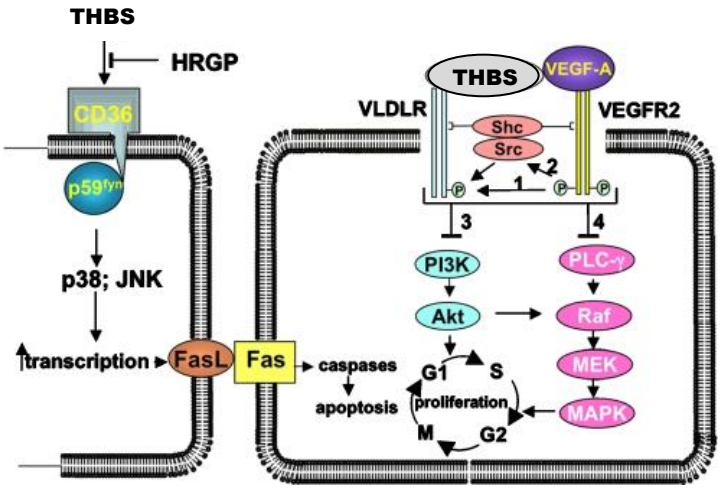

Figure 51: A scheme that describes the apoptotic (left) and homeostatic (right) functions of the THBSs
Left: the mechanism for the apoptotic function of thrombospondin-1 or -2 (THBS1 or THBS2). Activation of CD36 also leads directly to an increase in transcription of caspases and the TNF-R. Right: the coordinated and integrated interaction of THBS1 or THBS2 with the very low density lipoprotein receptor (VLDLR) and vascular endothelial growth factor (VEGF)-bound VEGF receptor (VERFR), together with the activation of Src and the adapter protein, Shc, leads to an inhibition of the PI3K and MAPK pathways, and consequently, of the cell cycle progression in endothelial cells (Bornstein 2009).

5.5.2.3 EPCs: Reflection on results affiliated to osteogenesis

There are numerous reports demonstrating that EPCs are the cells of choice for angiogenesis **(Risau 1994; Folkman & Shing 1992; Tonnesen et al. 2000; Liu & Velazquez 2010)**. The present study shows that EPCs are also beneficial for the purpose of osteogenesis. The microanalysis of EPCs$^{co\text{-}cu}$ revealed some differentially expressed genes involved in the migration, recruitment and differentiation of MSCs, e.g. two members of the CCN protein family (CYR61/CCN1 and CTGF/CCN2), integrin-binding sialoprotein (IBSP), fibroblast growth factor 2 (FGF2), bone morphogenetic protein 2 (BMP2), vascular endothelial growth factor (VEGF) and cadherin 11 type II (CDH11).

Luo et al. demonstrated that the exogenous expression of CTGF (CCN2) was able to promote cell migration and recruitment of mesenchymal stem cells in various *in vitro* assays. Furthermore, tight regulation of CTGF expression may be essential for normal osteoblast differentiation of mesenchymal stem cells and bone formation **(Luo et al. 2004)**. CYR61 (CCN1) stimulates osteoblast differentiation through an $\alpha_v\beta_3$/integrin-linked kinase-dependent pathway but inhibits osteoclastogenesis, suggesting its role as a bifunctional regulator of bone remodeling that promotes bone formation but inhibits bone resorption **(Lau 2011)**.

BMP/TGF-ß pathways are major signaling cascades responsible for osteogenesis. TGF-ß signaling promotes osteoprogenitor proliferation, early differentiation, and commitment to the osteoblastic lineage through the selective MAPKs and Smad2/3 pathways **(Matsunobu et al. 2009)**.

Tsuji et al. showed in mice lacking the ability to produce BMP2 that BMP2 is a necessary component of the signaling cascade that governs fracture repair. The authors also demonstrated that the high expression level of BMPs was generated by endothelial cells **(Tsuji et al. 2006)**. In addition, BMP2-elicited bone formation and bone healing is enhanced by the delivery of exogenous VEGF. The administration of the soluble form of fms-like tyrosine kinase 1 (sFlt1), a specific antagonist of VEGF, significantly inhibited BMP2-induced bone formation whereas the delivery of exogenous VEGF enhanced BMP2-induced bone formation and bone healing through modulation of angiogenesis **(Peng et al. 2005)**.

The FGF pathway has been shown to be involved in osteogenesis as well as several other cellular processes, such as angiogenesis and wound healing. Normally, the FGF pathway stimulates osteoblast differentiation and inhibits osteocyte differentiation. It has also been shown that runt-related transcription factor 2 (Runx2) is phosphorylated and activated by FGF2 via the MAPK pathway, which suggests an important role for FGF2 in the regulation of Runx2 function and bone formation **(Hayrapetyan et al. 2014)**.

Integrin-binding bone sialoprotein (IBSP, also known as BSP) is a secreted glycoprotein primarily found in sites of biomineralization. In bone, IBSP has been shown to mediate the attachment of osteoblasts and osteoclasts via $\alpha_v\beta_3$ integrin receptors. Ligands for $\alpha_v\beta_3$ integrin are considered to play a central role during angiogenesis. Therefore, IBSP could play a critical role in angiogenesis associated with bone formation **(Bellahcène et al. 2000)**.

Cadherin-mediated cell-cell adhesion is a fundamental mechanism involved in cell fate specification, tissue organization and morphogenesis during embryonic development. Cadherin 11 (CDH11, also known as osteoblast-cadherin) is a crucial regulator of postnatal skeletal growth and bone mass maintenance, serving distinct functions in the osteogenic lineage **(Di Benedetto et al. 2010)**.

In summary, the present study has identified specific genes and pathways associated with the osteogenic and angiogenic potential of EPCs, thus providing significant information toward improved understanding of the use of EPCs for functional bone tissue engineering applications.

5.5.2.4 Klotho: A gene differentially expressed in EPCs co-cultured with MSCs

In Greek mythology, Clotho was one of the Three Fates. She was responsible for spinning the thread of life. This meaningful name was given to a new gene that had been identified to be involved in the suppression of several ageing phenotypes (Figure 52). Kuro-o et al. were the first ones who described in their study in 1997 that a defect in klotho gene (*kl*) expression in the mouse results in a syndrome that resembles human ageing, including a short lifespan, infertility, arteriosclerosis, skin atrophy, osteoporosis and emphysema **(Kuro-o et al. 1997)**.

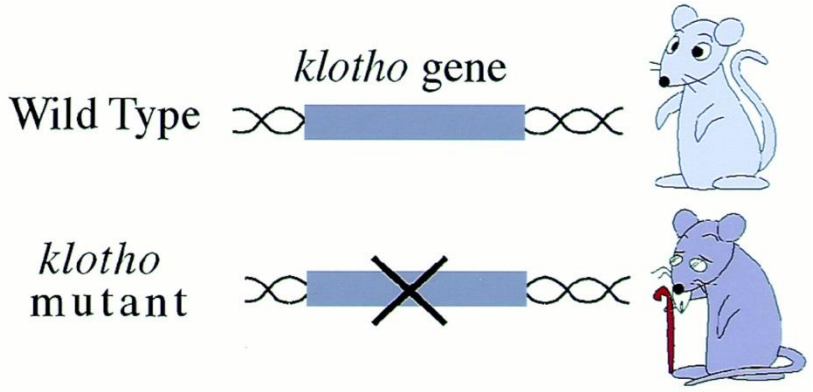

Figure 52: The klotho mouse model
A mutant model mouse is useful for studies of aging. The klotho phenotype (premature aging) is caused by a disruption of the single gene, klotho (Takahashi et al. 2000).

The mouse *kl* gene is a member of the beta-glucosidase gene family and encodes a single-pass membrane protein. Matsumura et al. identified two transcripts that encode a membrane (also known as isoform 1) or secreted (also known as isoform 2) protein. These transcripts arise from a single *kl* gene through alternative RNA splicing. Expression of the putative secreted form predominates over that of the membrane form **(Matsumura et al. 1998)**. In addition, the *kl* gene has been reported to encode two other klotho proteins, ß-klotho and klotho-related protein **(Xu & Sun 2015)**. Therefore, the originally described klotho variant is also known as α-klotho (α-KL). The full-length α-KL protein is a transmembrane protein that contains two separate glycosyl hydrolase domains, KL1 and KL2 (Figure 53). An interesting post-translational modification is the cleavage of α-KL in a process named α-cut. The cleaved product is a soluble α-KL protein (approximately 130 kDa) that lacks both transmembrane and intracellular domains. Another mechanism named β-cut, cleaves α-KL between the KL1 and KL2 domains and generates two fragments (approximately 65 kDa each). This truncated α-KL protein is also known as the soluble α-KL protein. In contrast, the secreted α-KL protein contains an N-terminal signal peptide that is followed by the KL1 domain only (approximately 65 kDa). It should be mentioned that circulating klotho may include both soluble and secreted klotho **(Xu & Sun 2015; Chen et al. 2014)**.

The microarray analysis of the EPCs$^{co\text{-}cu}$ revealed an up-regulation of the *kl* gene. Re-evaluation of the findings by RT-PCR confirmed the microarray results. In addition, the RT-PCR revealed an up-regulation of both, the mRNA of the full-length and the secreted form (Figure 37, Page 85). To date, there are no publications reporting the expression of KL in EPCs, neither in general nor upon contact with MSCs. As discussed above, it is known that mutation of the *kl* gene causes extensive aging phenotypes. To date, it is believed that KL is being expressed in only a few tissues. However, the mechanisms by which one protein causes such extensive aging phenotypes remains poorly understood. The present study reports for the first time that klotho is involved in the crosstalk of MSCs and EPCs. However, the determination of the exact role of KL in this cell-cell communication requires further validation. Future studies are warranted to explore the biochemical and physiological functions of KL.

In this issue, the latest review on klotho by Xu and Sun summarizes state-of-the-art knowledge about the structure of the *kl* gene and the factors that regulate *kl* gene transcription. The authors postulate that circulating KL may function as a hormone and regulate the functions of cells or tissues that do not express KL, e.g. vascular endothelial cells and smooth muscle cells. However, the authors conclude that further studies are needed to determine the nature of the generation and regulation of secreted KL and the mechanism of action of secreted KL, including the identification and characterization of the binding sites or receptors of KL **(Xu & Sun 2015)**.

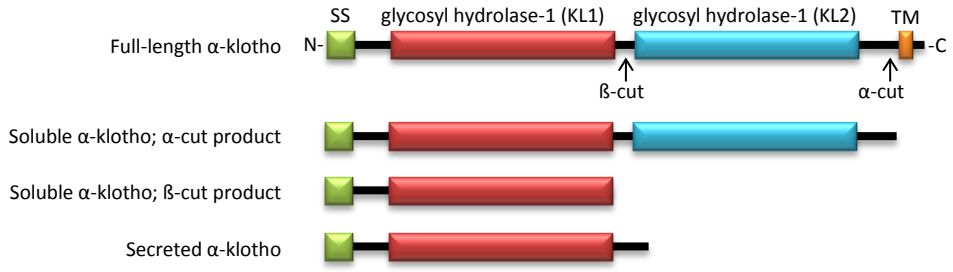

Figure 53: Architecture of the human klotho protein
The transmembrane protein (full-length) consists of two glycosyl hydrolase domains, named KL1 and KL2. The truncated α-klotho protein, which is also known as the soluble α-klotho protein, is released from the cell membrane by post-translational cleavage and contains either KL1 only (ß-cut product) or both KL1 and KL2 (α-cut product). Secreted α-Klotho is generated by the alternative mRNA splicing of α-klotho. The protein sequence of the secreted α-klotho protein is similar to that of the KL1 domain of α-klotho except for the C-terminus. The amino acids 535–549 (DTTLSQFTDLNVYLW) in the α-klotho protein are replaced with the sequence SQLTKPISSLTKPYH in secreted α-klotho. SS, signal sequence; TM, transmembrane domain. Figure adapted from Xu & Sun 2015.

Nonetheless, the present study raised the question: How is klotho related to the crosstalk of EPCs and MSCs? Despite the fact that functional studies remain to be elucidated to prove the results of this study, the following discussion summarizes briefly the current understanding of the role of klotho in this issue and tries to draw a picture that places the findings of the present study into state-of-the-art models of biological functions and cell signaling with special focus on the wingless (Wnt) signaling pathway. It should be mentioned that KL influences several intracellular signaling pathways which underlie the molecular mechanism of KL function. The exact biological functions of KL and the underlying molecular mechanisms are not fully understood **(Wang & Sun 2009)**.

Resident and circulating stem and progenitor cells are critical for ongoing tissue maintenance and repair, and it is often postulated that stem and progenitor cell depletion or dysfunction might contribute to aging. Liu et al. examined stem cell dynamics in a genetic model of accelerated aging, using mice lacking KL expression. The authors reported that tissues and organs from KL-deficient animals showed evidence of increased Wnt signaling, and ectopic expression of KL antagonized the activity of endogenous and exogenous Wnt **(Liu et al. 2007)**. It was recently reported that the extracellular domain of klotho protein binds to multiple Wnt ligands and inhibits their ability to activate Wnt signaling. Klotho may therefore suppress Wnt signaling **(Camilli et al. 2011; Liu et al. 2007; Wang & Sun 2009; Xu & Sun 2015)**.

Signaling by the Wnt family of secreted glycolipoproteins is one of the fundamental mechanisms that direct cell proliferation, cell polarity and cell fate determination during embryonic development and tissue homeostasis **(MacDonald et al. 2009)**. Wnt signaling is modulated by a number of evolutionarily conserved inhibitors and activators. Wnt inhibitors belong to small protein families, including secreted frizzled-related proteins (sFRP), dickkopf Wnt signaling pathway inhibitor proteins (DKK), Wnt-inhibitory factor 1 (WIF1), insulin-like growth factor binding protein 4 (IGFBP4), Shisa, and adenomatosis polyposis coli down-regulated 1 (APCDD1). Antagonists and agonists are of great importance, as they control the fine-tuning of Wnt signaling and inhibit or activate Wnt-regulated developmental processes, such as angiogenesis, vasculogenesis, and limb, bone, tooth, and eye

formation, and they are implicated in pathological events, including cancer and bone disease. **(Cruciat & Niehrs 2013)**.

The microarray analysis of the EPCs$^{co\text{-}cu}$ had unraveled an up-regulation of the gene encoding klotho. As discussed above, the subsequent literature search had identified klotho as a potent Wnt signaling inhibitor. Thus, the question rose if EPCs differentially express more genes affiliated with Wnt signaling upon direct cell-cell contact with MSCs. Therefore the list of differentially regulated genes was searched for further genes known to be involved in the Wnt signaling pathway. The results are displayed in Table 23 (Page 72). The results show that besides the up-regulation of the *kl* gene, EPCs differentially express a cluster of genes affiliated with the inhibition of the Wnt signaling pathway, e.g. DKK1, Kremen 1 and IGFBP4 upon direct cell-cell contact with MSCs.

Recently published data revealed that the Wnt signaling pathway is activated during postnatal bone regenerative events, such as ectopic endochondral bone formation and fracture repair. Dysregulation of this pathway greatly inhibits bone formation and healing process. Interestingly, activation of Wnt pathway has potential to improve bone healing, but only utilized after mesenchymal cells have become committed to the osteoblast lineage. In early pluripotent mesenchymal stem cells, Wnt/beta-catenin signaling needs to be precisely regulated to facilitate the differentiation of osteoblasts **(Chen & Alman 2009; Silkstone et al. 2008)**.

Summarizing the findings leads to the following conclusions:

Brack et al. found that Wnt signaling appeared to be more active in aging animals and Liu et al. reported that both *in vitro* and *in vivo*, continuous Wnt exposure triggered accelerated cellular senescence. These results indicate that the Wnt signaling pathway may play a critical role in tissue-specific stem cell aging. Thus, klotho appears to be a secreted Wnt antagonist and Wnt proteins have an unexpected role in mammalian aging **(Liu et al. 2007; Brack et al. 2007)**.

During the last decade, canonical Wnt signaling has been shown to play a significant role in the control of osteoblastogenesis and bone formation. Once mesenchymal stem cells are committed to the osteoblast lineage, activation of Wnt/β-catenin signaling enhances bone formation **(Silkstone et al. 2008; Yavropoulou & Yovos 2007)**.

The klotho gene expression is up-regulated in EPCs after direct cell-cell contact with MSCs. As discussed above, KL is a key player in several important physiological processes. The crucial role of KL discloses with age when KL levels decrease and age-dependent phenotypes increase. This was demonstrated and confirmed in several studies employing the *kl/kl* mouse model. Further studies unraveled the role of KL in physiological conditions, e.g. as an important regulator of the Wnt signaling pathway. The *in vivo* regulation of Wnt/ß-catenin by KL, including its role in aging, requires further validation. The changes of the global gene expression patterns of EPCs upon direct cell-cell contact with MSCs revealed in addition further genes affiliated with the Wnt signaling pathway. It is known that the fine-tuning of the Wnt/ß-catenin signaling is crucial for normal bone formation. The role of EPCs and MSCs in the formation of bone has been discussed in detail in the previous chapters and will be summarized in the following chapter.

In conclusion, the present study gives interesting insights in the crosstalk of EPCs and MSCs and sheds light on the connection and orchestrated interplay between these cells and the key players involved.

5.5.3 Summary of the crosstalk of EPCs and MSCs

While the importance of vascularization to bone healing has been recognized, the molecular and cellular mechanisms regulating angiogenesis and their relationship to the mechanisms of bone repair are not fully understood. Recent studies have shown that both, vascular and skeletal morphogenesis, are interdependent on each other. There is a reciprocal co-dependency between vascular and skeletal tissues in which each tissue provides morphogenetic signals or environmental cues that are crucial for the other's development **(Matsubara et al. 2012)**. The previous chapters have introduced some important genes differentially expressed in either EPCs or MSCs upon direct cell-cell contact or by humoral mediated effects through the distribution of conditioned medium. The results have been discussed with special focus on inflammation, immunomodulation, ECM remodeling, angiogenesis and osteogenesis. The genes of interest were observed with regard to the individual cell types and the findings were compared to state-of-the-art data. Since the present study aimed to give insights into the crosstalk of EPCs and MSCs, this chapter will focus on the communication between the two main actors in angiogenesis and bone formation. As the playground of this communication are sites of injured or damaged tissue, this summary will first provide a short introduction on the processes involved in wound healing and tissue repair before discussing the means of the differentially expressed genes on the respective other cell type.

Hemostasis begins after the disruption of blood vessels, which leads to a series of events designed to halt blood loss. The next phase in healing is the inflammatory phase, which is characterized by the sequential influx of immune cells that, among their other activities, remove bacteria, debris, and devitalized tissue. The proliferative phase is characterized by the formation of granulation tissue – new blood vessels, macrophages, fibroblasts, and loose connective tissue – as well as early wound contraction and re-epithelialization. During the proliferative phase, fibroblasts that are initially bound to fibronectin via $\alpha_v\beta_5$ or $\alpha_v\beta_3$ integrins migrate and proliferate in response to platelet-derived growth factor (PDGF), producing an extracellular matrix (ECM) that is relatively sparse but enriched in hyaluronan and with relatively higher levels of type III collagen. Under the influence of transforming growth factor beta (TGF-β) and connective tissue growth factor (CTGF), collagen I becomes the predominant fibrous protein **(Schultz et al. 2011)**. An example of the dynamic reciprocity (DR) in different stages of wound healing is provided in Figure 54.
Arnott et al. demonstrated that CTGF (also known as CCN2) is an essential downstream mediator for TGF-ß 1-induced ECM production in osteoblasts **(Arnott et al. 2007)**. Furthermore, exogenous expression of CTGF was shown to promote cell migration and recruitment of mesenchymal stem cells **(Luo et al. 2004)**. CTGF was amongst the top 10 up-regulated genes found in $EPCs^{co\text{-}cu}$ indicating its important role in the crosstalk of EPCs and MSCs. Besides its beneficial contribution towards osteogenesis, Ivkovic et al. showed in CTGF-null mice that CTGF also is a key regulator coupling extracellular matrix remodeling to angiogenesis. Coordinated production and remodeling of the extracellular matrix is essential during development. It is of particular importance for skeletogenesis (Figure 55), as the ability of cartilage and bone to provide structural support is determined by the composition and organization of the ECM **(Ivkovic et al. 2003)**. The microarray analysis of $EPCs^{co\text{-}cu}$ identified numerous differentially expressed genes involved in ECM remodeling, e.g. collagens, fibronectin and laminins. Their means and implications towards angiogenesis have been discussed in detail in Chapter 5.5.2.1. However, ECM deposition, subsequent matrix remodeling, and corresponding integrin expression profiles influence as well osteogenesis in MSCs **(Kundu et al. 2009)**.
Bone formation is tightly controlled by a balance between anabolism, in which osteoblasts are the main players, and catabolism, mediated by the osteoclasts. Osteoblasts and osteoclasts express specific integrin receptors and the pattern of expression varies depending on the stage of cell differentiation. Integrins are a superfamily of cell surface receptors involved in cell-cell and cell-matrix adhesion **(Grzesik 1997)**. These αβ heterodimeric transmembrane glycoproteins mediate adhesion of a wide range of cells to matrix proteins, such as fibronectin, collagen, and laminin, and

may therefore be important for cell-matrix interactions in bone **(Hughes et al. 1993)**. For example, the $\alpha_5\beta_1$ integrin, a cell surface receptor for fibronectin, controls osteoblast adhesion and survival and plays a critical role in MSC osteogenic differentiation, bone formation and repair **(Saidak et al. 2015)**. Mutations in type I collagen genes result in osteogenesis imperfecta. Osteogenesis imperfecta, commonly known as "brittle bone disease", is a dominant autosomal disorder characterized by bone fragility and abnormalities of connective tissue **(Gajko-Galicka 2002)**. However, cell-matrix interactions are not only of interest in physiological and pathological conditions. Scientists have also studied these interactions for the use of ECM components in the generation of (cell-based) tissue-engineered constructs. With the aging population, the incidence of bone defects due to fractures, tumors and infection will increase. Therefore, bone replacement will become an ever bigger and more costly problem. The control of bone tissue cell adhesion to biomaterials is an important requirement for the successful incorporation of implants or the colonization of scaffolds for tissue repair. Controlling cell-biomaterial interactions appears of prime importance to influence subsequent biological processes such as cell proliferation and differentiation **(Marquis et al. 2009)**.

A better understanding of the natural occurring cell-cell communication as well as cell-matrix interactions and therefore knowledge about the microenvironment created or mediated by the cells has proven to be beneficial for the generation of ECM-inspired coatings or scaffolds in the field of tissue engineering. Different *in vitro* studies have already shown the successful use of e.g. collagen, collagen-mimetic peptide or laminin-derived peptide-coated grafts and reported improved bone formation **(Rentsch et al. 2014; Min et al. 2013; Wojtowicz et al. 2010; Liu et al. 2004)**. The efforts in trying *in vitro* tissue reconstruction must be driven toward the exact knowledge of cell function on the one hand, and, on the other hand, toward the knowledge of interactions and signals that cells must receive from the environment to behave as in natural tissues **(Rosso et al. 2004)**. The present study shows that MSCs organize their surrounding microenvironment by employing EPCs to differentially express genes belonging to ECM components. In return, these components subsequently administering an effect to MSCs by influencing cell migration, proliferation, differentiation and adhesion.

Osteoblast lineage-specific differentiation from the pluripotent MSCs is a well-orchestrated process. Bone morphogenetic proteins (BMPs) that belong to the TGF-β superfamily play an important role in regulating osteoblast differentiation and subsequent bone formation. Luo et al. demonstrated that osteogenic BMPs (e.g. BMP2, BMP6, and BMP9) regulate a distinct set of downstream targets that may play a role in regulating BMP-induced osteoblast differentiation **(Luo et al. 2004)**. Especially BMP2 was shown to mediate the crosstalk between angiogenesis and osteogenesis during bone repair. The observed up-regulation of the BMP2 gene in $EPCs^{co\text{-}cu}$ correlates with the findings of Matsubara et al. who described that vascular tissues are a primary source of BMP2 during bone formation **(Matsubara et al. 2012)**.

The discovery of the RANKL/RANK/OPG system for the regulation of bone resorption in the mid-1990s has led to major advances in the understanding of how bone modeling and remodeling are regulated. Receptor activator of nuclear factor kappa-B (NF-κB) ligand (RANKL), receptor activator of NF-κB (RANK) and osteoprotegerin (OPG) are members of the tumor necrosis factor (TNF) and TNF receptor (TNFR) superfamilies (SF) and share signaling characteristics common to many members of each (they are also known as TNFSF11, TNFRSF11a and TNFRSF11b, respectively). Developmentally regulated and cell-type specific expression patterns of each of these factors have revealed key regulatory functions for RANKL/RANK/OPG in bone homeostasis, organogenesis, immune tolerance, and cancer **(Boyce & Xing 2008; Walsh & Choi 2014)**. RANKL/RANK signaling regulates osteoclast formation, activation and survival in normal bone modeling and remodeling and in a variety of pathologic conditions characterized by increased bone turnover. OPG, a physiological decoy receptor of RANKL, protects bone from excessive resorption by binding to RANKL and preventing it from binding to RANK **(Boyce & Xing 2008)**.

OPG (TNFRSF11b) was amongst the genes found to be differentially expressed in $EPCs^{co\text{-}cu}$.

Köttstorfer et al. monitored serum levels of OPG and soluble RANKL (sRANKL) in 64 patients with a long bone fracture over a time period of 48 weeks after injury. The authors found that OPG levels in patients with a long bone fracture were strongly enhanced compared to healthy controls (n = 33).

Further, levels of free sRANKL were decreased during regular fracture repair. In non-unions sRANKL and OPG levels showed a variable course, with no statistical significance **(Köttstorfer et al. 2014)**. At first glance, an up-regulation of the gene encoding OPG thus seems to be reasonable and beneficial towards osteoblastogenesis and bone formation. However, since OPG functions as a negative regulator of RANK signaling, is capable of inhibiting osteoclastogenesis *in vitro*, and of inducing osteoporosis when transgenically overexpressed in mice, it is of no surprise that a tight regulation of the RANKL/RANK/OPG triad is crucial **(Walsh & Choi 2014)**. And indeed, there are additional ligands of OPG that confer various biological functions. OPG can promote cell survival, cell proliferation and facilitates migration by binding TNF-related apoptosis inducing ligand (TRAIL), glycosaminoglycans or proteoglycans **(Baud'huin et al. 2013)**. TRAIL (also known as TNFSF10) is a tumor necrosis factor-related ligand that induces apoptosis upon binding to its death domain-containing receptors, DR4 and DR5. Two additional TRAIL receptors, TRID/DcR1 and DcR2, lack functional death domains and function as decoy receptors for TRAIL. Emery et al. identified a fifth TRAIL receptor, namely OPG. The authors showed that OPG inhibits TRAIL-induced apoptosis *in vitro*. Conversely, TRAIL blocks the anti-osteoclastogenic activity of OPG. These data suggest potential cross-regulatory mechanisms by OPG and TRAIL **(Emery et al. 1998)**.

The gene encoding TRAIL was found to be up-regulated in MSCs$^{co\text{-}cu}$.

There are little data on the interactions between OPG, RANKL, and TRAIL. However, there are studies highlighting the pivotal role of OPG in regulating the biology of both RANKL and TRAIL **(Vitovski et al. 2007)**. It was reported by Corallini et al. that OPG is abundantly released by endothelial cells upon stimulation with inflammatory cytokines. The authors showed that administering recombinant TRAIL decreased the spontaneous OPG release. In addition, OPG down-regulation was not due to induction of cytotoxic effects by TRAIL, since the degree of apoptosis in response to TRAIL was negligible in all primary cell types **(Corallini et al. 2011)**.

Besides additional binding partners for OPG, there are also other cells than osteoblasts expressing RANKL. Cells involved in the processes of innate and adaptive immunity express RANKL, RANK or OPG molecules. RANKL is produced not only by bone marrow stromal cells and osteoblasts, but also by T cells. The RANK receptor is expressed by monocytes and dendritic cells. OPG is expressed by mature osteoblasts and B cells **(Ferrari-Lacraz & Ferrari 2009)**. Emerging understanding that key cellular regulators of the immune and bone systems were responsive to the same cytokine systems and derived from common progenitors was one of the key impetuses in developing a new field of study, osteoimmunology, which seeks to examine the interactions between the bone and immune systems **(Walsh & Choi 2014)**. The microarray analysis of MSCs$^{co\text{-}cu}$ identified numerous differentially expressed genes involved in inflammation and immunomodulation, e.g. BIRC3, CTSS, chemokine (C-X-C motif) ligands (CXCL9, CXCL11), human leukocyte antigens (HLA-DQA1, HLA-DQB1, HLA-DRA), indoleamine 2,3-dioxygenase 1 (IDO1), lysozyme (LYZ) and S100 calcium binding protein A8 (S100A8). Their means and implications toward tissue regeneration and healing with focus on MSCs have been discussed in detail in Chapter 5.5.1.1. As described at the beginning of this chapter and also illustrated in Figure 54, the inflammatory phase is an important process during wound healing. The effect of inflammatory cytokines on EPCs referring to the release of OPG has been discussed above.

Although the link between angiogenesis and inflammation has received much attention in recent years, there has long been evidence suggesting that these are two closely related processes. It should be emphasized that while inflammation and angiogenesis are capable of potentiating each other, these processes are distinct and separable. The balance between angiogenic and angiostatic factors determines the existence and rate of blood vessel proliferation in a tissue. In inflammation, this balance is clearly tipped in favor of angiogenesis. This response results, in part, because an inflammatory locus is often hypoxic and hypoxia is an important pro-angiogenic signal that activates the hypoxia-inducible factor signaling pathway, which elicits the transcription-dependent production of vascular endothelial growth factor (VEGF) and fibroblast growth factor (FGF) **(Granger & Senchenkova 2010)**. Both growth factors were among the differentially regulated genes in EPCs$^{co\text{-}cu}$.

This inflammation-induced angiogenesis and the subsequent remodeling steps are in large part mediated by ECM proteins and proteases. Further matrix remodeling and vascular regression contribute to the resolution of the inflammatory response and facilitate tissue repair **(Arroyo &**

Iruela-Arispe 2010). Motz and Coukos describe a fundamental biological program that involves the activation of both angiogenesis and immunosuppressive responses, often through the same cell types or soluble factors. The authors suggest that the initiation of these responses is part of a physiological and homeostatic tissue repair program which can be co-opted in pathological states, notably by tumors **(Motz & Coukos 2011)**. One factor with the capacity to promote both immunosuppression and angiogenesis is indoleamine 2,3-dioxygenase (IDO). The gene encoding for IDO was among the top 20 up-regulated genes in MSCs$^{co\text{-}cu}$. IDO is an intracellular enzyme that catalyzes tryptophan catabolism at the initial and rate-limiting step. Studies have clarified the mechanisms of IDO immunosuppression in tumors. IDO expressed by tumor cells depletes tryptophan locally and produces a toxic tryptophan catabolite kynurenine, which causes growth arrest and the apoptosis of effector T-cells or natural killer cells that are extremely sensitive to tryptophan shortage, and also suppresses their killer functions **(Yuko Tanizaki 2013)**. Kynurenine, a major metabolite of IDO, has significant roles in regulating vascular tone and endothelial dilation and may directly regulate angiogenesis. Thus, expression of IDO is potentially crucial to endothelial cell biology and may link angiogenesis and immune suppression **(Gabrilovich & Hurwitz 2014)**.

Much has been learned about the role of ECM remodeling in inflammation-driven angiogenesis. There is also a lot of knowledge about the different stages of wound healing and the mechanisms directing these different stages. However, the molecular regulatory events that mediate tissue-specific ECM changes, inflammatory response, repair and reconstruction are as complex as the factors, components and cells involved in these processes. It has become clear that the microenvironment organized and created by cells is as important as the crosstalk of the cells itself. It has also been shown that these processes are highly interdependent and that each tissue provides morphogenetic signals or environmental cues that are crucial for each other's development. Some of these exciting interactions and mechanisms have been discussed in the present thesis.

The present study aimed to shed light on some of these interactions. Key players involved in the crosstalk of EPCs and MSCs have been identified and analyzed in the context of ECM interaction, inflammation and immunomodulation, angiogenesis and osteogenesis. Thus, the present study provides significant information toward improved understanding of the use of EPCs and MSCs for functional bone tissue engineering applications and may be as well beneficial to other therapeutic applications. The results are a useful tool and a rich source of information for researchers from different scientific fields, e.g. tissue engineering, osteoimmunology and cancer research.

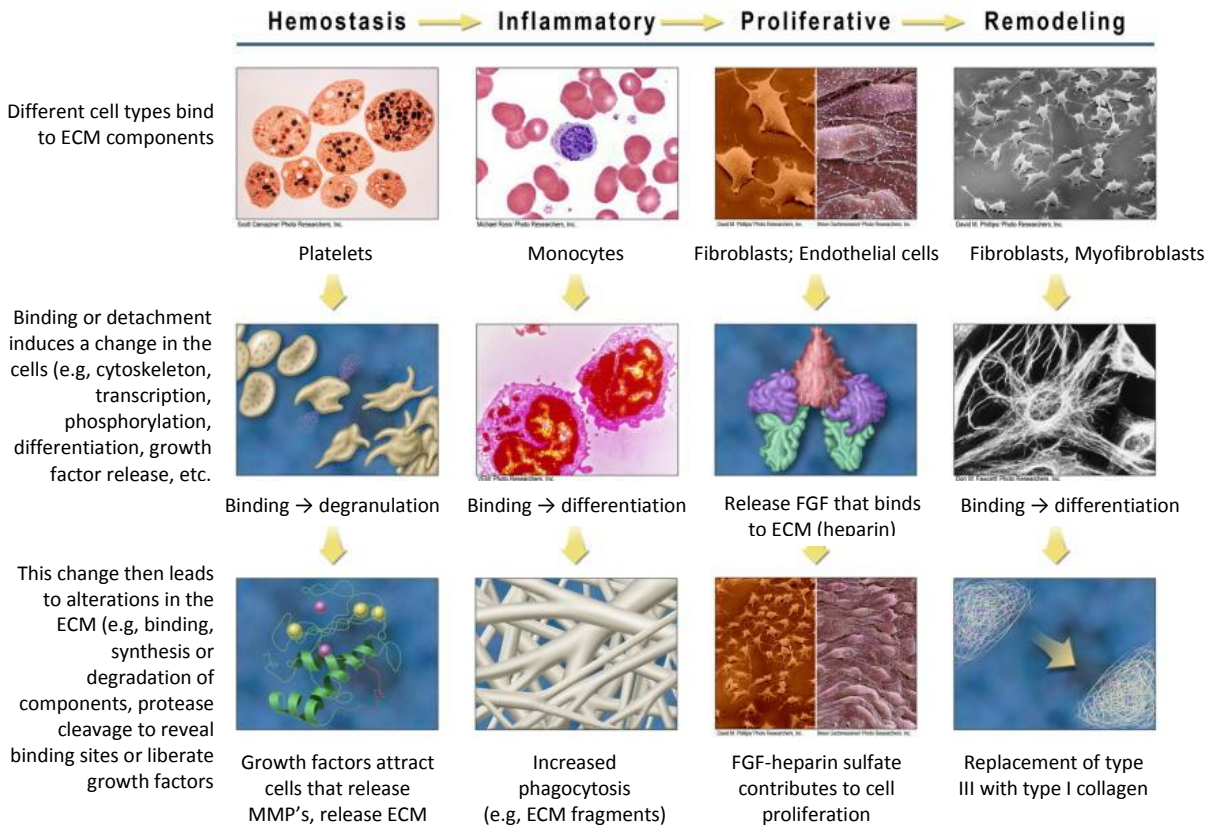

Figure 54: Key cellular examples of dynamic reciprocity in different stages of wound healing
Dynamic reciprocity (DR) is defined as an ongoing, bidirectional interaction amongst cells and their surrounding microenvironment. The figure shows key cellular examples of DR at each wound healing stage. The left-most column summarizes a general mechanism that invokes DR, beginning with the binding of cell types to ECM components. This binding (adhesion) or reduced/altered adhesion then leads to changes in the cells, which in turn leads to changes in the ECM. Examples of DR are provided at each wound healing stage, using one or two cell types for the purposes of illustration (Schultz et al. 2011).

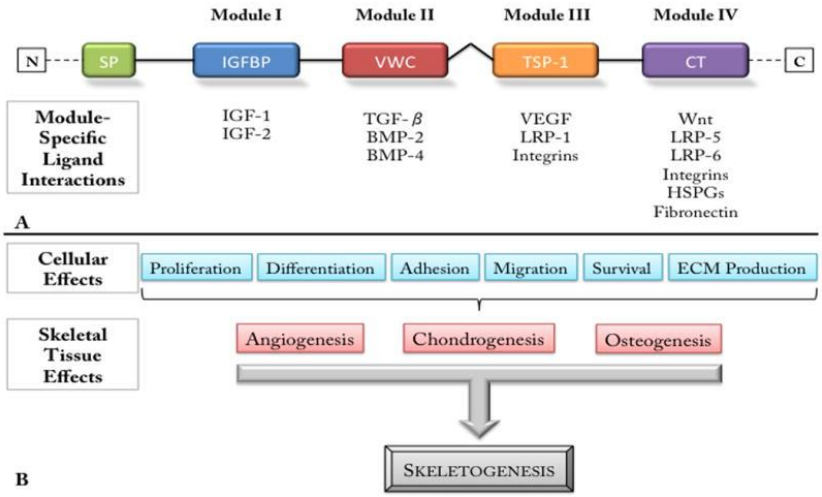

Figure 55: The modular structure and function of CTGF
A: The CTGF transcript contains a signal peptide (SP) as well as four modules: module 1 is an insulin-like growth factor (IGF)-binding domain; module 2 is a von Willebrand type C domain; module 3 is a thrombospondin-1 domain; and module 4 is a C-terminal domain containing a putative cysteine knot. Modules II and III are separated by a variable hinge region susceptible to enzymatic cleavage. Also shown below each module are molecules known to interact with this region of the secreted CTGF protein. B: The mosaic structure of these proteins allows for their involvement in many normal cellular events that contribute to key physiologic processes necessary for skeletogenesis (Arnott et al. 2011).

5.6 The klotho ELISA

The second part of the present study was the development of an ELISA (enzyme-linked immunosorbent assay) for a target protein chosen from the microarray findings in cooperation with Immundiagnostik AG, Bensheim, Germany. The protein of choice was klotho (KL). KL has been called an "aging suppressor gene" and has been suggested to delay age-related declines in physiological functioning **(Kuro-o et al. 1997)**. Both the membrane and secreted forms of KL have biological activity that include regulatory effects on general metabolism and a more specific effect on mineral metabolism that correlates with its effect on aging **(Dërmaku-Sopjani et al. 2013)**. Within the past few years there was growing interest to learn more about the role of KL since there is growing evidence about its importance in different conditions in health and disease, e.g. KL as a regulator of oxidative stress and senescence **(Kuro-o 2008)**, the role of KL in aging, phosphate metabolism, and chronic kidney disease **(John et al. 2011; Shimamura et al. 2012; Koizumi et al. 2013; Rotondi et al. 2015)** as well as cardiovascular disease **(Hu et al. 2014; Martín-Núñez et al. 2014; Kitagawa et al. 2013)** and vascular calcification **(Hu et al. 2011; Vervloet et al. 2014)**. For further investigations, there is a need to have tools to detect serum KL levels in healthy subjects and patients. Up to date, there are only a few assays available on the market and the methods for the measurement of α-klotho differ in quality. Heijboer et al. suggested in their study comparing 3 different ELISAs that some of the manufacturers should improve their assays in order to produce accurate results so that reliable conclusions can be drawn from studies in which these assays are used **(Heijboer et al. 2013)**.
The aim of this study was to develop an ELISA for the determination of KL in human serum and to generate a tool which could be highly beneficial in several fields of research, e.g. nephrology, osteology. The results show that the prototype of the assay has a linear standard curve in the range of 0 – 100 ng/ml. The antibodies used are custom-made and highly specific to KL (soluble KL and secreted KL). Serum samples of healthy subjects were detectable although the concentrations were at low levels. The prototype ELISA uses a specific scFV antibody immobilized to a microtiterplate and a rabbit-IgG1-Fc antibody as detection antibody followed by an anti-rabbit-HRP conjugate. Preliminary tests using a biotinylated rabbit-IgG1-Fc antibody as detection antibody followed by a Streptavidin-HRP conjugate showed that this second generation of the assay is more sensitive (range of the standard curve: 0 – 6 ng/ml). Further optimization steps including the new mouse-IgG1-Fc anti-KL antibody as coating antibody and an improved blocking solution are currently under investigation. In parallel, a sample preparation procedure will be tested to elevate/concentrate the KL levels before the sample is added to the assay.
In conclusion, the results look very promising. A first generation of an anti-klotho ELISA has been generated. However, it is a long way from R&D to be ready for the market and further studies are needed to demonstrate the performance of the assay. Nevertheless, as soon as the final version is ready and the regulatory requirements are fulfilled the product will be introduced to the market. The IDK® total klotho ELISA will be commercially available soon followed by the IDK® secreted klotho ELISA.

5.7 Conclusions

The present study successfully established a protocol to isolate and expand EPCs from buffy coat. The cells were characterized and used for experiments to assess the crosstalk of EPCs and MSCs. Therefore two different experimental settings were generated: experiments with conditioned medium and direct co-culture. The RNA gained from these experiments was used for microarray analyses. For each setting, 4 individual experiments were performed.
The bioinformatic analysis of the microarray data revealed lists of differential expressed genes that were successfully confirmed by RT-PCR re-evaluation. The differentially regulated genes were analyzed regarding to their role in angiogenesis, osteogenesis, immunomodulation, inflammation, ECM remodeling and Wnt signaling. The results shed light on some important biological processes and gave interesting insights into the communication of EPCs and MSCs. Several follow-up experiments are needed to investigate the role of e.g. klotho and CYR61 in the crosstalk of EPCs and MSCs, but the present thesis generated an essential fundament for further examinations.

In addition, in the second part of the present study, recombinant klotho protein as well as anti-klotho antibodies were generated and used to develop a prototype of a klotho ELISA. Suitable antibody combinations were identified and the standard curve as well as the antibody concentrations optimized. The current version of the ELISA is suitable to detect klotho in serum samples of healthy subjects. Currently, a sample preparation procedure is under investigation which aims to lift the optical densities of samples with low klotho concentration into the optimal range of the calibration curve. The klotho ELISA will be a useful tool to study the role of klotho in physiological and pathological conditions, e.g. in *in vivo* and *in vitro* models for the assessment of tissue regeneration processes or age related diseases.

5.8 Perspectives

The present study uncovered a lot of differentially expressed genes involved in the crosstalk of EPCs and MSCs. The results are very exciting and some of them confirmed existing knowledge, others unraveled new insights into the communication of these cells and some others also raised new questions. In any case, the results opened a platform that could be used as a rich source of information for all scientists working in the field of e.g. tissue engineering, osteoimmunology, or cancer research.
Amongst all these interesting results two findings aroused special attention:

- The up-regulation and alternative splicing of the CYR61 gene in EPCs after direct cell-cell contact with MSCs.
- The up-regulation of the klotho gene in EPCs after direct cell-cell contact with MSCs and its possible role in the Wnt signaling pathway.

The microarray results were successfully validated by RT-PCR. Functional studies on the protein level remain to be elucidated to confirm the results and shed light on some important biological processes.

The second part of the present study aimed to develop an ELISA for the determination of klotho. Therefore specific antibodies were generated and a prototype of the klotho ELISA was successfully developed. The results showed that the current version of the ELISA is suitable to determine samples of normal subjects. However, it is known from the literature that klotho concentrations are declining with age **(Carpenter et al. 2010)** and are decreased in some pathological conditions, e.g. diabetes **(Liu et al. 2014)**, chronic kidney disease **(Shimamura et al. 2012)** or anorexia nervosa and obesity **(Amitani et al. 2013)**. Taking this information into account, the development of the ELISA needs in addition an optimization of the sample preparation to be able to detect samples with lower klotho concentrations, too. The development of a sample preparation procedure aims to lift the optical densities of especially samples with low klotho concentrations into the optimal range of the standard curve. Preliminary tests showed that the use of disposable affinity columns that are filled with an immobilized antibody suspension (so called slurry) could be a useful tool to optimize the sample preparation procedure. Further optimization procedures are currently under investigation.
Since there is not only one form of klotho the ELISA also needs to be tested for its specificity to detect full-length klotho, soluble klotho and secreted klotho. It would be also interesting to know whether the antibodies recognize only human klotho or in addition e.g. mouse klotho. Rat and mouse klotho cDNA and protein have about 80 % homology with those of humans **(Wang & Sun 2009)**. The antibodies were raised against the KL1 domain of secreted klotho. Preliminary tests with full-length klotho (purchased from R&D systems) showed that the current version of the ELISA is not only able to bind the standard material the antibodies were raised against, but is also able to detect the full-length form. However, only one antibody combination was tested so far and further tests are required to optimize the standard curve using this standard material. Despite the fact that the optical densities were lower than with the previously used standard material, the full-length klotho material was linear dilutable and showed an acceptable low blank. Therefore, the results look very promising.
Finally, the ELISA needs to be validated and compared to commercially available kits.
In addition, the antibodies are currently tested in further applications, e.g. immunohistochemistry and western blot.

6 BIBLIOGRAPHY

Aguirre, A., Planell, J.A. & Engel, E., 2010. Dynamics of bone marrow-derived endothelial progenitor cell/mesenchymal stem cell interaction in co-culture and its implications in angiogenesis. *Biochemical and Biophysical Research Communications*, 400(2), pp.284–291.

Ahn, J.B. et al., 2010. Circulating endothelial progenitor cells (EPC) for tumor vasculogenesis in gastric cancer patients. *Cancer Letters*, 288(1), pp.124–132.

Aicher, A., Zeiher, A.M. & Dimmeler, S., 2005. Mobilizing Endothelial Progenitor Cells. *Hypertension*, 45(3), pp.321 –325.

Ambati, B.K. et al., 2006. Corneal avascularity is due to soluble VEGF receptor-1. *Nature*, 443(7114), pp.993–997.

Amitani, M. et al., 2013. Plasma klotho levels decrease in both anorexia nervosa and obesity. *Nutrition (Burbank, Los Angeles County, Calif.)*, 29(9), pp.1106–1109.

Anon, Introduction to Flow Cytometry: A Learning Guide.pdf. Available at: http://medicine.yale.edu/labmed/cellsorter/start/411_66019_Introduction.pdf [Accessed June 29, 2014].

António, N. et al., 2010. Challenges in vascular repair by endothelial progenitor cells in diabetic patients. *Cardiovascular & Hematological Disorders Drug Targets*, 10(3), pp.161–166.

Arnott, J.A. et al., 2007. Connective tissue growth factor (CTGF/CCN2) is a downstream mediator for TGF-beta1-induced extracellular matrix production in osteoblasts. *Journal of Cellular Physiology*, 210(3), pp.843–852.

Arnott, J.A. et al., 2011. The role of connective tissue growth factor (CTGF/CCN2) in skeletogenesis. *Critical Reviews in Eukaryotic Gene Expression*, 21(1), pp.43–69.

Arroyo, A.G. & Iruela-Arispe, M.L., 2010. Extracellular matrix, inflammation, and the angiogenic response. *Cardiovascular Research*, 86(2), pp.226–235.

Asahara, T. et al., 1997. Isolation of Putative Progenitor Endothelial Cells for Angiogenesis. *Science*, 275(5302), pp.964 –966.

Asahara, T. et al., 1999. VEGF contributes to postnatal neovascularization by mobilizing bone marrow-derived endothelial progenitor cells. *The EMBO Journal*, 18(14), pp.3964–3972.

Asahara, T. & Kawamoto, A., 2004. Endothelial progenitor cells for postnatal vasculogenesis. *American Journal of Physiology - Cell Physiology*, 287(3), pp.C572–C579.

Assar, M. El, Angulo, J. & Rodríguez-Mañas, L., 2013. Oxidative stress and vascular inflammation in aging. *Free Radical Biology and Medicine*, 65, pp.380–401.

Avin, K.G. et al., 2014. Skeletal muscle as a regulator of the longevity protein, Klotho. *Striated Muscle Physiology*, 5, p.189.

Bahlmann, F.H. et al., 2004. Erythropoietin regulates endothelial progenitor cells. *Blood*, 103(3), pp.921–926.

Balasubramanian, R. et al., 2011. The Puzzles Of the Prokineticin 2 Pathway in Human Reproduction. *Molecular and cellular endocrinology*, 346(1-2), pp.44–50.

Bancroft, T. et al., 2014. Upregulation of Thrombospondin-2 in Akt1-null Mice Contributes to Compromised Tissue Repair due to Abnormalities in Fibroblast Function. *The Journal of Biological Chemistry*.

Barber, T. et al., 2014. Vitamin A Deficiency and Alterations in the Extracellular Matrix. *Nutrients*, 6(11), pp.4984–5017.

Barry, F.P. & Murphy, J.M., 2004. Mesenchymal stem cells: clinical applications and biological characterization. *The International Journal of Biochemistry & Cell Biology*, 36(4), pp.568–584.

Bartaula-Brevik, S. et al., 2014. Leukocyte transmigration into tissue-engineered constructs is influenced by endothelial cells through toll-like receptor signaling. *Stem Cell Research & Therapy*, 5(6), p.143.

Baud'huin, M. et al., 2013. Osteoprotegerin: multiple partners for multiple functions. *Cytokine & Growth Factor Reviews*, 24(5), pp.401–409.

Bellahcène, A. et al., 2000. Bone Sialoprotein Mediates Human Endothelial Cell Attachment and Migration and Promotes Angiogenesis. *Circulation Research*, 86(8), pp.885–891.

Di Benedetto, A. et al., 2010. N-cadherin and cadherin 11 modulate postnatal bone growth and osteoblast differentiation by distinct mechanisms. *Journal of Cell Science*, 123(15), pp.2640–2648.

Bielby, R., Jones, E. & McGonagle, D., 2007. The role of mesenchymal stem cells in maintenance and repair of bone. *Injury*, 38 Suppl 1, pp.S26–32.

Bi, J. & Yi, L., 2014. Effects of integrins and integrin αvβ3 inhibitor on angiogenesis in cerebral ischemic stroke. *Journal of Huazhong University of Science and Technology. Medical Sciences = Hua Zhong Ke Ji Da Xue Xue Bao. Yi Xue Ying De Wen Ban = Huazhong Keji Daxue Xuebao. Yixue Yingdewen Ban*, 34(3), pp.299–305.

Billottet, C., Quemener, C. & Bikfalvi, A., 2013. CXCR3, a double-edged sword in tumor progression and angiogenesis. *Biochimica Et Biophysica Acta*, 1836(2), pp.287–295.

Bizenjima, T. et al., 2014. Fibroblast growth factor-2 promotes healing of surgically created periodontal defects in streptozotocin-induced early diabetic rats via increasing cell proliferation and regulating angiogenesis. *Journal of Clinical Periodontology*.

Bobis, S., Jarocha, D. & Majka, M., 2006. Mesenchymal stem cells: characteristics and clinical applications. *Folia Histochemica Et Cytobiologica / Polish Academy of Sciences, Polish Histochemical and Cytochemical Society*, 44(4), pp.215–230.

Bornstein, P., 2009. Thrombospondins function as regulators of angiogenesis. *Journal of Cell Communication and Signaling*, 3(3-4), pp.189–200.

Borst, O. et al., 2014. CXCL16 is a novel diagnostic marker and predictor of mortality in inflammatory cardiomyopathy and heart failure. *International Journal of Cardiology*, 176(3), pp.896–903.

Boyce, B.F. & Xing, L., 2008. Functions of RANKL/RANK/OPG in bone modeling and remodeling. *Archives of biochemistry and biophysics*, 473(2), pp.139–146.

Brack, A.S. et al., 2007. Increased Wnt signaling during aging alters muscle stem cell fate and increases fibrosis. *Science (New York, N.Y.)*, 317(5839), pp.807–810.

Bradford, M.M., 1976. A rapid and sensitive method for the quantitation of microgram quantities of protein utilizing the principle of protein-dye binding. *Analytical Biochemistry*, 72, pp.248–254.

Brigstock, D.R., 2002. Regulation of angiogenesis and endothelial cell function by connective tissue growth factor (CTGF) and cysteine-rich 61 (CYR61). *Angiogenesis*, 5(3), pp.153–165.

Bruder, S.P., Fink, D.J. & Caplan, A.I., 1994. Mesenchymal stem cells in bone development, bone repair, and skeletal regeneration therapy. *Journal of Cellular Biochemistry*, 56(3), pp.283–294.

Brunt, K.R. et al., 2007. Endothelial progenitor cell and mesenchymal stem cell isolation, characterization, viral transduction. *Methods in Molecular Medicine*, 139, pp.197–210.

Buschmann, I. & Schaper, W., 1999. Arteriogenesis Versus Angiogenesis: Two Mechanisms of Vessel Growth. *Physiology*, 14(3), pp.121 –125.

Camilli, T.C. et al., 2011. Loss of Klotho during melanoma progression leads to increased filamin cleavage, increased Wnt5A expression, and enhanced melanoma cell motility. *Pigment Cell & Melanoma Research*, 24(1), pp.175–186.

Carmeliet, P., 2000. Mechanisms of angiogenesis and arteriogenesis. *Nat Med*, 6(4), pp.389–395.

Carow, B. & Rottenberg, M.E., 2014. SOCS3, a Major Regulator of Infection and Inflammation. *Frontiers in Immunology*, 5. Available at: http://www.ncbi.nlm.nih.gov/pmc/articles/PMC3928676/ [Accessed February 1, 2015].

Carpenter, T.O. et al., 2010. Circulating levels of soluble klotho and FGF23 in X-linked hypophosphatemia: circadian variance, effects of treatment, and relationship to parathyroid status. *The Journal of Clinical Endocrinology and Metabolism*, 95(11), pp.E352–357.

Case, J. et al., 2007. Human CD34+AC133+VEGFR-2+ cells are not endothelial progenitor cells but distinct, primitive hematopoietic progenitors. *Experimental Hematology*, 35(7), pp.1109–1118.

Chang, C.-C. et al., 2006. Effect of Connective Tissue Growth Factor on Hypoxia-Inducible Factor 1α Degradation and Tumor Angiogenesis. *Journal of the National Cancer Institute*, 98(14), pp.984–995.

Chang, Q. et al., 2005. The ß-Glucuronidase Klotho Hydrolyzes and Activates the TRPV5 Channel. *Science*, 310(5747), pp.490–493.

Chan, J.L. et al., 2006. Antigen-presenting property of mesenchymal stem cells occurs during a narrow window at low levels of interferon-gamma. *Blood*, 107(12), pp.4817–4824.

Chan, J.L. et al., 2004. Mesenchymal Stem Cells (MSC) Exhibit Antigen Presenting (APC) and Phagocytic Properties: Implicatins to Bnone Marrow Failure during Inflammation. *ASH Annual Meeting Abstracts*, 104(11), p.4249.

Chen, C.-D. et al., 2014. Identification of cleavage sites leading to the shed form of the anti-aging protein klotho. *Biochemistry*, 53(34), pp.5579–5587.

Chen, D. et al., 2014. Increased expression of Id1 and Id3 promotes tumorigenicity by enhancing angiogenesis and suppressing apoptosis in small cell lung cancer. *Genes & Cancer*, 5(5-6), pp.212–225.

Chen, H.I. et al., 2014. The sinus venosus contributes to coronary vasculature through VEGFC-stimulated angiogenesis. *Development (Cambridge, England)*, 141(23), pp.4500–4512.

Chen, Y. & Alman, B.A., 2009. Wnt pathway, an essential role in bone regeneration. *Journal of Cellular Biochemistry*, 106(3), pp.353–362.

Chu, L.-Y., Ramakrishnan, D.P. & Silverstein, R.L., 2013. Thrombospondin-1 modulates VEGF signaling via CD36 by recruiting SHP-1 to VEGFR2 complex in microvascular endothelial cells. *Blood*, 122(10), pp.1822–1832.

Corallini, F. et al., 2011. Trail down-regulates the release of osteoprotegerin (OPG) by primary stromal cells. *Journal of Cellular Physiology*, 226(9), pp.2279–2286.

Cruciat, C.-M. & Niehrs, C., 2013. Secreted and Transmembrane Wnt Inhibitors and Activators. *Cold Spring Harbor Perspectives in Biology*, 5(3), p.a015081.

Daley, W.P., Peters, S.B. & Larsen, M., 2008. Extracellular matrix dynamics in development and regenerative medicine. *Journal of Cell Science*, 121(3), pp.255–264.

Damgaard, R.B. & Gyrd-Hansen, M., 2011. Inhibitor of Apoptosis (IAP) Proteins in Regulation of Inflammation and Innate Immunity. *Discovery Medicine*, 11(58), pp.221–231.

DeLisser, H.M. et al., 1997. Involvement of endothelial PECAM-1/CD31 in angiogenesis. *The American Journal of Pathology*, 151(3), pp.671–677.

Dërmaku-Sopjani, M. et al., 2013. Significance of the anti-aging protein Klotho. *Molecular Membrane Biology*, 30(8), pp.369–385.

Devaraj, S. et al., 2012. Validation of an Immunoassay for Soluble Klotho Protein Decreased Levels in Diabetes and Increased Levels in Chronic Kidney Disease. *American Journal of Clinical Pathology*, 137(3), pp.479–485.

Dimmeler, S. et al., 2001. HMG-CoA reductase inhibitors (statins) increase endothelial progenitor cells via the PI 3-kinase/Akt pathway. *The Journal of Clinical Investigation*, 108(3), pp.391–397.

Donate-Correa, J. et al., 2014. Pathophysiological Implications of Fibroblast Growth Factor-23 and Klotho and Their Potential Role as Clinical Biomarkers. *Clinical Chemistry*, 60(7), pp.933–940.

Dotterweich, J. et al., 2014. Mesenchymal stem cell contact promotes CCN1 splicing and transcription in myeloma cells. *Cell Communication and Signaling : CCS*, 12, p.36.

Drozina, G. et al., 2005. Expression of MHC II genes. *Current Topics in Microbiology and Immunology*, 290, pp.147–170.

Drüeke, T.B. & Prié, D., 2007. Klotho spins the thread of life—what does Klotho do to the receptors of fibroblast growth factor-23 (FGF23)? *Nephrology Dialysis Transplantation*, 22(6), pp.1524–1526.

Dubois, R.N. et al., 1998. Cyclooxygenase in biology and disease. *The FASEB Journal*, 12(12), pp.1063–1073.

Ebert, R. et al., 2015. Acute phase serum amyloid A induces proinflammatory cytokines and mineralization via toll-like receptor 4 in mesenchymal stem cells. *Stem Cell Research*, 15(1), pp.231–239.

Eggenhofer, E. et al., 2014. The Life and Fate of Mesenchymal Stem Cells. *Frontiers in Immunology*, 5. Available at: http://www.ncbi.nlm.nih.gov/pmc/articles/PMC4032901/ [Accessed November 9, 2014].

Emery, J.G. et al., 1998. Osteoprotegerin Is a Receptor for the Cytotoxic Ligand TRAIL. *Journal of Biological Chemistry*, 273(23), pp.14363–14367.

Estes, M.L. et al., Identification of Endothelial Cells and Progenitor Cell Subsets in Human Peripheral Blood. Available at: http://onlinelibrary.wiley.com/doi/10.1002/0471142956.cy0933s52/abstract [Accessed January 13, 2012].

Fadini, G.P. et al., 2006. Number and Function of Endothelial Progenitor Cells as a Marker of Severity for Diabetic Vasculopathy. *Arteriosclerosis, Thrombosis, and Vascular Biology*, 26(9), pp.2140–2146.

Feng, X. & McDonald, J.M., 2011. Disorders of Bone Remodeling. *Annual review of pathology*, 6, pp.121–145.

Ferrari-Lacraz, S. & Ferrari, S., 2009. Effects of RANKL inhibition on inflammation and immunity. *IBMS BoneKEy*, 6(3), pp.116–126.

Ferreira, E. et al., 2013. Inflammatory cytokines induce a unique mineralizing phenotype in mesenchymal stem cells derived from human bone marrow. *The Journal of Biological Chemistry*, 288(41), pp.29494–29505.

Folkman, J. & Klagsbrun, M., 1987. Angiogenic factors. *Science (New York, N.Y.)*, 235(4787), pp.442–447.

Folkman, J. & Shing, Y., 1992. Angiogenesis. *Journal of Biological Chemistry*, 267(16), pp.10931 – 10934.

Foresta, C. et al., 2007. Oestrogen stimulates endothelial progenitor cells via oestrogen receptor-alpha. *Clinical Endocrinology*, 67(4), pp.520–525.

França, C.N. et al., 2011. Endothelial Progenitor Cell Mobilization and Platelet Microparticle Release Are Influenced by Clopidogrel Plasma Levels in Stable Coronary Heart Disease. *Circulation Journal: Official Journal of the Japanese Circulation Society*. Available at: http://www.ncbi.nlm.nih.gov/pubmed/22214900 [Accessed January 9, 2012].

François, M. et al., 2009. Mesenchymal stromal cells cross-present soluble exogenous antigens as part of their antigen-presenting cell properties. *Blood*, 114(13), pp.2632–2638.

Gabrilovich, D.I. & Hurwitz, A.A., 2014. *Tumor-Induced Immune Suppression: Mechanisms and Therapeutic Reversal*, Springer Science & Business Media.

Gajko-Galicka, A., 2002. Mutations in type I collagen genes resulting in osteogenesis imperfecta in humans. *Acta Biochimica Polonica*, 49(2), pp.433–441.

Gao, A. & Van Dyke, T.E., 2014. Role of suppressors of cytokine signaling 3 in bone inflammatory responses. *Frontiers in Immunology*, 4, p.506.

Garlanda, C. & Dejana, E., 1997. Heterogeneity of endothelial cells. Specific markers. *Arteriosclerosis, Thrombosis, and Vascular Biology*, 17(7), pp.1193–1202.

Georgescu, A. et al., 2011. The promise of EPC-based therapies on vascular dysfunction in diabetes. *European Journal of Pharmacology*, 669(1-3), pp.1–6.

Gerhardt, H., 2008. VEGF and endothelial guidance in angiogenic sprouting. *Organogenesis*, 4(4), pp.241–246.

Giannotti, G. et al., 2010. Impaired Endothelial Repair Capacity of Early Endothelial Progenitor Cells in Prehypertension. *Hypertension*, 55(6), pp.1389 –1397.

Goodell, M.A., 1999. CD34+ or CD34−: Does it Really Matter? *Blood*, 94(8), pp.2545–2547.

Grainger, S.J. & Putnam, A.J., 2013. ECM Remodeling in Angiogenesis. In C. A. Reinhart-King, ed. *Mechanical and Chemical Signaling in Angiogenesis*. Studies in Mechanobiology, Tissue Engineering and Biomaterials. Springer Berlin Heidelberg, pp. 185–209. Available at: http://link.springer.com/chapter/10.1007/978-3-642-30856-7_9 [Accessed February 7, 2015].

Granger, D. & Senchenkova, E., 2010. Inflammation and the Microcirculation - Chapter 6: Angiogenesis - NCBI Bookshelf. Available at: http://www.ncbi.nlm.nih.gov/books/NBK53377/ [Accessed February 21, 2015].

Grellier, M., Bordenave, L. & Amédée, J., 2009. Cell-to-cell communication between osteogenic and endothelial lineages: implications for tissue engineering. *Trends in Biotechnology*, 27(10), pp.562–571.

Grevers, L.C. et al., 2011. S100A8 enhances osteoclastic bone resorption in vitro through activation of Toll-like receptor 4: Implications for bone destruction in murine antigen-induced arthritis. *Arthritis & Rheumatism*, 63(5), pp.1365–1375.

Grote, K. et al., 2007. The angiogenic factor CCN1 promotes adhesion and migration of circulating CD34+ progenitor cells: potential role in angiogenesis and endothelial regeneration. *Blood*, 110(3), pp.877 –885.

Grzesik, W.J., 1997. Integrins and bone--cell adhesion and beyond. *Archivum Immunologiae Et Therapiae Experimentalis*, 45(4), pp.271–275.

Hale, J.S. et al., 2012. Context dependent role of the CD36--thrombospondin--histidine-rich glycoprotein axis in tumor angiogenesis and growth. *PloS One*, 7(7), p.e40033.

Han, Q., Liu, F. & Zhou, Y., 2013. Increased expression of heparanase in osteogenic differentiation of rat marrow stromal cells. *Experimental and Therapeutic Medicine*, 5(6), pp.1697–1700.

Hari, A. et al., 2014. Redirecting soluble antigen for MHC class I cross-presentation during phagocytosis. *European Journal of Immunology*, p.n/a–n/a.

Hass, R. et al., 2011. Different populations and sources of human mesenchymal stem cells (MSC): A comparison of adult and neonatal tissue-derived MSC. *Cell Communication and Signaling : CCS*, 9, p.12.

Hattori, K. et al., 2001. Vascular endothelial growth factor and angiopoietin-1 stimulate postnatal hematopoiesis by recruitment of vasculogenic and hematopoietic stem cells. *The Journal of Experimental Medicine*, 193(9), pp.1005–1014.

Hayrapetyan, A., Jansen, J.A. & van den Beucken, J.J.J.P., 2014. Signaling Pathways Involved in Osteogenesis and Their Application for Bone Regenerative Medicine. *Tissue Engineering. Part B, Reviews*.

He, C., Nie, W. & Feng, W., 2014. Engineering of biomimetic nanofibrous matrices for drug delivery and tissue engineering. *Journal of Materials Chemistry B*, 2(45), pp.7828–7848.

Heeschen, C. et al., 2003. Erythropoietin is a potent physiologic stimulus for endothelial progenitor cell mobilization. *Blood*, 102(4), pp.1340–1346.

Heijboer, A.C. et al., 2013. Laboratory aspects of circulating α-Klotho. *Nephrology, Dialysis, Transplantation: Official Publication of the European Dialysis and Transplant Association - European Renal Association*, 28(9), pp.2283–2287.

Heldin, C.-H., 2013. Targeting the PDGF signaling pathway in tumor treatment. *Cell Communication and Signaling*, 11(1), p.97.

Hillen, F. & Griffioen, A.W., 2007. Tumour vascularization: sprouting angiogenesis and beyond. *Cancer Metastasis Reviews*, 26(3-4), pp.489–502.

Hill, P.A., 1998. Bone remodelling. *Journal of Orthodontics*, 25(2), pp.101–107.

Hirschfeld, M. et al., 2009. Alternative splicing of Cyr61 is regulated by hypoxia and significantly changed in breast cancer. *Cancer Research*, 69(5), pp.2082–2090.

Hofmann, A.K., 2010. Ex vivo Expansion von endothelialen Vorläuferzellen. Available at: http://opus.bibliothek.uni-wuerzburg.de/volltexte/2011/6487/ [Accessed January 9, 2012].

Holthöfer, H. et al., 1982. Ulex europaeus I lectin as a marker for vascular endothelium in human tissues. *Laboratory Investigation; a Journal of Technical Methods and Pathology*, 47(1), pp.60–66.

Hristov, M. et al., 2007. Regulation of endothelial progenitor cell homing after arterial injury. *Thrombosis and Haemostasis*. Available at: http://www.schattauer.de/index.php?id=1214&doi=10.1160/TH07-03-0181 [Accessed January 14, 2012].

Huang, Y.-C. & Liu, T.-J., 2011. Mobilization of mesenchymal stem cells by stromal cell-derived factor-1 released from chitosan/tripolyphosphate/fucoidan nanoparticles. *Acta Biomaterialia*. Available at: http://www.ncbi.nlm.nih.gov/pubmed/22200609 [Accessed January 11, 2012].

Huen, A.C. & Wells, A., 2012. The Beginning of the End: CXCR3 Signaling in Late-Stage Wound Healing. *Advances in Wound Care*, 1(6), pp.244–248.

Hughes, D.E. et al., 1993. Integrin expression in human bone. *Journal of Bone and Mineral Research: The Official Journal of the American Society for Bone and Mineral Research*, 8(5), pp.527–533.

Hu, M.C. et al., 2011. Klotho deficiency causes vascular calcification in chronic kidney disease. *Journal of the American Society of Nephrology: JASN*, 22(1), pp.124–136.

Hu, M.C., Kuro-o, M. & Moe, O.W., 2014. αKlotho and vascular calcification: an evolving paradigm. *Current Opinion in Nephrology and Hypertension*, 23(4), pp.331–339.

Ivkovic, S. et al., 2003. Connective tissue growth factor coordinates chondrogenesis and angiogenesis during skeletal development. *Development (Cambridge, England)*, 130(12), pp.2779–2791.

Iwakura, A. et al., 2003. Estrogen-mediated, endothelial nitric oxide synthase-dependent mobilization of bone marrow-derived endothelial progenitor cells contributes to reendothelialization after arterial injury. *Circulation*, 108(25), pp.3115–3121.

Jalili, R.B. et al., 2007. The immunoregulatory function of indoleamine 2, 3 dioxygenase and its application in allotransplantation. *Iranian Journal of Allergy, Asthma, and Immunology*, 6(4), pp.167–179.

John, G.B., Cheng, C.-Y. & Kuro-o, M., 2011. Role of Klotho in aging, phosphate metabolism, and CKD. *American Journal of Kidney Diseases: The Official Journal of the National Kidney Foundation*, 58(1), pp.127–134.

Kalfas, I.H., 2001. Principles of bone healing. *Neurosurgical Focus*, 10(4), p.E1.

Kalka, C. et al., 2000. VEGF gene transfer mobilizes endothelial progenitor cells in patients with inoperable coronary disease. *The Annals of Thoracic Surgery*, 70(3), pp.829–834.

Kanczler, J.M. & Oreffo, R.O.C., 2008. Osteogenesis and angiogenesis: the potential for engineering bone. *European cells & materials*, 15, pp.100–114.

Kitagawa, M. et al., 2013. A Decreased Level of Serum Soluble Klotho Is an Independent Biomarker Associated with Arterial Stiffness in Patients with Chronic Kidney Disease. *PLoS ONE*, 8(2). Available at: http://www.ncbi.nlm.nih.gov/pmc/articles/PMC3576368/ [Accessed July 12, 2014].

Klotzsche-von Ameln, A. et al., 2013. PHD4 stimulates tumor angiogenesis in osteosarcoma cells via TGF-α. *Molecular cancer research: MCR*, 11(11), pp.1337–1348.

Kneser, U. et al., 2006. Tissue engineering of bone: the reconstructive surgeon's point of view. *Journal of Cellular and Molecular Medicine*, 10(1), pp.7–19.

Koizumi, M., Komaba, H. & Fukagawa, M., 2013. Parathyroid function in chronic kidney disease: role of FGF23-Klotho axis. *Contributions to Nephrology*, 180, pp.110–123.

Kon, T. et al., 2001. Expression of osteoprotegerin, receptor activator of NF-kappaB ligand (osteoprotegerin ligand) and related proinflammatory cytokines during fracture healing. *Journal of Bone and Mineral Research: The Official Journal of the American Society for Bone and Mineral Research*, 16(6), pp.1004–1014.

Korevaar, T.I.M. et al., 2014. Soluble Flt1 and placental growth factor are novel determinants of newborn thyroid (dys)function: the generation R study. *The Journal of Clinical Endocrinology and Metabolism*, 99(9), pp.E1627–1634.

Köttstorfer, J. et al., 2014. Are OPG and RANKL involved in human fracture healing? *Journal of Orthopaedic Research: Official Publication of the Orthopaedic Research Society*, 32(12), pp.1557–1561.

Kuhn, N.Z. & Tuan, R.S., 2010. Regulation of stemness and stem cell niche of mesenchymal stem cells: Implications in tumorigenesis and metastasis. *Journal of Cellular Physiology*, 222(2), pp.268–277.

Kundu, A.K., Khatiwala, C.B. & Putnam, A.J., 2009. Extracellular matrix remodeling, integrin expression, and downstream signaling pathways influence the osteogenic differentiation of mesenchymal stem cells on poly(lactide-co-glycolide) substrates. *Tissue Engineering. Part A*, 15(2), pp.273–283.

Kuro-o, M., 2010. Klotho. *Pflügers Archiv: European Journal of Physiology*, 459(2), pp.333–343.

Kuro-o, M., 2008. Klotho as a regulator of oxidative stress and senescence. *Biological Chemistry*, 389(3), pp.233–241.

Kuro-o, M. et al., 1997. Mutation of the mouse klotho gene leads to a syndrome resembling ageing. *Nature*, 390(6655), pp.45–51.

Kurosu, H. & Kuro-o, M., 2009. The Klotho gene family as a regulator of endocrine fibroblast growth factors. *Molecular and Cellular Endocrinology*, 299(1), pp.72–78.

Kusumbe, A.P., Ramasamy, S.K. & Adams, R.H., 2014. Coupling of angiogenesis and osteogenesis by a specific vessel subtype in bone. *Nature*, 507(7492), pp.323–328.

Lacotte, S. et al., 2009. CXCR3, inflammation, and autoimmune diseases. *Annals of the New York Academy of Sciences*, 1173, pp.310–317.

Lau, L.F., 2011. CCN1/CYR61: The Very Model of a Modern Matricellular Protein. *Cellular and molecular life sciences : CMLS*, 68(19), pp.3149–3163.

Lee, D. et al., 2014. Id proteins regulate capillary repair and perivascular cell proliferation following ischemia-reperfusion injury. *PloS One*, 9(2), p.e88417.

Leng, E. et al., 2002. Organization and expression of the Cyr61 gene in normal human fibroblasts. *Journal of Biomedical Science*, 9(1), pp.59–67.

Leunissen, E.H.P. et al., 2013. The epithelial calcium channel TRPV5 is regulated differentially by klotho and sialidase. *The Journal of Biological Chemistry*, 288(41), pp.29238–29246.

Lewin, E. & Olgaard, K., 2006. Klotho, an important new factor for the activity of Ca2+ channels, connecting calcium homeostasis, ageing and uraemia. *Nephrology Dialysis Transplantation*, 21(7), pp.1770–1772.

Li, B. et al., 2006. VEGF and PlGF promote adult vasculogenesis by enhancing EPC recruitment and vessel formation at the site of tumor neovascularization. *The FASEB Journal*, 20(9), pp.1495 – 1497.

Lienau, J. et al., 2006. CYR61 (CCN1) protein expression during fracture healing in an ovine tibial model and its relation to the mechanical fixation stability. *Journal of Orthopaedic Research: Official Publication of the Orthopaedic Research Society*, 24(2), pp.254–262.

Li, H. et al., 2013. 17β-Estradiol enhances the recruitment of bone marrow-derived endothelial progenitor cells into infarcted myocardium by inducing CXCR4 expression. *International Journal of Cardiology*, 162(2), pp.100–106.

Li, J., Zhang, Y.-P. & Kirsner, R.S., 2003. Angiogenesis in wound repair: angiogenic growth factors and the extracellular matrix. *Microscopy Research and Technique*, 60(1), pp.107–114.

Li, S.-A. et al., 2004. Immunohistochemical localization of Klotho protein in brain, kidney, and reproductive organs of mice. *Cell Structure and Function*, 29(4), pp.91–99.

Liu, B.Y. et al., 2012. Mammary tumor regression elicited by Wnt signaling inhibitor requires IGFBP5. *Cancer Research*, 72(6), pp.1568–1578.

Liu, G. et al., 2004. Effect of type I collagen on the adhesion, proliferation, and osteoblastic gene expression of bone marrow-derived mesenchymal stem cells. *Chinese Journal of Traumatology = Zhonghua Chuang Shang Za Zhi / Chinese Medical Association*, 7(6), pp.358–362.

Liu, H. et al., 2007. Augmented Wnt Signaling in a Mammalian Model of Accelerated Aging. *Science*, 317(5839), pp.803–806.

Liu, J.-J. et al., 2014. Association of plasma soluble α-klotho with pro-endothelin-1 in patients with type 2 diabetes. *Atherosclerosis*, 233(2), pp.415–418.

Liu, Y., Chan, J.K.Y. & Teoh, S.-H., 2012. Review of vascularised bone tissue-engineering strategies with a focus on co-culture systems. *Journal of tissue engineering and regenerative medicine*.

Liu, Z.-J. & Velazquez, O.C., 2010. Angiogenesis in Wound Healing. In *Encyclopedia of the Eye*. Oxford: Academic Press, pp. 99–105. Available at: http://www.sciencedirect.com/science/article/pii/B978012374203200124X [Accessed January 16, 2012].

Llevadot, J. et al., 2001. HMG-CoA reductase inhibitor mobilizes bone marrow--derived endothelial progenitor cells. *The Journal of Clinical Investigation*, 108(3), pp.399–405.

Luo, Q. et al., 2004. Connective Tissue Growth Factor (CTGF) Is Regulated by Wnt and Bone Morphogenetic Proteins Signaling in Osteoblast Differentiation of Mesenchymal Stem Cells. *Journal of Biological Chemistry*, 279(53), pp.55958–55968.

Lu, P. et al., 2011. Extracellular Matrix Degradation and Remodeling in Development and Disease. *Cold Spring Harbor Perspectives in Biology*, 3(12). Available at: http://www.ncbi.nlm.nih.gov/pmc/articles/PMC3225943/ [Accessed February 8, 2015].

Lyden, D. et al., 1999. Id1 and Id3 are required for neurogenesis, angiogenesis and vascularization of tumour xenografts. *Nature*, 401(6754), pp.670–677.

MacDonald, B.T., Tamai, K. & He, X., 2009. Wnt/β-catenin signaling: components, mechanisms, and diseases. *Developmental cell*, 17(1), pp.9–26.

Maclauchlan, S. et al., 2009. Enhanced angiogenesis and reduced contraction in thrombospondin-2-null wounds is associated with increased levels of matrix metalloproteinases-2 and -9, and soluble VEGF. *The Journal of Histochemistry and Cytochemistry: Official Journal of the Histochemistry Society*, 57(4), pp.301–313.

Maity, G. et al., 2014. Pancreatic tumor cell secreted CCN1/Cyr61 promotes endothelial cell migration and aberrant neovascularization. *Scientific Reports*, 4, p.4995.

Marquis, M.-E. et al., 2009. Bone cells-biomaterials interactions. *Frontiers in Bioscience (Landmark Edition)*, 14, pp.1023–1067.

Martin, A., David, V. & Quarles, L.D., 2012. Regulation and Function of the FGF23/Klotho Endocrine Pathways. *Physiological Reviews*, 92(1), pp.131–155.

Martín-Núñez, E. et al., 2014. Implications of Klotho in vascular health and disease. *World Journal of Cardiology*, 6(12), pp.1262–1269.

Matsubara, H. et al., 2012. Vascular tissues are a primary source of BMP2 expression during bone formation induced by distraction osteogenesis. *Bone*, 51(1), pp.168–180.

Matsumoto, K. & Ema, M., 2014. Roles of VEGF-A signalling in development, regeneration, and tumours. *Journal of Biochemistry*, 156(1), pp.1–10.

Matsumura, Y. et al., 1998. Identification of the human klotho gene and its two transcripts encoding membrane and secreted klotho protein. *Biochemical and Biophysical Research Communications*, 242(3), pp.626–630.

Matsunobu, T. et al., 2009. Critical roles of the TGF-beta type I receptor ALK5 in perichondrial formation and function, cartilage integrity, and osteoblast differentiation during growth plate development. *Developmental Biology*, 332(2), pp.325–338.

Meisel, R. et al., 2004. Human bone marrow stromal cells inhibit allogeneic T-cell responses by indoleamine 2,3-dioxygenase-mediated tryptophan degradation. *Blood*, 103(12), pp.4619–4621.

De Miguel, M.P. et al., 2012. Immunosuppressive properties of mesenchymal stem cells: advances and applications. *Current Molecular Medicine*, 12(5), pp.574–591.

Min, S.-K. et al., 2013. Titanium Surface Coating with a Laminin-Derived Functional Peptide Promotes Bone Cell Adhesion. *BioMed Research International*, 2013. Available at: http://www.ncbi.nlm.nih.gov/pmc/articles/PMC3622367/ [Accessed February 20, 2015].

Motz, G.T. & Coukos, G., 2011. The parallel lives of angiogenesis and immunosuppression: cancer and other tales. *Nature Reviews. Immunology*, 11(10), pp.702–711.

Müller, M. et al., 2010. Review: The chemokine receptor CXCR3 and its ligands CXCL9, CXCL10 and CXCL11 in neuroimmunity--a tale of conflict and conundrum. *Neuropathology and Applied Neurobiology*, 36(5), pp.368–387.

Murohara, T. et al., 2000. Transplanted cord blood–derived endothelial precursor cells augment postnatal neovascularization. *Journal of Clinical Investigation*, 105(11), pp.1527–1536.

Nguyen, L.H. et al., 2012. Vascularized bone tissue engineering: approaches for potential improvement. *Tissue engineering. Part B, Reviews*, 18(5), pp.363–382.

Nickoloff, B.J. & Turka, L.A., 1994. Immunological functions of non-professional antigen-presenting cells: new insights from studies of T-cell interactions with keratinocytes. *Immunology Today*, 15(10), pp.464–469.

Nöth, U. et al., 2002. Multilineage mesenchymal differentiation potential of human trabecular bone-derived cells. *Journal of Orthopaedic Research*, 20(5), pp.1060–1069.

Novosel, E.C., Kleinhans, C. & Kluger, P.J., 2011. Vascularization is the key challenge in tissue engineering. *Advanced drug delivery reviews*, 63(4-5), pp.300–311.

Oikonomopoulos, A. et al., 2011. Wnt signaling exerts an antiproliferative effect on adult cardiac progenitor cells through IGFBP3. *Circulation Research*, 109(12), pp.1363–1374.

Okada, S. et al., 2000. Impairment of B lymphopoiesis in precocious aging (klotho) mice. *International Immunology*, 12(6), pp.861–871.

Parfitt, A.M., 2002. Targeted and nontargeted bone remodeling: relationship to basic multicellular unit origination and progression. *Bone*, 30(1), pp.5–7.

Patenaude, A., Parker, J. & Karsan, A., 2010. Involvement of endothelial progenitor cells in tumor vascularization. *Microvascular Research*, 79(3), pp.217–223.

Pedersen, L. et al., 2013. Soluble serum Klotho levels in healthy subjects. Comparison of two different immunoassays. *Clinical Biochemistry*, 46(12), pp.1079–1083.

Pedersen, T.O. et al., 2013. Endothelial microvascular networks affect gene-expression profiles and osteogenic potential of tissue-engineered constructs. *Stem Cell Research & Therapy*, 4(3), p.52.

Pedersen, T.O. et al., 2014. Mesenchymal stem cells induce endothelial cell quiescence and promote capillary formation. *Stem Cell Research & Therapy*, 5(1), p.23.

Peichev, M. et al., 2000. Expression of VEGFR-2 and AC133 by circulating human CD34+ cells identifies a population of functional endothelial precursors. *Blood*, 95(3), pp.952 –958.

Peng, H. et al., 2005. VEGF improves, whereas sFlt1 inhibits, BMP2-induced bone formation and bone healing through modulation of angiogenesis. *Journal of Bone and Mineral Research: The Official Journal of the American Society for Bone and Mineral Research*, 20(11), pp.2017–2027.

Peplow, P.V., 2014. Influence of growth factors and cytokines on angiogenic function of endothelial progenitor cells: a review of in vitro human studies. *Growth Factors (Chur, Switzerland)*, 32(3-4), pp.83–116.

Perbal, B., 2009. Alternative splicing of CCN mRNAs …. it has been upon us. *Journal of Cell Communication and Signaling*, 3(2), pp.153–157.

Presta, M. et al., 2005. Fibroblast growth factor/fibroblast growth factor receptor system in angiogenesis. *Cytokine & Growth Factor Reviews*, 16(2), pp.159–178.

Przybylski, M., 2009. A review of the current research on the role of bFGF and VEGF in angiogenesis. *Journal of Wound Care*, 18(12), pp.516–519.

Qian, X. et al., 1997. Thrombospondin-1 modulates angiogenesis in vitro by up-regulation of matrix metalloproteinase-9 in endothelial cells. *Experimental Cell Research*, 235(2), pp.403–412.

Qin, Y., Guan, J. & Zhang, C., 2014. Mesenchymal stem cells: mechanisms and role in bone regeneration. *Postgraduate Medical Journal*, 90(1069), pp.643–647.

Rafat, M. et al., 2012. Engineered endothelial cell adhesion via VCAM1 and E-selectin antibody-presenting alginate hydrogels. *Acta Biomaterialia*, 8(7), pp.2697–2703.

Ramasamy, S.K. et al., 2014. Endothelial Notch activity promotes angiogenesis and osteogenesis in bone. *Nature*, 507(7492), pp.376–380.

Rauner, M. et al., 2012. WNT5A is induced by inflammatory mediators in bone marrow stromal cells and regulates cytokine and chemokine production. *Journal of Bone and Mineral Research: The Official Journal of the American Society for Bone and Mineral Research*, 27(3), pp.575–585.

Razzaque, M.S., 2012. The role of Klotho in energy metabolism. *Nature Reviews Endocrinology*, 8(10), pp.579–587.

Reed, M.J. et al., 2003. Inhibition of TIMP1 enhances angiogenesis in vivo and cell migration in vitro. *Microvascular Research*, 65(1), pp.9–17.

Rentsch, C. et al., 2014. ECM inspired coating of embroidered 3D scaffolds enhances calvaria bone regeneration. *BioMed Research International*, 2014, p.217078.

Ribatti, D. et al., 2002. Endothelial cell heterogeneity and organ specificity. *Journal of Hematotherapy & Stem Cell Research*, 11(1), pp.81–90.

Risau, W., 1994. Angiogenesis and endothelial cell function. *Arzneimittel-Forschung*, 44(3A), pp.416–417.

Risau, W. & Flamme, I., 1995. Vasculogenesis. *Annual Review of Cell and Developmental Biology*, 11(1), pp.73–91.

Rivilis, I. et al., 2002. Differential involvement of MMP-2 and VEGF during muscle stretch- versus shear stress-induced angiogenesis. *American Journal of Physiology. Heart and Circulatory Physiology*, 283(4), pp.H1430–1438.

Rochefort, G.Y., 2014. The osteocyte as a therapeutic target in the treatment of osteoporosis. *Therapeutic Advances in Musculoskeletal Disease*, 6(3), pp.79–91.

Rosso, F. et al., 2004. From Cell–ECM interactions to tissue engineering. *Journal of Cellular Physiology*, 199(2), pp.174–180.

Rotondi, S. et al., 2015. Soluble α -Klotho Serum Levels in Chronic Kidney Disease. *International Journal of Endocrinology*, 2015, p.872193.

Saidak, Z. et al., 2015. Wnt-β-Catenin Signaling Mediates Osteoblast Differentiation Triggered by Peptide-Induced α5β1 Integrin Priming in Mesenchymal Skeletal Cells. *Journal of Biological Chemistry*, p.jbc.M114.621219.

Sato, T., Laver, J.H. & Ogawa, M., 1999. Reversible expression of CD34 by murine hematopoietic stem cells. *Blood*, 94(8), pp.2548–2554.

Scheller, J. et al., 2011. The pro- and anti-inflammatory properties of the cytokine interleukin-6. *Biochimica Et Biophysica Acta*, 1813(5), pp.878–888.

Schenk, R., 2007. Impact of the CCN-proteins CYR61/CCN1 and WISP3/CCN6 on mesenchymal stem cells and endothelial progenitor cells. Available at: http://opus.bibliothek.uni-wuerzburg.de/volltexte/2008/2776/ [Accessed January 9, 2012].

Schlegelmilch, K., 2012. Molecular function of WISP1/CCN4 in the musculoskeletal system with special reference to apoptosis and cell survival, Funktionsüberprüfung von WISP1/CCN4 im mukuloskelettalen System mit besonderem Augenmerk auf Apoptose und das Überleben der Zellen. Available at: http://opus.bibliothek.uni-wuerzburg.de/frontdoor/index/index/docId/6217 [Accessed July 5, 2014].

Schlegelmilch, K. et al., 2014. WISP 1 is an important survival factor in human mesenchymal stromal cells. *Gene*.

Schmidt-Lucke, C. et al., 2010. Quantification of Circulating Endothelial Progenitor Cells Using the Modified ISHAGE Protocol. *PLoS ONE*, 5(11).

Schmidt, T. & Carmeliet, P., 2010. Blood-vessel formation: Bridges that guide and unite. *Nature*, 465(7299), pp.697–699.

Schmitz, S., 2011. Zellbiologische und Routinemethoden. In *Der Experimentator: Zellkultur*. Experimentator. Spektrum Akademischer Verlag, pp. 205–222. Available at: http://link.springer.com/chapter/10.1007/978-3-8274-2573-7_13 [Accessed July 12, 2014].

Schultz, G.S. et al., 2011. Dynamic Reciprocity in the Wound Microenvironment. *Wound repair and regeneration : official publication of the Wound Healing Society [and] the European Tissue Repair Society*, 19(2), pp.134–148.

Schütze, N. et al., 2005. Expression, purification, and functional testing of recombinant CYR61/CCN1. *Protein Expression and Purification*, 42(1), pp.219–225.

Seghezzi, G. et al., 1998. Fibroblast Growth Factor-2 (FGF-2) Induces Vascular Endothelial Growth Factor (VEGF) Expression in the Endothelial Cells of Forming Capillaries: An Autocrine Mechanism Contributing to Angiogenesis. *The Journal of Cell Biology*, 141(7), pp.1659–1673.

Shahmoon, S. et al., 2014. The aging suppressor klotho: A potential regulator of growth hormone secretion. *American Journal of Physiology. Endocrinology and Metabolism*.

Shimada, T. et al., 2004. Angiogenesis and Vasculogenesis Are Impaired in the Precocious-Aging klotho Mouse. *Circulation*, 110(9), pp.1148–1155.

Shimamura, Y. et al., 2012. Serum levels of soluble secreted α-Klotho are decreased in the early stages of chronic kidney disease, making it a probable novel biomarker for early diagnosis. *Clinical and Experimental Nephrology*, 16(5), pp.722–729.

Shi, Y. et al., 2010. Mesenchymal stem cells: a new strategy for immunosuppression and tissue repair. *Cell Research*, 20(5), pp.510–518.

Sidney, L.E. et al., 2014. Concise review: evidence for CD34 as a common marker for diverse progenitors. *Stem Cells (Dayton, Ohio)*, 32(6), pp.1380–1389.

Silkstone, D., Hong, H. & Alman, B.A., 2008. Beta-catenin in the race to fracture repair: in it to Wnt. *Nature Clinical Practice. Rheumatology*, 4(8), pp.413–419.

Silver, J. & Naveh-Many, T., 2009. Phosphate and the parathyroid. *Kidney International*, 75(9), pp.898–905.

Silverstein, R.L. & Febbraio, M., 2007. CD36-TSP-HRGP interactions in the regulation of angiogenesis. *Current Pharmaceutical Design*, 13(35), pp.3559–3567.

Smart, N., Dubé, K.N. & Riley, P.R., 2009. Coronary vessel development and insight towards neovascular therapy. *International Journal of Experimental Pathology*, 90(3), pp.262–283.

Sottile, J., 2004. Regulation of angiogenesis by extracellular matrix. *Biochimica Et Biophysica Acta*, 1654(1), pp.13–22.

Strehlow, K. et al., 2003. Estrogen increases bone marrow-derived endothelial progenitor cell production and diminishes neointima formation. *Circulation*, 107(24), pp.3059–3065.

Subramani, J. et al., 2013. Tyrosine phosphorylation of CD13 regulates inflammatory cell-cell adhesion and monocyte trafficking. *Journal of Immunology (Baltimore, Md.: 1950)*, 191(7), pp.3905–3912.

Suda, T., Takahashi, N. & Martin, T.J., 1992. Modulation of osteoclast differentiation. *Endocrine Reviews*, 13(1), pp.66–80.

Sugimoto, T. et al., 2014. CD34+/CD144+ Circulating Endothelial Cells as an Indicator of Carotid Atherosclerosis. *Journal of Stroke and Cerebrovascular Diseases: The Official Journal of National Stroke Association*.

Sumimoto, S. et al., 2014. Vascular endothelial cells promote cortical neurite outgrowth via an integrin β3-dependent mechanism. *Biochemical and Biophysical Research Communications*, 450(1), pp.593–597.

Sun, X.-T. et al., 2005. Differential gene expression during capillary morphogenesis in a microcarrier-based three-dimensional in vitro model of angiogenesis with focus on chemokines and chemokine receptors. *World journal of gastroenterology: WJG*, 11(15), pp.2283–2290.

Surlin, P. et al., 2014. Involvement of TSP1 and MMP9/NGAL in Angiogenesis during Orthodontic Periodontal Remodeling. *The Scientific World Journal*, 2014. Available at: http://www.ncbi.nlm.nih.gov/pmc/articles/PMC4054803/ [Accessed November 23, 2014].

Takahashi, T. et al., 1999. Ischemia- and cytokine-induced mobilization of bone marrow-derived endothelial progenitor cells for neovascularization. *Nat Med*, 5(4), pp.434–438.

Takahashi, Y., Kuro-o, M. & Ishikawa, F., 2000. Aging mechanisms. *Proceedings of the National Academy of Sciences*, 97(23), pp.12407–12408.

Tan, B.M. et al., 2013. Baculoviral inhibitors of apoptosis repeat containing (BIRC) proteins fine-tune TNF-induced nuclear factor κB and c-Jun N-terminal kinase signalling in mouse pancreatic beta cells. *Diabetologia*, 56(3), pp.520–532.

Tian, H. et al., 2014. HIF-1α Plays a Role in the Chemotactic Migration of Hepatocarcinoma Cells Through the Modulation of CXCL6 Expression. *Cellular Physiology and Biochemistry: International Journal of Experimental Cellular Physiology, Biochemistry, and Pharmacology*, 34(5), pp.1536–1546.

Timmermans, F. et al., 2009. Endothelial progenitor cells: identity defined? *Journal of Cellular and Molecular Medicine*, 13(1), pp.87–102.

Tonnesen, M.G., Feng, X. & Clark, R.A., 2000. Angiogenesis in wound healing. *The Journal of Investigative Dermatology. Symposium Proceedings / the Society for Investigative Dermatology, Inc. [and] European Society for Dermatological Research*, 5(1), pp.40–46.

Toyoda, H. et al., 1997. Distribution of mRNA for human epiregulin, a differentially expressed member of the epidermal growth factor family. *Biochemical Journal*, 326(Pt 1), pp.69–75.

Troeger, A. & Williams, D.A., 2013. Hematopoietic-specific Rho GTPases Rac2 and RhoH and human blood disorders. *Experimental cell research*, 319(15), pp.2375–2383.

Tsuji, K. et al., 2006. BMP2 activity, although dispensable for bone formation, is required for the initiation of fracture healing. *Nature Genetics*, 38(12), pp.1424–1429.

Untergasser, G. et al., 2006. CD34+/CD133- circulating endothelial precursor cells (CEP): characterization, senescence and in vivo application. *Experimental Gerontology*, 41(6), pp.600–608.

Urakawa, I. et al., 2006. Klotho converts canonical FGF receptor into a specific receptor for FGF23. *Nature*, 444(7120), pp.770–774.

Vaananen, H. k. et al., 2000. The cell biology of osteoclast function. *Journal of Cell Science*, 113(3), pp.377 –381.

Vadivel, A. et al., 2013. The axonal guidance cue semaphorin 3C contributes to alveolar growth and repair. *PloS One*, 8(6), p.e67225.

Vasa, M. et al., 2001. Increase in circulating endothelial progenitor cells by statin therapy in patients with stable coronary artery disease. *Circulation*, 103(24), pp.2885–2890.

VascuBone, 2010. Vascubone. Available at: http://www.vascubone.eu [Accessed July 14, 2014].

Vervloet, M.G. et al., 2014. The role of klotho on vascular calcification and endothelial function in chronic kidney disease. *Seminars in Nephrology*, 34(6), pp.578–585.

Vitovski, S. et al., 2007. Investigating the Interaction between Osteoprotegerin and Receptor Activator of NF-κB or Tumor Necrosis Factor-related Apoptosis-inducing Ligand EVIDENCE FOR A PIVOTAL ROLE FOR OSTEOPROTEGERIN IN REGULATING TWO DISTINCT PATHWAYS. *Journal of Biological Chemistry*, 282(43), pp.31601–31609.

Voelkl, J. et al., 2013. Spironolactone ameliorates PIT1-dependent vascular osteoinduction in klotho-hypomorphic mice. *The Journal of Clinical Investigation*, 123(2), pp.812–822.

Voyta, J.C. et al., 1984. Identification and isolation of endothelial cells based on their increased uptake of acetylated-low density lipoprotein. *The Journal of Cell Biology*, 99(6), pp.2034–2040.

Wahl, P., Bloch, W. & Schmidt, A., 2007. Exercise has a Positive Effect on Endothelial Progenitor Cells, which Could be Necessary for Vascular Adaptation Processes. *International Journal of Sports Medicine*, 28(5), pp.374–380.

Walsh, M.C. & Choi, Y., 2014. Biology of the RANKL–RANK–OPG System in Immunity, Bone, and Beyond. *Frontiers in Immunology*, 5. Available at: http://www.ncbi.nlm.nih.gov/pmc/articles/PMC4202272/ [Accessed February 21, 2015].

Wang, D., Xia, D. & Dubois, R.N., 2011. The Crosstalk of PTGS2 and EGF Signaling Pathways in Colorectal Cancer. *Cancers*, 3(4), pp.3894–3908.

Wang, J. et al., 2014. Transforming growth factor-β2 induces morphological alteration of human corneal endothelial cells in vitro. *International Journal of Ophthalmology*, 7(5), pp.759–763.

Wang, Y. & Sun, Z., 2009. Current Understanding of Klotho. *Ageing research reviews*, 8(1), pp.43–51.

Wojtowicz, A.M. et al., 2010. Coating of biomaterial scaffolds with the collagen-mimetic peptide GFOGER for bone defect repair. *Biomaterials*, 31(9), pp.2574–2582.

Wolf, M.T.F. et al., 2014. Klotho upregulates renal calcium channel transient receptor potential vanilloid 5 (TRPV5) by intra- and extracellular N-glycosylation dependent mechanisms. *Journal of Biological Chemistry*, p.jbc.M114.616649.

Wu, J. et al., 2014. Plasminogen Activator Inhibitor-1 Inhibits Angiogenic Signaling by Uncoupling Vascular Endothelial Growth Factor Receptor-2-αVβ3 Integrin Cross Talk. *Arteriosclerosis, Thrombosis, and Vascular Biology*.

www.atlasgeneticsoncology.org, 2015. CYR61 (cysteine-rich, angiogenic inducer, 61). *Atlas of Genetics and Cytogenetics in Oncology and Haematology*. Available at: http://atlasgeneticsoncology.org/Genes/CYR61ID40256ch1p22.html [Accessed February 15, 2015].

Xing, Z. et al., 2011. Effect of endothelial cells on bone regeneration using poly(L-lactide-co-1,5-dioxepan-2-one) scaffolds. *Journal of Biomedical Materials Research. Part A*, 96(2), pp.349–357.

Xue, Y. et al., 2013. Co-culture of human bone marrow stromal cells with endothelial cells alters gene expression profiles. *The International journal of artificial organs*, 36(9), pp.650–662.

Xue, Y. et al., 2009. Endothelial cells influence the osteogenic potential of bone marrow stromal cells. *BioMedical Engineering OnLine*, 8, p.34.

Xu, Y. & Sun, Z., 2015. Molecular Basis of Klotho: From Gene to Function in Aging. *Endocrine Reviews*, p.er20131079.

Yagi, H. et al., 2010. Mesenchymal Stem Cells: Mechanisms of Immunomodulation and Homing. *Cell transplantation*, 19(6), pp.667–679.

Yamazaki, Y. et al., 2010. Establishment of sandwich ELISA for soluble alpha-Klotho measurement: Age-dependent change of soluble alpha-Klotho levels in healthy subjects. *Biochemical and Biophysical Research Communications*, 398(3), pp.513–518.

Yang, J. et al., 2011. CD34+ Cells Represent Highly Functional Endothelial Progenitor Cells in Murine Bone Marrow. *PLoS ONE*, 6(5).

Yao, L. et al., 2014. Overexpression of Wnt5a promotes angiogenesis in NSCLC. *BioMed Research International*, 2014, p.832562.

Yaqoob, U. et al., 2014. FGF21 Promotes Endothelial Cell Angiogenesis through a Dynamin-2 and Rab5 Dependent Pathway. *PLoS ONE*, 9(5). Available at: http://www.ncbi.nlm.nih.gov/pmc/articles/PMC4029959/ [Accessed July 7, 2014].

Yavropoulou, M.P. & Yovos, J.G., 2007. The role of the Wnt signaling pathway in osteoblast commitment and differentiation. *Hormones (Athens, Greece)*, 6(4), pp.279–294.

Yin, A.H. et al., 1997. AC133, a Novel Marker for Human Hematopoietic Stem and Progenitor Cells. *Blood*, 90(12), pp.5002 –5012.

Yu, H. et al., 2008. Promotion of osteogenesis in tissue-engineered bone by pre-seeding endothelial progenitor cells-derived endothelial cells. *Journal of Orthopaedic Research: Official Publication of the Orthopaedic Research Society*, 26(8), pp.1147–1152.

Yuko Tanizaki, K.I., 2013. Role of the Immune Tolerance-Inducing Molecule Indoleamine 2,3-Dioxygenase in Gynecologic Cancers. *Journal of Cancer Science & Therapy*, 05(08). Available at: http://www.omicsonline.org/role-of-the-immune-toleranceinducing-molecule-indoleamine-dioxygenase-in-gynecologic-cancers-1948-5956.S13-001.php?aid=6656 [Accessed February 22, 2015].

Yu, Y. et al., 2010. CCN1 promotes the differentiation of endothelial progenitor cells and reendothelialization in the early phase after vascular injury. *Basic Research in Cardiology*, 105(6), pp.713–724.

Zhao, P. et al., 2014. Cathepsin S causes inflammatory pain via biased agonism of PAR2 and TRPV4. *The Journal of Biological Chemistry*, 289(39), pp.27215–27234.

Zigdon-Giladi, H. et al., 2013. Co-Transplantation of Endothelial Progenitor Cells and Mesenchymal Stem Cells Promote Neovascularization and Bone Regeneration. *Clinical Implant Dentistry and Related Research*.

Zreiqat, H. et al., 2007. S100A8/S100A9 and their association with cartilage and bone. *Journal of Molecular Histology*, 38(5), pp.381–391.

7 APPENDIX

7.1 Appendix A: Differentially expressed probe sets of EPCs$^{con\text{-}med}$

Table 36: Differentially expressed probe sets during microarray of EPCs$^{con\text{-}med}$ (array group A)
Listed are all 769 differentially expressed probe sets between EPCs subjected to conditioned medium of MSCs and their corresponding control assays (n = 4). Probe sets are ordered according to their descending statistical score (logFc) from highest up-regulation to highest down-regulation. Additional information reflects the probe set ID, their corresponding gene symbol and name as well as the adjusted (corrected for multiple comparisons) p-value (adj.P.Val).

ID	Symbol	GeneName	logFC	adj.P.Val
206336_at	CXCL6	chemokine (C-X-C motif) ligand 6 (granulocyte chemotactic protein 2)	6.27	4.15E-04
201110_s_at	THBS1	thrombospondin 1	6.16	4.95E-04
224354_at	NA	NA	6.02	2.38E-04
233847_x_at	NA	NA	6.00	1.08E-04
203963_at	CA12	carbonic anhydrase XII	5.74	2.95E-05
201109_s_at	THBS1	thrombospondin 1	5.41	2.87E-04
225491_at	SLC1A2	solute carrier family 1 (glial high affinity glutamate transporter), member 2	5.35	3.44E-04
215646_s_at	VCAN	versican	5.06	3.18E-04
210118_s_at	IL1A	interleukin 1, alpha	5.04	1.81E-04
221731_x_at	VCAN	versican	4.99	4.11E-04
214164_x_at	CA12	carbonic anhydrase XII	4.97	3.56E-05
215867_x_at	CA12	carbonic anhydrase XII	4.87	2.35E-05
243296_at	NAMPT	nicotinamide phosphoribosyltransferase	4.85	4.43E-05
204620_s_at	VCAN	versican	4.76	3.61E-04
234623_x_at	NA	NA	4.68	3.20E-04
204619_s_at	VCAN	versican	4.66	2.62E-04
204508_s_at	CA12	carbonic anhydrase XII	4.61	2.92E-05
219093_at	PID1	phosphotyrosine interaction domain containing 1	4.56	2.50E-04
204470_at	CXCL1	chemokine (C-X-C motif) ligand 1 (melanoma growth stimulating activity, alpha)	4.55	9.61E-04
205767_at	EREG	epiregulin	4.51	2.35E-05
210029_at	IDO1	indoleamine 2,3-dioxygenase 1	4.42	8.98E-04
206025_s_at	TNFAIP6	tumor necrosis factor, alpha-induced protein 6	4.35	3.61E-04
212977_at	CXCR7	chemokine (C-X-C motif) receptor 7	4.35	6.74E-04
1554997_a_at	PTGS2	prostaglandin-endoperoxide synthase 2 (prostaglandin G/H synthase and cyclooxygenase)	4.29	3.12E-04
1555167_s_at	NAMPT	nicotinamide phosphoribosyltransferase	4.24	4.86E-05
205863_at	S100A12	S100 calcium binding protein A12	4.22	4.81E-04
207850_at	CXCL3	chemokine (C-X-C motif) ligand 3	4.22	1.20E-03
211506_s_at	IL8	interleukin 8	4.18	6.90E-04
217738_at	NAMPT	nicotinamide phosphoribosyltransferase	4.13	2.35E-05
206026_s_at	TNFAIP6	tumor necrosis factor, alpha-induced protein 6	4.05	3.61E-04
205207_at	IL6	interleukin 6 (interferon, beta 2)	4.00	7.25E-04
205816_at	ITGB8	integrin, beta 8	3.98	4.86E-05
205990_s_at	WNT5A	wingless-type MMTV integration site family, member 5A	3.95	3.61E-04
204748_at	PTGS2	prostaglandin-endoperoxide synthase 2 (prostaglandin G/H synthase and cyclooxygenase)	3.88	3.58E-04
235086_at	THBS1	thrombospondin 1	3.86	3.58E-04
207533_at	CCL1	chemokine (C-C motif) ligand 1	3.84	3.79E-04
208389_s_at	SLC1A2	solute carrier family 1 (glial high affinity glutamate transporter), member 2	3.80	7.25E-04
226189_at	ITGB8	integrin, beta 8	3.74	1.08E-04
217739_s_at	NAMPT	nicotinamide phosphoribosyltransferase	3.71	6.47E-05
201108_s_at	THBS1	thrombospondin 1	3.60	6.72E-04
213425_at	WNT5A	wingless-type MMTV integration site family, member 5A	3.60	3.20E-04

39402_at	IL1B	interleukin 1, beta	3.59	3.61E-04
205067_at	IL1B	interleukin 1, beta	3.59	4.11E-04
206022_at	NDP	Norrie disease (pseudoglioma)	3.59	3.61E-04
211571_s_at	VCAN	versican	3.58	8.41E-04
209774_x_at	CXCL2	chemokine (C-X-C motif) ligand 2	3.58	8.96E-04
210512_s_at	VEGFA	vascular endothelial growth factor A	3.47	3.20E-04
210724_at	EMR3	egf-like module containing, mucin-like, hormone receptor-like 3	3.33	8.28E-04
236220_at	NA	NA	3.23	2.22E-04
211488_s_at	ITGB8	integrin, beta 8	3.23	1.08E-04
239887_at	NA	NA	3.14	1.93E-04
210772_at	FPR2	formyl peptide receptor 2	3.10	4.04E-04
220528_at	VNN3	vanin 3	3.09	2.95E-05
229566_at	LOC645638	WDNM1-like pseudogene	3.05	1.33E-03
230170_at	OSM	oncostatin M	3.03	6.45E-04
210773_s_at	FPR2	formyl peptide receptor 2	3.02	7.54E-04
219915_s_at	SLC16A10	solute carrier family 16, member 10 (aromatic amino acid transporter)	2.86	2.15E-04
206002_at	GPR64	G protein-coupled receptor 64	2.85	3.12E-04
221541_at	CRISPLD2	cysteine-rich secretory protein LCCL domain containing 2	2.84	2.33E-04
224358_s_at	MS4A7	membrane-spanning 4-domains, subfamily A, member 7	2.83	7.72E-04
227361_at	HS3ST3B1	heparan sulfate (glucosamine) 3-O-sulfotransferase 3B1	2.79	2.22E-04
206341_at	IL2RA	interleukin 2 receptor, alpha	2.78	4.72E-04
213524_s_at	G0S2	G0/G1switch 2	2.77	9.61E-04
203510_at	MET	met proto-oncogene (hepatocyte growth factor receptor)	2.76	1.57E-03
227697_at	SOCS3	suppressor of cytokine signaling 3	2.76	1.09E-03
202859_x_at	IL8	interleukin 8	2.75	1.35E-03
211269_s_at	IL2RA	interleukin 2 receptor, alpha	2.71	1.35E-03
203708_at	PDE4B	phosphodiesterase 4B, cAMP-specific	2.71	3.61E-04
227554_at	MAGI2-AS3	MAGI2 antisense RNA 3 (non-protein coding)	2.70	2.24E-04
210004_at	OLR1	oxidized low density lipoprotein (lectin-like) receptor 1	2.69	2.33E-04
210735_s_at	CA12	carbonic anhydrase XII	2.66	1.09E-04
207674_at	FCAR	Fc fragment of IgA, receptor for	2.62	3.12E-04
220655_at	TNIP3	TNFAIP3 interacting protein 3	2.61	4.04E-04
1556378_a_at	LOC440896	uncharacterized LOC440896	2.60	4.28E-04
242982_x_at	ITGB8	integrin, beta 8	2.56	3.20E-04
201505_at	LAMB1	laminin, beta 1	2.54	6.33E-04
204148_s_at	NA	NA	2.54	2.26E-04
215078_at	SOD2	superoxide dismutase 2, mitochondrial	2.52	4.04E-04
205083_at	AOX1	aldehyde oxidase 1	2.51	8.96E-04
211307_s_at	FCAR	Fc fragment of IgA, receptor for	2.46	8.41E-04
44783_s_at	HEY1	hairy/enhancer-of-split related with YRPW motif 1	2.45	3.12E-04
205330_at	MN1	meningioma (disrupted in balanced translocation) 1	2.44	3.12E-04
206118_at	STAT4	signal transducer and activator of transcription 4	2.44	4.17E-04
211302_s_at	PDE4B	phosphodiesterase 4B, cAMP-specific	2.43	7.25E-04
201631_s_at	IER3	immediate early response 3	2.43	2.38E-04
222939_s_at	SLC16A10	solute carrier family 16, member 10 (aromatic amino acid transporter)	2.41	1.08E-04
205119_s_at	FPR1	formyl peptide receptor 1	2.36	1.49E-03
205922_at	VNN2	vanin 2	2.34	1.33E-03
223217_s_at	NFKBIZ	nuclear factor of kappa light polypeptide gene enhancer in B-cells inhibitor, zeta	2.33	2.38E-04
242807_at	FSD1L	fibronectin type III and SPRY domain containing 1-like	2.31	8.63E-04
211651_s_at	LAMB1	laminin, beta 1	2.30	7.42E-04
213624_at	SMPDL3A	sphingomyelin phosphodiesterase, acid-like 3A	2.27	2.92E-05
203650_at	PROCR	protein C receptor, endothelial	2.26	1.51E-03
215977_x_at	GK	glycerol kinase	2.26	8.59E-04
223218_s_at	NFKBIZ	nuclear factor of kappa light polypeptide gene enhancer in B-cells inhibitor, zeta	2.26	3.29E-04
218810_at	ZC3H12A	zinc finger CCCH-type containing 12A	2.25	1.81E-04
210662_at	KYNU	kynureninase	2.25	4.56E-04
215966_x_at	GK3P	glycerol kinase 3 pseudogene	2.25	1.54E-03

242649_x_at	HMGN2P46	high mobility group nucleosomal binding domain 2 pseudogene 46	2.25	8.00E-04
229510_at	MS4A14	membrane-spanning 4-domains, subfamily A, member 14	2.24	3.12E-04
206176_at	BMP6	bone morphogenetic protein 6	2.22	1.41E-04
202887_s_at	DDIT4	DNA-damage-inducible transcript 4	2.22	1.23E-03
217167_x_at	GK	glycerol kinase	2.21	9.61E-04
217507_at	SLC11A1	solute carrier family 11 (proton-coupled divalent metal ion transporters), member 1	2.19	3.61E-04
1554676_at	SRGN	serglycin	2.18	5.92E-04
231227_at	WNT5A	wingless-type MMTV integration site family, member 5A	2.17	3.20E-04
1553602_at	MUCL1	mucin-like 1	2.17	1.79E-03
207387_s_at	GK	glycerol kinase	2.17	9.50E-04
205476_at	CCL20	chemokine (C-C motif) ligand 20	2.15	1.18E-03
228846_at	MXD1	MAX dimerization protein 1	2.14	2.26E-04
204567_s_at	ABCG1	ATP-binding cassette, sub-family G (WHITE), member 1	2.13	9.12E-04
1569203_at	CXCL2	chemokine (C-X-C motif) ligand 2	2.12	4.11E-04
222995_s_at	RHBDD2	rhomboid domain containing 2	2.12	5.60E-04
214681_at	GK	glycerol kinase	2.11	7.54E-04
218880_at	FOSL2	FOS-like antigen 2	2.10	3.61E-04
217553_at	STEAP1B	STEAP family member 1B	2.09	7.74E-04
228188_at	FOSL2	FOS-like antigen 2	2.09	3.18E-04
205013_s_at	NA	NA	2.09	1.96E-04
218839_at	HEY1	hairy/enhancer-of-split related with YRPW motif 1	2.09	3.12E-04
225262_at	FOSL2	FOS-like antigen 2	2.06	3.20E-04
216316_x_at	NA	NA	2.05	1.31E-03
229480_at	MAGI2-AS3	MAGI2 antisense RNA 3 (non-protein coding)	2.05	2.88E-04
211527_x_at	VEGFA	vascular endothelial growth factor A	2.03	4.43E-05
229053_at	SYT17	synaptotagmin XVII	2.02	2.26E-04
227230_s_at	KIAA1211	KIAA1211	2.02	7.50E-04
222326_at	NA	NA	1.98	1.56E-03
206907_at	TNFSF9	tumor necrosis factor (ligand) superfamily, member 9	1.98	2.33E-04
206359_at	SOCS3	suppressor of cytokine signaling 3	1.95	4.04E-04
207038_at	SLC16A6	solute carrier family 16, member 6 (monocarboxylic acid transporter 7)	1.94	7.87E-04
230913_at	NA	NA	1.93	2.38E-04
224807_at	GRAMD1A	GRAM domain containing 1A	1.92	1.04E-04
233388_at	NA	NA	1.91	9.12E-04
227799_at	MYO1G	myosin IG	1.91	8.96E-04
232081_at	NA	NA	1.90	2.03E-04
205027_s_at	MAP3K8	mitogen-activated protein kinase kinase kinase 8	1.89	1.61E-03
240232_at	NA	NA	1.87	1.54E-03
223343_at	MS4A7	membrane-spanning 4-domains, subfamily A, member 7	1.86	1.42E-03
230748_at	SLC16A6	solute carrier family 16, member 6 (monocarboxylic acid transporter 7)	1.86	9.36E-04
241824_at	NA	NA	1.85	4.81E-04
226275_at	MXD1	MAX dimerization protein 1	1.85	1.96E-04
201666_at	TIMP1	TIMP metallopeptidase inhibitor 1	1.84	4.95E-04
202888_s_at	ANPEP	alanyl (membrane) aminopeptidase	1.83	7.25E-04
210513_s_at	VEGFA	vascular endothelial growth factor A	1.82	1.86E-04
222934_s_at	CLEC4E	C-type lectin domain family 4, member E	1.81	4.15E-04
217475_s_at	LIMK2	LIM domain kinase 2	1.80	4.04E-04
227231_at	KIAA1211	KIAA1211	1.79	9.60E-04
1558871_at	NA	NA	1.77	5.06E-04
211924_s_at	PLAUR	plasminogen activator, urokinase receptor	1.77	2.56E-04
212171_x_at	VEGFA	vascular endothelial growth factor A	1.74	3.29E-04
1555116_s_at	SLC11A1	solute carrier family 11 (proton-coupled divalent metal ion transporters), member 1	1.74	4.04E-04
200920_s_at	BTG1	B-cell translocation gene 1, anti-proliferative	1.70	9.60E-04
202237_at	NNMT	nicotinamide N-methyltransferase	1.69	9.50E-04
203895_at	PLCB4	phospholipase C, beta 4	1.66	1.02E-03
219869_s_at	SLC39A8	solute carrier family 39 (zinc transporter), member 8	1.66	1.49E-03
1555689_at	CD80	CD80 molecule	1.64	1.49E-03
203921_at	CHST2	carbohydrate (N-acetylglucosamine-6-O) sulfotransferase 2	1.63	4.86E-05

202464_s_at	PFKFB3	6-phosphofructo-2-kinase/fructose-2,6-biphosphatase 3	1.62	9.12E-04
211113_s_at	ABCG1	ATP-binding cassette, sub-family G (WHITE), member 1	1.62	8.85E-04
1554519_at	CD80	CD80 molecule	1.60	1.70E-03
241916_at	NA	NA	1.59	1.54E-03
215559_at	ABCC6	ATP-binding cassette, sub-family C (CFTR/MRP), member 6	1.59	3.92E-04
209566_at	INSIG2	insulin induced gene 2	1.59	1.08E-04
205613_at	SYT17	synaptotagmin XVII	1.58	3.12E-04
227250_at	KREMEN1	kringle containing transmembrane protein 1	1.58	6.54E-04
212830_at	MEGF9	multiple EGF-like-domains 9	1.57	8.79E-04
210663_s_at	KYNU	kynureninase	1.57	5.06E-04
213817_at	IRAK3	interleukin-1 receptor-associated kinase 3	1.57	4.93E-04
208322_s_at	ST3GAL1	ST3 beta-galactoside alpha-2,3-sialyltransferase 1	1.56	2.87E-04
202388_at	RGS2	regulator of G-protein signaling 2, 24kDa	1.56	4.04E-04
225033_at	ST3GAL1	ST3 beta-galactoside alpha-2,3-sialyltransferase 1	1.55	3.12E-04
1553514_a_at	VNN3	vanin 3	1.55	3.20E-04
200921_s_at	BTG1	B-cell translocation gene 1, anti-proliferative	1.54	1.84E-03
207528_s_at	SLC7A11	solute carrier family 7 (anionic amino acid transporter light chain, xc- system), member 11	1.54	8.96E-04
210845_s_at	PLAUR	plasminogen activator, urokinase receptor	1.53	2.33E-04
201041_s_at	DUSP1	dual specificity phosphatase 1	1.53	3.12E-04
206675_s_at	SKIL	SKI-like oncogene	1.52	3.20E-04
230245_s_at	LOC283663	uncharacterized LOC283663	1.51	1.09E-03
207196_s_at	TNIP1	TNFAIP3 interacting protein 1	1.51	6.72E-04
204385_at	KYNU	kynureninase	1.50	9.60E-04
216920_s_at	NA	NA	1.50	7.07E-04
222288_at	NA	NA	1.50	1.11E-03
210146_x_at	LILRB2	leukocyte immunoglobulin-like receptor, subfamily B (with TM and ITIM domains), member 2	1.49	1.49E-03
229699_at	LOC100129550	uncharacterized LOC100129550	1.48	4.15E-04
202255_s_at	SIPA1L1	signal-induced proliferation-associated 1 like 1	1.48	7.42E-04
224336_s_at	DUSP16	dual specificity phosphatase 16	1.48	3.20E-04
244808_at	GRAMD1A	GRAM domain containing 1A	1.47	8.85E-04
202446_s_at	PLSCR1	phospholipid scramblase 1	1.46	1.19E-03
219859_at	CLEC4E	C-type lectin domain family 4, member E	1.46	4.29E-04
1560520_at	LOC401312	uncharacterized LOC401312	1.46	3.20E-04
1561654_at	NA	NA	1.46	2.38E-04
215838_at	LILRA5	leukocyte immunoglobulin-like receptor, subfamily A (with TM domain), member 5	1.45	1.53E-03
228325_at	KIAA0146	KIAA0146	1.45	8.45E-04
235661_at	NA	NA	1.45	3.36E-04
227854_at	NA	NA	1.45	9.10E-04
205896_at	SLC22A4	solute carrier family 22 (organic cation/ergothioneine transporter), member 4	1.43	1.30E-03
240656_at	NA	NA	1.42	1.38E-03
224832_at	DUSP16	dual specificity phosphatase 16	1.40	8.28E-04
229934_at	NA	NA	1.40	9.12E-04
1558397_at	PECAM1	platelet/endothelial cell adhesion molecule 1	1.40	4.81E-04
212561_at	DENND5A	DENN/MADD domain containing 5A	1.38	6.93E-04
214033_at	ABCC6	ATP-binding cassette, sub-family C (CFTR/MRP), member 6	1.37	2.33E-04
243509_at	NA	NA	1.36	1.47E-03
36612_at	FAM168A	family with sequence similarity 168, member A	1.36	8.24E-04
238319_at	LOC644090	uncharacterized LOC644090	1.36	4.95E-04
221697_at	MAP1LC3C	microtubule-associated protein 1 light chain 3 gamma	1.36	4.28E-04
209034_at	PNRC1	proline-rich nuclear receptor coactivator 1	1.35	8.85E-04
1566901_at	TGIF1	TGFB-induced factor homeobox 1	1.35	3.23E-04
212942_s_at	KIAA1199	KIAA1199	1.35	9.41E-04
226804_at	FAM20A	family with sequence similarity 20, member A	1.35	1.84E-03
1569599_at	SAMSN1	SAM domain, SH3 domain and nuclear localization signals 1	1.34	8.63E-04
201416_at	SOX4	SRY (sex determining region Y)-box 4	1.34	1.41E-03
202254_at	SIPA1L1	signal-induced proliferation-associated 1 like 1	1.34	1.30E-03
227099_s_at	C11orf96	chromosome 11 open reading frame 96	1.33	1.33E-03
235733_at	GXYLT2	glucoside xylosyltransferase 2	1.33	3.58E-04
226140_s_at	OTUD1	OTU domain containing 1	1.32	1.49E-03

160020_at	MMP14	matrix metallopeptidase 14 (membrane-inserted)	1.32	4.57E-04
218988_at	SLC35E3	solute carrier family 35, member E3	1.31	1.01E-03
209921_at	SLC7A11	solute carrier family 7 (anionic amino acid transporter light chain, xc- system), member 11	1.31	1.30E-03
227970_at	GPR157	G protein-coupled receptor 157	1.31	9.44E-04
244219_at	NA	NA	1.31	9.60E-04
210285_x_at	WTAP	Wilms tumor 1 associated protein	1.30	7.25E-04
232053_x_at	RHBDD2	rhomboid domain containing 2	1.30	1.53E-03
202828_s_at	MMP14	matrix metallopeptidase 14 (membrane-inserted)	1.30	3.20E-04
213107_at	TNIK	TRAF2 and NCK interacting kinase	1.30	1.82E-03
208092_s_at	FAM49A	family with sequence similarity 49, member A	1.29	5.63E-04
223683_at	ZMYND15	zinc finger, MYND-type containing 15	1.29	4.04E-04
213038_at	RNF19B	ring finger protein 19B	1.29	1.86E-03
210660_at	LILRA1	leukocyte immunoglobulin-like receptor, subfamily A (with TM domain), member 1	1.28	9.12E-04
217529_at	ORAI2	ORAI calcium release-activated calcium modulator 2	1.28	9.50E-04
241722_x_at	NA	NA	1.28	1.93E-03
204140_at	TPST1	tyrosylprotein sulfotransferase 1	1.28	1.65E-03
235089_at	FBXL20	F-box and leucine-rich repeat protein 20	1.27	5.06E-04
232504_at	LOC285628	uncharacterized LOC285628	1.27	7.54E-04
226026_at	DIRC2	disrupted in renal carcinoma 2	1.26	1.23E-03
231779_at	IRAK2	interleukin-1 receptor-associated kinase 2	1.26	9.50E-04
229937_x_at	LILRB1	leukocyte immunoglobulin-like receptor, subfamily B (with TM and ITIM domains), member 1	1.26	1.14E-03
44790_s_at	KIAA0226L	KIAA0226-like	1.26	8.96E-04
243299_at	VRK2	vaccinia related kinase 2	1.26	8.96E-04
207176_s_at	CD80	CD80 molecule	1.26	1.42E-03
225224_at	C20orf112	chromosome 20 open reading frame 112	1.26	8.15E-04
203556_at	ZHX2	zinc fingers and homeoboxes 2	1.26	2.38E-04
227749_at	POU2F2	POU class 2 homeobox 2	1.25	8.96E-04
202643_s_at	TNFAIP3	tumor necrosis factor, alpha-induced protein 3	1.25	3.31E-04
219788_at	PILRA	paired immunoglobin-like type 2 receptor alpha	1.25	4.28E-04
220034_at	IRAK3	interleukin-1 receptor-associated kinase 3	1.24	7.50E-04
201941_at	CPD	carboxypeptidase D	1.24	4.04E-04
223454_at	CXCL16	chemokine (C-X-C motif) ligand 16	1.24	8.14E-04
219317_at	POLI	polymerase (DNA directed) iota	1.24	3.18E-04
204802_at	RRAD	Ras-related associated with diabetes	1.24	9.55E-04
216504_s_at	SLC39A8	solute carrier family 39 (zinc transporter), member 8	1.24	1.70E-03
219889_at	FRAT1	frequently rearranged in advanced T-cell lymphomas	1.23	1.63E-03
204735_at	PDE4A	phosphodiesterase 4A, cAMP-specific	1.23	2.26E-04
206881_s_at	LILRA3	leukocyte immunoglobulin-like receptor, subfamily A (without TM domain), member 3	1.22	4.08E-04
225034_at	ST3GAL1	ST3 beta-galactoside alpha-2,3-sialyltransferase 1	1.22	1.70E-03
1553770_a_at	SLAMF9	SLAM family member 9	1.21	1.35E-03
207697_x_at	LILRB2	leukocyte immunoglobulin-like receptor, subfamily B (with TM and ITIM domains), member 2	1.21	1.49E-03
201502_s_at	NFKBIA	nuclear factor of kappa light polypeptide gene enhancer in B-cells inhibitor, alpha	1.21	2.51E-04
216199_s_at	MAP3K4	mitogen-activated protein kinase kinase kinase 4	1.21	3.18E-04
206877_at	MXD1	MAX dimerization protein 1	1.20	7.09E-04
231035_s_at	OTUD1	OTU domain containing 1	1.20	1.56E-03
232412_at	FBXL20	F-box and leucine-rich repeat protein 20	1.20	1.59E-03
225227_at	SKIL	SKI-like oncogene	1.19	5.40E-04
217279_x_at	MMP14	matrix metallopeptidase 14 (membrane-inserted)	1.19	5.29E-04
209606_at	CYTIP	cytohesin 1 interacting protein	1.19	9.97E-04
224889_at	FOXO3	forkhead box O3	1.19	4.81E-04
203408_s_at	SATB1	SATB homeobox 1	1.19	6.26E-04
212357_at	FAM168A	family with sequence similarity 168, member A	1.18	4.95E-04
236937_at	LOC100505729	uncharacterized LOC100505729	1.18	1.74E-03
228037_at	NA	NA	1.18	8.07E-04
201417_at	SOX4	SRY (sex determining region Y)-box 4	1.18	1.25E-03
202827_s_at	MMP14	matrix metallopeptidase 14 (membrane-inserted)	1.17	7.54E-04
215411_s_at	TRAF3IP2	TRAF3 interacting protein 2	1.17	3.61E-04

230333_at	NA	NA	1.17	1.64E-03
222450_at	PMEPA1	prostate transmembrane protein, androgen induced 1	1.17	6.72E-04
211776_s_at	EPB41L3	erythrocyte membrane protein band 4.1-like 3	1.17	6.93E-04
204803_s_at	RRAD	Ras-related associated with diabetes	1.17	1.87E-03
210664_s_at	TFPI	tissue factor pathway inhibitor (lipoprotein-associated coagulation inhibitor)	1.17	7.03E-04
203137_at	WTAP	Wilms tumor 1 associated protein	1.17	6.76E-04
211828_s_at	TNIK	TRAF2 and NCK interacting kinase	1.16	7.36E-04
227621_at	WTAP	Wilms tumor 1 associated protein	1.16	2.38E-04
203827_at	WIPI1	WD repeat domain, phosphoinositide interacting 1	1.16	1.68E-03
204089_x_at	MAP3K4	mitogen-activated protein kinase kinase kinase 4	1.16	2.38E-04
203313_s_at	TGIF1	TGFB-induced factor homeobox 1	1.16	2.50E-04
228910_at	NA	NA	1.16	7.39E-04
1553513_at	VNN3	vanin 3	1.16	6.74E-04
241365_at	SATB1	SATB homeobox 1	1.16	1.68E-03
220054_at	IL23A	interleukin 23, alpha subunit p19	1.16	1.49E-03
205126_at	VRK2	vaccinia related kinase 2	1.16	7.55E-04
1556332_at	NA	NA	1.16	1.29E-03
203238_s_at	NOTCH3	notch 3	1.15	3.20E-04
226575_at	ZNF462	zinc finger protein 462	1.15	1.84E-03
208018_s_at	HCK	hemopoietic cell kinase	1.15	7.25E-04
231406_at	ORAI2	ORAI calcium release-activated calcium modulator 2	1.14	1.25E-03
223196_s_at	SESN2	sestrin 2	1.14	3.61E-04
213159_at	PCNX	pecanex homolog (Drosophila)	1.14	4.11E-04
228945_s_at	SLC39A8	solute carrier family 39 (zinc transporter), member 8	1.14	7.54E-04
207630_s_at	CREM	cAMP responsive element modulator	1.14	8.96E-04
206710_s_at	EPB41L3	erythrocyte membrane protein band 4.1-like 3	1.13	6.93E-04
212960_at	TBC1D9	TBC1 domain family, member 9 (with GRAM domain)	1.13	1.16E-03
215046_at	KANSL1L	KAT8 regulatory NSL complex subunit 1-like	1.13	8.96E-04
201061_s_at	STOM	stomatin	1.12	1.66E-03
229213_at	DIRC2	disrupted in renal carcinoma 2	1.12	1.65E-03
209813_x_at	NA	NA	1.11	1.35E-03
219471_at	KIAA0226L	KIAA0226-like	1.11	8.96E-04
229287_at	PCNX	pecanex homolog (Drosophila)	1.11	1.39E-03
205443_at	SNAPC1	small nuclear RNA activating complex, polypeptide 1, 43kDa	1.11	1.49E-03
204132_s_at	NA	NA	1.11	3.20E-04
202625_at	LYN	v-yes-1 Yamaguchi sarcoma viral related oncogene homolog	1.10	9.12E-04
1553960_at	SNX21	sorting nexin family member 21	1.10	1.02E-03
210665_at	TFPI	tissue factor pathway inhibitor (lipoprotein-associated coagulation inhibitor)	1.10	1.47E-03
217388_s_at	KYNU	kynureninase	1.10	9.50E-04
239100_x_at	PCNX	pecanex homolog (Drosophila)	1.09	8.63E-04
209967_s_at	CREM	cAMP responsive element modulator	1.09	4.04E-04
224891_at	FOXO3	forkhead box O3	1.09	3.58E-04
209272_at	NAB1	NGFI-A binding protein 1 (EGR1 binding protein 1)	1.08	3.12E-04
235556_at	C5orf41	chromosome 5 open reading frame 41	1.08	1.49E-03
226842_at	FBXL20	F-box and leucine-rich repeat protein 20	1.07	2.33E-04
227020_at	YPEL2	yippee-like 2 (Drosophila)	1.06	1.03E-03
205499_at	SRPX2	sushi-repeat containing protein, X-linked 2	1.06	1.65E-03
202644_s_at	TNFAIP3	tumor necrosis factor, alpha-induced protein 3	1.06	4.28E-04
228153_at	RNF144B	ring finger protein 144B	1.05	1.34E-03
204131_s_at	FOXO3	forkhead box O3	1.05	1.04E-03
204157_s_at	SIK3	SIK family kinase 3	1.05	1.60E-03
217591_at	NA	NA	1.05	6.67E-04
214508_x_at	CREM	cAMP responsive element modulator	1.05	1.23E-03
231944_at	ERO1LB	ERO1-like beta (S. cerevisiae)	1.05	1.16E-03
1563357_at	NA	NA	1.04	2.05E-03
228343_at	POU2F2	POU class 2 homeobox 2	1.04	1.89E-03
213258_at	TFPI	tissue factor pathway inhibitor (lipoprotein-associated coagulation inhibitor)	1.04	2.05E-03
213173_at	PCNX	pecanex homolog (Drosophila)	1.04	1.16E-03
231296_at	GNA12	guanine nucleotide binding protein (G protein) alpha 12	1.04	9.64E-04

202693_s_at	STK17A	serine/threonine kinase 17a	1.03	4.11E-04
235675_at	DHFRL1	dihydrofolate reductase-like 1	1.03	1.02E-03
210785_s_at	C1orf38	chromosome 1 open reading frame 38	1.03	3.20E-04
212681_at	EPB41L3	erythrocyte membrane protein band 4.1-like 3	1.03	9.86E-04
210754_s_at	LYN	v-yes-1 Yamaguchi sarcoma viral related oncogene homolog	1.03	8.96E-04
205686_s_at	CD86	CD86 molecule	1.02	1.03E-03
201940_at	CPD	carboxypeptidase D	1.02	8.28E-04
223482_at	TMEM120A	transmembrane protein 120A	1.02	9.12E-04
209267_s_at	SLC39A8	solute carrier family 39 (zinc transporter), member 8	1.02	1.94E-03
226261_at	ZNRF2	zinc and ring finger 2	1.02	2.05E-03
202820_at	AHR	aryl hydrocarbon receptor	1.01	1.49E-03
202626_s_at	LYN	v-yes-1 Yamaguchi sarcoma viral related oncogene homolog	1.01	1.16E-03
205685_at	CD86	CD86 molecule	1.01	6.61E-04
214104_at	GPR161	G protein-coupled receptor 161	1.01	1.10E-03
1560625_s_at	NA	NA	1.00	2.38E-04
212761_at	TCF7L2	transcription factor 7-like 2 (T-cell specific, HMG-box)	1.00	2.04E-03
210895_s_at	CD86	CD86 molecule	1.00	8.96E-04
210422_x_at	SLC11A1	solute carrier family 11 (proton-coupled divalent metal ion transporters), member 1	1.00	1.16E-03
230511_at	CREM	cAMP responsive element modulator	1.00	4.04E-04
230561_s_at	KANSL1L	KAT8 regulatory NSL complex subunit 1-like	1.00	1.12E-03
203904_x_at	CD82	CD82 molecule	1.00	1.30E-03
204908_s_at	BCL3	B-cell CLL/lymphoma 3	1.00	6.72E-04
207571_x_at	C1orf38	chromosome 1 open reading frame 38	1.00	4.08E-04
207442_at	CSF3	colony stimulating factor 3 (granulocyte)	0.99	8.96E-04
229630_s_at	WTAP	Wilms tumor 1 associated protein	0.99	7.25E-04
203278_s_at	PHF21A	PHD finger protein 21A	0.98	7.25E-04
212110_at	SLC39A14	solute carrier family 39 (zinc transporter), member 14	0.98	1.67E-03
200797_s_at	MCL1	myeloid cell leukemia sequence 1 (BCL2-related)	0.98	1.75E-03
1559034_at	SIRPB2	signal-regulatory protein beta 2	0.98	9.91E-04
212956_at	TBC1D9	TBC1 domain family, member 9 (with GRAM domain)	0.97	6.72E-04
228562_at	ZBTB10	zinc finger and BTB domain containing 10	0.97	3.12E-04
209198_s_at	SYT11	synaptotagmin XI	0.97	9.61E-04
217473_x_at	SLC11A1	solute carrier family 11 (proton-coupled divalent metal ion transporters), member 1	0.96	9.12E-04
201942_s_at	CPD	carboxypeptidase D	0.96	2.09E-03
223484_at	C15orf48	chromosome 15 open reading frame 48	0.96	3.20E-04
200989_at	HIF1A	hypoxia inducible factor 1, alpha subunit (basic helix-loop-helix transcription factor)	0.95	3.61E-04
229795_at	NA	NA	0.95	1.02E-03
215175_at	PCNX	pecanex homolog (Drosophila)	0.94	8.63E-04
230380_at	THAP2	THAP domain containing, apoptosis associated protein 2	0.93	1.35E-03
218834_s_at	TMEM132A	transmembrane protein 132A	0.93	8.96E-04
214866_at	PLAUR	plasminogen activator, urokinase receptor	0.93	3.20E-04
204542_at	ST6GALNAC2	ST6 (alpha-N-acetyl-neuraminyl-2,3-beta-galactosyl-1,3)-N-acetylgalactosaminide alpha-2,6-sialyltransferase 2	0.93	4.81E-04
1555193_a_at	ZNF277	zinc finger protein 277	0.93	5.45E-04
230815_at	LOC389765	kinesin family member 27 pseudogene	0.92	1.50E-03
220091_at	SLC2A6	solute carrier family 2 (facilitated glucose transporter), member 6	0.92	2.88E-04
212614_at	ARID5B	AT rich interactive domain 5B (MRF1-like)	0.92	8.13E-04
218881_s_at	FOSL2	FOS-like antigen 2	0.92	9.44E-04
218645_at	ZNF277	zinc finger protein 277	0.91	3.20E-04
221752_at	SSH1	slingshot homolog 1 (Drosophila)	0.91	9.61E-04
224197_s_at	C1QTNF1	C1q and tumor necrosis factor related protein 1	0.91	6.74E-04
209197_at	SYT11	synaptotagmin XI	0.91	4.81E-04
224710_at	RAB34	RAB34, member RAS oncogene family	0.91	1.21E-03
211139_s_at	NAB1	NGFI-A binding protein 1 (EGR1 binding protein 1)	0.91	6.72E-04
226181_at	TUBE1	tubulin, epsilon 1	0.90	3.61E-04
222218_s_at	PILRA	paired immunoglobin-like type 2 receptor alpha	0.90	1.35E-03
1554153_a_at	PHF21A	PHD finger protein 21A	0.90	1.49E-03

205003_at	DOCK4	dedicator of cytokinesis 4	0.90	8.96E-04
210357_s_at	SMOX	spermine oxidase	0.90	1.16E-03
238792_at	PCNX	pecanex homolog (Drosophila)	0.90	9.60E-04
203195_s_at	NUP98	nucleoporin 98kDa	0.89	3.61E-04
203194_s_at	NUP98	nucleoporin 98kDa	0.89	4.28E-04
1559573_at	LOC100506229	uncharacterized LOC100506229	0.89	1.24E-03
205599_at	TRAF1	TNF receptor-associated factor 1	0.88	1.46E-03
210387_at	NA	NA	0.88	1.81E-03
1562749_at	LOC644090	uncharacterized LOC644090	0.88	3.61E-04
211690_at	RPS6	ribosomal protein S6	0.88	1.31E-03
1555630_a_at	RAB34	RAB34, member RAS oncogene family	0.88	1.06E-03
226489_at	TMCC3	transmembrane and coiled-coil domain family 3	0.88	1.36E-03
225919_s_at	C9orf72	chromosome 9 open reading frame 72	0.88	1.87E-03
213034_at	SIK3	SIK family kinase 3	0.87	2.01E-03
222693_at	FNDC3B	fibronectin type III domain containing 3B	0.87	1.05E-03
236125_at	NA	NA	0.87	1.85E-03
235360_at	PLEKHM3	pleckstrin homology domain containing, family M, member 3	0.87	1.75E-03
226454_at	MARCH9	membrane-associated ring finger (C3HC4) 9	0.87	6.72E-04
215555_at	NA	NA	0.86	1.33E-03
223195_s_at	SESN2	sestrin 2	0.85	1.28E-03
212989_at	SGMS1	sphingomyelin synthase 1	0.85	1.63E-03
233986_s_at	PLEKHG2	pleckstrin homology domain containing, family G (with RhoGef domain) member 2	0.85	4.81E-04
209102_s_at	HBP1	HMG-box transcription factor 1	0.85	1.30E-03
206219_s_at	VAV1	vav 1 guanine nucleotide exchange factor	0.84	5.36E-04
220936_s_at	H2AFJ	H2A histone family, member J	0.83	9.20E-04
202925_s_at	PLAGL2	pleiomorphic adenoma gene-like 2	0.83	6.54E-04
207104_x_at	LILRB1	leukocyte immunoglobulin-like receptor, subfamily B (with TM and ITIM domains), member 1	0.83	1.20E-03
226731_at	NA	NA	0.82	9.44E-04
201990_s_at	CREBL2	cAMP responsive element binding protein-like 2	0.82	1.31E-03
201883_s_at	B4GALT1	UDP-Gal:betaGlcNAc beta 1,4- galactosyltransferase, polypeptide 1	0.82	2.14E-03
211711_s_at	PTEN	phosphatase and tensin homolog	0.82	1.65E-03
204912_at	IL10RA	interleukin 10 receptor, alpha	0.81	6.93E-04
1556385_at	NA	NA	0.81	2.01E-03
239223_s_at	FBXL20	F-box and leucine-rich repeat protein 20	0.80	7.25E-04
215732_s_at	DTX2	deltex homolog 2 (Drosophila)	0.80	1.18E-03
227408_s_at	SNX25	sorting nexin 25	0.80	8.13E-04
219312_s_at	ZBTB10	zinc finger and BTB domain containing 10	0.80	9.60E-04
238987_at	B4GALT1	UDP-Gal:betaGlcNAc beta 1,4- galactosyltransferase, polypeptide 1	0.80	2.18E-03
225328_at	FBXO32	F-box protein 32	0.79	1.39E-03
207275_s_at	ACSL1	acyl-CoA synthetase long-chain family member 1	0.79	1.32E-03
205548_s_at	BTG3	BTG family, member 3	0.79	1.47E-03
1555950_a_at	CD55	CD55 molecule, decay accelerating factor for complement (Cromer blood group)	0.79	2.07E-03
223264_at	MESDC1	mesoderm development candidate 1	0.79	2.29E-03
202695_s_at	STK17A	serine/threonine kinase 17a	0.79	1.73E-03
211336_x_at	LILRB1	leukocyte immunoglobulin-like receptor, subfamily B (with TM and ITIM domains), member 1	0.79	1.38E-03
205407_at	RECK	reversion-inducing-cysteine-rich protein with kazal motifs	0.78	1.23E-03
222692_s_at	FNDC3B	fibronectin type III domain containing 3B	0.78	7.25E-04
228702_at	FLJ43663	uncharacterized LOC378805	0.78	1.75E-03
225414_at	RNF149	ring finger protein 149	0.78	1.79E-03
217875_s_at	PMEPA1	prostate transmembrane protein, androgen induced 1	0.78	1.86E-03
201926_s_at	CD55	CD55 molecule, decay accelerating factor for complement (Cromer blood group)	0.77	1.50E-03
201988_s_at	CREBL2	cAMP responsive element binding protein-like 2	0.77	2.20E-03
211538_s_at	HSPA2	heat shock 70kDa protein 2	0.77	1.27E-03
217122_s_at	SLC35E2B	solute carrier family 35, member E2B	0.77	9.24E-04
201490_s_at	PPIF	peptidylprolyl isomerase F	0.76	1.93E-03

224596_at	SLC44A1	solute carrier family 44, member 1	0.76	1.07E-03
209551_at	YIPF4	Yip1 domain family, member 4	0.76	2.01E-03
208869_s_at	GABARAPL1	GABA(A) receptor-associated protein like 1	0.76	2.26E-03
225059_at	AGTRAP	angiotensin II receptor-associated protein	0.76	9.12E-04
203853_s_at	GAB2	GRB2-associated binding protein 2	0.76	1.42E-03
224783_at	FAM100B	family with sequence similarity 100, member B	0.76	2.24E-03
221062_at	HS3ST3B1	heparan sulfate (glucosamine) 3-O-sulfotransferase 3B1	0.76	2.04E-03
236217_at	SLC31A1	solute carrier family 31 (copper transporters), member 1	0.76	2.33E-03
224681_at	GNA12	guanine nucleotide binding protein (G protein) alpha 12	0.75	1.47E-03
208983_s_at	PECAM1	platelet/endothelial cell adhesion molecule 1	0.75	9.50E-04
225368_at	HIPK2	homeodomain interacting protein kinase 2	0.74	1.75E-03
227755_at	NA	NA	0.74	9.60E-04
214435_x_at	RALA	v-ral simian leukemia viral oncogene homolog A (ras related)	0.74	1.71E-03
225097_at	HIPK2	homeodomain interacting protein kinase 2	0.74	1.86E-03
213134_x_at	BTG3	BTG family, member 3	0.74	9.61E-04
228485_s_at	SLC44A1	solute carrier family 44, member 1	0.74	1.80E-03
226763_at	SESTD1	SEC14 and spectrin domains 1	0.73	2.06E-03
235267_at	MAGI2-AS3	MAGI2 antisense RNA 3 (non-protein coding)	0.73	1.95E-03
224595_at	SLC44A1	solute carrier family 44, member 1	0.73	2.53E-03
244041_at	NA	NA	0.72	2.29E-03
214743_at	CUX1	cut-like homeobox 1	0.72	2.27E-03
203504_s_at	ABCA1	ATP-binding cassette, sub-family A (ABC1), member 1	0.72	2.31E-03
218499_at	MST4	serine/threonine protein kinase MST4	0.71	2.28E-03
203221_at	TLE1	transducin-like enhancer of split 1 (E(sp1) homolog, Drosophila)	0.71	1.96E-03
229678_at	LOC728431	uncharacterized LOC728431	0.71	5.06E-04
212799_at	STX6	syntaxin 6	0.71	1.29E-03
228964_at	PRDM1	PR domain containing 1, with ZNF domain	0.71	1.05E-03
210655_s_at	NA	NA	0.71	1.87E-03
229226_at	NA	NA	0.70	8.96E-04
209935_at	ATP2C1	ATPase, Ca++ transporting, type 2C, member 1	0.70	1.75E-03
1552329_at	RBBP6	retinoblastoma binding protein 6	0.70	1.61E-03
219458_s_at	NSUN3	NOP2/Sun domain family, member 3	0.70	7.25E-04
242866_x_at	POU2F2	POU class 2 homeobox 2	0.70	8.63E-04
227905_s_at	AZI2	5-azacytidine induced 2	0.70	2.13E-03
218277_s_at	DHX40	DEAH (Asp-Glu-Ala-His) box polypeptide 40	0.69	2.51E-03
210564_x_at	CFLAR	CASP8 and FADD-like apoptosis regulator	0.69	2.24E-03
228751_at	CLK4	CDC-like kinase 4	0.69	1.16E-03
214130_s_at	PDE4DIP	phosphodiesterase 4D interacting protein	0.69	2.07E-03
242230_at	ATXN1	ataxin 1	0.68	1.89E-03
221669_s_at	ACAD8	acyl-CoA dehydrogenase family, member 8	0.67	1.80E-03
229603_at	BBS12	Bardet-Biedl syndrome 12	0.66	2.27E-03
228213_at	H2AFJ	H2A histone family, member J	0.66	1.31E-03
209934_s_at	ATP2C1	ATPase, Ca++ transporting, type 2C, member 1	0.66	1.66E-03
211771_s_at	POU2F2	POU class 2 homeobox 2	0.66	1.33E-03
228486_at	SLC44A1	solute carrier family 44, member 1	0.66	2.73E-03
209239_at	NFKB1	nuclear factor of kappa light polypeptide gene enhancer in B-cells 1	0.66	9.97E-04
213922_at	TTBK2	tau tubulin kinase 2	0.66	1.90E-03
210346_s_at	CLK4	CDC-like kinase 4	0.65	1.98E-03
232145_at	C2orf68	chromosome 2 open reading frame 68	0.65	2.04E-03
210047_at	SLC11A2	solute carrier family 11 (proton-coupled divalent metal ion transporters), member 2	0.65	1.47E-03
218641_at	C11orf95	chromosome 11 open reading frame 95	0.65	2.09E-03
211316_x_at	CFLAR	CASP8 and FADD-like apoptosis regulator	0.65	2.34E-03
209394_at	ASMTL	acetylserotonin O-methyltransferase-like	0.65	2.39E-03
208981_at	PECAM1	platelet/endothelial cell adhesion molecule 1	0.65	1.56E-03
213137_s_at	PTPN2	protein tyrosine phosphatase, non-receptor type 2	0.65	2.44E-03
202197_at	MTMR3	myotubularin related protein 3	0.65	2.51E-03
204601_at	N4BP1	NEDD4 binding protein 1	0.64	2.68E-03
212677_s_at	CEP68	centrosomal protein 68kDa	0.64	9.75E-04
225245_x_at	H2AFJ	H2A histone family, member J	0.64	2.55E-03

224508_at	MGC12916	uncharacterized protein MGC12916	0.63	1.38E-03
222421_at	UBE2H	ubiquitin-conjugating enzyme E2H	0.63	9.44E-04
204173_at	MYL6B	myosin, light chain 6B, alkali, smooth muscle and non-muscle	0.63	2.80E-03
241985_at	JMY	junction mediating and regulatory protein, p53 cofactor	0.63	1.70E-03
214129_at	PDE4DIP	phosphodiesterase 4D interacting protein	0.62	1.87E-03
201963_at	ACSL1	acyl-CoA synthetase long-chain family member 1	0.62	1.31E-03
227785_at	SDCCAG8	serologically defined colon cancer antigen 8	0.61	2.88E-03
225803_at	FBXO32	F-box protein 32	0.61	2.10E-03
1553956_at	TMEM237	transmembrane protein 237	0.61	1.77E-03
209508_x_at	CFLAR	CASP8 and FADD-like apoptosis regulator	0.61	1.98E-03
226037_s_at	TAF9B	TAF9B RNA polymerase II, TATA box binding protein (TBP)-associated factor, 31kDa	0.61	1.53E-03
219210_s_at	RAB8B	RAB8B, member RAS oncogene family	0.61	1.66E-03
239600_at	NA	NA	0.61	2.50E-03
203149_at	PVRL2	poliovirus receptor-related 2 (herpesvirus entry mediator B)	0.60	1.80E-03
238327_at	ODF3B	outer dense fiber of sperm tails 3B	0.60	1.80E-03
1556321_a_at	NA	NA	0.59	2.68E-03
1552950_at	C15orf26	chromosome 15 open reading frame 26	0.59	1.49E-03
203602_s_at	ZBTB17	zinc finger and BTB domain containing 17	0.59	2.26E-03
212268_at	SERPINB1	serpin peptidase inhibitor, clade B (ovalbumin), member 1	0.58	2.47E-03
214660_at	ITGA1	integrin, alpha 1	0.58	2.99E-03
209845_at	MKRN1	makorin ring finger protein 1	0.58	2.73E-03
209359_x_at	RUNX1	runt-related transcription factor 1	0.58	1.97E-03
211135_x_at	LILRB3	leukocyte immunoglobulin-like receptor, subfamily B (with TM and ITIM domains), member 3	0.58	2.44E-03
209333_at	ULK1	unc-51-like kinase 1 (C. elegans)	0.58	2.29E-03
204054_at	PTEN	phosphatase and tensin homolog	0.58	1.24E-03
55065_at	MARK4	MAP/microtubule affinity-regulating kinase 4	0.58	1.21E-03
226195_at	IFT43	intraflagellar transport 43 homolog (Chlamydomonas)	0.57	1.65E-03
215889_at	SKIL	SKI-like oncogene	0.57	2.91E-03
227169_at	DNAJC18	DnaJ (Hsp40) homolog, subfamily C, member 18	0.57	2.53E-03
232204_at	EBF1	early B-cell factor 1	0.57	1.28E-03
217763_s_at	RAB31	RAB31, member RAS oncogene family	0.57	2.04E-03
231861_at	LRP10	low density lipoprotein receptor-related protein 10	0.57	2.56E-03
215164_at	NA	NA	0.57	1.70E-03
202245_at	LSS	lanosterol synthase (2,3-oxidosqualene-lanosterol cyclase)	0.57	1.81E-03
207860_at	NCR1	natural cytotoxicity triggering receptor 1	0.57	2.01E-03
201772_at	AZIN1	antizyme inhibitor 1	0.56	1.97E-03
213379_at	COQ2	coenzyme Q2 homolog, prenyltransferase (yeast)	0.56	2.06E-03
243395_at	NA	NA	0.56	2.53E-03
210784_x_at	NA	NA	0.56	3.02E-03
235258_at	DCP2	DCP2 decapping enzyme homolog (S. cerevisiae)	0.56	2.17E-03
226956_at	MTMR3	myotubularin related protein 3	0.56	3.26E-03
1554291_at	UHRF1BP1L	UHRF1 binding protein 1-like	0.55	3.28E-03
219492_at	CHIC2	cysteine-rich hydrophobic domain 2	0.55	2.53E-03
201189_s_at	ITPR3	inositol 1,4,5-trisphosphate receptor, type 3	0.54	2.72E-03
225519_at	PPP4R2	protein phosphatase 4, regulatory subunit 2	0.54	2.74E-03
221641_s_at	ACOT9	acyl-CoA thioesterase 9	0.54	2.18E-03
219693_at	AGPAT4	1-acylglycerol-3-phosphate O-acyltransferase 4 (lysophosphatidic acid acyltransferase, delta)	0.53	2.96E-03
204118_at	CD48	CD48 molecule	0.53	1.94E-03
222863_at	ZBTB10	zinc finger and BTB domain containing 10	0.53	2.68E-03
217762_s_at	RAB31	RAB31, member RAS oncogene family	0.52	2.51E-03
202252_at	RAB13	RAB13, member RAS oncogene family	0.52	2.07E-03
216015_s_at	NLRP3	NLR family, pyrin domain containing 3	0.52	2.82E-03
203227_s_at	TSPAN31	tetraspanin 31	0.51	3.16E-03
213627_at	MAGED2	melanoma antigen family D, 2	0.51	2.47E-03
205791_x_at	NA	NA	0.51	3.14E-03
228386_s_at	DDX59	DEAD (Asp-Glu-Ala-Asp) box polypeptide 59	0.51	3.41E-03
228536_at	PRMT10	protein arginine methyltransferase 10 (putative)	0.51	2.34E-03
203825_at	BRD3	bromodomain containing 3	0.50	3.08E-03
217764_s_at	RAB31	RAB31, member RAS oncogene family	0.50	3.14E-03

209377_s_at	HMGN3	high mobility group nucleosomal binding domain 3	-0.50	2.68E-03
206050_s_at	RNH1	ribonuclease/angiogenin inhibitor 1	-0.50	2.01E-03
225484_at	CEP41	centrosomal protein 41kDa	-0.50	3.28E-03
213334_x_at	HAUS7	HAUS augmin-like complex, subunit 7	-0.51	2.04E-03
218705_s_at	SNX24	sorting nexin 24	-0.51	3.27E-03
230264_s_at	AP1S2	adaptor-related protein complex 1, sigma 2 subunit	-0.51	2.17E-03
201740_at	NDUFS3	NADH dehydrogenase (ubiquinone) Fe-S protein 3, 30kDa (NADH-coenzyme Q reductase)	-0.51	3.62E-03
210624_s_at	ILVBL	ilvB (bacterial acetolactate synthase)-like	-0.51	3.09E-03
218557_at	NIT2	nitrilase family, member 2	-0.51	3.60E-03
233498_at	ERBB4	v-erb-a erythroblastic leukemia viral oncogene homolog 4 (avian)	-0.51	3.90E-03
209478_at	STRA13	stimulated by retinoic acid 13 homolog (mouse)	-0.51	2.80E-03
226958_s_at	MED11	mediator complex subunit 11	-0.51	1.59E-03
204046_at	PLCB2	phospholipase C, beta 2	-0.52	3.60E-03
229426_at	COX5A	cytochrome c oxidase subunit Va	-0.53	3.26E-03
222622_at	PGP	phosphoglycolate phosphatase	-0.53	2.64E-03
219043_s_at	NA	NA	-0.53	1.98E-03
213892_s_at	APRT	adenine phosphoribosyltransferase	-0.54	3.23E-03
209104_s_at	NHP2	NHP2 ribonucleoprotein homolog (yeast)	-0.54	2.05E-03
224335_s_at	BACE1	beta-site APP-cleaving enzyme 1	-0.54	2.56E-03
231917_at	GFM2	G elongation factor, mitochondrial 2	-0.55	2.50E-03
217751_at	GSTK1	glutathione S-transferase kappa 1	-0.55	3.23E-03
214501_s_at	H2AFY	H2A histone family, member Y	-0.55	2.61E-03
210872_x_at	GAS7	growth arrest-specific 7	-0.55	3.28E-03
219491_at	LRFN4	leucine rich repeat and fibronectin type III domain containing 4	-0.55	2.74E-03
218481_at	EXOSC5	exosome component 5	-0.55	2.74E-03
218597_s_at	CISD1	CDGSH iron sulfur domain 1	-0.55	2.97E-03
224869_s_at	MRPS25	mitochondrial ribosomal protein S25	-0.56	1.98E-03
200768_s_at	MAT2A	methionine adenosyltransferase II, alpha	-0.56	2.65E-03
200617_at	MLEC	malectin	-0.56	2.26E-03
202053_s_at	ALDH3A2	aldehyde dehydrogenase 3 family, member A2	-0.56	1.86E-03
204875_s_at	GMDS	GDP-mannose 4,6-dehydratase	-0.56	2.05E-03
235339_at	SETDB2	SET domain, bifurcated 2	-0.56	3.05E-03
225676_s_at	DCAF13	DDB1 and CUL4 associated factor 13	-0.57	3.30E-03
1555037_a_at	IDH1	isocitrate dehydrogenase 1 (NADP+), soluble	-0.57	2.68E-03
227782_at	ZBTB7C	zinc finger and BTB domain containing 7C	-0.57	1.69E-03
203092_at	TIMM44	translocase of inner mitochondrial membrane 44 homolog (yeast)	-0.57	3.17E-03
224283_x_at	IL18BP	interleukin 18 binding protein	-0.57	2.61E-03
222640_at	DNMT3A	DNA (cytosine-5-)-methyltransferase 3 alpha	-0.58	1.87E-03
218108_at	UBR7	ubiquitin protein ligase E3 component n-recognin 7 (putative)	-0.59	2.58E-03
203093_s_at	TIMM44	translocase of inner mitochondrial membrane 44 homolog (yeast)	-0.59	1.67E-03
205085_at	ORC1	origin recognition complex, subunit 1	-0.59	2.84E-03
210950_s_at	FDFT1	farnesyl-diphosphate farnesyltransferase 1	-0.60	1.75E-03
209527_at	EXOSC2	exosome component 2	-0.60	2.26E-03
235025_at	WDR89	WD repeat domain 89	-0.61	2.26E-03
225096_at	C17orf79	chromosome 17 open reading frame 79	-0.61	2.15E-03
208647_at	FDFT1	farnesyl-diphosphate farnesyltransferase 1	-0.61	2.15E-03
215165_x_at	UMPS	uridine monophosphate synthetase	-0.61	2.52E-03
200845_s_at	PRDX6	peroxiredoxin 6	-0.62	1.51E-03
216212_s_at	DKC1	dyskeratosis congenita 1, dyskerin	-0.62	2.69E-03
227117_at	NA	NA	-0.62	1.47E-03
222584_at	MSTO1	misato homolog 1 (Drosophila)	-0.62	1.79E-03
218981_at	ACN9	ACN9 homolog (S. cerevisiae)	-0.62	1.90E-03
228810_at	CCNYL1	cyclin Y-like 1	-0.63	9.60E-04
218358_at	CRELD2	cysteine-rich with EGF-like domains 2	-0.63	1.31E-03
212638_s_at	WWP1	WW domain containing E3 ubiquitin protein ligase 1	-0.63	2.19E-03
233328_x_at	SLC17A9	solute carrier family 17, member 9	-0.63	1.81E-03

210802_s_at	DIMT1	DIM1 dimethyladenosine transferase 1 homolog (S. cerevisiae)	-0.63	2.63E-03
204839_at	POP5	processing of precursor 5, ribonuclease P/MRP subunit (S. cerevisiae)	-0.65	1.49E-03
209567_at	RRS1	RRS1 ribosome biogenesis regulator homolog (S. cerevisiae)	-0.65	8.98E-04
209440_at	PRPS1	phosphoribosyl pyrophosphate synthetase 1	-0.65	1.47E-03
202054_s_at	ALDH3A2	aldehyde dehydrogenase 3 family, member A2	-0.65	2.68E-03
232589_at	NA	NA	-0.65	1.14E-03
208813_at	GOT1	glutamic-oxaloacetic transaminase 1, soluble (aspartate aminotransferase 1)	-0.66	2.23E-03
201280_s_at	DAB2	disabled homolog 2, mitogen-responsive phosphoprotein (Drosophila)	-0.66	1.60E-03
221830_at	RAP2A	RAP2A, member of RAS oncogene family	-0.66	2.64E-03
209626_s_at	OSBPL3	oxysterol binding protein-like 3	-0.66	1.18E-03
208923_at	CYFIP1	cytoplasmic FMR1 interacting protein 1	-0.66	1.53E-03
228051_at	KIAA1244	KIAA1244	-0.66	2.68E-03
219110_at	GAR1	GAR1 ribonucleoprotein homolog (yeast)	-0.66	1.66E-03
228624_at	TMEM144	transmembrane protein 144	-0.66	2.72E-03
203405_at	PSMG1	proteasome (prosome, macropain) assembly chaperone 1	-0.66	1.23E-03
1556667_at	FONG	uncharacterized LOC348751	-0.67	2.46E-03
225851_at	FNTB	farnesyltransferase, CAAX box, beta	-0.67	2.09E-03
221539_at	EIF4EBP1	eukaryotic translation initiation factor 4E binding protein 1	-0.67	1.70E-03
203299_s_at	AP1S2	adaptor-related protein complex 1, sigma 2 subunit	-0.67	1.72E-03
219420_s_at	SELRC1	Sel1 repeat containing 1	-0.67	1.30E-03
229061_s_at	SLC25A13	solute carrier family 25, member 13 (citrin)	-0.68	2.06E-03
218493_at	SNRNP25	small nuclear ribonucleoprotein 25kDa (U11/U12)	-0.68	1.53E-03
229241_at	LDHD	lactate dehydrogenase D	-0.69	1.87E-03
202246_s_at	CDK4	cyclin-dependent kinase 4	-0.69	2.08E-03
204168_at	MGST2	microsomal glutathione S-transferase 2	-0.70	1.24E-03
218024_at	BRP44L	brain protein 44-like	-0.70	2.27E-03
219419_at	RBFA	ribosome binding factor A (putative)	-0.70	2.54E-03
224523_s_at	C3orf26	chromosome 3 open reading frame 26	-0.70	1.90E-03
235338_s_at	SETDB2	SET domain, bifurcated 2	-0.71	1.97E-03
227960_s_at	FAHD1	fumarylacetoacetate hydrolase domain containing 1	-0.71	1.66E-03
223774_at	SNHG12	small nucleolar RNA host gene 12 (non-protein coding)	-0.71	1.19E-03
200616_s_at	MLEC	malectin	-0.72	1.33E-03
205135_s_at	NUFIP1	nuclear fragile X mental retardation protein interacting protein 1	-0.72	1.74E-03
228661_s_at	NA	NA	-0.72	1.54E-03
208758_at	ATIC	5-aminoimidazole-4-carboxamide ribonucleotide formyltransferase/IMP cyclohydrolase	-0.73	1.41E-03
218270_at	MRPL24	mitochondrial ribosomal protein L24	-0.73	1.49E-03
222500_at	PPIL1	peptidylprolyl isomerase (cyclophilin)-like 1	-0.74	1.49E-03
208787_at	MRPL3	mitochondrial ribosomal protein L3	-0.74	1.98E-03
226106_at	RNF141	ring finger protein 141	-0.74	1.29E-03
225609_at	GSR	glutathione reductase	-0.74	9.44E-04
222532_at	SRPRB	signal recognition particle receptor, B subunit	-0.74	9.61E-04
1554067_at	C12orf66	chromosome 12 open reading frame 66	-0.74	2.26E-03
208881_x_at	IDI1	isopentenyl-diphosphate delta isomerase 1	-0.75	2.27E-03
206420_at	IGSF6	immunoglobulin superfamily, member 6	-0.75	1.10E-03
204615_x_at	IDI1	isopentenyl-diphosphate delta isomerase 1	-0.75	1.30E-03
203402_at	KCNAB2	potassium voltage-gated channel, shaker-related subfamily, beta member 2	-0.76	2.22E-03
202655_at	MANF	mesencephalic astrocyte-derived neurotrophic factor	-0.76	2.12E-03
223035_s_at	FARSB	phenylalanyl-tRNA synthetase, beta subunit	-0.77	2.26E-03
221666_s_at	PYCARD	PYD and CARD domain containing	-0.77	1.56E-03
221045_s_at	PER3	period homolog 3 (Drosophila)	-0.78	8.96E-04
218710_at	TTC27	tetratricopeptide repeat domain 27	-0.78	1.53E-03
235026_at	C12orf66	chromosome 12 open reading frame 66	-0.78	2.37E-03
205823_at	RGS12	regulator of G-protein signaling 12	-0.78	1.92E-03
205225_at	ESR1	estrogen receptor 1	-0.79	1.31E-03
202138_x_at	AIMP2	aminoacyl tRNA synthetase complex-interacting multifunctional protein 2	-0.79	1.84E-03

238622_at	RAP2B	RAP2B, member of RAS oncogene family	-0.79	9.20E-04
225868_at	TRIM47	tripartite motif containing 47	-0.79	2.19E-03
209971_x_at	AIMP2	aminoacyl tRNA synthetase complex-interacting multifunctional protein 2	-0.80	1.05E-03
205770_at	GSR	glutathione reductase	-0.80	1.11E-03
211569_s_at	HADH	hydroxyacyl-CoA dehydrogenase	-0.80	1.49E-03
221245_s_at	FZD5	frizzled family receptor 5	-0.80	1.31E-03
220246_at	CAMK1D	calcium/calmodulin-dependent protein kinase ID	-0.81	1.49E-03
226938_at	DCAF4	DDB1 and CUL4 associated factor 4	-0.81	1.42E-03
224973_at	FAM46A	family with sequence similarity 46, member A	-0.81	1.32E-03
221766_s_at	FAM46A	family with sequence similarity 46, member A	-0.81	1.79E-03
209960_at	HGF	hepatocyte growth factor (hepapoietin A; scatter factor)	-0.82	1.54E-03
213133_s_at	NA	NA	-0.82	1.79E-03
208639_x_at	PDIA6	protein disulfide isomerase family A, member 6	-0.82	1.74E-03
220061_at	ACSM5	acyl-CoA synthetase medium-chain family member 5	-0.82	2.11E-03
207668_x_at	PDIA6	protein disulfide isomerase family A, member 6	-0.83	1.83E-03
217809_at	BZW2	basic leucine zipper and W2 domains 2	-0.83	2.19E-03
227144_at	KIAA0930	KIAA0930	-0.84	1.56E-03
223773_s_at	SNHG12	small nucleolar RNA host gene 12 (non-protein coding)	-0.84	8.96E-04
211192_s_at	CD84	CD84 molecule	-0.84	1.56E-03
222613_at	C12orf4	chromosome 12 open reading frame 4	-0.85	1.89E-03
211190_x_at	CD84	CD84 molecule	-0.85	1.03E-03
228990_at	SNHG12	small nucleolar RNA host gene 12 (non-protein coding)	-0.85	2.07E-03
214830_at	SLC38A6	solute carrier family 38, member 6	-0.86	9.44E-04
219037_at	RRP15	ribosomal RNA processing 15 homolog (S. cerevisiae)	-0.86	1.54E-03
218893_at	ISOC2	isochorismatase domain containing 2	-0.87	8.96E-04
218140_x_at	SRPRB	signal recognition particle receptor, B subunit	-0.88	1.53E-03
200903_s_at	AHCY	adenosylhomocysteinase	-0.88	8.13E-04
219525_at	SLC47A1	solute carrier family 47, member 1	-0.88	2.19E-03
216640_s_at	PDIA6	protein disulfide isomerase family A, member 6	-0.89	1.61E-03
213302_at	PFAS	phosphoribosylformylglycinamidine synthase	-0.90	1.47E-03
204689_at	HHEX	hematopoietically expressed homeobox	-0.90	8.79E-04
211189_x_at	CD84	CD84 molecule	-0.91	8.72E-04
205237_at	FCN1	ficolin (collagen/fibrinogen domain containing) 1	-0.91	2.05E-03
217966_s_at	FAM129A	family with sequence similarity 129, member A	-0.91	1.65E-03
224950_at	PTGFRN	prostaglandin F2 receptor negative regulator	-0.91	1.71E-03
221523_s_at	RRAGD	Ras-related GTP binding D	-0.91	1.35E-03
242786_at	LOC283104	uncharacterized LOC283104	-0.92	1.02E-03
207655_s_at	BLNK	B-cell linker	-0.94	8.28E-04
225826_at	MMAB	methylmalonic aciduria (cobalamin deficiency) cblB type	-0.94	9.44E-04
200790_at	ODC1	ornithine decarboxylase 1	-0.95	1.02E-03
227374_at	EARS2	glutamyl-tRNA synthetase 2, mitochondrial (putative)	-0.95	1.45E-03
243252_at	NA	NA	-0.95	1.73E-03
201872_s_at	ABCE1	ATP-binding cassette, sub-family E (OABP), member 1	-0.96	1.45E-03
209608_s_at	ACAT2	acetyl-CoA acetyltransferase 2	-0.97	1.49E-03
225943_at	NLN	neurolysin (metallopeptidase M3 family)	-0.98	1.49E-03
223312_at	PRADC1	protease-associated domain containing 1	-1.00	9.75E-04
204059_s_at	ME1	malic enzyme 1, NADP(+)-dependent, cytosolic	-1.00	1.89E-03
226423_at	PAQR8	progestin and adipoQ receptor family member VIII	-1.00	4.28E-04
227756_at	FAM81A	family with sequence similarity 81, member A	-1.01	8.13E-04
226923_at	SCFD2	sec1 family domain containing 2	-1.01	4.57E-04
207216_at	TNFSF8	tumor necrosis factor (ligand) superfamily, member 8	-1.01	1.87E-03
244546_at	CYCS	cytochrome c, somatic	-1.02	1.11E-03
227626_at	PAQR8	progestin and adipoQ receptor family member VIII	-1.02	7.50E-04
203196_at	ABCC4	ATP-binding cassette, sub-family C (CFTR/MRP), member 4	-1.03	8.96E-04
222118_at	CENPN	centromere protein N	-1.04	1.56E-03
210145_at	PLA2G4A	phospholipase A2, group IVA (cytosolic, calcium-dependent)	-1.05	8.96E-04
234974_at	GALM	galactose mutarotase (aldose 1-epimerase)	-1.05	1.96E-03
1553906_s_at	FGD2	FYVE, RhoGEF and PH domain containing 2	-1.07	4.04E-04
202923_s_at	GCLC	glutamate-cysteine ligase, catalytic subunit	-1.08	6.74E-04
213129_s_at	NA	NA	-1.10	8.96E-04

226382_at	NA	NA	-1.11	1.54E-03
236834_at	SCFD2	sec1 family domain containing 2	-1.13	3.20E-04
200862_at	DHCR24	24-dehydrocholesterol reductase	-1.14	7.25E-04
209218_at	SQLE	squalene epoxidase	-1.14	1.30E-03
215933_s_at	HHEX	hematopoietically expressed homeobox	-1.16	6.26E-04
202922_at	GCLC	glutamate-cysteine ligase, catalytic subunit	-1.17	9.60E-04
218096_at	AGPAT5	1-acylglycerol-3-phosphate O-acyltransferase 5 (lysophosphatidic acid acyltransferase, epsilon)	-1.18	6.41E-04
241068_at	NA	NA	-1.22	9.55E-04
204959_at	MNDA	myeloid cell nuclear differentiation antigen	-1.24	9.74E-04
235122_at	HIVEP3	human immunodeficiency virus type I enhancer binding protein 3	-1.24	1.49E-03
213562_s_at	SQLE	squalene epoxidase	-1.27	8.96E-04
204547_at	RAB40B	RAB40B, member RAS oncogene family	-1.28	1.35E-03
1553639_a_at	PPARGC1B	peroxisome proliferator-activated receptor gamma, coactivator 1 beta	-1.29	1.78E-03
221019_s_at	COLEC12	collectin sub-family member 12	-1.29	8.96E-04
207213_s_at	USP2	ubiquitin specific peptidase 2	-1.31	1.82E-03
204039_at	CEBPA	CCAAT/enhancer binding protein (C/EBP), alpha	-1.31	8.28E-04
212279_at	TMEM97	transmembrane protein 97	-1.32	7.25E-04
235709_at	GAS2L3	growth arrest-specific 2 like 3	-1.34	1.51E-03
227559_at	NDUFAF4	NADH dehydrogenase (ubiquinone) 1 alpha subcomplex, assembly factor 4	-1.34	1.80E-03
212510_at	GPD1L	glycerol-3-phosphate dehydrogenase 1-like	-1.36	8.96E-04
231747_at	CYSLTR1	cysteinyl leukotriene receptor 1	-1.39	9.75E-04
222773_s_at	GALNT12	UDP-N-acetyl-alpha-D-galactosamine:polypeptide N-acetylgalactosaminyltransferase 12 (GalNAc-T12)	-1.40	1.75E-03
218885_s_at	GALNT12	UDP-N-acetyl-alpha-D-galactosamine:polypeptide N-acetylgalactosaminyltransferase 12 (GalNAc-T12)	-1.41	1.86E-03
230866_at	CYSLTR1	cysteinyl leukotriene receptor 1	-1.47	3.12E-04
201310_s_at	NREP	neuronal regeneration related protein homolog (rat)	-1.50	9.61E-04
235780_at	PRKACB	protein kinase, cAMP-dependent, catalytic, beta	-1.51	1.28E-03
221022_s_at	PMFBP1	polyamine modulated factor 1 binding protein 1	-1.55	1.80E-03
219697_at	HS3ST2	heparan sulfate (glucosamine) 3-O-sulfotransferase 2	-1.60	1.49E-03
206170_at	ADRB2	adrenergic, beta-2-, receptor, surface	-1.64	4.04E-04
212281_s_at	TMEM97	transmembrane protein 97	-1.65	9.75E-04
212282_at	TMEM97	transmembrane protein 97	-1.68	3.12E-04
235735_at	TNFSF8	tumor necrosis factor (ligand) superfamily, member 8	-1.92	1.54E-03
238756_at	GAS2L3	growth arrest-specific 2 like 3	-1.96	1.51E-03
219142_at	RASL11B	RAS-like, family 11, member B	-2.08	8.31E-04
228281_at	C11orf82	chromosome 11 open reading frame 82	-2.26	1.27E-03
228376_at	GGTA1P	glycoprotein, alpha-galactosyltransferase 1 pseudogene	-2.35	3.61E-04
220005_at	P2RY13	purinergic receptor P2Y, G-protein coupled, 13	-2.70	1.10E-03
230550_at	MS4A6A	membrane-spanning 4-domains, subfamily A, member 6A	-2.73	1.47E-03

7.2 Appendix B: Differentially expressed probe sets of MSCs$^{con\text{-}med}$

Table 37: Differentially expressed probe sets during microarray of MSCs$^{con\text{-}med}$ (array group B)
Listed are all 180 differentially expressed probe sets between MSCs subjected to conditioned medium of EPCs and their corresponding control assays (n = 4). Probe sets are ordered according to their descending statistical score (logFC) from highest up-regulation to highest down-regulation. Additional information reflects the probe set ID, their corresponding gene symbol and name as well as the adjusted (corrected for multiple comparisons) p-value (adj.P.Val).

ID	Symbol	GeneName	logFC	adj.P.Val
210538_s_at	BIRC3	baculoviral IAP repeat containing 3	1.85	4.39E-03
1554997_a_at	PTGS2	prostaglandin-endoperoxide synthase 2 (prostaglandin G/H synthase and cyclooxygenase)	1.48	7.02E-03
204748_at	PTGS2	prostaglandin-endoperoxide synthase 2 (prostaglandin G/H synthase and cyclooxygenase)	1.36	7.02E-03
206100_at	CPM	carboxypeptidase M	1.34	1.07E-02
204595_s_at	STC1	stanniocalcin 1	1.32	4.64E-03
204597_x_at	STC1	stanniocalcin 1	1.30	6.51E-03
230746_s_at	NA	NA	1.30	7.02E-03
221477_s_at	SOD2	superoxide dismutase 2, mitochondrial	1.25	7.02E-03
205207_at	IL6	interleukin 6 (interferon, beta 2)	1.21	1.13E-02
204224_s_at	GCH1	GTP cyclohydrolase 1	1.20	6.51E-03
242907_at	NA	NA	1.19	4.64E-03
240450_at	NA	NA	1.19	8.64E-03
219888_at	SPAG4	sperm associated antigen 4	1.13	6.51E-03
222150_s_at	PION	pigeon homolog (Drosophila)	1.09	7.02E-03
1554919_s_at	C7orf63	chromosome 7 open reading frame 63	1.07	8.98E-03
209583_s_at	CD200	CD200 molecule	1.05	7.02E-03
209582_s_at	CD200	CD200 molecule	1.03	7.02E-03
202902_s_at	CTSS	cathepsin S	0.98	1.30E-02
202748_at	GBP2	guanylate binding protein 2, interferon-inducible	0.97	1.07E-02
213142_x_at	PION	pigeon homolog (Drosophila)	0.97	1.08E-02
235706_at	CPM	carboxypeptidase M	0.95	1.64E-02
1553141_at	LACC1	laccase (multicopper oxidoreductase) domain containing 1	0.94	1.30E-02
215078_at	SOD2	superoxide dismutase 2, mitochondrial	0.93	1.67E-02
220244_at	LINC00312	long intergenic non-protein coding RNA 312	0.93	9.14E-03
204596_s_at	STC1	stanniocalcin 1	0.92	1.64E-02
219455_at	C7orf63	chromosome 7 open reading frame 63	0.91	1.16E-02
212946_at	KIAA0564	KIAA0564	0.90	1.64E-02
227223_at	NA	NA	0.89	1.00E-02
213256_at	MARCH3	membrane-associated ring finger (C3HC4) 3, E3 ubiquitin protein ligase	0.89	1.89E-02
234989_at	NEAT1	nuclear paraspeckle assembly transcript 1 (non-protein coding)	0.88	1.30E-02
202901_x_at	CTSS	cathepsin S	0.87	1.54E-02
223217_s_at	NFKBIZ	nuclear factor of kappa light polypeptide gene enhancer in B-cells inhibitor, zeta	0.86	1.30E-02
240038_at	NA	NA	0.86	1.54E-02
202687_s_at	TNFSF10	tumor necrosis factor (ligand) superfamily, member 10	0.86	2.14E-02
1558714_at	NA	NA	0.86	8.64E-03
227677_at	JAK3	Janus kinase 3	0.85	1.07E-02
230318_at	SERPINA1	serpin peptidase inhibitor, clade A (alpha-1 antiproteinase, antitrypsin), member 1	0.83	1.86E-02
213817_at	IRAK3	interleukin-1 receptor-associated kinase 3	0.83	1.07E-02
215253_s_at	RCAN1	regulator of calcineurin 1	0.82	1.83E-02
232935_at	NA	NA	0.82	1.64E-02
223940_x_at	MALAT1	metastasis associated lung adenocarcinoma transcript 1 (non-protein coding)	0.80	1.54E-02
209863_s_at	TP63	tumor protein p63	0.80	2.23E-02

205027_s_at	MAP3K8	mitogen-activated protein kinase kinase kinase 8	0.80	2.20E-02
223218_s_at	NFKBIZ	nuclear factor of kappa light polypeptide gene enhancer in B-cells inhibitor, zeta	0.78	1.64E-02
233607_at	NA	NA	0.77	1.30E-02
213247_at	SVEP1	sushi, von Willebrand factor type A, EGF and pentraxin domain containing 1	0.76	1.89E-02
235592_at	NA	NA	0.75	2.23E-02
205782_at	FGF7	fibroblast growth factor 7	0.75	2.40E-02
228325_at	KIAA0146	KIAA0146	0.74	2.33E-02
244774_at	PHACTR2	phosphatase and actin regulator 2	0.74	2.14E-02
209546_s_at	APOL1	apolipoprotein L, 1	0.74	2.40E-02
223578_x_at	MALAT1	metastasis associated lung adenocarcinoma transcript 1 (non-protein coding)	0.74	2.33E-02
1556462_a_at	NA	NA	0.73	2.33E-02
208370_s_at	RCAN1	regulator of calcineurin 1	0.73	2.23E-02
210367_s_at	PTGES	prostaglandin E synthase	0.72	2.50E-02
200878_at	EPAS1	endothelial PAS domain protein 1	0.72	2.29E-02
211527_x_at	VEGFA	vascular endothelial growth factor A	0.72	2.33E-02
219558_at	ATP13A3	ATPase type 13A3	0.71	2.33E-02
226561_at	AGFG1	ArfGAP with FG repeats 1	0.71	2.33E-02
1556364_at	ADAMTS9-AS2	ADAMTS9 antisense RNA 2 (non-protein coding)	0.71	1.74E-02
228771_at	ADRBK2	adrenergic, beta, receptor kinase 2	0.71	2.33E-02
232472_at	NA	NA	0.71	2.50E-02
232453_at	NA	NA	0.71	2.29E-02
214657_s_at	NEAT1	nuclear paraspeckle assembly transcript 1 (non-protein coding)	0.70	2.50E-02
225239_at	NA	NA	0.70	2.51E-02
214329_x_at	TNFSF10	tumor necrosis factor (ligand) superfamily, member 10	0.70	2.14E-02
211596_s_at	LRIG1	leucine-rich repeats and immunoglobulin-like domains 1	0.70	2.14E-02
227250_at	KREMEN1	kringle containing transmembrane protein 1	0.69	2.50E-02
221978_at	HLA-F	major histocompatibility complex, class I, F	0.69	2.50E-02
204881_s_at	UGCG	UDP-glucose ceramide glucosyltransferase	0.68	2.33E-02
213926_s_at	AGFG1	ArfGAP with FG repeats 1	0.67	2.50E-02
226756_at	CCDC71L	coiled-coil domain containing 71-like	0.67	2.65E-02
202022_at	ALDOC	aldolase C, fructose-bisphosphate	0.67	2.33E-02
213006_at	CEBPD	CCAAT/enhancer binding protein (C/EBP), delta	0.66	2.50E-02
233090_at	NA	NA	0.65	2.40E-02
230085_at	PDK3	pyruvate dehydrogenase kinase, isozyme 3	0.65	2.50E-02
204070_at	RARRES3	retinoic acid receptor responder (tazarotene induced) 3	0.65	2.92E-02
215206_at	NA	NA	0.65	2.51E-02
241925_x_at	NA	NA	0.64	2.50E-02
205205_at	RELB	v-rel reticuloendotheliosis viral oncogene homolog B	0.64	2.29E-02
236599_at	NA	NA	0.64	2.78E-02
204105_s_at	NRCAM	neuronal cell adhesion molecule	0.64	2.51E-02
232458_at	COL3A1	collagen, type III, alpha 1	0.64	2.50E-02
222846_at	RAB8B	RAB8B, member RAS oncogene family	0.64	2.50E-02
211828_s_at	TNIK	TRAF2 and NCK interacting kinase	0.64	2.64E-02
224568_x_at	MALAT1	metastasis associated lung adenocarcinoma transcript 1 (non-protein coding)	0.63	2.33E-02
213194_at	ROBO1	roundabout, axon guidance receptor, homolog 1 (Drosophila)	0.63	2.65E-02
202531_at	IRF1	interferon regulatory factor 1	0.62	2.51E-02
244625_at	NA	NA	0.62	2.40E-02
1564378_a_at	NA	NA	0.61	3.15E-02
221087_s_at	APOL3	apolipoprotein L, 3	0.61	3.09E-02
238725_at	IRF1	interferon regulatory factor 1	0.61	2.50E-02
220866_at	ADAMTS6	ADAM metallopeptidase with thrombospondin type 1 motif, 6	0.61	2.64E-02
1559067_a_at	NA	NA	0.61	2.50E-02
219410_at	TMEM45A	transmembrane protein 45A	0.60	2.77E-02
226325_at	ADSSL1	adenylosuccinate synthase like 1	0.60	3.28E-02
205729_at	OSMR	oncostatin M receptor	0.60	3.28E-02
203293_s_at	LMAN1	lectin, mannose-binding, 1	0.60	3.28E-02

230003_at	NA	NA	0.59	3.21E-02
210852_s_at	AASS	aminoadipate-semialdehyde synthase	0.59	2.92E-02
206701_x_at	EDNRB	endothelin receptor type B	0.59	2.78E-02
244026_at	NA	NA	0.59	3.15E-02
236610_at	NA	NA	0.59	2.76E-02
218717_s_at	LEPREL1	leprecan-like 1	0.58	3.28E-02
219622_at	RAB20	RAB20, member RAS oncogene family	0.58	3.25E-02
227742_at	CLIC6	chloride intracellular channel 6	0.58	3.21E-02
230821_at	ZNF148	zinc finger protein 148	0.58	2.64E-02
229302_at	TMEM178	transmembrane protein 178	0.57	3.42E-02
218983_at	C1RL	complement component 1, r subcomponent-like	0.57	3.28E-02
214012_at	ERAP1	endoplasmic reticulum aminopeptidase 1	0.57	3.31E-02
223423_at	GPR160	G protein-coupled receptor 160	0.57	3.29E-02
222088_s_at	NA	NA	0.57	3.28E-02
1559296_at	ADAMTS9-AS2	ADAMTS9 antisense RNA 2 (non-protein coding)	0.57	3.28E-02
221765_at	UGCG	UDP-glucose ceramide glucosyltransferase	0.57	3.28E-02
221957_at	PDK3	pyruvate dehydrogenase kinase, isozyme 3	0.57	3.27E-02
1559391_s_at	NA	NA	0.56	3.27E-02
209318_x_at	PLAGL1	pleiomorphic adenoma gene-like 1	0.56	3.28E-02
204508_s_at	CA12	carbonic anhydrase XII	0.56	3.48E-02
236808_at	FGFR1OP2	FGFR1 oncogene partner 2	0.56	3.28E-02
200737_at	PGK1	phosphoglycerate kinase 1	0.56	3.28E-02
226663_at	ANKRD10	ankyrin repeat domain 10	0.56	3.28E-02
219213_at	JAM2	junctional adhesion molecule 2	0.56	3.28E-02
218810_at	ZC3H12A	zinc finger CCCH-type containing 12A	0.56	3.42E-02
222592_s_at	ACSL5	acyl-CoA synthetase long-chain family member 5	0.56	3.50E-02
203758_at	CTSO	cathepsin O	0.55	3.55E-02
233648_at	NA	NA	0.55	3.21E-02
227510_x_at	MALAT1	metastasis associated lung adenocarcinoma transcript 1 (non-protein coding)	0.55	3.15E-02
203542_s_at	KLF9	Kruppel-like factor 9	0.55	3.48E-02
227361_at	HS3ST3B1	heparan sulfate (glucosamine) 3-O-sulfotransferase 3B1	0.55	3.30E-02
203963_at	CA12	carbonic anhydrase XII	0.54	3.55E-02
207002_s_at	PLAGL1	pleiomorphic adenoma gene-like 1	0.54	3.37E-02
221569_at	AHI1	Abelson helper integration site 1	0.54	3.43E-02
231980_at	DOK6	docking protein 6	0.54	3.64E-02
228439_at	BATF2	basic leucine zipper transcription factor, ATF-like 2	0.53	3.55E-02
226982_at	ELL2	elongation factor, RNA polymerase II, 2	0.53	3.28E-02
242853_at	NA	NA	0.53	3.28E-02
215505_s_at	STRN3	striatin, calmodulin binding protein 3	0.53	3.28E-02
227260_at	NA	NA	0.53	3.64E-02
238987_at	B4GALT1	UDP-Gal:betaGlcNAc beta 1,4- galactosyltransferase, polypeptide 1	0.53	3.64E-02
220580_at	BICC1	bicaudal C homolog 1 (Drosophila)	0.52	3.61E-02
213295_at	CYLD	cylindromatosis (turban tumor syndrome)	0.52	3.50E-02
206673_at	GPR176	G protein-coupled receptor 176	0.52	3.75E-02
209959_at	NR4A3	nuclear receptor subfamily 4, group A, member 3	0.52	3.85E-02
235751_s_at	VMO1	vitelline membrane outer layer 1 homolog (chicken)	0.52	4.01E-02
230025_at	GJD3	gap junction protein, delta 3, 31.9kDa	0.51	4.03E-02
227846_at	GPR176	G protein-coupled receptor 176	0.51	4.04E-02
239274_at	NA	NA	0.51	3.48E-02
226621_at	NA	NA	0.51	3.93E-02
228937_at	LACC1	laccase (multicopper oxidoreductase) domain containing 1	0.51	3.68E-02
232002_at	NA	NA	0.51	3.61E-02
239049_at	NA	NA	0.51	3.48E-02
217356_s_at	PGK1	phosphoglycerate kinase 1	0.51	3.80E-02
204646_at	DPYD	dihydropyrimidine dehydrogenase	0.51	3.61E-02
223454_at	CXCL16	chemokine (C-X-C motif) ligand 16	0.50	3.48E-02
236917_at	LRRC34	leucine rich repeat containing 34	-0.50	3.64E-02
222305_at	HK2	hexokinase 2	-0.50	3.82E-02
1553982_a_at	RAB7B	RAB7B, member RAS oncogene family	-0.51	3.30E-02
208396_s_at	PDE1A	phosphodiesterase 1A, calmodulin-dependent	-0.51	3.64E-02
217979_at	TSPAN13	tetraspanin 13	-0.51	3.61E-02

205379_at	CBR3	carbonyl reductase 3	-0.51	3.61E-02
216247_at	NA	NA	-0.52	3.61E-02
222075_s_at	OAZ3	ornithine decarboxylase antizyme 3	-0.52	3.61E-02
220698_at	MGC4294	uncharacterized MGC4294	-0.53	3.48E-02
202586_at	POLR2L	polymerase (RNA) II (DNA directed) polypeptide L, 7.6kDa	-0.54	3.61E-02
219308_s_at	AK5	adenylate kinase 5	-0.57	3.28E-02
205698_s_at	MAP2K6	mitogen-activated protein kinase kinase 6	-0.58	3.28E-02
202345_s_at	FABP5	fatty acid binding protein 5 (psoriasis-associated)	-0.59	2.64E-02
1554830_a_at	STEAP3	STEAP family member 3, metalloreductase	-0.59	2.92E-02
223274_at	TCF19	transcription factor 19	-0.60	2.50E-02
207147_at	DLX2	distal-less homeobox 2	-0.61	2.40E-02
235273_at	DYX1C1	dyslexia susceptibility 1 candidate 1	-0.63	2.45E-02
222862_s_at	AK5	adenylate kinase 5	-0.64	2.51E-02
239410_at	NA	NA	-0.67	2.40E-02
204796_at	EML1	echinoderm microtubule associated protein like 1	-0.67	2.23E-02
223749_at	C1QTNF2	C1q and tumor necrosis factor related protein 2	-0.68	2.50E-02
203819_s_at	NA	NA	-0.76	1.64E-02
204529_s_at	TOX	thymocyte selection-associated high mobility group box	-0.91	1.64E-02
227226_at	MRAP2	melanocortin 2 receptor accessory protein 2	-0.97	1.54E-02
203820_s_at	IGF2BP3	insulin-like growth factor 2 mRNA binding protein 3	-0.98	7.02E-03
205381_at	LRRC17	leucine rich repeat containing 17	-1.22	4.64E-03

7.3 Appendix C: Differentially expressed probe sets of EPCs$^{co\text{-}cu}$

Table 38: Differentially expressed probe sets during microarray of EPCs$^{co\text{-}cu}$ (array group C)
Listed are all 923 differentially expressed probe sets between co-cultured EPCs and their corresponding control assays (n = 4). Probe sets are ordered according to their descending statistical score (logFc) from highest up-regulation to highest down-regulation. Additional information reflects the probe set ID, their corresponding gene symbol and name as well as the adjusted (corrected for multiple comparisons) p-value (adj.P.Val).

ID	Symbol	GeneName	logFC	adj.P.Val
1556499_s_at	COL1A1	collagen, type I, alpha 1	8.32	8.17E-08
202404_s_at	COL1A2	collagen, type I, alpha 2	7.84	8.09E-08
201667_at	GJA1	gap junction protein, alpha 1, 43kDa	7.38	8.94E-08
215076_s_at	COL3A1	collagen, type III, alpha 1	7.14	9.21E-08
201744_s_at	LUM	lumican	7.11	8.94E-08
210809_s_at	POSTN	periostin, osteoblast specific factor	6.87	8.17E-08
212077_at	CALD1	caldesmon 1	6.67	1.18E-07
201852_x_at	COL3A1	collagen, type III, alpha 1	6.43	2.53E-07
209101_at	CTGF	connective tissue growth factor	6.29	8.23E-08
202403_s_at	COL1A2	collagen, type I, alpha 2	6.27	1.92E-07
210095_s_at	IGFBP3	insulin-like growth factor binding protein 3	6.14	4.39E-07
202620_s_at	PLOD2	procollagen-lysine, 2-oxoglutarate 5-dioxygenase 2	6.14	9.21E-08
209278_s_at	TFPI2	tissue factor pathway inhibitor 2	6.11	9.21E-08
223395_at	ABI3BP	ABI family, member 3 (NESH) binding protein	6.10	8.94E-08
211161_s_at	COL3A1	collagen, type III, alpha 1	5.99	2.46E-07
225275_at	EDIL3	EGF-like repeats and discoidin I-like domains 3	5.92	1.50E-06
215446_s_at	LOX	lysyl oxidase	5.83	1.43E-07
212353_at	SULF1	sulfatase 1	5.60	4.39E-07
212097_at	CAV1	caveolin 1, caveolae protein, 22kDa	5.59	2.71E-06
208782_at	FSTL1	follistatin-like 1	5.40	2.53E-07
207173_x_at	CDH11	cadherin 11, type 2, OB-cadherin (osteoblast)	5.38	1.39E-06
201438_at	COL6A3	collagen, type VI, alpha 3	5.32	1.32E-05
202310_s_at	COL1A1	collagen, type I, alpha 1	5.19	2.53E-06
225681_at	CTHRC1	collagen triple helix repeat containing 1	5.14	4.90E-06
221729_at	COL5A2	collagen, type V, alpha 2	5.10	1.09E-06
203939_at	NT5E	5'-nucleotidase, ecto (CD73)	5.07	1.50E-06
212190_at	SERPINE2	serpin peptidase inhibitor, clade E (nexin, plasminogen activator inhibitor type 1), member 2	5.06	9.13E-06
201842_s_at	EFEMP1	EGF containing fibulin-like extracellular matrix protein 1	4.90	1.29E-05
1555778_a_at	POSTN	periostin, osteoblast specific factor	4.81	3.79E-07
201109_s_at	THBS1	thrombospondin 1	4.80	2.49E-03
201110_s_at	THBS1	thrombospondin 1	4.79	2.24E-03
201289_at	CYR61	cysteine-rich, angiogenic inducer, 61	4.78	1.77E-06
202619_s_at	PLOD2	procollagen-lysine, 2-oxoglutarate 5-dioxygenase 2	4.78	1.92E-06
206432_at	HAS2	hyaluronan synthase 2	4.63	5.92E-06
236220_at	NA	NA	4.63	4.59E-04
219915_s_at	SLC16A10	solute carrier family 16, member 10 (aromatic amino acid transporter)	4.55	8.75E-04
201215_at	PLS3	plastin 3	4.52	1.37E-05
202766_s_at	FBN1	fibrillin 1	4.50	3.79E-06
202311_s_at	COL1A1	collagen, type I, alpha 1	4.50	1.16E-05
226834_at	NA	NA	4.49	5.17E-06
222162_s_at	ADAMTS1	ADAM metallopeptidase with thrombospondin type 1 motif, 1	4.48	2.67E-05
212143_s_at	IGFBP3	insulin-like growth factor binding protein 3	4.42	9.41E-06
226237_at	COL8A1	collagen, type VIII, alpha 1	4.37	6.61E-05
215646_s_at	VCAN	versican	4.31	6.93E-05
201893_x_at	DCN	decorin	4.19	2.06E-05
211896_s_at	DCN	decorin	4.18	1.32E-05
202237_at	NNMT	nicotinamide N-methyltransferase	4.15	2.59E-05
221730_at	COL5A2	collagen, type V, alpha 2	4.15	1.68E-05

202133_at	WWTR1	WW domain containing transcription regulator 1	4.10	6.93E-05
204475_at	MMP1	matrix metallopeptidase 1 (interstitial collagenase)	4.10	2.73E-05
225664_at	COL12A1	collagen, type XII, alpha 1	4.06	6.93E-05
222939_s_at	SLC16A10	solute carrier family 16, member 10 (aromatic amino acid transporter)	4.06	7.05E-04
209277_at	TFPI2	tissue factor pathway inhibitor 2	4.05	2.53E-06
202949_s_at	FHL2	four and a half LIM domains 2	3.97	5.15E-05
209094_at	DDAH1	dimethylarginine dimethylaminohydrolase 1	3.94	1.46E-05
225242_s_at	CCDC80	coiled-coil domain containing 80	3.91	2.82E-05
201445_at	CNN3	calponin 3, acidic	3.90	3.78E-05
204620_s_at	VCAN	versican	3.90	6.61E-05
205990_s_at	WNT5A	wingless-type MMTV integration site family, member 5A	3.88	4.97E-04
204619_s_at	VCAN	versican	3.87	9.52E-05
225481_at	FRMD6	FERM domain containing 6	3.87	2.80E-05
221731_x_at	VCAN	versican	3.84	8.24E-05
203083_at	THBS2	thrombospondin 2	3.84	9.52E-05
201617_x_at	CALD1	caldesmon 1	3.82	1.46E-05
224894_at	YAP1	Yes-associated protein 1	3.78	6.61E-05
204298_s_at	LOX	lysyl oxidase	3.77	1.91E-05
226695_at	PRRX1	paired related homeobox 1	3.77	4.10E-05
212354_at	SULF1	sulfatase 1	3.75	5.15E-05
201108_s_at	THBS1	thrombospondin 1	3.75	5.45E-03
203570_at	LOXL1	lysyl oxidase-like 1	3.74	1.82E-04
230372_at	HAS2	hyaluronan synthase 2	3.73	2.67E-05
235086_at	THBS1	thrombospondin 1	3.73	1.07E-02
209210_s_at	FERMT2	fermitin family member 2	3.73	2.59E-05
215101_s_at	CXCL5	chemokine (C-X-C motif) ligand 5	3.70	4.30E-03
203963_at	CA12	carbonic anhydrase XII	3.67	3.91E-03
203065_s_at	CAV1	caveolin 1, caveolae protein, 22kDa	3.62	9.52E-05
211571_s_at	VCAN	versican	3.61	1.14E-04
203131_at	PDGFRA	platelet-derived growth factor receptor, alpha polypeptide	3.61	1.11E-04
209386_at	TM4SF1	transmembrane 4 L six family member 1	3.60	5.92E-06
215034_s_at	TM4SF1	transmembrane 4 L six family member 1	3.59	6.85E-06
227628_at	GPX8	glutathione peroxidase 8 (putative)	3.56	4.81E-05
201505_at	LAMB1	laminin, beta 1	3.53	3.78E-05
205542_at	STEAP1	six transmembrane epithelial antigen of the prostate 1	3.53	7.30E-05
205828_at	MMP3	matrix metallopeptidase 3 (stromelysin 1, progelatinase)	3.53	2.46E-03
201645_at	TNC	tenascin C	3.50	7.05E-04
211813_x_at	DCN	decorin	3.49	1.30E-04
212977_at	CXCR7	chemokine (C-X-C motif) receptor 7	3.49	6.12E-03
209946_at	VEGFC	vascular endothelial growth factor C	3.48	1.46E-05
226847_at	FST	follistatin	3.48	1.56E-04
214146_s_at	PPBP	pro-platelet basic protein (chemokine (C-X-C motif) ligand 7)	3.44	1.24E-02
203510_at	MET	met proto-oncogene (hepatocyte growth factor receptor)	3.43	5.99E-04
213139_at	SNAI2	snail homolog 2 (Drosophila)	3.42	4.54E-04
202458_at	PRSS23	protease, serine, 23	3.42	5.15E-05
224955_at	TEAD1	TEA domain family member 1 (SV40 transcriptional enhancer factor)	3.41	6.61E-05
204017_at	KDELR3	KDEL (Lys-Asp-Glu-Leu) endoplasmic reticulum protein retention receptor 3	3.40	1.93E-04
209656_s_at	TMEM47	transmembrane protein 47	3.34	9.66E-05
214164_x_at	CA12	carbonic anhydrase XII	3.34	6.15E-03
217820_s_at	ENAH	enabled homolog (Drosophila)	3.33	1.80E-04
202765_s_at	FBN1	fibrillin 1	3.30	1.08E-04
213425_at	WNT5A	wingless-type MMTV integration site family, member 5A	3.29	3.24E-04
202363_at	SPOCK1	sparc/osteonectin, cwcv and kazal-like domains proteoglycan (testican) 1	3.27	9.33E-05
225464_at	FRMD6	FERM domain containing 6	3.26	9.52E-05
209387_s_at	TM4SF1	transmembrane 4 L six family member 1	3.23	1.61E-05
206336_at	CXCL6	chemokine (C-X-C motif) ligand 6 (granulocyte chemotactic protein 2)	3.22	1.26E-02
215867_x_at	CA12	carbonic anhydrase XII	3.20	6.75E-03
226621_at	NA	NA	3.20	9.56E-05
203002_at	AMOTL2	angiomotin like 2	3.17	9.62E-05

213943_at	TWIST1	twist homolog 1 (Drosophila)	3.17	7.20E-04
205767_at	EREG	epiregulin	3.16	3.86E-03
225782_at	MSRB3	methionine sulfoxide reductase B3	3.14	2.35E-04
210724_at	EMR3	egf-like module containing, mucin-like, hormone receptor-like 3	3.13	3.57E-03
211980_at	COL4A1	collagen, type IV, alpha 1	3.09	2.82E-05
211651_s_at	LAMB1	laminin, beta 1	3.08	9.36E-05
228297_at	CNN3	calponin 3, acidic	3.07	2.06E-04
203324_s_at	CAV2	caveolin 2	3.07	1.08E-04
202011_at	TJP1	tight junction protein 1 (zona occludens 1)	2.99	8.84E-04
228708_at	RAB27B	RAB27B, member RAS oncogene family	2.99	1.18E-03
226189_at	ITGB8	integrin, beta 8	2.98	1.38E-02
226279_at	PRSS23	protease, serine, 23	2.97	3.46E-04
217507_at	SLC11A1	solute carrier family 11 (proton-coupled divalent metal ion transporters), member 1	2.97	4.55E-04
226777_at	ADAM12	ADAM metallopeptidase domain 12	2.96	1.18E-03
202238_s_at	NNMT	nicotinamide N-methyltransferase	2.96	2.37E-04
210764_s_at	CYR61	cysteine-rich, angiogenic inducer, 61	2.96	1.62E-04
204115_at	GNG11	guanine nucleotide binding protein (G protein), gamma 11	2.96	2.85E-04
204457_s_at	GAS1	growth arrest-specific 1	2.95	4.05E-03
201616_s_at	CALD1	caldesmon 1	2.94	6.34E-04
205422_s_at	ITGBL1	integrin, beta-like 1 (with EGF-like repeat domains)	2.94	1.89E-04
205978_at	KL	klotho	2.94	6.42E-03
201579_at	FAT1	FAT tumor suppressor homolog 1 (Drosophila)	2.93	6.94E-04
226282_at	PTPN14	protein tyrosine phosphatase, non-receptor type 14	2.92	7.83E-04
203325_s_at	COL5A1	collagen, type V, alpha 1	2.91	2.37E-04
214974_x_at	CXCL5	chemokine (C-X-C motif) ligand 5	2.89	4.30E-03
218468_s_at	GREM1	gremlin 1	2.88	4.88E-04
214022_s_at	IFITM1	interferon induced transmembrane protein 1 (9-27)	2.86	5.71E-03
228407_at	SCUBE3	signal peptide, CUB domain, EGF-like 3	2.86	2.46E-03
212942_s_at	KIAA1199	KIAA1199	2.84	4.05E-04
205695_at	SDS	serine dehydratase	2.82	7.72E-03
229357_at	ADAMTS5	ADAM metallopeptidase with thrombospondin type 1 motif, 5	2.81	4.15E-03
225381_at	MIR100HG	mir-100-let-7a-2 cluster host gene (non-protein coding)	2.81	4.55E-04
228128_x_at	PAPPA	pregnancy-associated plasma protein A, pappalysin 1	2.81	5.01E-04
209335_at	DCN	decorin	2.77	2.16E-03
202202_s_at	LAMA4	laminin, alpha 4	2.77	9.86E-04
203650_at	PROCR	protein C receptor, endothelial	2.76	5.59E-03
203887_s_at	THBD	thrombomodulin	2.75	8.89E-04
224823_at	MYLK	myosin light chain kinase	2.75	8.70E-04
201185_at	HTRA1	HtrA serine peptidase 1	2.74	5.17E-03
203038_at	PTPRK	protein tyrosine phosphatase, receptor type, K	2.72	6.32E-04
213429_at	BICC1	bicaudal C homolog 1 (Drosophila)	2.69	1.39E-03
203888_at	THBD	thrombomodulin	2.69	5.44E-04
204422_s_at	FGF2	fibroblast growth factor 2 (basic)	2.66	2.98E-04
225491_at	SLC1A2	solute carrier family 1 (glial high affinity glutamate transporter), member 2	2.65	2.69E-02
214039_s_at	LAPTM4B	lysosomal protein transmembrane 4 beta	2.65	1.81E-02
212344_at	SULF1	sulfatase 1	2.61	4.93E-04
1555116_s_at	SLC11A1	solute carrier family 11 (proton-coupled divalent metal ion transporters), member 1	2.61	2.32E-03
212509_s_at	MXRA7	matrix-remodelling associated 7	2.60	4.56E-04
236565_s_at	LARP6	La ribonucleoprotein domain family, member 6	2.60	4.43E-04
224940_s_at	PAPPA	pregnancy-associated plasma protein A, pappalysin 1	2.59	1.35E-03
205100_at	GFPT2	glutamine-fructose-6-phosphate transaminase 2	2.58	5.59E-04
211964_at	COL4A2	collagen, type IV, alpha 2	2.58	6.69E-04
227623_at	CACNA2D1	calcium channel, voltage-dependent, alpha 2/delta subunit 1	2.57	6.87E-04
213423_x_at	TUSC3	tumor suppressor candidate 3	2.56	4.97E-04
206111_at	RNASE2	ribonuclease, RNase A family, 2 (liver, eosinophil-derived neurotoxin)	2.53	1.88E-03
214247_s_at	DKK3	dickkopf 3 homolog (Xenopus laevis)	2.53	1.97E-03
224895_at	YAP1	Yes-associated protein 1	2.52	4.09E-04
225688_s_at	PHLDB2	pleckstrin homology-like domain, family B, member 2	2.51	7.05E-04

203180_at	ALDH1A3	aldehyde dehydrogenase 1 family, member A3	2.51	1.21E-03
203440_at	CDH2	cadherin 2, type 1, N-cadherin (neuronal)	2.50	8.41E-04
213790_at	ADAM12	ADAM metallopeptidase domain 12	2.50	2.84E-03
208075_s_at	CCL7	chemokine (C-C motif) ligand 7	2.49	2.48E-02
226311_at	ADAMTS2	ADAM metallopeptidase with thrombospondin type 1 motif, 2	2.49	8.41E-04
221541_at	CRISPLD2	cysteine-rich secretory protein LCCL domain containing 2	2.48	4.20E-03
227061_at	LOC100506621	uncharacterized LOC100506621	2.48	8.87E-03
234994_at	TMEM200A	transmembrane protein 200A	2.47	9.86E-04
212110_at	SLC39A14	solute carrier family 39 (zinc transporter), member 14	2.46	2.09E-03
222433_at	ENAH	enabled homolog (Drosophila)	2.46	2.24E-03
210004_at	OLR1	oxidized low density lipoprotein (lectin-like) receptor 1	2.46	4.30E-03
235751_s_at	VMO1	vitelline membrane outer layer 1 homolog (chicken)	2.45	6.30E-03
218469_at	GREM1	gremlin 1	2.45	1.10E-03
229638_at	IRX3	iroquois homeobox 3	2.44	2.24E-03
212724_at	RND3	Rho family GTPase 3	2.43	4.02E-03
212294_at	GNG12	guanine nucleotide binding protein (G protein), gamma 12	2.42	2.07E-03
209651_at	TGFB1I1	transforming growth factor beta 1 induced transcript 1	2.42	2.29E-03
212488_at	COL5A1	collagen, type V, alpha 1	2.41	1.73E-03
210986_s_at	TPM1	tropomyosin 1 (alpha)	2.40	7.27E-04
207738_s_at	NCKAP1	NCK-associated protein 1	2.39	1.61E-03
222486_s_at	ADAMTS1	ADAM metallopeptidase with thrombospondin type 1 motif, 1	2.39	1.04E-03
203323_at	CAV2	caveolin 2	2.39	2.07E-03
230170_at	OSM	oncostatin M	2.38	1.55E-03
227099_s_at	C11orf96	chromosome 11 open reading frame 96	2.38	7.13E-03
223315_at	NTN4	netrin 4	2.38	3.38E-03
217890_s_at	PARVA	parvin, alpha	2.37	6.32E-04
225105_at	C12orf75	chromosome 12 open reading frame 75	2.36	1.58E-02
210002_at	GATA6	GATA binding protein 6	2.35	4.09E-04
204992_s_at	PFN2	profilin 2	2.35	1.21E-03
202627_s_at	SERPINE1	serpin peptidase inhibitor, clade E (nexin, plasminogen activator inhibitor type 1), member 1	2.35	5.02E-03
219935_at	ADAMTS5	ADAM metallopeptidase with thrombospondin type 1 motif, 5	2.34	1.27E-02
227399_at	VGLL3	vestigial like 3 (Drosophila)	2.34	1.20E-03
203868_s_at	VCAM1	vascular cell adhesion molecule 1	2.34	1.48E-02
204508_s_at	CA12	carbonic anhydrase XII	2.34	1.92E-02
205896_at	SLC22A4	solute carrier family 22 (organic cation/ergothioneine transporter), member 4	2.34	2.11E-03
204083_s_at	TPM2	tropomyosin 2 (beta)	2.33	1.13E-03
201843_s_at	EFEMP1	EGF containing fibulin-like extracellular matrix protein 1	2.33	2.46E-03
209687_at	CXCL12	chemokine (C-X-C motif) ligand 12	2.32	7.72E-03
204614_at	SERPINB2	serpin peptidase inhibitor, clade B (ovalbumin), member 2	2.32	3.91E-02
213905_x_at	BGN	biglycan	2.31	1.08E-03
203476_at	TPBG	trophoblast glycoprotein	2.30	1.44E-03
212233_at	MAP1B	microtubule-associated protein 1B	2.30	2.07E-03
219093_at	PID1	phosphotyrosine interaction domain containing 1	2.30	2.52E-02
213791_at	PENK	proenkephalin	2.30	3.93E-03
227140_at	INHBA	inhibin, beta A	2.30	2.64E-02
211719_x_at	FN1	fibronectin 1	2.29	3.22E-02
227566_at	NTM	neurotrimin	2.28	2.59E-03
212489_at	COL5A1	collagen, type V, alpha 1	2.28	2.12E-03
204932_at	TNFRSF11B	tumor necrosis factor receptor superfamily, member 11b	2.27	7.18E-04
219295_s_at	PCOLCE2	procollagen C-endopeptidase enhancer 2	2.26	8.58E-04
210549_s_at	CCL23	chemokine (C-C motif) ligand 23	2.26	1.34E-02
207852_at	CXCL5	chemokine (C-X-C motif) ligand 5	2.25	1.39E-02
212364_at	MYO1B	myosin IB	2.25	1.48E-03
209955_s_at	FAP	fibroblast activation protein, alpha	2.25	2.63E-03
202052_s_at	RAI14	retinoic acid induced 14	2.25	2.21E-03
229218_at	COL1A2	collagen, type I, alpha 2	2.25	4.72E-03
210517_s_at	AKAP12	A kinase (PRKA) anchor protein 12	2.24	2.07E-03
225442_at	DDR2	discoidin domain receptor tyrosine kinase 2	2.24	1.44E-03
216442_x_at	FN1	fibronectin 1	2.23	3.00E-02

210548_at	CCL23	chemokine (C-C motif) ligand 23	2.23	1.06E-02
202998_s_at	LOXL2	lysyl oxidase-like 2	2.22	5.84E-04
212464_s_at	FN1	fibronectin 1	2.22	3.11E-02
204114_at	NID2	nidogen 2 (osteonidogen)	2.22	3.02E-03
204823_at	NAV3	neuron navigator 3	2.21	1.18E-03
205523_at	HAPLN1	hyaluronan and proteoglycan link protein 1	2.21	1.10E-03
218332_at	BEX1	brain expressed, X-linked 1	2.20	2.05E-02
210423_s_at	SLC11A1	solute carrier family 11 (proton-coupled divalent metal ion transporters), member 1	2.19	1.10E-03
208937_s_at	ID1	inhibitor of DNA binding 1, dominant negative helix-loop-helix protein	2.19	5.34E-03
213194_at	ROBO1	roundabout, axon guidance receptor, homolog 1 (Drosophila)	2.19	2.27E-03
206118_at	STAT4	signal transducer and activator of transcription 4	2.18	6.27E-03
210762_s_at	DLC1	deleted in liver cancer 1	2.18	2.37E-03
202933_s_at	YES1	v-yes-1 Yamaguchi sarcoma viral oncogene homolog 1	2.17	3.93E-03
228850_s_at	SLIT2	slit homolog 2 (Drosophila)	2.16	2.30E-03
210495_x_at	FN1	fibronectin 1	2.16	3.16E-02
219434_at	TREM1	triggering receptor expressed on myeloid cells 1	2.15	5.97E-03
1553613_s_at	FOXC1	forkhead box C1	2.15	6.30E-03
205466_s_at	HS3ST1	heparan sulfate (glucosamine) 3-O-sulfotransferase 1	2.14	3.54E-02
213348_at	CDKN1C	cyclin-dependent kinase inhibitor 1C (p57, Kip2)	2.14	1.19E-02
208789_at	PTRF	polymerase I and transcript release factor	2.14	1.43E-03
217553_at	STEAP1B	STEAP family member 1B	2.14	2.07E-03
205158_at	RNASE4	ribonuclease, RNase A family, 4	2.13	1.02E-02
203423_at	RBP1	retinol binding protein 1, cellular	2.13	2.23E-02
224941_at	PAPPA	pregnancy-associated plasma protein A, pappalysin 1	2.11	2.49E-03
221898_at	PDPN	podoplanin	2.10	5.35E-03
225079_at	EMP2	epithelial membrane protein 2	2.09	3.38E-03
201601_x_at	IFITM1	interferon induced transmembrane protein 1 (9-27)	2.09	1.66E-02
210772_at	FPR2	formyl peptide receptor 2	2.08	7.57E-03
37892_at	COL11A1	collagen, type XI, alpha 1	2.08	2.47E-03
205088_at	MAMLD1	mastermind-like domain containing 1	2.08	1.11E-02
205863_at	S100A12	S100 calcium binding protein A12	2.08	2.71E-02
210773_s_at	FPR2	formyl peptide receptor 2	2.08	8.34E-03
205547_s_at	TAGLN	transgelin	2.07	2.01E-03
220014_at	PRR16	proline rich 16	2.07	2.24E-03
207826_s_at	ID3	inhibitor of DNA binding 3, dominant negative helix-loop-helix protein	2.07	1.31E-02
206157_at	PTX3	pentraxin 3, long	2.06	1.05E-02
205119_s_at	FPR1	formyl peptide receptor 1	2.06	2.24E-03
210987_x_at	TPM1	tropomyosin 1 (alpha)	2.06	1.18E-03
202628_s_at	SERPINE1	serpin peptidase inhibitor, clade E (nexin, plasminogen activator inhibitor type 1), member 1	2.06	1.75E-02
226930_at	FNDC1	fibronectin type III domain containing 1	2.06	6.64E-03
202729_s_at	LTBP1	latent transforming growth factor beta binding protein 1	2.06	2.09E-03
236028_at	IBSP	integrin-binding sialoprotein	2.04	2.50E-02
202465_at	PCOLCE	procollagen C-endopeptidase enhancer	2.03	5.77E-03
206858_s_at	HOXC6	homeobox C6	2.03	5.39E-03
237252_at	THBD	thrombomodulin	2.01	2.24E-03
212012_at	PXDN	peroxidasin homolog (Drosophila)	2.00	3.78E-03
205573_s_at	SNX7	sorting nexin 7	2.00	4.22E-02
224911_s_at	DCBLD2	discoidin, CUB and LCCL domain containing 2	1.98	7.53E-03
224588_at	XIST	X (inactive)-specific transcript (non-protein coding)	1.98	3.34E-02
227646_at	EBF1	early B-cell factor 1	1.98	4.14E-03
206028_s_at	MERTK	c-mer proto-oncogene tyrosine kinase	1.97	3.80E-03
205798_at	IL7R	interleukin 7 receptor	1.97	2.62E-02
202952_s_at	ADAM12	ADAM metallopeptidase domain 12	1.96	2.07E-03
225728_at	SORBS2	sorbin and SH3 domain containing 2	1.96	1.47E-02
200771_at	LAMC1	laminin, gamma 1 (formerly LAMB2)	1.95	4.30E-03
213428_s_at	COL6A1	collagen, type VI, alpha 1	1.95	1.41E-02
211913_s_at	MERTK	c-mer proto-oncogene tyrosine kinase	1.94	4.76E-03
204686_at	IRS1	insulin receptor substrate 1	1.94	1.08E-02
228141_at	GPX8	glutathione peroxidase 8 (putative)	1.94	5.64E-03

224694_at	ANTXR1	anthrax toxin receptor 1	1.94	1.19E-02
239058_at	FOXC2	forkhead box C2 (MFH-1, mesenchyme forkhead 1)	1.92	8.87E-03
213397_x_at	NA	NA	1.92	1.39E-02
219682_s_at	TBX3	T-box 3	1.92	1.47E-02
226223_at	NA	NA	1.91	7.53E-03
219815_at	GAL3ST4	galactose-3-O-sulfotransferase 4	1.91	3.75E-03
210422_x_at	SLC11A1	solute carrier family 11 (proton-coupled divalent metal ion transporters), member 1	1.91	2.04E-03
205568_at	AQP9	aquaporin 9	1.89	6.08E-03
229510_at	MS4A14	membrane-spanning 4-domains, subfamily A, member 14	1.88	9.52E-03
1553995_a_at	NT5E	5'-nucleotidase, ecto (CD73)	1.88	3.39E-03
226218_at	IL7R	interleukin 7 receptor	1.88	2.28E-02
203874_s_at	SMARCA1	SWI/SNF related, matrix associated, actin dependent regulator of chromatin, subfamily a, member 1	1.88	2.63E-03
206116_s_at	TPM1	tropomyosin 1 (alpha)	1.88	2.63E-03
230204_at	HAPLN1	hyaluronan and proteoglycan link protein 1	1.88	3.06E-03
204491_at	PDE4D	phosphodiesterase 4D, cAMP-specific	1.87	6.34E-03
226342_at	SPTBN1	spectrin, beta, non-erythrocytic 1	1.87	1.97E-03
201163_s_at	IGFBP7	insulin-like growth factor binding protein 7	1.87	2.40E-03
1557080_s_at	ITGBL1	integrin, beta-like 1 (with EGF-like repeat domains)	1.86	9.48E-03
200606_at	DSP	desmoplakin	1.86	8.15E-03
222881_at	HPSE	heparanase	1.86	2.55E-02
221024_s_at	SLC2A10	solute carrier family 2 (facilitated glucose transporter), member 10	1.86	4.30E-03
210664_s_at	TFPI	tissue factor pathway inhibitor (lipoprotein-associated coagulation inhibitor)	1.86	7.53E-03
205180_s_at	ADAM8	ADAM metallopeptidase domain 8	1.86	3.03E-03
210511_s_at	INHBA	inhibin, beta A	1.86	3.70E-02
205660_at	OASL	2'-5'-oligoadenylate synthetase-like	1.85	3.70E-02
209120_at	NR2F2	nuclear receptor subfamily 2, group F, member 2	1.85	9.46E-03
227828_s_at	FAM176A	family with sequence similarity 176, member A	1.85	2.46E-03
206877_at	MXD1	MAX dimerization protein 1	1.85	9.74E-03
215838_at	LILRA5	leukocyte immunoglobulin-like receptor, subfamily A (with TM domain), member 5	1.84	2.65E-02
202887_s_at	DDIT4	DNA-damage-inducible transcript 4	1.84	2.12E-02
222608_s_at	ANLN	anillin, actin binding protein	1.84	4.30E-02
210612_s_at	SYNJ2	synaptojanin 2	1.84	1.23E-02
238983_at	NSUN7	NOP2/Sun domain family, member 7	1.84	1.74E-02
213125_at	OLFML2B	olfactomedin-like 2B	1.84	1.97E-02
238623_at	NA	NA	1.84	5.67E-03
227126_at	PTPRG	protein tyrosine phosphatase, receptor type, G	1.83	1.20E-02
219403_s_at	HPSE	heparanase	1.83	3.19E-02
232235_at	DSEL	dermatan sulfate epimerase-like	1.83	2.02E-02
213258_at	TFPI	tissue factor pathway inhibitor (lipoprotein-associated coagulation inhibitor)	1.82	1.11E-02
226084_at	MAP1B	microtubule-associated protein 1B	1.81	2.46E-03
222258_s_at	SH3BP4	SH3-domain binding protein 4	1.81	1.14E-02
219410_at	TMEM45A	transmembrane protein 45A	1.81	8.26E-03
231335_at	MS4A6E	membrane-spanning 4-domains, subfamily A, member 6E	1.80	3.69E-02
210367_s_at	PTGES	prostaglandin E synthase	1.80	4.39E-02
202254_at	SIPA1L1	signal-induced proliferation-associated 1 like 1	1.80	6.98E-03
44790_s_at	KIAA0226L	KIAA0226-like	1.80	3.86E-03
205289_at	BMP2	bone morphogenetic protein 2	1.80	1.27E-02
225975_at	PCDH18	protocadherin 18	1.79	8.87E-03
1554741_s_at	NA	NA	1.79	8.28E-03
204933_s_at	TNFRSF11B	tumor necrosis factor receptor superfamily, member 11b	1.79	2.63E-03
224358_s_at	MS4A7	membrane-spanning 4-domains, subfamily A, member 7	1.79	1.81E-02
202932_at	YES1	v-yes-1 Yamaguchi sarcoma viral oncogene homolog 1	1.79	7.12E-03
225078_at	EMP2	epithelial membrane protein 2	1.78	8.80E-03
1553994_at	NT5E	5'-nucleotidase, ecto (CD73)	1.78	4.57E-03
212590_at	RRAS2	related RAS viral (r-ras) oncogene homolog 2	1.78	9.66E-03
203404_at	ARMCX2	armadillo repeat containing, X-linked 2	1.77	6.12E-03
204879_at	PDPN	podoplanin	1.77	1.32E-02
235318_at	FBN1	fibrillin 1	1.77	6.12E-03

206932_at	CH25H	cholesterol 25-hydroxylase	1.77	8.87E-03
212764_at	ZEB1	zinc finger E-box binding homeobox 1	1.76	3.22E-02
209487_at	RBPMS	RNA binding protein with multiple splicing	1.75	5.68E-03
228347_at	SIX1	SIX homeobox 1	1.75	3.73E-03
232458_at	COL3A1	collagen, type III, alpha 1	1.75	1.30E-02
227769_at	GPR27	G protein-coupled receptor 27	1.75	3.04E-02
217473_x_at	SLC11A1	solute carrier family 11 (proton-coupled divalent metal ion transporters), member 1	1.75	3.39E-03
1555643_s_at	LILRA5	leukocyte immunoglobulin-like receptor, subfamily A (with TM domain), member 5	1.75	2.96E-02
202878_s_at	CD93	CD93 molecule	1.74	1.07E-02
226989_at	RGMB	RGM domain family, member B	1.74	1.01E-02
206953_s_at	LPHN2	latrophilin 2	1.74	5.88E-03
210512_s_at	VEGFA	vascular endothelial growth factor A	1.74	1.81E-02
224215_s_at	DLL1	delta-like 1 (Drosophila)	1.74	2.26E-02
228962_at	PDE4D	phosphodiesterase 4D, cAMP-specific	1.74	1.02E-02
1555724_s_at	TAGLN	transgelin	1.73	5.81E-03
231227_at	WNT5A	wingless-type MMTV integration site family, member 5A	1.73	1.28E-02
222995_s_at	RHBDD2	rhomboid domain containing 2	1.73	1.01E-02
212154_at	SDC2	syndecan 2	1.72	8.87E-03
228918_at	NA	NA	1.72	1.58E-02
238852_at	NA	NA	1.72	1.07E-02
224657_at	ERRFI1	ERBB receptor feedback inhibitor 1	1.71	6.36E-03
205290_s_at	BMP2	bone morphogenetic protein 2	1.71	2.23E-02
204337_at	RGS4	regulator of G-protein signaling 4	1.71	1.31E-02
203851_at	IGFBP6	insulin-like growth factor binding protein 6	1.71	4.17E-03
1563445_x_at	CTSL1P8	cathepsin L1 pseudogene 8	1.70	8.22E-03
212589_at	RRAS2	related RAS viral (r-ras) oncogene homolog 2	1.70	1.52E-02
226225_at	MCC	mutated in colorectal cancers	1.70	1.69E-02
213183_s_at	CDKN1C	cyclin-dependent kinase inhibitor 1C (p57, Kip2)	1.69	2.26E-02
201939_at	PLK2	polo-like kinase 2	1.69	2.70E-02
239336_at	THBS1	thrombospondin 1	1.69	3.67E-02
212915_at	PDZRN3	PDZ domain containing ring finger 3	1.68	2.92E-02
237032_x_at	SIPA1L1	signal-induced proliferation-associated 1 like 1	1.68	1.01E-02
201162_at	IGFBP7	insulin-like growth factor binding protein 7	1.68	5.35E-03
1555167_s_at	NAMPT	nicotinamide phosphoribosyltransferase	1.68	2.92E-02
213624_at	SMPDL3A	sphingomyelin phosphodiesterase, acid-like 3A	1.68	9.35E-03
212157_at	SDC2	syndecan 2	1.68	7.39E-03
201860_s_at	PLAT	plasminogen activator, tissue	1.67	4.70E-03
202686_s_at	AXL	AXL receptor tyrosine kinase	1.67	5.68E-03
203908_at	SLC4A4	solute carrier family 4, sodium bicarbonate cotransporter, member 4	1.66	1.44E-02
222834_s_at	GNG12	guanine nucleotide binding protein (G protein), gamma 12	1.66	1.15E-02
226658_at	PDPN	podoplanin	1.66	1.81E-02
226302_at	ATP8B1	ATPase, aminophospholipid transporter, class I, type 8B, member 1	1.66	1.43E-02
235146_at	TMCC3	transmembrane and coiled-coil domain family 3	1.66	1.07E-02
209291_at	ID4	inhibitor of DNA binding 4, dominant negative helix-loop-helix protein	1.65	1.93E-02
223344_s_at	MS4A7	membrane-spanning 4-domains, subfamily A, member 7	1.65	1.98E-02
204682_at	LTBP2	latent transforming growth factor beta binding protein 2	1.65	1.13E-02
227998_at	S100A16	S100 calcium binding protein A16	1.64	4.96E-03
207172_s_at	CDH11	cadherin 11, type 2, OB-cadherin (osteoblast)	1.64	5.88E-03
210665_at	TFPI	tissue factor pathway inhibitor (lipoprotein-associated coagulation inhibitor)	1.63	2.04E-02
228121_at	TGFB2	transforming growth factor, beta 2	1.63	1.81E-02
223918_at	ACSL6	acyl-CoA synthetase long-chain family member 6	1.63	2.77E-02
213664_at	SLC1A1	solute carrier family 1 (neuronal/epithelial high affinity glutamate transporter, system Xag), member 1	1.63	1.39E-02
229635_at	LOC100505702	uncharacterized LOC100505702	1.63	6.08E-03
203903_s_at	HEPH	hephaestin	1.62	9.15E-03
223690_at	LTBP2	latent transforming growth factor beta binding protein 2	1.62	8.80E-03
228188_at	FOSL2	FOS-like antigen 2	1.62	8.52E-03
1555728_a_at	MS4A4A	membrane-spanning 4-domains, subfamily A, member 4A	1.62	1.01E-02
225308_s_at	TANC1	tetratricopeptide repeat, ankyrin repeat and coiled-coil	1.61	4.17E-03

		containing 1		
227705_at	TCEAL7	transcription elongation factor A (SII)-like 7	1.61	1.92E-02
218880_at	FOSL2	FOS-like antigen 2	1.61	1.52E-02
222450_at	PMEPA1	prostate transmembrane protein, androgen induced 1	1.61	2.63E-02
227058_at	C13orf33	chromosome 13 open reading frame 33	1.61	5.35E-03
240656_at	NA	NA	1.61	2.04E-02
235368_at	ADAMTS5	ADAM metallopeptidase with thrombospondin type 1 motif, 5	1.61	3.10E-02
236179_at	CDH11	cadherin 11, type 2, OB-cadherin (osteoblast)	1.60	1.55E-02
201042_at	TGM2	transglutaminase 2 (C polypeptide, protein-glutamine-gamma-glutamyltransferase)	1.60	1.11E-02
227059_at	GPC6	glypican 6	1.60	1.77E-02
215411_s_at	TRAF3IP2	TRAF3 interacting protein 2	1.60	1.11E-02
226112_at	SGCB	sarcoglycan, beta (43kDa dystrophin-associated glycoprotein)	1.58	2.02E-02
207630_s_at	CREM	cAMP responsive element modulator	1.58	1.11E-02
232231_at	RUNX2	runt-related transcription factor 2	1.58	1.79E-02
214033_at	ABCC6	ATP-binding cassette, sub-family C (CFTR/MRP), member 6	1.58	3.31E-02
227613_at	ZNF331	zinc finger protein 331	1.58	2.33E-02
227443_at	LURAP1L	leucine rich adaptor protein 1-like	1.58	2.82E-02
214508_x_at	CREM	cAMP responsive element modulator	1.58	1.14E-02
235568_at	C19orf59	chromosome 19 open reading frame 59	1.57	2.96E-02
229802_at	WISP1	WNT1 inducible signaling pathway protein 1	1.57	2.55E-02
222449_at	PMEPA1	prostate transmembrane protein, androgen induced 1	1.57	1.97E-02
201261_x_at	BGN	biglycan	1.57	1.10E-02
202255_s_at	SIPA1L1	signal-induced proliferation-associated 1 like 1	1.56	1.52E-02
212828_at	SYNJ2	synaptojanin 2	1.56	3.23E-02
215071_s_at	HIST1H2AC	histone cluster 1, H2ac	1.56	1.97E-02
204042_at	WASF3	WAS protein family, member 3	1.56	1.61E-02
235629_at	NA	NA	1.56	2.14E-02
204256_at	ELOVL6	ELOVL fatty acid elongase 6	1.56	1.91E-02
223454_at	CXCL16	chemokine (C-X-C motif) ligand 16	1.55	9.74E-03
1559975_at	BTG1	B-cell translocation gene 1, anti-proliferative	1.55	1.81E-02
212560_at	SORL1	sortilin-related receptor, L(DLR class) A repeats containing	1.55	1.96E-02
204602_at	DKK1	dickkopf 1 homolog (Xenopus laevis)	1.54	6.30E-03
204320_at	COL11A1	collagen, type XI, alpha 1	1.54	9.50E-03
214651_s_at	NA	NA	1.54	1.35E-02
1569583_at	EREG	epiregulin	1.53	2.57E-02
211924_s_at	PLAUR	plasminogen activator, urokinase receptor	1.53	2.12E-02
226771_at	ATP8B2	ATPase, class I, type 8B, member 2	1.53	2.77E-02
201059_at	CTTN	cortactin	1.52	1.85E-02
205141_at	ANG	angiogenin, ribonuclease, RNase A family, 5	1.52	2.14E-02
201069_at	MMP2	matrix metallopeptidase 2 (gelatinase A, 72kDa gelatinase, 72kDa type IV collagenase)	1.51	3.69E-02
201666_at	TIMP1	TIMP metallopeptidase inhibitor 1	1.51	7.72E-03
212013_at	PXDN	peroxidasin homolog (Drosophila)	1.51	1.66E-02
226489_at	TMCC3	transmembrane and coiled-coil domain family 3	1.51	1.01E-02
230511_at	CREM	cAMP responsive element modulator	1.51	1.21E-02
209209_s_at	FERMT2	fermitin family member 2	1.51	1.48E-02
241394_at	NA	NA	1.51	1.69E-02
204567_s_at	ABCG1	ATP-binding cassette, sub-family G (WHITE), member 1	1.51	1.66E-02
229800_at	DCLK1	doublecortin-like kinase 1	1.50	2.68E-02
231766_s_at	COL12A1	collagen, type XII, alpha 1	1.50	2.45E-02
219607_s_at	MS4A4A	membrane-spanning 4-domains, subfamily A, member 4A	1.50	1.58E-02
242722_at	LMO7	LIM domain 7	1.50	1.58E-02
218326_s_at	LGR4	leucine-rich repeat containing G protein-coupled receptor 4	1.50	3.37E-02
208850_s_at	THY1	Thy-1 cell surface antigen	1.50	1.05E-02
204948_s_at	FST	follistatin	1.49	7.54E-03
207030_s_at	CSRP2	cysteine and glycine-rich protein 2	1.49	7.53E-03
229479_at	NA	NA	1.49	3.73E-02
227195_at	ZNF503	zinc finger protein 503	1.49	1.01E-02
219534_x_at	CDKN1C	cyclin-dependent kinase inhibitor 1C (p57, Kip2)	1.49	2.69E-02
209676_at	TFPI	tissue factor pathway inhibitor (lipoprotein-associated coagulation inhibitor)	1.49	1.52E-02

1552619_a_at	ANLN	anillin, actin binding protein	1.49	3.83E-02
209967_s_at	CREM	cAMP responsive element modulator	1.49	1.47E-02
209897_s_at	SLIT2	slit homolog 2 (Drosophila)	1.49	8.64E-03
217738_at	NAMPT	nicotinamide phosphoribosyltransferase	1.48	2.76E-02
209228_x_at	TUSC3	tumor suppressor candidate 3	1.48	1.58E-02
234513_at	ELOVL3	ELOVL fatty acid elongase 3	1.48	1.33E-02
204030_s_at	NA	NA	1.48	1.15E-02
212158_at	SDC2	syndecan 2	1.47	1.21E-02
229554_at	NA	NA	1.47	1.36E-02
222455_s_at	PARVA	parvin, alpha	1.47	1.62E-02
209031_at	CADM1	cell adhesion molecule 1	1.47	3.12E-02
219228_at	ZNF331	zinc finger protein 331	1.47	2.86E-02
219134_at	ELTD1	EGF, latrophilin and seven transmembrane domain containing 1	1.47	1.49E-02
204749_at	NAP1L3	nucleosome assembly protein 1-like 3	1.47	2.82E-02
201508_at	IGFBP4	insulin-like growth factor binding protein 4	1.47	1.01E-02
209758_s_at	MFAP5	microfibrillar associated protein 5	1.46	8.89E-03
1553770_a_at	SLAMF9	SLAM family member 9	1.46	1.23E-02
219985_at	HS3ST3A1	heparan sulfate (glucosamine) 3-O-sulfotransferase 3A1	1.45	1.07E-02
215506_s_at	DIRAS3	DIRAS family, GTP-binding RAS-like 3	1.45	3.47E-02
211981_at	COL4A1	collagen, type IV, alpha 1	1.45	8.75E-03
217963_s_at	NGFRAP1	nerve growth factor receptor (TNFRSF16) associated protein 1	1.45	2.46E-02
204944_at	PTPRG	protein tyrosine phosphatase, receptor type, G	1.44	1.38E-02
228846_at	MXD1	MAX dimerization protein 1	1.44	2.09E-02
212372_at	MYH10	myosin, heavy chain 10, non-muscle	1.44	2.37E-02
225241_at	CCDC80	coiled-coil domain containing 80	1.44	1.52E-02
204165_at	WASF1	WAS protein family, member 1	1.44	9.74E-03
227070_at	GLT8D2	glycosyltransferase 8 domain containing 2	1.44	2.32E-02
210845_s_at	PLAUR	plasminogen activator, urokinase receptor	1.43	2.20E-02
227970_at	GPR157	G protein-coupled receptor 157	1.43	2.67E-02
225262_at	FOSL2	FOS-like antigen 2	1.43	1.58E-02
205782_at	FGF7	fibroblast growth factor 7	1.43	2.55E-02
208029_s_at	LAPTM4B	lysosomal protein transmembrane 4 beta	1.42	2.70E-02
1558397_at	PECAM1	platelet/endothelial cell adhesion molecule 1	1.42	2.96E-02
206307_s_at	FOXD1	forkhead box D1	1.41	1.97E-02
44783_s_at	HEY1	hairy/enhancer-of-split related with YRPW motif 1	1.41	4.52E-02
206580_s_at	EFEMP2	EGF containing fibulin-like extracellular matrix protein 2	1.41	1.48E-02
203789_s_at	SEMA3C	sema domain, immunoglobulin domain (Ig), short basic domain, secreted, (semaphorin) 3C	1.40	1.57E-02
230130_at	NA	NA	1.40	3.36E-02
204975_at	EMP2	epithelial membrane protein 2	1.40	1.61E-02
225871_at	STEAP2	STEAP family member 2, metalloreductase	1.40	2.02E-02
221728_x_at	XIST	X (inactive)-specific transcript (non-protein coding)	1.40	4.53E-02
203509_at	SORL1	sortilin-related receptor, L(DLR class) A repeats containing	1.40	2.82E-02
232629_at	PROK2	prokineticin 2	1.40	4.25E-02
219471_at	KIAA0226L	KIAA0226-like	1.39	1.15E-02
1556698_a_at	GPRIN3	GPRIN family member 3	1.39	1.35E-02
202888_s_at	ANPEP	alanyl (membrane) aminopeptidase	1.39	3.70E-02
226051_at	SELM	selenoprotein M	1.39	1.14E-02
224590_at	XIST	X (inactive)-specific transcript (non-protein coding)	1.38	5.18E-02
202196_s_at	DKK3	dickkopf 3 homolog (Xenopus laevis)	1.38	2.12E-02
1555539_at	SDS	serine dehydratase	1.37	4.56E-02
207480_s_at	MEIS2	Meis homeobox 2	1.37	1.58E-02
227799_at	MYO1G	myosin IG	1.36	4.20E-02
203910_at	ARHGAP29	Rho GTPase activating protein 29	1.36	2.28E-02
214702_at	FN1	fibronectin 1	1.36	1.85E-02
208394_x_at	ESM1	endothelial cell-specific molecule 1	1.36	1.35E-02
222446_s_at	BACE2	beta-site APP-cleaving enzyme 2	1.36	1.47E-02
229641_at	CCBE1	collagen and calcium binding EGF domains 1	1.35	2.04E-02
214212_x_at	FERMT2	fermitin family member 2	1.35	1.07E-02
203562_at	FEZ1	fasciculation and elongation protein zeta 1 (zygin I)	1.35	1.52E-02
228033_at	E2F7	E2F transcription factor 7	1.35	4.01E-02

232081_at	NA	NA	1.35	1.79E-02
230913_at	NA	NA	1.34	3.42E-02
242649_x_at	HMGN2P46	high mobility group nucleosomal binding domain 2 pseudogene 46	1.34	5.61E-02
208767_s_at	LAPTM4B	lysosomal protein transmembrane 4 beta	1.34	3.36E-02
209032_s_at	CADM1	cell adhesion molecule 1	1.34	2.95E-02
229014_at	FLJ42709	uncharacterized LOC441094	1.33	1.11E-02
202555_s_at	MYLK	myosin light chain kinase	1.33	1.79E-02
204797_s_at	EML1	echinoderm microtubule associated protein like 1	1.32	3.06E-02
228776_at	GJC1	gap junction protein, gamma 1, 45kDa	1.32	2.55E-02
201417_at	SOX4	SRY (sex determining region Y)-box 4	1.32	3.36E-02
236646_at	C12orf59	chromosome 12 open reading frame 59	1.31	3.19E-02
221911_at	ETV1	ets variant 1	1.31	4.56E-02
205016_at	TGFA	transforming growth factor, alpha	1.31	2.40E-02
210119_at	KCNJ15	potassium inwardly-rectifying channel, subfamily J, member 15	1.31	4.01E-02
227554_at	MAGI2-AS3	MAGI2 antisense RNA 3 (non-protein coding)	1.30	3.69E-02
240173_at	NA	NA	1.30	3.17E-02
204627_s_at	ITGB3	integrin, beta 3 (platelet glycoprotein IIIa, antigen CD61)	1.30	2.04E-02
227123_at	RAB3B	RAB3B, member RAS oncogene family	1.30	1.81E-02
205234_at	SLC16A4	solute carrier family 16, member 4 (monocarboxylic acid transporter 5)	1.30	1.52E-02
229435_at	GLIS3	GLIS family zinc finger 3	1.30	5.49E-02
212771_at	FAM171A1	family with sequence similarity 171, member A1	1.30	1.92E-02
207265_s_at	KDELR3	KDEL (Lys-Asp-Glu-Leu) endoplasmic reticulum protein retention receptor 3	1.29	1.71E-02
201681_s_at	DLG5	discs, large homolog 5 (Drosophila)	1.29	1.81E-02
221029_s_at	WNT5B	wingless-type MMTV integration site family, member 5B	1.29	2.68E-02
224822_at	DLC1	deleted in liver cancer 1	1.29	1.85E-02
209356_x_at	EFEMP2	EGF containing fibulin-like extracellular matrix protein 2	1.29	1.66E-02
218656_s_at	LHFP	lipoma HMGIC fusion partner	1.29	1.81E-02
201431_s_at	DPYSL3	dihydropyrimidinase-like 3	1.28	1.58E-02
214637_at	OSM	oncostatin M	1.28	2.59E-02
224357_s_at	MS4A4A	membrane-spanning 4-domains, subfamily A, member 4A	1.28	2.15E-02
205120_s_at	SGCB	sarcoglycan, beta (43kDa dystrophin-associated glycoprotein)	1.28	2.32E-02
202464_s_at	PFKFB3	6-phosphofructo-2-kinase/fructose-2,6-biphosphatase 3	1.28	3.22E-02
218717_s_at	LEPREL1	leprecan-like 1	1.28	1.66E-02
205407_at	RECK	reversion-inducing-cysteine-rich protein with kazal motifs	1.28	1.59E-02
237411_at	ADAMTS6	ADAM metallopeptidase with thrombospondin type 1 motif, 6	1.27	3.02E-02
204994_at	MX2	myxovirus (influenza virus) resistance 2 (mouse)	1.27	5.47E-02
217739_s_at	NAMPT	nicotinamide phosphoribosyltransferase	1.27	3.34E-02
212365_at	MYO1B	myosin IB	1.27	1.85E-02
228037_at	NA	NA	1.27	2.02E-02
218901_at	PLSCR4	phospholipid scramblase 4	1.27	2.35E-02
203561_at	FCGR2A	Fc fragment of IgG, low affinity IIa, receptor (CD32)	1.26	1.98E-02
202430_s_at	PLSCR1	phospholipid scramblase 1	1.26	2.71E-02
214866_at	PLAUR	plasminogen activator, urokinase receptor	1.26	2.67E-02
204688_at	SGCE	sarcoglycan, epsilon	1.26	2.01E-02
211737_x_at	PTN	pleiotrophin	1.25	1.45E-02
207714_s_at	SERPINH1	serpin peptidase inhibitor, clade H (heat shock protein 47), member 1, (collagen binding protein 1)	1.25	1.52E-02
235944_at	HMCN1	hemicentin 1	1.25	2.76E-02
240815_at	NA	NA	1.25	5.32E-02
215388_s_at	NA	NA	1.25	2.71E-02
218574_s_at	LMCD1	LIM and cysteine-rich domains 1	1.24	2.62E-02
228335_at	CLDN11	claudin 11	1.24	2.69E-02
202446_s_at	PLSCR1	phospholipid scramblase 1	1.24	1.95E-02
204254_s_at	VDR	vitamin D (1,25- dihydroxyvitamin D3) receptor	1.24	2.63E-02
200920_s_at	BTG1	B-cell translocation gene 1, anti-proliferative	1.24	3.36E-02
206857_s_at	FKBP1B	FK506 binding protein 1B, 12.6 kDa	1.24	2.28E-02
201416_at	SOX4	SRY (sex determining region Y)-box 4	1.24	5.12E-02
220952_s_at	PLEKHA5	pleckstrin homology domain containing, family A member 5	1.23	4.83E-02
229441_at	PRSS23	protease, serine, 23	1.23	2.21E-02

225842_at	PHLDA1	pleckstrin homology-like domain, family A, member 1	1.23	2.09E-02
201925_s_at	CD55	CD55 molecule, decay accelerating factor for complement (Cromer blood group)	1.23	3.34E-02
217771_at	GOLM1	golgi membrane protein 1	1.22	3.69E-02
213909_at	LRRC15	leucine rich repeat containing 15	1.22	2.11E-02
207610_s_at	EMR2	egf-like module containing, mucin-like, hormone receptor-like 2	1.22	2.81E-02
238378_at	NA	NA	1.22	3.60E-02
213342_at	YAP1	Yes-associated protein 1	1.22	3.05E-02
1556697_at	GPRIN3	GPRIN family member 3	1.22	2.63E-02
228176_at	NA	NA	1.22	3.82E-02
227250_at	KREMEN1	kringle containing transmembrane protein 1	1.22	2.96E-02
223000_s_at	F11R	F11 receptor	1.22	2.62E-02
241365_at	SATB1	SATB homeobox 1	1.22	4.91E-02
204726_at	CDH13	cadherin 13, H-cadherin (heart)	1.22	4.06E-02
227697_at	SOCS3	suppressor of cytokine signaling 3	1.21	2.96E-02
235548_at	APCDD1L	adenomatosis polyposis coli down-regulated 1-like	1.21	2.60E-02
213765_at	MFAP5	microfibrillar associated protein 5	1.21	2.32E-02
227812_at	TNFRSF19	tumor necrosis factor receptor superfamily, member 19	1.21	2.92E-02
203666_at	CXCL12	chemokine (C-X-C motif) ligand 12	1.21	2.55E-02
201792_at	AEBP1	AE binding protein 1	1.20	2.32E-02
226275_at	MXD1	MAX dimerization protein 1	1.20	3.86E-02
209030_s_at	CADM1	cell adhesion molecule 1	1.20	5.56E-02
212599_at	AUTS2	autism susceptibility candidate 2	1.20	4.58E-02
202273_at	PDGFRB	platelet-derived growth factor receptor, beta polypeptide	1.20	2.32E-02
205066_s_at	ENPP1	ectonucleotide pyrophosphatase/phosphodiesterase 1	1.20	3.52E-02
202132_at	WWTR1	WW domain containing transcription regulator 1	1.20	2.57E-02
206675_s_at	SKIL	SKI-like oncogene	1.20	3.75E-02
223343_at	MS4A7	membrane-spanning 4-domains, subfamily A, member 7	1.20	2.86E-02
234725_s_at	SEMA4B	sema domain, immunoglobulin domain (Ig), transmembrane domain (TM) and short cytoplasmic domain, (semaphorin) 4B	1.20	1.81E-02
225575_at	LIFR	leukemia inhibitory factor receptor alpha	1.19	2.95E-02
228707_at	CLDN23	claudin 23	1.19	2.86E-02
238429_at	TMEM71	transmembrane protein 71	1.19	5.23E-02
218418_s_at	KANK2	KN motif and ankyrin repeat domains 2	1.19	2.92E-02
224772_at	NAV1	neuron navigator 1	1.19	2.32E-02
227992_s_at	LINC00085	long intergenic non-protein coding RNA 85	1.19	3.84E-02
242100_at	CHSY3	chondroitin sulfate synthase 3	1.18	2.23E-02
213906_at	MYBL1	v-myb myeloblastosis viral oncogene homolog (avian)-like 1	1.18	4.27E-02
205880_at	PRKD1	protein kinase D1	1.18	2.57E-02
212203_x_at	IFITM3	interferon induced transmembrane protein 3	1.18	4.95E-02
203408_s_at	SATB1	SATB homeobox 1	1.18	4.31E-02
214435_x_at	RALA	v-ral simian leukemia viral oncogene homolog A (ras related)	1.17	2.77E-02
224999_at	EGFR	epidermal growth factor receptor	1.17	2.70E-02
231879_at	COL12A1	collagen, type XII, alpha 1	1.17	5.18E-02
220528_at	VNN3	vanin 3	1.16	6.74E-02
228904_at	HOXB3	homeobox B3	1.16	3.45E-02
204005_s_at	PAWR	PRKC, apoptosis, WT1, regulator	1.16	2.81E-02
213069_at	HEG1	HEG homolog 1 (zebrafish)	1.16	2.00E-02
222803_at	PRTFDC1	phosphoribosyl transferase domain containing 1	1.16	3.24E-02
204951_at	RHOH	ras homolog family member H	1.16	5.35E-02
202732_at	PKIG	protein kinase (cAMP-dependent, catalytic) inhibitor gamma	1.16	2.70E-02
1560625_s_at	NA	NA	1.16	3.42E-02
212104_s_at	RBFOX2	RNA binding protein, fox-1 homolog (C. elegans) 2	1.15	2.71E-02
228486_at	SLC44A1	solute carrier family 44, member 1	1.15	2.12E-02
218162_at	OLFML3	olfactomedin-like 3	1.15	3.93E-02
225328_at	FBXO32	F-box protein 32	1.15	6.56E-02
212171_x_at	VEGFA	vascular endothelial growth factor A	1.15	6.61E-02
202016_at	MEST	mesoderm specific transcript homolog (mouse)	1.15	2.91E-02
226804_at	FAM20A	family with sequence similarity 20, member A	1.14	3.14E-02
230369_at	GPR161	G protein-coupled receptor 161	1.14	2.74E-02
206359_at	SOCS3	suppressor of cytokine signaling 3	1.14	3.69E-02
202391_at	BASP1	brain abundant, membrane attached signal protein 1	1.14	5.89E-02

238021_s_at	CRNDE	colorectal neoplasia differentially expressed (non-protein coding)	1.14	5.47E-02
1558871_at	NA	NA	1.14	3.98E-02
229461_x_at	NEGR1	neuronal growth regulator 1	1.14	5.60E-02
222108_at	AMIGO2	adhesion molecule with Ig-like domain 2	1.14	4.06E-02
52837_at	KIAA1644	KIAA1644	1.13	4.01E-02
202936_s_at	SOX9	SRY (sex determining region Y)-box 9	1.13	2.92E-02
215559_at	ABCC6	ATP-binding cassette, sub-family C (CFTR/MRP), member 6	1.13	6.33E-02
228082_at	CLMP	CXADR-like membrane protein	1.13	3.47E-02
203946_s_at	ARG2	arginase, type II	1.13	4.20E-02
213764_s_at	MFAP5	microfibrillar associated protein 5	1.13	3.68E-02
231807_at	KIAA1217	KIAA1217	1.13	5.67E-02
211113_s_at	ABCG1	ATP-binding cassette, sub-family G (WHITE), member 1	1.13	3.17E-02
203574_at	NFIL3	nuclear factor, interleukin 3 regulated	1.13	3.92E-02
221261_x_at	NA	NA	1.13	3.67E-02
225946_at	RASSF8	Ras association (RalGDS/AF-6) domain family (N-terminal) member 8	1.12	4.11E-02
222662_at	PPP1R3B	protein phosphatase 1, regulatory subunit 3B	1.12	2.67E-02
221276_s_at	SYNC	syncoilin, intermediate filament protein	1.12	5.32E-02
227224_at	RALGPS2	Ral GEF with PH domain and SH3 binding motif 2	1.12	2.83E-02
209109_s_at	TSPAN6	tetraspanin 6	1.12	3.35E-02
1555950_a_at	CD55	CD55 molecule, decay accelerating factor for complement (Cromer blood group)	1.12	2.92E-02
1558199_at	FN1	fibronectin 1	1.12	4.80E-02
209911_x_at	HIST1H2BD	histone cluster 1, H2bd	1.12	4.01E-02
203875_at	SMARCA1	SWI/SNF related, matrix associated, actin dependent regulator of chromatin, subfamily a, member 1	1.11	2.84E-02
239675_at	LOC283143	uncharacterized LOC283143	1.11	3.12E-02
204255_s_at	VDR	vitamin D (1,25- dihydroxyvitamin D3) receptor	1.11	3.71E-02
210139_s_at	PMP22	peripheral myelin protein 22	1.11	3.73E-02
222288_at	NA	NA	1.11	3.40E-02
209108_at	TSPAN6	tetraspanin 6	1.11	3.34E-02
201107_s_at	THBS1	thrombospondin 1	1.11	5.03E-02
217867_x_at	BACE2	beta-site APP-cleaving enzyme 2	1.11	2.61E-02
228706_s_at	CLDN23	claudin 23	1.10	3.32E-02
229373_at	NA	NA	1.10	2.45E-02
200921_s_at	BTG1	B-cell translocation gene 1, anti-proliferative	1.10	3.17E-02
1554679_a_at	LAPTM4B	lysosomal protein transmembrane 4 beta	1.10	5.34E-02
223378_at	GLIS2	GLIS family zinc finger 2	1.09	2.84E-02
215966_x_at	GK3P	glycerol kinase 3 pseudogene	1.09	4.74E-02
223816_at	SLC46A2	solute carrier family 46, member 2	1.09	2.71E-02
229566_at	LOC645638	WDNM1-like pseudogene	1.09	6.82E-02
223463_at	RAB23	RAB23, member RAS oncogene family	1.09	3.14E-02
216894_x_at	CDKN1C	cyclin-dependent kinase inhibitor 1C (p57, Kip2)	1.09	3.70E-02
225227_at	SKIL	SKI-like oncogene	1.09	3.10E-02
223683_at	ZMYND15	zinc finger, MYND-type containing 15	1.09	4.08E-02
208436_s_at	IRF7	interferon regulatory factor 7	1.08	7.43E-02
38037_at	HBEGF	heparin-binding EGF-like growth factor	1.08	6.32E-02
224942_at	NA	NA	1.08	3.92E-02
213836_s_at	WIPI1	WD repeat domain, phosphoinositide interacting 1	1.08	3.57E-02
232113_at	NA	NA	1.08	4.30E-02
204004_at	PAWR	PRKC, apoptosis, WT1, regulator	1.08	3.17E-02
224097_s_at	F11R	F11 receptor	1.08	3.81E-02
204006_s_at	NA	NA	1.08	2.83E-02
221664_s_at	F11R	F11 receptor	1.08	4.22E-02
211959_at	IGFBP5	insulin-like growth factor binding protein 5	1.08	2.96E-02
218839_at	HEY1	hairy/enhancer-of-split related with YRPW motif 1	1.08	5.95E-02
209290_s_at	NFIB	nuclear factor I/B	1.08	3.85E-02
228485_s_at	SLC44A1	solute carrier family 44, member 1	1.07	2.71E-02
229770_at	GLT1D1	glycosyltransferase 1 domain containing 1	1.07	3.37E-02
238423_at	SYTL3	synaptotagmin-like 3	1.07	6.13E-02
225224_at	C20orf112	chromosome 20 open reading frame 112	1.07	3.93E-02
225303_at	KIRREL	kin of IRRE like (Drosophila)	1.07	3.16E-02
227370_at	FAM171B	family with sequence similarity 171, member B	1.07	3.82E-02

203827_at	WIPI1	WD repeat domain, phosphoinositide interacting 1	1.07	3.91E-02
212830_at	MEGF9	multiple EGF-like-domains 9	1.07	4.08E-02
205991_s_at	PRRX1	paired related homeobox 1	1.06	3.20E-02
243509_at	NA	NA	1.06	6.74E-02
209576_at	GNAI1	guanine nucleotide binding protein (G protein), alpha inhibiting activity polypeptide 1	1.06	3.85E-02
203821_at	HBEGF	heparin-binding EGF-like growth factor	1.06	6.77E-02
225202_at	RHOBTB3	Rho-related BTB domain containing 3	1.06	4.84E-02
213869_x_at	THY1	Thy-1 cell surface antigen	1.06	2.96E-02
215977_x_at	GK	glycerol kinase	1.06	4.82E-02
208456_s_at	RRAS2	related RAS viral (r-ras) oncogene homolog 2	1.05	3.67E-02
243601_at	LOC285957	uncharacterized LOC285957	1.05	4.63E-02
228790_at	FAM110B	family with sequence similarity 110, member B	1.05	3.95E-02
232687_at	NA	NA	1.05	3.51E-02
212330_at	TFDP1	transcription factor Dp-1	1.05	3.67E-02
231993_at	ITGBL1	integrin, beta-like 1 (with EGF-like repeat domains)	1.05	4.91E-02
213182_x_at	CDKN1C	cyclin-dependent kinase inhibitor 1C (p57, Kip2)	1.05	5.67E-02
210513_s_at	VEGFA	vascular endothelial growth factor A	1.05	7.48E-02
232053_x_at	RHBDD2	rhomboid domain containing 2	1.05	3.86E-02
201315_x_at	IFITM2	interferon induced transmembrane protein 2 (1-8D)	1.05	7.42E-02
243299_at	VRK2	vaccinia related kinase 2	1.05	6.78E-02
207315_at	CD226	CD226 molecule	1.04	4.80E-02
202988_s_at	RGS1	regulator of G-protein signaling 1	1.04	6.65E-02
208025_s_at	HMGA2	high mobility group AT-hook 2	1.04	3.72E-02
209156_s_at	COL6A2	collagen, type VI, alpha 2	1.04	5.28E-02
201926_s_at	CD55	CD55 molecule, decay accelerating factor for complement (Cromer blood group)	1.04	3.57E-02
206472_s_at	TLE3	transducin-like enhancer of split 3 (E(sp1) homolog, Drosophila)	1.04	4.60E-02
235497_at	LOC643837	uncharacterized LOC643837	1.04	6.71E-02
227339_at	RGMB	RGM domain family, member B	1.03	3.69E-02
208690_s_at	PDLIM1	PDZ and LIM domain 1	1.03	3.60E-02
205579_at	HRH1	histamine receptor H1	1.03	5.13E-02
242939_at	TFDP1	transcription factor Dp-1	1.03	3.60E-02
214255_at	ATP10A	ATPase, class V, type 10A	1.03	5.56E-02
203708_at	PDE4B	phosphodiesterase 4B, cAMP-specific	1.03	8.03E-02
234985_at	LDLRAD3	low density lipoprotein receptor class A domain containing 3	1.03	3.79E-02
214104_at	GPR161	G protein-coupled receptor 161	1.03	3.92E-02
209655_s_at	TMEM47	transmembrane protein 47	1.02	3.42E-02
202877_s_at	CD93	CD93 molecule	1.02	4.63E-02
225097_at	HIPK2	homeodomain interacting protein kinase 2	1.02	3.36E-02
242281_at	GLUL	glutamate-ammonia ligase	1.02	2.95E-02
202733_at	P4HA2	prolyl 4-hydroxylase, alpha polypeptide II	1.02	3.24E-02
219179_at	DACT1	dapper, antagonist of beta-catenin, homolog 1 (Xenopus laevis)	1.02	3.93E-02
217167_x_at	GK	glycerol kinase	1.02	5.14E-02
222528_s_at	SLC25A37	solute carrier family 25, member 37	1.01	4.01E-02
218284_at	SMAD3	SMAD family member 3	1.01	3.76E-02
207510_at	BDKRB1	bradykinin receptor B1	1.01	4.01E-02
211071_s_at	MLLT11	myeloid/lymphoid or mixed-lineage leukemia (trithorax homolog, Drosophila); translocated to, 11	1.01	4.18E-02
210992_x_at	FCGR2C	Fc fragment of IgG, low affinity IIc, receptor for (CD32) (gene/pseudogene)	1.01	3.43E-02
212624_s_at	CHN1	chimerin (chimaerin) 1	1.01	3.92E-02
212185_x_at	MT2A	metallothionein 2A	1.01	7.48E-02
225368_at	HIPK2	homeodomain interacting protein kinase 2	1.01	3.05E-02
212813_at	JAM3	junctional adhesion molecule 3	1.00	3.42E-02
229088_at	ENPP1	ectonucleotide pyrophosphatase/phosphodiesterase 1	1.00	6.18E-02
212800_at	STX6	syntaxin 6	1.00	3.91E-02
200644_at	MARCKSL1	MARCKS-like 1	1.00	7.48E-02
214587_at	COL8A1	collagen, type VIII, alpha 1	1.00	3.67E-02
216607_s_at	CYP51A1	cytochrome P450, family 51, subfamily A, polypeptide 1	-1.00	4.56E-02
210287_s_at	FLT1	fms-related tyrosine kinase 1 (vascular endothelial growth factor/vascular permeability factor receptor)	-1.00	8.03E-02
1556121_at	NAP1L1	nucleosome assembly protein 1-like 1	-1.00	4.80E-02

227228_s_at	CCDC88C	coiled-coil domain containing 88C	-1.01	4.39E-02
1553787_at	C11orf45	chromosome 11 open reading frame 45	-1.01	6.14E-02
238778_at	MPP7	membrane protein, palmitoylated 7 (MAGUK p55 subfamily member 7)	-1.02	7.37E-02
223773_s_at	SNHG12	small nucleolar RNA host gene 12 (non-protein coding)	-1.02	5.03E-02
201468_s_at	NQO1	NAD(P)H dehydrogenase, quinone 1	-1.02	3.73E-02
228797_at	NLN	neurolysin (metallopeptidase M3 family)	-1.02	3.73E-02
235213_at	ITPKB	inositol-trisphosphate 3-kinase B	-1.03	7.98E-02
216685_s_at	MTAP	methylthioadenosine phosphorylase	-1.03	7.48E-02
202800_at	SLC1A3	solute carrier family 1 (glial high affinity glutamate transporter), member 3	-1.03	3.92E-02
221035_s_at	TEX14	testis expressed 14	-1.03	3.86E-02
238520_at	TRERF1	transcriptional regulating factor 1	-1.03	5.46E-02
229773_at	SNAP23	synaptosomal-associated protein, 23kDa	-1.03	4.70E-02
235803_at	NA	NA	-1.04	3.92E-02
202741_at	PRKACB	protein kinase, cAMP-dependent, catalytic, beta	-1.04	6.69E-02
239252_at	COX7B	cytochrome c oxidase subunit VIIb	-1.04	5.43E-02
222292_at	CD40	CD40 molecule, TNF receptor superfamily member 5	-1.04	4.36E-02
208916_at	SLC1A5	solute carrier family 1 (neutral amino acid transporter), member 5	-1.04	2.82E-02
231899_at	ZC3H12C	zinc finger CCCH-type containing 12C	-1.04	3.60E-02
226848_at	NA	NA	-1.04	3.77E-02
232916_at	NA	NA	-1.05	3.97E-02
203196_at	ABCC4	ATP-binding cassette, sub-family C (CFTR/MRP), member 4	-1.05	7.28E-02
202970_at	DYRK2	dual-specificity tyrosine-(Y)-phosphorylation regulated kinase 2	-1.05	3.82E-02
224851_at	CDK6	cyclin-dependent kinase 6	-1.06	4.22E-02
1561334_at	LOC285181	uncharacterized LOC285181	-1.06	7.02E-02
230494_at	SLC20A1	solute carrier family 20 (phosphate transporter), member 1	-1.06	5.46E-02
225942_at	NLN	neurolysin (metallopeptidase M3 family)	-1.06	3.60E-02
215343_at	CCDC88C	coiled-coil domain containing 88C	-1.06	3.11E-02
238953_at	LOC100506325	uncharacterized LOC100506325	-1.06	7.65E-02
202551_s_at	CRIM1	cysteine rich transmembrane BMP regulator 1 (chordin-like)	-1.06	4.90E-02
219648_at	MREG	melanoregulin	-1.07	5.13E-02
239108_at	FAR2	fatty acyl CoA reductase 2	-1.07	6.79E-02
226066_at	MITF	microphthalmia-associated transcription factor	-1.07	2.95E-02
219006_at	NDUFAF4	NADH dehydrogenase (ubiquinone) 1 alpha subcomplex, assembly factor 4	-1.07	7.42E-02
225143_at	SFXN4	sideroflexin 4	-1.07	4.95E-02
221577_x_at	GDF15	growth differentiation factor 15	-1.08	6.76E-02
209735_at	ABCG2	ATP-binding cassette, sub-family G (WHITE), member 2	-1.08	6.31E-02
212500_at	ADO	2-aminoethanethiol (cysteamine) dioxygenase	-1.09	3.66E-02
223939_at	SUCNR1	succinate receptor 1	-1.09	4.24E-02
240555_at	NA	NA	-1.09	2.80E-02
39817_s_at	C6orf108	chromosome 6 open reading frame 108	-1.11	3.69E-02
237186_at	NA	NA	-1.11	5.97E-02
204027_s_at	METTL1	methyltransferase like 1	-1.11	6.49E-02
207233_s_at	MITF	microphthalmia-associated transcription factor	-1.11	2.21E-02
205770_at	GSR	glutathione reductase	-1.11	2.70E-02
240788_at	NA	NA	-1.12	5.44E-02
235244_at	CCDC58	coiled-coil domain containing 58	-1.12	4.81E-02
202552_s_at	CRIM1	cysteine rich transmembrane BMP regulator 1 (chordin-like)	-1.12	3.87E-02
218096_at	AGPAT5	1-acylglycerol-3-phosphate O-acyltransferase 5 (lysophosphatidic acid acyltransferase, epsilon)	-1.12	5.75E-02
233465_at	NA	NA	-1.12	5.51E-02
224063_at	NLN	neurolysin (metallopeptidase M3 family)	-1.13	2.76E-02
235626_at	CAMK1D	calcium/calmodulin-dependent protein kinase ID	-1.13	3.10E-02
212638_s_at	WWP1	WW domain containing E3 ubiquitin protein ligase 1	-1.14	4.03E-02
244332_at	NA	NA	-1.14	2.96E-02
215435_at	NA	NA	-1.14	6.57E-02
232682_at	MREG	melanoregulin	-1.14	5.57E-02
226117_at	TIFA	TRAF-interacting protein with forkhead-associated domain	-1.15	3.97E-02
205633_s_at	ALAS1	aminolevulinate, delta-, synthase 1	-1.15	3.92E-02
1556185_a_at	STEAP4	STEAP family member 4	-1.15	4.01E-02

36711_at	MAFF	v-maf musculoaponeurotic fibrosarcoma oncogene homolog F (avian)	-1.15	6.01E-02
1563088_a_at	LOC284837	uncharacterized LOC284837	-1.15	3.74E-02
241418_at	LOC344887	NmrA-like family domain containing 1 pseudogene	-1.16	2.57E-02
1569362_at	ALCAM	activated leukocyte cell adhesion molecule	-1.16	3.60E-02
202968_s_at	DYRK2	dual-specificity tyrosine-(Y)-phosphorylation regulated kinase 2	-1.16	3.00E-02
235374_at	MDH1	malate dehydrogenase 1, NAD (soluble)	-1.17	2.52E-02
244610_x_at	NA	NA	-1.17	3.57E-02
228496_s_at	CRIM1	cysteine rich transmembrane BMP regulator 1 (chordin-like)	-1.17	3.95E-02
204956_at	MTAP	methylthioadenosine phosphorylase	-1.17	6.55E-02
217838_s_at	EVL	Enah/Vasp-like	-1.17	2.86E-02
209218_at	SQLE	squalene epoxidase	-1.19	4.01E-02
210222_s_at	RTN1	reticulon 1	-1.19	3.67E-02
212224_at	ALDH1A1	aldehyde dehydrogenase 1 family, member A1	-1.19	2.02E-02
232471_at	NA	NA	-1.19	2.82E-02
228416_at	ACVR2A	activin A receptor, type IIA	-1.19	5.23E-02
204039_at	CEBPA	CCAAT/enhancer binding protein (C/EBP), alpha	-1.19	3.72E-02
240655_at	NA	NA	-1.20	2.86E-02
209288_s_at	CDC42EP3	CDC42 effector protein (Rho GTPase binding) 3	-1.20	2.96E-02
204984_at	GPC4	glypican 4	-1.20	4.90E-02
244413_at	CLECL1	C-type lectin-like 1	-1.20	2.06E-02
204032_at	BCAR3	breast cancer anti-estrogen resistance 3	-1.21	2.83E-02
221266_s_at	TM7SF4	transmembrane 7 superfamily member 4	-1.21	4.44E-02
241472_at	NA	NA	-1.21	3.66E-02
220560_at	C11orf21	chromosome 11 open reading frame 21	-1.22	3.73E-02
225609_at	GSR	glutathione reductase	-1.22	2.52E-02
206206_at	CD180	CD180 molecule	-1.23	5.21E-02
227556_at	NME7	non-metastatic cells 7, protein expressed in (nucleoside-diphosphate kinase)	-1.24	1.93E-02
212510_at	GPD1L	glycerol-3-phosphate dehydrogenase 1-like	-1.24	3.76E-02
229437_at	MIR155HG	MIR155 host gene (non-protein coding)	-1.24	4.80E-02
228990_at	SNHG12	small nucleolar RNA host gene 12 (non-protein coding)	-1.25	3.24E-02
213475_s_at	ITGAL	integrin, alpha L (antigen CD11A (p180), lymphocyte function-associated antigen 1; alpha polypeptide)	-1.25	2.83E-02
230741_at	NA	NA	-1.26	1.66E-02
205934_at	PLCL1	phospholipase C-like 1	-1.26	1.92E-02
207091_at	P2RX7	purinergic receptor P2X, ligand-gated ion channel, 7	-1.27	1.39E-02
1561195_at	NA	NA	-1.27	2.83E-02
227232_at	EVL	Enah/Vasp-like	-1.27	1.91E-02
1558292_s_at	PIGW	phosphatidylinositol glycan anchor biosynthesis, class W	-1.28	3.94E-02
201872_s_at	ABCE1	ATP-binding cassette, sub-family E (OABP), member 1	-1.32	5.92E-02
1554240_a_at	ITGAL	integrin, alpha L (antigen CD11A (p180), lymphocyte function-associated antigen 1; alpha polypeptide)	-1.32	2.91E-02
225944_at	NLN	neurolysin (metallopeptidase M3 family)	-1.33	2.19E-02
203485_at	RTN1	reticulon 1	-1.34	3.60E-02
241068_at	NA	NA	-1.34	3.43E-02
236313_at	CDKN2B	cyclin-dependent kinase inhibitor 2B (p15, inhibits CDK4)	-1.34	1.91E-02
201243_s_at	ATP1B1	ATPase, Na+/K+ transporting, beta 1 polypeptide	-1.34	1.07E-02
213562_s_at	SQLE	squalene epoxidase	-1.34	3.73E-02
201873_s_at	ABCE1	ATP-binding cassette, sub-family E (OABP), member 1	-1.36	4.58E-02
206488_s_at	CD36	CD36 molecule (thrombospondin receptor)	-1.36	3.09E-02
205890_s_at	NA	NA	-1.36	2.26E-02
201242_s_at	ATP1B1	ATPase, Na+/K+ transporting, beta 1 polypeptide	-1.37	1.47E-02
236198_at	NA	NA	-1.38	2.23E-02
238756_at	GAS2L3	growth arrest-specific 2 like 3	-1.38	4.51E-02
235199_at	RNF125	ring finger protein 125, E3 ubiquitin protein ligase	-1.39	4.36E-02
205327_s_at	ACVR2A	activin A receptor, type IIA	-1.39	1.85E-02
202923_s_at	GCLC	glutamate-cysteine ligase, catalytic subunit	-1.40	1.35E-02
222868_s_at	IL18BP	interleukin 18 binding protein	-1.40	2.28E-02
225943_at	NLN	neurolysin (metallopeptidase M3 family)	-1.40	2.23E-02
209555_s_at	CD36	CD36 molecule (thrombospondin receptor)	-1.40	4.22E-02
202742_s_at	PRKACB	protein kinase, cAMP-dependent, catalytic, beta	-1.40	4.08E-02
212637_s_at	WWP1	WW domain containing E3 ubiquitin protein ligase 1	-1.40	2.71E-02

204238_s_at	C6orf108	chromosome 6 open reading frame 108	-1.40	2.63E-02
230499_at	BIRC3	baculoviral IAP repeat containing 3	-1.40	1.47E-02
202969_at	DYRK2	dual-specificity tyrosine-(Y)-phosphorylation regulated kinase 2	-1.41	2.09E-02
205659_at	HDAC9	histone deacetylase 9	-1.41	1.01E-02
244375_at	NA	NA	-1.41	1.19E-02
236673_at	TIFAB	TRAF-interacting protein with forkhead-associated domain, family member B	-1.42	3.69E-02
202922_at	GCLC	glutamate-cysteine ligase, catalytic subunit	-1.42	1.38E-02
217966_s_at	FAM129A	family with sequence similarity 129, member A	-1.42	3.37E-02
226382_at	NA	NA	-1.43	3.05E-02
204440_at	CD83	CD83 molecule	-1.44	1.11E-02
204011_at	SPRY2	sprouty homolog 2 (Drosophila)	-1.45	2.82E-02
206765_at	KCNJ2	potassium inwardly-rectifying channel, subfamily J, member 2	-1.45	2.34E-02
215322_at	NA	NA	-1.48	2.09E-02
241929_at	NA	NA	-1.48	4.65E-02
1560762_at	LOC285972	uncharacterized LOC285972	-1.50	2.40E-02
1553639_a_at	PPARGC1B	peroxisome proliferator-activated receptor gamma, coactivator 1 beta	-1.50	1.35E-02
226038_at	LONRF1	LON peptidase N-terminal domain and ring finger 1	-1.50	2.56E-02
235020_at	TAF4B	TAF4b RNA polymerase II, TATA box binding protein (TBP)-associated factor, 105kDa	-1.50	1.32E-02
231513_at	KCNJ2	potassium inwardly-rectifying channel, subfamily J, member 2	-1.53	2.37E-02
206115_at	EGR3	early growth response 3	-1.54	1.85E-02
220301_at	CCDC102B	coiled-coil domain containing 102B	-1.54	1.75E-02
222071_s_at	SLCO4C1	solute carrier organic anion transporter family, member 4C1	-1.55	2.28E-02
229041_s_at	LOC100505746	uncharacterized LOC100505746	-1.56	9.74E-03
214967_at	NA	NA	-1.56	2.12E-02
217967_s_at	FAM129A	family with sequence similarity 129, member A	-1.57	2.71E-02
228766_at	CD36	CD36 molecule (thrombospondin receptor)	-1.57	3.65E-02
219895_at	FAM70A	family with sequence similarity 70, member A	-1.58	1.48E-02
228281_at	C11orf82	chromosome 11 open reading frame 82	-1.62	2.82E-02
225645_at	EHF	ets homologous factor	-1.66	2.67E-02
209716_at	CSF1	colony stimulating factor 1 (macrophage)	-1.67	1.81E-02
205249_at	EGR2	early growth response 2	-1.67	1.52E-02
202971_s_at	DYRK2	dual-specificity tyrosine-(Y)-phosphorylation regulated kinase 2	-1.72	4.62E-03
235539_at	NUMA1	nuclear mitotic apparatus protein 1	-1.78	1.58E-02
210538_s_at	BIRC3	baculoviral IAP repeat containing 3	-1.78	1.89E-02
220146_at	TLR7	toll-like receptor 7	-1.81	2.87E-02
226560_at	NA	NA	-1.86	2.50E-02
203178_at	GATM	glycine amidinotransferase (L-arginine:glycine amidinotransferase)	-1.87	2.19E-02
232181_at	PPARGC1B	peroxisome proliferator-activated receptor gamma, coactivator 1 beta	-1.89	1.49E-02
216733_s_at	GATM	glycine amidinotransferase (L-arginine:glycine amidinotransferase)	-1.90	2.04E-02
239529_at	C5orf20	chromosome 5 open reading frame 20	-1.91	1.49E-02
203548_s_at	LPL	lipoprotein lipase	-1.96	2.11E-02
228376_at	GGTA1P	glycoprotein, alpha-galactosyltransferase 1 pseudogene	-1.97	2.78E-02
206682_at	CLEC10A	C-type lectin domain family 10, member A	-1.99	3.79E-02
204363_at	F3	coagulation factor III (thromboplastin, tissue factor)	-2.01	3.60E-02
205738_s_at	FABP3	fatty acid binding protein 3, muscle and heart (mammary-derived growth inhibitor)	-2.02	2.67E-02
209301_at	CA2	carbonic anhydrase II	-2.03	1.19E-02
203549_s_at	LPL	lipoprotein lipase	-2.04	2.50E-02
214285_at	FABP3	fatty acid binding protein 3, muscle and heart (mammary-derived growth inhibitor)	-2.09	1.76E-02
1556314_a_at	NA	NA	-2.10	6.75E-03
206637_at	P2RY14	purinergic receptor P2Y, G-protein coupled, 14	-2.23	2.96E-02
220187_at	STEAP4	STEAP family member 4	-2.62	2.96E-03
220005_at	P2RY13	purinergic receptor P2Y, G-protein coupled, 13	-2.64	1.35E-02
225987_at	STEAP4	STEAP family member 4	-3.79	3.80E-03

7.4 Appendix D: Differentially expressed probe sets of MSCs$^{co\text{-}cu}$

Table 39: Differentially expressed probe sets during microarray of MSCs$^{co\text{-}cu}$ (array group D)
Listed are all 458 differentially expressed probe sets between co-cultured MSCs and their corresponding control assays (n = 4). Probe sets are ordered according to their descending statistical score (logFC) from highest up-regulation to highest down-regulation. Additional information reflects the probe set ID, their corresponding gene symbol and name as well as the adjusted (corrected for multiple comparisons) p-value (adj.P.Val).

ID	Symbol	GeneName	logFC	adj.P.Val
211122_s_at	CXCL11	chemokine (C-X-C motif) ligand 11	5.48	3.58E-03
1555745_a_at	LYZ	lysozyme	5.00	1.35E-03
203915_at	CXCL9	chemokine (C-X-C motif) ligand 9	4.96	3.17E-03
213975_s_at	LYZ	lysozyme	4.93	1.90E-03
202687_s_at	TNFSF10	tumor necrosis factor (ligand) superfamily, member 10	4.77	2.10E-04
210163_at	CXCL11	chemokine (C-X-C motif) ligand 11	4.72	3.82E-03
212671_s_at	NA	NA	4.49	2.10E-04
202917_s_at	S100A8	S100 calcium binding protein A8	4.49	1.28E-04
202688_at	TNFSF10	tumor necrosis factor (ligand) superfamily, member 10	4.36	2.10E-04
213831_at	HLA-DQA1	major histocompatibility complex, class II, DQ alpha 1	4.29	1.11E-04
214329_x_at	TNFSF10	tumor necrosis factor (ligand) superfamily, member 10	4.28	3.82E-04
206134_at	ADAMDEC1	ADAM-like, decysin 1	4.23	1.37E-05
220330_s_at	SAMSN1	SAM domain, SH3 domain and nuclear localization signals 1	3.94	3.89E-04
203923_s_at	CYBB	cytochrome b-245, beta polypeptide	3.85	2.86E-04
202901_x_at	CTSS	cathepsin S	3.85	5.20E-04
223343_at	MS4A7	membrane-spanning 4-domains, subfamily A, member 7	3.83	2.02E-03
212588_at	PTPRC	protein tyrosine phosphatase, receptor type, C	3.81	2.67E-04
202638_s_at	ICAM1	intercellular adhesion molecule 1	3.76	3.01E-03
210029_at	IDO1	indoleamine 2,3-dioxygenase 1	3.68	3.63E-03
208894_at	HLA-DRA	major histocompatibility complex, class II, DR alpha	3.63	1.87E-03
202902_s_at	CTSS	cathepsin S	3.58	8.54E-04
214038_at	CCL8	chemokine (C-C motif) ligand 8	3.53	3.58E-03
210982_s_at	HLA-DRA	major histocompatibility complex, class II, DR alpha	3.48	2.00E-03
242907_at	NA	NA	3.46	1.81E-03
206214_at	PLA2G7	phospholipase A2, group VII (platelet-activating factor acetylhydrolase, plasma)	3.42	5.20E-04
202748_at	GBP2	guanylate binding protein 2, interferon-inducible	3.37	1.37E-03
203936_s_at	MMP9	matrix metallopeptidase 9 (gelatinase B, 92kDa gelatinase, 92kDa type IV collagenase)	3.33	8.54E-04
210538_s_at	BIRC3	baculoviral IAP repeat containing 3	3.32	2.97E-03
1554899_s_at	FCER1G	Fc fragment of IgE, high affinity I, receptor for; gamma polypeptide	3.31	5.20E-04
219386_s_at	SLAMF8	SLAM family member 8	3.27	1.34E-03
204122_at	TYROBP	TYRO protein tyrosine kinase binding protein	3.19	1.15E-03
219607_s_at	MS4A4A	membrane-spanning 4-domains, subfamily A, member 4A	3.10	3.82E-03
232617_at	CTSS	cathepsin S	3.09	7.11E-04
202637_s_at	ICAM1	intercellular adhesion molecule 1	3.06	3.58E-03
212998_x_at	HLA-DQB1	major histocompatibility complex, class II, DQ beta 1	3.04	1.83E-03
201721_s_at	LAPTM5	lysosomal protein transmembrane 5	3.02	1.35E-03
216834_at	RGS1	regulator of G-protein signaling 1	2.91	1.81E-03
205114_s_at	NA	NA	2.88	3.66E-03
215223_s_at	SOD2	superoxide dismutase 2, mitochondrial	2.82	1.35E-03
206420_at	IGSF6	immunoglobulin superfamily, member 6	2.80	4.16E-04
222868_s_at	IL18BP	interleukin 18 binding protein	2.79	3.82E-03
204070_at	RARRES3	retinoic acid receptor responder (tazarotene induced) 3	2.77	3.66E-03
217497_at	TYMP	thymidine phosphorylase	2.76	7.11E-04
223502_s_at	TNFSF13B	tumor necrosis factor (ligand) superfamily, member 13b	2.73	1.37E-03
238725_at	IRF1	interferon regulatory factor 1	2.72	3.01E-03
212587_s_at	PTPRC	protein tyrosine phosphatase, receptor type, C	2.71	1.64E-03

204232_at	FCER1G	Fc fragment of IgE, high affinity I, receptor for; gamma polypeptide	2.71	7.83E-04
209480_at	HLA-DQB1	major histocompatibility complex, class II, DQ beta 1	2.68	3.22E-04
229560_at	TLR8	toll-like receptor 8	2.67	2.00E-03
202269_x_at	GBP1	guanylate binding protein 1, interferon-inducible	2.67	3.58E-03
208075_s_at	CCL7	chemokine (C-C motif) ligand 7	2.63	7.83E-04
216841_s_at	SOD2	superoxide dismutase 2, mitochondrial	2.58	1.35E-03
223501_at	TNFSF13B	tumor necrosis factor (ligand) superfamily, member 13b	2.50	2.12E-03
231577_s_at	GBP1	guanylate binding protein 1, interferon-inducible	2.47	3.87E-03
210895_s_at	CD86	CD86 molecule	2.47	2.78E-03
203416_at	CD53	CD53 molecule	2.45	7.11E-04
221477_s_at	SOD2	superoxide dismutase 2, mitochondrial	2.44	8.54E-04
214022_s_at	IFITM1	interferon induced transmembrane protein 1 (9-27)	2.44	3.58E-03
206513_at	AIM2	absent in melanoma 2	2.44	1.28E-03
201601_x_at	IFITM1	interferon induced transmembrane protein 1 (9-27)	2.39	4.00E-03
218404_at	SNX10	sorting nexin 10	2.34	1.83E-03
209546_s_at	APOL1	apolipoprotein L, 1	2.34	1.83E-03
202270_at	GBP1	guanylate binding protein 1, interferon-inducible	2.34	3.82E-03
202531_at	IRF1	interferon regulatory factor 1	2.33	3.58E-03
204446_s_at	ALOX5	arachidonate 5-lipoxygenase	2.32	4.05E-03
205269_at	LCP2	lymphocyte cytosolic protein 2 (SH2 domain containing leukocyte protein of 76kDa)	2.30	5.20E-04
230422_at	FPR3	formyl peptide receptor 3	2.29	3.66E-03
204279_at	PSMB9	proteasome (prosome, macropain) subunit, beta type, 9 (large multifunctional peptidase 2)	2.25	1.99E-03
209619_at	CD74	CD74 molecule, major histocompatibility complex, class II invariant chain	2.24	2.71E-03
205098_at	CCR1	chemokine (C-C motif) receptor 1	2.24	1.15E-03
201743_at	CD14	CD14 molecule	2.21	2.71E-03
222150_s_at	PION	pigeon homolog (Drosophila)	2.20	4.05E-03
207238_s_at	PTPRC	protein tyrosine phosphatase, receptor type, C	2.17	1.72E-03
211991_s_at	HLA-DPA1	major histocompatibility complex, class II, DP alpha 1	2.14	3.26E-03
1557236_at	APOL6	apolipoprotein L, 6	2.14	3.66E-03
209906_at	C3AR1	complement component 3a receptor 1	2.13	1.72E-03
227697_at	SOCS3	suppressor of cytokine signaling 3	2.12	8.54E-04
211990_at	HLA-DPA1	major histocompatibility complex, class II, DP alpha 1	2.11	2.71E-03
203932_at	HLA-DMB	major histocompatibility complex, class II, DM beta	2.10	1.13E-03
221897_at	TRIM52	tripartite motif containing 52	2.08	3.80E-03
206715_at	TFEC	transcription factor EC	2.05	8.54E-04
206359_at	SOCS3	suppressor of cytokine signaling 3	2.04	2.74E-03
227609_at	EPSTI1	epithelial stromal interaction 1 (breast)	2.04	3.12E-03
222253_s_at	POM121L9P	POM121 membrane glycoprotein-like 9, pseudogene	2.02	4.04E-03
213537_at	HLA-DPA1	major histocompatibility complex, class II, DP alpha 1	2.02	1.37E-03
203535_at	S100A9	S100 calcium binding protein A9	1.97	5.20E-04
204670_x_at	NA	NA	1.96	3.66E-03
201641_at	BST2	bone marrow stromal cell antigen 2	1.94	3.72E-03
235276_at	EPSTI1	epithelial stromal interaction 1 (breast)	1.94	3.58E-03
225502_at	DOCK8	dedicator of cytokinesis 8	1.93	2.97E-03
216598_s_at	CCL2	chemokine (C-C motif) ligand 2	1.92	3.67E-03
1557116_at	APOL6	apolipoprotein L, 6	1.87	4.04E-03
204912_at	IL10RA	interleukin 10 receptor, alpha	1.87	2.68E-03
232024_at	GIMAP2	GTPase, IMAP family member 2	1.86	3.82E-03
230391_at	CD84	CD84 molecule	1.86	3.99E-03
203561_at	FCGR2A	Fc fragment of IgG, low affinity IIa, receptor (CD32)	1.84	2.73E-03
205992_s_at	IL15	interleukin 15	1.83	4.05E-03
219716_at	APOL6	apolipoprotein L, 6	1.82	3.66E-03
239587_at	NA	NA	1.82	2.08E-03
1566342_at	SOD2	superoxide dismutase 2, mitochondrial	1.82	1.64E-03
229937_x_at	LILRB1	leukocyte immunoglobulin-like receptor, subfamily B (with TM and ITIM domains), member 1	1.82	3.66E-03
202659_at	PSMB10	proteasome (prosome, macropain) subunit, beta type, 10	1.80	3.13E-03
202953_at	C1QB	complement component 1, q subcomponent, B chain	1.79	1.37E-03
206819_at	POM121L9P	POM121 membrane glycoprotein-like 9, pseudogene	1.77	4.13E-03

222592_s_at	ACSL5	acyl-CoA synthetase long-chain family member 5	1.75	3.29E-03
217388_s_at	KYNU	kynureninase	1.75	3.66E-03
211654_x_at	HLA-DQB1	major histocompatibility complex, class II, DQ beta 1	1.75	3.23E-03
221698_s_at	CLEC7A	C-type lectin domain family 7, member A	1.74	3.68E-03
231769_at	FBXO6	F-box protein 6	1.73	3.58E-03
241869_at	APOL6	apolipoprotein L, 6	1.73	3.99E-03
209949_at	NCF2	neutrophil cytosolic factor 2	1.69	3.68E-03
226459_at	PIK3AP1	phosphoinositide-3-kinase adaptor protein 1	1.66	5.20E-04
203868_s_at	VCAM1	vascular cell adhesion molecule 1	1.66	5.20E-04
201422_at	IFI30	interferon, gamma-inducible protein 30	1.65	1.35E-03
201649_at	UBE2L6	ubiquitin-conjugating enzyme E2L 6	1.63	1.37E-03
235458_at	HAVCR2	hepatitis A virus cellular receptor 2	1.63	3.26E-03
220358_at	BATF3	basic leucine zipper transcription factor, ATF-like 3	1.63	3.58E-03
202307_s_at	TAP1	transporter 1, ATP-binding cassette, sub-family B (MDR/TAP)	1.63	3.82E-03
205568_at	AQP9	aquaporin 9	1.62	3.36E-03
204385_at	KYNU	kynureninase	1.61	3.66E-03
207610_s_at	EMR2	egf-like module containing, mucin-like, hormone receptor-like 2	1.60	1.42E-03
203922_s_at	CYBB	cytochrome b-245, beta polypeptide	1.57	7.83E-04
211138_s_at	KMO	kynurenine 3-monooxygenase (kynurenine 3-hydroxylase)	1.57	1.88E-03
225353_s_at	C1QC	complement component 1, q subcomponent, C chain	1.57	3.53E-03
211656_x_at	HLA-DQB1	major histocompatibility complex, class II, DQ beta 1	1.55	3.87E-03
205100_at	GFPT2	glutamine-fructose-6-phosphate transaminase 2	1.55	3.54E-03
201720_s_at	LAPTM5	lysosomal protein transmembrane 5	1.55	3.58E-03
218035_s_at	RBM47	RNA binding motif protein 47	1.54	2.23E-03
220244_at	LINC00312	long intergenic non-protein coding RNA 312	1.54	3.38E-03
204798_at	MYB	v-myb myeloblastosis viral oncogene homolog (avian)	1.53	1.87E-03
212999_x_at	HLA-DQB1	major histocompatibility complex, class II, DQ beta 1	1.53	1.35E-03
225973_at	TAP2	transporter 2, ATP-binding cassette, sub-family B (MDR/TAP)	1.53	3.82E-03
230499_at	BIRC3	baculoviral IAP repeat containing 3	1.51	2.02E-03
242868_at	NA	NA	1.51	4.14E-03
201288_at	ARHGDIB	Rho GDP dissociation inhibitor (GDI) beta	1.48	4.19E-03
204858_s_at	TYMP	thymidine phosphorylase	1.48	2.48E-03
239979_at	NA	NA	1.48	2.18E-03
219574_at	MARCH1	membrane-associated ring finger (C3HC4) 1, E3 ubiquitin protein ligase	1.47	4.18E-03
203148_s_at	TRIM14	tripartite motif containing 14	1.47	4.19E-03
204588_s_at	SLC7A7	solute carrier family 7 (amino acid transporter light chain, y+L system), member 7	1.46	1.76E-03
208018_s_at	HCK	hemopoietic cell kinase	1.45	3.26E-03
218574_s_at	LMCD1	LIM and cysteine-rich domains 1	1.41	4.32E-03
206271_at	TLR3	toll-like receptor 3	1.41	3.85E-03
232375_at	NA	NA	1.40	4.17E-03
208885_at	LCP1	lymphocyte cytosolic protein 1 (L-plastin)	1.39	1.35E-03
234987_at	SAMHD1	SAM domain and HD domain 1	1.38	3.53E-03
232311_at	B2M	beta-2-microglobulin	1.38	3.58E-03
205841_at	JAK2	Janus kinase 2	1.38	4.04E-03
204787_at	VSIG4	V-set and immunoglobulin domain containing 4	1.35	4.05E-03
1555638_a_at	SAMSN1	SAM domain, SH3 domain and nuclear localization signals 1	1.34	2.05E-03
204118_at	CD48	CD48 molecule	1.33	3.13E-03
202295_s_at	CTSH	cathepsin H	1.30	3.58E-03
213095_x_at	AIF1	allograft inflammatory factor 1	1.30	2.74E-03
222218_s_at	PILRA	paired immunoglobin-like type 2 receptor alpha	1.27	3.67E-03
218232_at	C1QA	complement component 1, q subcomponent, A chain	1.27	4.04E-03
201762_s_at	PSME2	proteasome (prosome, macropain) activator subunit 2 (PA28 beta)	1.26	2.97E-03
201137_s_at	HLA-DPB1	major histocompatibility complex, class II, DP beta 1	1.25	3.44E-03
215051_x_at	AIF1	allograft inflammatory factor 1	1.24	2.78E-03
207571_x_at	C1orf38	chromosome 1 open reading frame 38	1.22	2.98E-03
205306_x_at	KMO	kynurenine 3-monooxygenase (kynurenine 3-hydroxylase)	1.21	4.32E-03
233177_s_at	PNKD	paroxysmal nonkinesigenic dyskinesia	1.21	2.97E-03

200904_at	HLA-E	major histocompatibility complex, class I, E	1.20	3.58E-03
204924_at	TLR2	toll-like receptor 2	1.20	3.53E-03
223454_at	CXCL16	chemokine (C-X-C motif) ligand 16	1.19	1.35E-03
219947_at	CLEC4A	C-type lectin domain family 4, member A	1.19	2.78E-03
210785_s_at	C1orf38	chromosome 1 open reading frame 38	1.18	3.82E-03
227677_at	JAK3	Janus kinase 3	1.18	8.54E-04
222496_s_at	RBM47	RNA binding motif protein 47	1.17	2.06E-03
229723_at	TAGAP	T-cell activation RhoGTPase activating protein	1.17	2.14E-03
236439_at	NA	NA	1.15	4.03E-03
206467_x_at	NA	NA	1.15	1.35E-03
225415_at	DTX3L	deltex 3-like (Drosophila)	1.12	4.31E-03
227184_at	PTAFR	platelet-activating factor receptor	1.12	1.64E-03
218834_s_at	TMEM132A	transmembrane protein 132A	1.12	3.36E-03
200905_x_at	HLA-E	major histocompatibility complex, class I, E	1.11	3.99E-03
211725_s_at	NA	NA	1.10	3.58E-03
219593_at	SLC15A3	solute carrier family 15, member 3	1.10	3.66E-03
204440_at	CD83	CD83 molecule	1.09	1.35E-03
237169_at	TNC	tenascin C	1.09	1.37E-03
223586_at	ARNTL2	aryl hydrocarbon receptor nuclear translocator-like 2	1.08	2.77E-03
208829_at	TAPBP	TAP binding protein (tapasin)	1.08	4.10E-03
235670_at	STX11	syntaxin 11	1.08	3.58E-03
212110_at	SLC39A14	solute carrier family 39 (zinc transporter), member 14	1.07	3.66E-03
228758_at	BCL6	B-cell CLL/lymphoma 6	1.07	3.38E-03
204715_at	PANX1	pannexin 1	1.06	3.23E-03
216950_s_at	NA	NA	1.05	3.99E-03
225868_at	TRIM47	tripartite motif containing 47	1.05	1.35E-03
222666_s_at	RCL1	RNA terminal phosphate cyclase-like 1	1.03	1.37E-03
210889_s_at	FCGR2B	Fc fragment of IgG, low affinity IIb, receptor (CD32)	1.03	4.93E-03
1559883_s_at	SAMHD1	SAM domain and HD domain 1	1.02	3.67E-03
207677_s_at	NCF4	neutrophil cytosolic factor 4, 40kDa	1.02	3.87E-03
227262_at	HAPLN3	hyaluronan and proteoglycan link protein 3	1.02	4.32E-03
204493_at	BID	BH3 interacting domain death agonist	1.02	2.31E-03
221558_s_at	LEF1	lymphoid enhancer-binding factor 1	1.01	3.99E-03
203471_s_at	PLEK	pleckstrin	1.00	3.99E-03
225293_at	COL27A1	collagen, type XXVII, alpha 1	1.00	4.61E-03
209354_at	TNFRSF14	tumor necrosis factor receptor superfamily, member 14	0.99	3.87E-03
202431_s_at	MYC	v-myc myelocytomatosis viral oncogene homolog (avian)	0.99	3.82E-03
205988_at	CD84	CD84 molecule	0.98	3.35E-03
203147_s_at	TRIM14	tripartite motif containing 14	0.97	3.58E-03
223322_at	RASSF5	Ras association (RalGDS/AF-6) domain family member 5	0.96	2.55E-03
202238_s_at	NNMT	nicotinamide N-methyltransferase	0.95	3.82E-03
219622_at	RAB20	RAB20, member RAS oncogene family	0.95	2.74E-03
241981_at	FAM20A	family with sequence similarity 20, member A	0.94	4.93E-03
220658_s_at	ARNTL2	aryl hydrocarbon receptor nuclear translocator-like 2	0.94	4.76E-03
204646_at	DPYD	dihydropyrimidine dehydrogenase	0.93	1.83E-03
227250_at	KREMEN1	kringle containing transmembrane protein 1	0.93	3.01E-03
201473_at	JUNB	jun B proto-oncogene	0.93	2.78E-03
227911_at	ARHGAP28	Rho GTPase activating protein 28	0.93	4.62E-03
218544_s_at	RCL1	RNA terminal phosphate cyclase-like 1	0.92	2.02E-03
203455_s_at	SAT1	spermidine/spermine N1-acetyltransferase 1	0.92	4.68E-03
203927_at	NFKBIE	nuclear factor of kappa light polypeptide gene enhancer in B-cells inhibitor, epsilon	0.92	3.60E-03
227143_s_at	BID	BH3 interacting domain death agonist	0.91	3.58E-03
227438_at	ALPK1	alpha-kinase 1	0.91	4.32E-03
209924_at	CCL18	chemokine (C-C motif) ligand 18 (pulmonary and activation-regulated)	0.91	4.14E-03
203710_at	ITPR1	inositol 1,4,5-trisphosphate receptor, type 1	0.91	2.71E-03
205205_at	RELB	v-rel reticuloendotheliosis viral oncogene homolog B	0.91	4.48E-03
218066_at	SLC12A7	solute carrier family 12 (potassium/chloride transporters), member 7	0.90	3.66E-03
216565_x_at	NA	NA	0.90	5.01E-03
240306_at	LINC00312	long intergenic non-protein coding RNA 312	0.89	4.96E-03
224204_x_at	ARNTL2	aryl hydrocarbon receptor nuclear translocator-like 2	0.89	4.88E-03

211582_x_at	LST1	leukocyte specific transcript 1	0.88	3.96E-03
204057_at	IRF8	interferon regulatory factor 8	0.85	3.24E-03
207536_s_at	TNFRSF9	tumor necrosis factor receptor superfamily, member 9	0.85	3.82E-03
202308_at	SREBF1	sterol regulatory element binding transcription factor 1	0.84	3.13E-03
213136_at	PTPN2	protein tyrosine phosphatase, non-receptor type 2	0.84	3.96E-03
47550_at	LZTS1	leucine zipper, putative tumor suppressor 1	0.84	1.83E-03
220066_at	NOD2	nucleotide-binding oligomerization domain containing 2	0.84	1.84E-03
217456_x_at	HLA-E	major histocompatibility complex, class I, E	0.84	5.73E-03
229537_at	LMO4	LIM domain only 4	0.82	3.82E-03
209640_at	PML	promyelocytic leukemia	0.81	1.83E-03
232406_at	NA	NA	0.81	3.90E-03
1553043_a_at	CD300LF	CD300 molecule-like family member f	0.81	3.58E-03
216944_s_at	ITPR1	inositol 1,4,5-trisphosphate receptor, type 1	0.79	4.31E-03
230640_at	NA	NA	0.79	3.82E-03
204935_at	PTPN2	protein tyrosine phosphatase, non-receptor type 2	0.79	5.18E-03
242945_at	FAM20A	family with sequence similarity 20, member A	0.79	4.04E-03
202237_at	NNMT	nicotinamide N-methyltransferase	0.79	5.10E-03
210772_at	FPR2	formyl peptide receptor 2	0.78	4.13E-03
208965_s_at	IFI16	interferon, gamma-inducible protein 16	0.78	5.10E-03
226804_at	FAM20A	family with sequence similarity 20, member A	0.78	4.88E-03
217771_at	GOLM1	golgi membrane protein 1	0.78	3.99E-03
223168_at	RHOU	ras homolog family member U	0.77	5.00E-03
211013_x_at	PML	promyelocytic leukemia	0.77	2.97E-03
205101_at	CIITA	class II, major histocompatibility complex, transactivator	0.76	4.00E-03
213137_s_at	PTPN2	protein tyrosine phosphatase, non-receptor type 2	0.76	4.31E-03
205542_at	STEAP1	six transmembrane epithelial antigen of the prostate 1	0.75	5.96E-03
229844_at	FOXP1	forkhead box P1	0.75	4.19E-03
226795_at	LRCH1	leucine-rich repeats and calponin homology (CH) domain containing 1	0.74	6.39E-03
210607_at	FLT3LG	fms-related tyrosine kinase 3 ligand	0.73	2.71E-03
214181_x_at	LST1	leukocyte specific transcript 1	0.73	4.34E-03
209734_at	NCKAP1L	NCK-associated protein 1-like	0.72	4.53E-03
211323_s_at	ITPR1	inositol 1,4,5-trisphosphate receptor, type 1	0.71	4.00E-03
208438_s_at	FGR	Gardner-Rasheed feline sarcoma viral (v-fgr) oncogene homolog	0.70	5.84E-03
217202_s_at	GLUL	glutamate-ammonia ligase	0.70	4.74E-03
211192_s_at	CD84	CD84 molecule	0.69	4.86E-03
219474_at	C3orf52	chromosome 3 open reading frame 52	0.68	6.26E-03
203528_at	SEMA4D	sema domain, immunoglobulin domain (Ig), transmembrane domain (TM) and short cytoplasmic domain, (semaphorin) 4D	0.68	3.38E-03
208991_at	STAT3	signal transducer and activator of transcription 3 (acute-phase response factor)	0.67	3.66E-03
229062_at	ARL9	ADP-ribosylation factor-like 9	0.67	6.73E-03
213839_at	CLMN	calmin (calponin-like, transmembrane)	0.67	6.26E-03
210184_at	ITGAX	integrin, alpha X (complement component 3 receptor 4 subunit)	0.65	6.27E-03
210992_x_at	FCGR2C	Fc fragment of IgG, low affinity IIc, receptor for (CD32) (gene/pseudogene)	0.65	6.56E-03
219042_at	LZTS1	leucine zipper, putative tumor suppressor 1	0.65	5.44E-03
220576_at	PGAP1	post-GPI attachment to proteins 1	0.65	3.99E-03
237849_at	NA	NA	0.65	3.78E-03
210644_s_at	LAIR1	leukocyte-associated immunoglobulin-like receptor 1	0.64	4.93E-03
207426_s_at	TNFSF4	tumor necrosis factor (ligand) superfamily, member 4	0.64	4.67E-03
200923_at	LGALS3BP	lectin, galactoside-binding, soluble, 3 binding protein	0.63	3.99E-03
1569203_at	CXCL2	chemokine (C-X-C motif) ligand 2	0.62	4.31E-03
1554676_at	SRGN	serglycin	0.62	7.82E-03
227125_at	IFNAR2	interferon (alpha, beta and omega) receptor 2	0.61	3.82E-03
227210_at	SFMBT2	Scm-like with four mbt domains 2	0.60	4.31E-03
225505_s_at	FAM113A	family with sequence similarity 113, member A	0.60	4.19E-03
209473_at	ENTPD1	ectonucleoside triphosphate diphosphohydrolase 1	0.60	7.95E-03
214574_x_at	LST1	leukocyte specific transcript 1	0.59	8.47E-03

211336_x_at	LILRB1	leukocyte immunoglobulin-like receptor, subfamily B (with TM and ITIM domains), member 1	0.59	7.11E-03
201489_at	PPIF	peptidylprolyl isomerase F	0.58	7.84E-03
225177_at	RAB11FIP1	RAB11 family interacting protein 1 (class I)	0.58	7.84E-03
221485_at	B4GALT5	UDP-Gal:betaGlcNAc beta 1,4- galactosyltransferase, polypeptide 5	0.56	5.10E-03
206503_x_at	PML	promyelocytic leukemia	0.56	9.30E-03
201490_s_at	PPIF	peptidylprolyl isomerase F	0.56	6.93E-03
1563075_s_at	NA	NA	0.55	9.48E-03
205038_at	IKZF1	IKAROS family zinc finger 1 (Ikaros)	0.54	5.32E-03
221484_at	B4GALT5	UDP-Gal:betaGlcNAc beta 1,4- galactosyltransferase, polypeptide 5	0.54	9.86E-03
216874_at	DKFZp686O1327	uncharacterized LOC401014	0.52	1.06E-02
205859_at	LY86	lymphocyte antigen 86	0.52	6.08E-03
202963_at	RFX5	regulatory factor X, 5 (influences HLA class II expression)	0.52	8.71E-03
38703_at	DNPEP	aspartyl aminopeptidase	0.51	9.34E-03
204341_at	TRIM16	tripartite motif containing 16	-0.51	1.12E-02
239598_s_at	LPCAT2	lysophosphatidylcholine acyltransferase 2	-0.51	1.12E-02
241434_at	NA	NA	-0.51	6.88E-03
206116_s_at	TPM1	tropomyosin 1 (alpha)	-0.51	1.10E-02
225180_at	TTC14	tetratricopeptide repeat domain 14	-0.52	9.39E-03
227408_s_at	SNX25	sorting nexin 25	-0.53	7.27E-03
212062_at	ATP9A	ATPase, class II, type 9A	-0.53	7.29E-03
212345_s_at	CREB3L2	cAMP responsive element binding protein 3-like 2	-0.54	3.99E-03
219321_at	MPP5	membrane protein, palmitoylated 5 (MAGUK p55 subfamily member 5)	-0.54	9.30E-03
202686_s_at	AXL	AXL receptor tyrosine kinase	-0.54	8.49E-03
243634_at	NA	NA	-0.54	9.97E-03
1555388_s_at	SNX25	sorting nexin 25	-0.54	8.77E-03
223079_s_at	GLS	glutaminase	-0.55	7.90E-03
229890_at	PRRT1	proline-rich transmembrane protein 1	-0.55	9.86E-03
217053_x_at	ETV1	ets variant 1	-0.56	8.65E-03
202080_s_at	TRAK1	trafficking protein, kinesin binding 1	-0.56	8.56E-03
1553108_at	C5orf24	chromosome 5 open reading frame 24	-0.56	9.24E-03
1554471_a_at	ANKRD13C	ankyrin repeat domain 13C	-0.57	9.02E-03
218613_at	PSD3	pleckstrin and Sec7 domain containing 3	-0.57	6.93E-03
212552_at	HPCAL1	hippocalcin-like 1	-0.57	7.13E-03
202045_s_at	ARHGAP35	Rho GTPase activating protein 35	-0.58	7.82E-03
207425_s_at	40057	septin 9	-0.58	8.77E-03
225567_at	NA	NA	-0.58	7.82E-03
229621_x_at	EBF3	early B-cell factor 3	-0.58	4.04E-03
213147_at	HOXA10	homeobox A10	-0.58	6.77E-03
236115_at	HTR7P1	5-hydroxytryptamine (serotonin) receptor 7 pseudogene 1	-0.58	6.24E-03
232636_at	SLITRK4	SLIT and NTRK-like family, member 4	-0.59	6.44E-03
209199_s_at	MEF2C	myocyte enhancer factor 2C	-0.59	7.06E-03
205462_s_at	HPCAL1	hippocalcin-like 1	-0.59	8.65E-03
224963_at	SLC26A2	solute carrier family 26 (sulfate transporter), member 2	-0.59	6.30E-03
202341_s_at	TRIM2	tripartite motif containing 2	-0.59	6.50E-03
244163_at	SEMA3A	sema domain, immunoglobulin domain (Ig), short basic domain, secreted, (semaphorin) 3A	-0.59	8.69E-03
238940_at	KLF12	Kruppel-like factor 12	-0.60	5.36E-03
211121_s_at	DOK1	docking protein 1, 62kDa (downstream of tyrosine kinase 1)	-0.60	6.00E-03
239466_at	LOC344595	uncharacterized LOC344595	-0.61	6.56E-03
202506_at	SSFA2	sperm specific antigen 2	-0.61	7.95E-03
205327_s_at	ACVR2A	activin A receptor, type IIA	-0.62	5.07E-03
242963_at	SGMS2	sphingomyelin synthase 2	-0.63	7.84E-03
201534_s_at	UBL3	ubiquitin-like 3	-0.63	4.04E-03
227115_at	LOC100506870	uncharacterized LOC100506870	-0.63	6.08E-03
234140_s_at	STIM2	stromal interaction molecule 2	-0.63	5.84E-03
222721_at	CNIH4	cornichon homolog 4 (Drosophila)	-0.63	5.10E-03
201283_s_at	TRAK1	trafficking protein, kinesin binding 1	-0.64	7.71E-03

210688_s_at	CPT1A	carnitine palmitoyltransferase 1A (liver)	-0.65	3.58E-03
212468_at	SPAG9	sperm associated antigen 9	-0.65	4.04E-03
219921_s_at	DOCK5	dedicator of cytokinesis 5	-0.66	3.01E-03
204546_at	KIAA0513	KIAA0513	-0.66	3.23E-03
1556308_at	PRRT3	proline-rich transmembrane protein 3	-0.66	6.56E-03
229735_s_at	NIPAL3	NIPA-like domain containing 3	-0.66	4.74E-03
205148_s_at	CLCN4	chloride channel, voltage-sensitive 4	-0.66	5.36E-03
1555830_s_at	ESYT2	extended synaptotagmin-like protein 2	-0.68	6.05E-03
215945_s_at	TRIM2	tripartite motif containing 2	-0.68	3.66E-03
226876_at	FAM101B	family with sequence similarity 101, member B	-0.68	6.05E-03
233335_at	NA	NA	-0.68	4.31E-03
212736_at	C16orf45	chromosome 16 open reading frame 45	-0.69	3.82E-03
227270_at	FAM200B	family with sequence similarity 200, member B	-0.69	3.01E-03
211379_x_at	B3GALNT1	beta-1,3-N-acetylgalactosaminyltransferase 1 (globoside blood group)	-0.69	6.08E-03
220092_s_at	ANTXR1	anthrax toxin receptor 1	-0.70	6.31E-03
229092_at	NR2F2	nuclear receptor subfamily 2, group F, member 2	-0.71	5.23E-03
218963_s_at	KRT23	keratin 23 (histone deacetylase inducible)	-0.71	4.00E-03
216493_s_at	IGF2BP3	insulin-like growth factor 2 mRNA binding protein 3	-0.71	2.97E-03
202214_s_at	CUL4B	cullin 4B	-0.73	3.58E-03
221534_at	C11orf68	chromosome 11 open reading frame 68	-0.73	3.87E-03
233509_at	HERC4	HECT and RLD domain containing E3 ubiquitin protein ligase 4	-0.73	4.96E-03
1555009_a_at	SYNJ2	synaptojanin 2	-0.73	5.10E-03
230207_s_at	DOCK5	dedicator of cytokinesis 5	-0.74	4.68E-03
226013_at	TRAK1	trafficking protein, kinesin binding 1	-0.74	4.33E-03
225162_at	SH3D19	SH3 domain containing 19	-0.74	5.01E-03
236798_at	NA	NA	-0.74	4.80E-03
213150_at	HOXA10	homeobox A10	-0.76	5.73E-03
202342_s_at	TRIM2	tripartite motif containing 2	-0.76	3.03E-03
230206_at	DOCK5	dedicator of cytokinesis 5	-0.76	3.17E-03
220260_at	TBC1D19	TBC1 domain family, member 19	-0.76	3.29E-03
230263_s_at	DOCK5	dedicator of cytokinesis 5	-0.78	2.68E-03
222016_s_at	ZNF323	zinc finger protein 323	-0.78	4.68E-03
203658_at	SLC25A20	solute carrier family 25 (carnitine/acylcarnitine translocase), member 20	-0.78	3.24E-03
243179_at	NA	NA	-0.79	4.05E-03
236396_at	NA	NA	-0.79	3.58E-03
222258_s_at	SH3BP4	SH3-domain binding protein 4	-0.79	4.93E-03
203397_s_at	GALNT3	UDP-N-acetyl-alpha-D-galactosamine:polypeptide N-acetylgalactosaminyltransferase 3 (GalNAc-T3)	-0.79	5.25E-03
204049_s_at	PHACTR2	phosphatase and actin regulator 2	-0.80	4.05E-03
235173_at	LOC401093	uncharacterized LOC401093	-0.81	4.93E-03
209119_x_at	NR2F2	nuclear receptor subfamily 2, group F, member 2	-0.81	4.31E-03
242277_at	NA	NA	-0.82	2.18E-03
209121_x_at	NR2F2	nuclear receptor subfamily 2, group F, member 2	-0.82	4.83E-03
203633_at	CPT1A	carnitine palmitoyltransferase 1A (liver)	-0.83	4.05E-03
229394_s_at	ARHGAP35	Rho GTPase activating protein 35	-0.84	3.99E-03
229397_s_at	ARHGAP35	Rho GTPase activating protein 35	-0.88	4.26E-03
239336_at	THBS1	thrombospondin 1	-0.88	5.23E-03
210519_s_at	NQO1	NAD(P)H dehydrogenase, quinone 1	-0.89	4.17E-03
214036_at	EFNA5	ephrin-A5	-0.89	3.82E-03
244774_at	PHACTR2	phosphatase and actin regulator 2	-0.92	4.14E-03
207469_s_at	PIR	pirin (iron-binding nuclear protein)	-0.92	4.26E-03
221031_s_at	APOLD1	apolipoprotein L domain containing 1	-0.93	3.68E-03
219543_at	PBLD	phenazine biosynthesis-like protein domain containing	-0.93	5.10E-03
239710_at	FIGN	fidgetin	-0.94	3.66E-03
215073_s_at	NR2F2	nuclear receptor subfamily 2, group F, member 2	-0.95	4.77E-03
203634_s_at	CPT1A	carnitine palmitoyltransferase 1A (liver)	-0.95	3.80E-03
214769_at	CLCN4	chloride channel, voltage-sensitive 4	-0.95	1.83E-03
236207_at	SSFA2	sperm specific antigen 2	-0.96	2.93E-03
229461_x_at	NEGR1	neuronal growth regulator 1	-0.96	3.31E-03

227556_at	NME7	non-metastatic cells 7, protein expressed in (nucleoside-diphosphate kinase)	-0.96	2.02E-03
202213_s_at	CUL4B	cullin 4B	-0.97	3.53E-03
227405_s_at	FZD8	frizzled family receptor 8	-0.97	2.77E-03
212188_at	KCTD12	potassium channel tetramerisation domain containing 12	-0.98	4.34E-03
210257_x_at	CUL4B	cullin 4B	-0.99	3.18E-03
228503_at	RPS6KA6	ribosomal protein S6 kinase, 90kDa, polypeptide 6	-1.01	3.99E-03
1553313_s_at	SLC5A3	solute carrier family 5 (sodium/myo-inositol cotransporter), member 3	-1.02	2.78E-03
201467_s_at	NQO1	NAD(P)H dehydrogenase, quinone 1	-1.04	2.78E-03
212944_at	SLC5A3	solute carrier family 5 (sodium/myo-inositol cotransporter), member 3	-1.04	3.66E-03
212838_at	DNMBP	dynamin binding protein	-1.05	3.72E-03
203820_s_at	IGF2BP3	insulin-like growth factor 2 mRNA binding protein 3	-1.06	2.02E-03
241726_at	NA	NA	-1.06	3.58E-03
226103_at	NEXN	nexilin (F actin binding protein)	-1.07	4.17E-03
209288_s_at	CDC42EP3	CDC42 effector protein (Rho GTPase binding) 3	-1.07	3.99E-03
229795_at	NA	NA	-1.08	4.14E-03
213164_at	NA	NA	-1.09	2.02E-03
223315_at	NTN4	netrin 4	-1.10	1.35E-03
203819_s_at	NA	NA	-1.10	1.37E-03
215997_s_at	CUL4B	cullin 4B	-1.11	2.82E-03
233814_at	EFNA5	ephrin-A5	-1.12	2.06E-03
221276_s_at	SYNC	syncoilin, intermediate filament protein	-1.12	4.68E-03
225685_at	CDC42EP3	CDC42 effector protein (Rho GTPase binding) 3	-1.16	3.99E-03
225989_at	HERC4	HECT and RLD domain containing E3 ubiquitin protein ligase 4	-1.17	2.71E-03
1552309_a_at	NEXN	nexilin (F actin binding protein)	-1.17	2.14E-03
205984_at	CRHBP	corticotropin releasing hormone binding protein	-1.17	2.48E-03
232298_at	LOC401093	uncharacterized LOC401093	-1.18	4.31E-03
242592_at	GPR137C	G protein-coupled receptor 137C	-1.19	3.66E-03
219483_s_at	PORCN	porcupine homolog (Drosophila)	-1.20	3.82E-03
213167_s_at	NA	NA	-1.21	3.67E-03
235337_at	SERTAD4	SERTA domain containing 4	-1.21	3.26E-03
224325_at	FZD8	frizzled family receptor 8	-1.23	2.68E-03
227955_s_at	EFNA5	ephrin-A5	-1.24	3.66E-03
201109_s_at	THBS1	thrombospondin 1	-1.27	3.86E-03
235236_at	NA	NA	-1.27	3.58E-03
227243_s_at	EBF3	early B-cell factor 3	-1.27	1.67E-03
222486_s_at	ADAMTS1	ADAM metallopeptidase with thrombospondin type 1 motif, 1	-1.27	4.05E-03
201468_s_at	NQO1	NAD(P)H dehydrogenase, quinone 1	-1.29	2.06E-03
209286_at	CDC42EP3	CDC42 effector protein (Rho GTPase binding) 3	-1.30	3.66E-03
218469_at	GREM1	gremlin 1	-1.31	8.54E-04
227242_s_at	EBF3	early B-cell factor 3	-1.35	2.48E-03
223614_at	MMP16	matrix metallopeptidase 16 (membrane-inserted)	-1.37	1.64E-03
210261_at	KCNK2	potassium channel, subfamily K, member 2	-1.37	3.58E-03
235230_at	PLCXD2	phosphatidylinositol-specific phospholipase C, X domain containing 2	-1.39	3.24E-03
219073_s_at	OSBPL10	oxysterol binding protein-like 10	-1.42	2.18E-03
218468_s_at	GREM1	gremlin 1	-1.43	8.54E-04
226632_at	CYGB	cytoglobin	-1.43	1.35E-03
214761_at	ZNF423	zinc finger protein 423	-1.44	4.05E-03
201860_s_at	PLAT	plasminogen activator, tissue	-1.45	2.78E-03
230660_at	SERTAD4	SERTA domain containing 4	-1.53	4.27E-03
235504_at	GREM2	gremlin 2	-1.58	3.58E-03
204284_at	PPP1R3C	protein phosphatase 1, regulatory subunit 3C	-1.58	2.78E-03
229354_at	AHRR	aryl-hydrocarbon receptor repressor	-1.58	1.35E-03
220161_s_at	EPB41L4B	erythrocyte membrane protein band 4.1 like 4B	-1.59	1.91E-03
212665_at	TIPARP	TCDD-inducible poly(ADP-ribose) polymerase	-1.62	1.04E-03
234880_x_at	KRTAP1-3	keratin associated protein 1-3	-1.62	4.26E-03
210138_at	RGS20	regulator of G-protein signaling 20	-1.65	4.14E-03
228104_at	PLXNA4	plexin A4	-1.69	2.74E-03

218858_at	DEPTOR	DEP domain containing MTOR-interacting protein	-1.70	3.02E-03
235086_at	THBS1	thrombospondin 1	-1.79	3.78E-03
207147_at	DLX2	distal-less homeobox 2	-1.81	1.64E-03
225207_at	PDK4	pyruvate dehydrogenase kinase, isozyme 4	-1.98	1.35E-03
203498_at	RCAN2	regulator of calcineurin 2	-2.02	1.64E-03
210026_s_at	CARD10	caspase recruitment domain family, member 10	-2.06	4.08E-03
205330_at	MN1	meningioma (disrupted in balanced translocation) 1	-2.11	3.66E-03
220794_at	GREM2	gremlin 2	-2.20	3.66E-03
240509_s_at	GREM2	gremlin 2	-2.20	2.06E-03
237435_at	NA	NA	-2.80	2.48E-03
230493_at	SHISA2	shisa homolog 2 (Xenopus laevis)	-2.91	3.99E-03

7.5 Abbreviations

°C	degree Celsius
µg	microgram(s)
µl	microliter
µm	micrometer
µM	micro molar (micromole per liter)
acLDL	acetylated-low density lipoprotein
AE	additional experiment
APC	allophycocyanin
BIRC3	baculoviral IAP repeat containing 3
BSA	bovine serum albumin
CCN1-2	intron-1 retaining RNA of CYR61
CCN2-3	intron-2 retaining RNA of CYR61
CCN3-4	intron-3 retaining RNA of CYR61
CCN4-5	intron-4 retaining RNA of CYR61
cm^2	square centimeter(s)
CTGF	connective tissue growth factor
CXCR4	chemokine (C-X-C motif) receptor 4
CYR61	cysteine-rich protein 61
DiI	(2*Z*)-2-[(*E*)-3-(3,3-dimethyl-1-octadecylindol-1-ium-2-yl)prop-2-enylidene]-3,3-dimethyl-1-octadecylindole; perchlorate
DNA	deoxyribonucleic acid
dNTPs	deoxynucleotide triphosphates
ECM	extracellular matrix
EDTA	ethylendiamintetraacetic acid
ELISA	enzyme-linked immunosorbent assay
EPCs	endothelial progenitor cells
$EPCs^{co\text{-}cu}$	EPCs co-cultured with MSCs
$EPCs^{con\text{-}med}$	EPCs treated with conditioned medium gained from MSCs
et al.	et alia
FACS	fluorescence-activated cell sorting
FBS	foetal bovine serum
FITC	fluorescein isothiocyanate
FST	follistatin
FSTL1	follistatin-like 1
g	gram(s)
g	gravitational force
GO	gene ontology
h	hour(s)
HLA-DQA1	major histocompatibility complex, class II, DQ alpha 1
IDO1	indoleamine 2,3-dioxygenase 1
IL1b	interleukin 1b
IL6	interleukin 6
IL8	interleukin 8
KEGG	Kyoto Encyclopedia of Genes and Genomes
KL	klotho
KL (iso1)	klotho (isoform 1)
KL (iso1)	klotho (isoform 2)
M	molar
mg	milligram(s)
min	minute(s)
ml	milliliter
mM	milli molar (millimol per liter)
mRNA	messenger RNA
MSCs	mesenchymal stem cells
$MSCs^{co\text{-}cu}$	MSCs co-cultured with EPCs
$MSCs^{con\text{-}med}$	MSCs treated with conditioned medium gained from EPCs
n	quantity

NaCl	sodium chloride
ng	nanogram(s)
nM	nano molar (nanomol per liter)
OD	optical density
ON	over night
PBS	phosphate buffered saline
PE	phycoerythrin
PFA	paraformaldehyde
pg	picogram(s)
pmol	picomole(s)
POSTN	periostin
r	recombinant
rbIgG-Fc	Immunoglobulin G (IgG) with rabbit (rb) fragment crystallizable (Fc) region
rCYR61	recombinant CYR61
RNA	ribonucleic acid
RT	room temperature
RT-PCR	reverse transcriptase polymerase chain reaction
scFV	single chain variable fragment
SOCS3	suppressor of cytokine signaling 3
SOD2	superoxide dismutase 2
T_A	annealing temperature
THBS1	thrombospondin 1
TNFSF10	tumor necrosis factor (ligand) superfamily, member 10
Tris	tris(hydroxymethyl)aminomethane
Ulex Lectin	Ulex europaeus I agglutinin
UV	ultraviolet
V	voltage
VCAN	versican
VEGFA	vascular endothelial growth factor A
Wnt5a	wingless-type MMTV integration site family, member 5A
x	times, -fold

7.6 List of Figures

7.7 List of Tables

7.8 List of Publications

7.8.1 Journal publications

Bettina Hafen, Susanne Wiesner, Kathrin Schlegelmilch, Alexander Keller, Regina Ebert, Heike Walles, Franz Jakob and Norbert Schütze *(Manuscript submitted 2015)*

"Physical contact between mesenchymal stem cells and endothelial precursors induces distinct signatures with relevance to tissue engineering and regeneration"
Manuscript submitted to Tisssue Engineering Part A

Anand-Ivell R, Hiendleder S, Viñoles C, Martin GB, Fitzsimmons C, Eurich A, **Hafen B**, Ivell R. (2011)

"INSL3 in the ruminant: a powerful indicator of gender- and genetic-specific feto-maternal dialogue."
In: PLoS One. 2011;6(5):e19821. doi: 10.1371/journal.pone.0019821. Epub 2011 May 16.

Anand-Ivell R, Heng K, **Hafen B**, Setchell B, Ivell R. (2009)

"Dynamics of INSL3 peptide expression in the rodent testis."
In: Biol Reprod. 2009 Sep;81(3):480-7. doi: 10.1095/biolreprod.109.077552. Epub 2009 May 6.

7.8.2 Oral presentations

B. Hafen, S. Wiesner, K.Schlegelmilch, A.Keller, R. Ebert, F. Jakob, and N. Schütze (2015)

„Physical contact between mesenchymal stem cells and endothelial progenitor cells induces distinct global gene expression patterns important for tissue regeneration"
WITE Congress 2015 in Würzburg, Germany

7.8.3 Poster presentations

Bettina Hafen, Katrin Schlegelmilch, Alexander Keller, Susanne Wiesner, Norbert Schütze (2013)

„Spezifische Genexpressionsänderungen durch Zellinteraktionen von endothelialen Vorläuferzellen und mesenchymalen Stammzellen"
Osteology Congress 2013 in Weimar, Germany

Bettina Hafen, Katrin Schlegelmilch, Alexander Keller, Susanne Wiesner, Norbert Schütze (2012)

„ Crosstalk between endothelial precursor cells and mesenchymal stem cells"
ASBMR 2012 in Minneapolis, Minnesota, USA